

6-24-2020

Development of Prefrontal Structure and Connectivity in Typical Children and Children with ADHD: Association with Language and Executive Function

Dea Garic
dgari004@fiu.edu

Follow this and additional works at: <https://digitalcommons.fiu.edu/etd>

 Part of the [Biological Psychology Commons](#), [Cognitive Neuroscience Commons](#), [Cognitive Psychology Commons](#), [Developmental Neuroscience Commons](#), and the [Developmental Psychology Commons](#)

Recommended Citation

Garic, Dea, "Development of Prefrontal Structure and Connectivity in Typical Children and Children with ADHD: Association with Language and Executive Function" (2020). *FIU Electronic Theses and Dissertations*. 4495.
<https://digitalcommons.fiu.edu/etd/4495>

This work is brought to you for free and open access by the University Graduate School at FIU Digital Commons. It has been accepted for inclusion in FIU Electronic Theses and Dissertations by an authorized administrator of FIU Digital Commons. For more information, please contact dcc@fiu.edu.

FLORIDA INTERNATIONAL UNIVERSITY
Miami, Florida

DEVELOPMENT OF PREFRONTAL STRUCTURE AND CONNECTIVITY IN
TYPICAL CHILDREN AND CHILDREN WITH ADHD: ASSOCIATION WITH
LANGUAGE AND EXECUTIVE FUNCTION

A dissertation submitted in partial fulfillment of the
requirements for the degree of
DOCTOR OF PHILOSOPHY
in
PSYCHOLOGY
by
Dea Garic

2020

To: Dean Michael R. Heithaus
College of Arts, Sciences, and Engineering

This dissertation, written by Dea Garic, and entitled Development of Prefrontal Structure and Connectivity in Typical Children and Children with ADHD: Association with Language and Executive Function, having been approved in respect to style and intellectual content, is referred to you for judgment.

We have read this dissertation and recommend that it be approved.

Paulo Graziano

Andy Pham

Bethany Reeb-Sutherland

Lucina Uddin

Anthony Dick, Major Professor

Date of Defense: June 24, 2020

The dissertation of Dea Garic is approved.

Dean Michael R. Heithaus
College of Arts, Sciences, and Engineering

Andres Gil
Vice President for Research and Economic Development
and Dean of the University Graduate School

Florida International University, 2020

© Copyright 2020 by Dea Garic

All rights reserved.

DEDICATION

I dedicate this to my parents, Biljana and Petko Garic, who instilled and continuously fostered my work ethic and sense of purpose. Thank you for the endless love, support, and encouragement.

ACKNOWLEDGMENTS

First and foremost, I would like to thank my advisor, Dr. Anthony Steven Dick, for all of his guidance and support over the last five years. He has been more than willing to spend countless hours discussing research ideas, helping me learn to code, and providing critical feedback on manuscript drafts. Beyond teaching me analytical methods and shaping my writing style, he has always encouraged me to approach science with the bigger picture in mind. I am fortunate to have been trained by an advisor who emphasizes independent problem-solving rather than assigns to-do lists. I cannot thank him enough for his endless commitment and availability to all his students, and for the invaluable skills and knowledge he has prepared me with as I start a career in academia.

I would also like to express my gratitude for my dissertation committee members, Drs. Paulo Graziano, Andy Pham, Bethany Reeb-Sutherland, and Lucina Uddin, who have never failed to provide support, encouragement, and thoughtful suggestions during this challenging dissertation process. Specifically, I would like to thank Dr. Graziano for contributing his extensive clinical expertise in ADHD, Drs. Pham and Reeb-Sutherland for suggesting alternative analytical approaches, and Dr. Uddin for imparting her knowledge in atypical neural networks.

I am extremely grateful for the past and present members of the DCN Lab, all of whom have uniquely contributed to my graduate journey. A special thank you to Iris Broce, the very first graduate student in DCN, who blazed the trail and guided everyone along the way. I would also like to thank Carolina Vias, who spent 5 years sharing an office and advice with me. The findings presented in the dissertation would not have been possible without the tireless commitment to data collection from our undergraduate research assistants and summer interns. I would like to thank Rina Badran, Hector Borges, Armando Torres, Alexis Rodriguez, Sophia

Lehrman, Kevin Roman, and Heidy Zetina. Additionally, I would like to thank Thandi Lyew and Judith Lobo, who are alumni research assistants that have gone on to become amazing members of the research field.

A special thank you goes out to all my external sources of support that I have received during this process. I am extremely grateful for the continued encouragement I have received from my undergraduate advisor, Dr. Scott Miller, who sparked my initial interest in the dynamic process of early child development and guided me in taking the steps needed to further my career. I would also like to thank my partner, Adam, for allowing me to talk incessantly about my work and providing me with a new perspective when I hit roadblocks. I am extremely appreciative of Myriah McNew, a member of my graduate cohort who quickly became a lifelong friend, for always being a bottomless source of advice, a statistical genius, and for providing much-needed comedic relief. Finally, I would like to thank my best friend, Bentley, for being with me every step of the way for the last decade.

Study 1 and 3 data for this dissertation were obtained from the Biosignatures of Executive Function and Emotion Regulation in Young Children with ADHD (Co-PIs: Graziano and Dick; 5R01MH112588-03). Study 2 adult data was provided [in part] by the Human Connectome Project, WU-Minn Consortium (PIs: Van Essen and Ugurbil; 1U54MH091657) funded by the 16 NIH Institutes and Centers that support the NIH Blueprint for Neuroscience Research; and by the McDonnell Center for Systems Neuroscience at Washington University. Study 2 child data were derived from the Cincinnati MR Imaging of NeuroDevelopment (C-MIND) database, provided by the Pediatric Functional Neuroimaging Research Network and supported by a contract from the Eunice Kennedy Shriver National Institute of Child Health and Human Development (HHSN275200900018C).

ABSTRACT OF THE DISSERTATION
DEVELOPMENT OF PREFRONTAL STRUCTURE AND CONNECTIVITY IN
TYPICAL CHILDREN AND CHILDREN WITH ADHD: ASSOCIATION WITH
LANGUAGE AND EXECUTIVE FUNCTION

by

Dea Garic

Florida International University, 2020

Miami, Florida

Professor Anthony Dick, Major Professor

The structure and connectivity of the prefrontal cortex has been extensively studied for its contribution to language and executive function (EF) development, but many questions still remain whether its microstructural tissue properties can reliably predict behavioral outcomes in very young typically and atypically developing populations. In particular, the bilateral frontal aslant tract (FAT) has garnered increasing interest with respect to its potential association with both language and EF, but has yet to be examined in childhood attention disorders, such Attention Deficit Hyperactivity Disorder (ADHD). At the same time, with advances in diffusion weighted imaging (DWI), new diffusion models offer more nuanced characterizations of specific tissue properties, namely neurite (axonal and dendritic) density and organization. Restricted diffusion imaging (RDI) and neurite orientation dispersion and density diffusion imaging (NODDI) are two advanced approaches to measuring density *in vivo* that have been tested in animal, infant, and adult studies, but have been sparsely examined in regards to their association with behavioral outcomes in young children. We can now apply these diffusion methods to the analysis of microstructure of the frontal lobe and its association with language and EF. Thus, across three studies, this dissertation aims to answer the following questions: Does

the FAT show age-related differences during the sensitive developmental period between 4- to 7-years of age, and do age-related differences differ in children diagnosed with ADHD? Are microstructural properties of the FAT differentially associated with language and EF outcomes in ADHD and control samples? Are novel DWI methods capable of reliably mapping neurite density in children and adults and expanding what we currently know about brain microstructure and maturation? And finally, is neurite density and orientation within prefrontal and subcortical brain regions associated with behavioral outcomes in typically and atypically developing children? To answer these questions, we used three DWI reconstruction methods to better elucidate neural tissue development, and examined its association to a battery of language and EF measures. We present compelling evidence that the FAT is a potential biomarker for ADHD, differentially associated with aspects of language and EF across these groups. Furthermore, we show that more precise diffusion-weighted imaging methods can inform our understanding of typical and atypical brain development as it relates to behavior in the domains of language and EF.

TABLE OF CONTENTS

CHAPTER	PAGE
1. INTRODUCTION	1
1.1 Attention Deficit Hyperactivity Disorder (ADHD)	2
1.2 Frontal Aslant Tract (FAT)	3
1.2.1 FAT and Language	4
1.2.2 FAT and Executive Function	6
1.3 Measuring Neuronal Density <i>in vivo</i>	7
1.3.1 Neurite Orientation Dispersion and Density Imaging (NODDI)	8
1.3.2 Restricted Diffusion Imaging (RDI)	10
1.4 Research Aims	11
2. STUDY 1	12
2.1 Research Question	12
2.2 Method	15
2.3 Statistical Analysis	27
2.4 Results	29
2.4.1 Language Findings	32
2.4.2 Executive Function Findings.	38
2.5 Discussion	45
3. STUDY 2	56
3.1 Research Question	56
3.2 Study 2.A: Adult Sample	61
3.2.1 Method	61
3.2.2 Results	67
3.3 Study 2.B: Developing Sample	68
3.3.1 Method	68
3.3.2 Results	69
3.4 Discussion	70
4. STUDY 3	76
4.1 Research Question	76
4.2 Method	81
4.3 Results	83
4.3.1 Language Findings	85
4.3.2 Executive Function Findings	88
4.4 Discussion	92

5. GENERAL DISCUSSION	99
5.1 Summary	99
5.2 Implications	112
5.3 Limitations	113
5.4 Future Directions	114
REFERENCES	116
APPENDICES	144
VITA	229

LIST OF TABLES

TABLE	PAGE
1 Group Differences in Demographics	175
2 Age-Related Differences in the FAT	176
3 Language Task Means and Main Effects of Demographic Variables	177
4 Group Differences on Language Tasks	178
5 The FAT's Association with Language	179
6 EF Means and Main Effects of Demographic Variables	181
7 Executive Functioning Group Differences.	182
8 The FAT's Association with Executive Function	183
9 DWI Metrics in Study 2.A and 2.B	185
10 Contrast Analyses for Axonal Density in Adult Sample	186
11 Contrast Analyses for Axonal Density in Developing Sample	188
12 NODDI Means and Group Differences	189
13 Region-Based Age Related Change	190
14 Neurite Density and Orientation Predicting Language Outcomes	191
15 Neurite Density and Orientation Predicting Executive Function	192

LIST OF FIGURES

FIGURE	PAGE
1 FAT Anatomy	194
2 Age-related differences in the FAT by DTI metric: Winsor.	195
3 Age-related changes in the FAT by HARDI metric: Winsor.	196
4 Significant Age-related differences in the CST: Winsor.	197
5 NEPSY Group Differences	198
6 FAT Predicting Phonemic and Semantic Scores in TD Sample	199
7 FAT Predicting Semantic Scores in ADHD Sample	200
8 FAT Lateralization Association with Semantic Scores in ADHD Sample	201
9 ADHD Diagnosis Moderates Relationship Between Right FAT and Semantics	202
10 ADHD Diagnosis Moderates Effect of PreSMA Op Laterality’s Relationship with Semantics	203
11 Left FAT Predicting Phoneme Articulation in Full Sample	204
12 Left Lateralization of the FAT Predicts SRT in Full Sample	205
13 Left FAT Predicting Flanker and DCCS Scores in Full Sample	206
14 Group Differences in NIH Toolbox Tasks	207
15 Bilateral FAT Predicting NIH Toolbox in ADHD Sample	208
16 Bilateral FAT Predicting HTKS Scores in Full Sample	209
17 Bilateral FAT Predicting HTKS Scores in TD Sample	210
18 FAT Laterality Predicting HTKS Scores in TD Sample	211
19 Bilateral FAT Predicting HTKS Scores in ADHD Sample	212
20 ADHD Diagnosis Moderates Relationship Between Left and Right FAT and HTKS	213
21 ADHD Diagnosis Moderates Effect of PreSMA to Op Laterality’s Relationship with HTKS	214
22 Corpus Callosum Segmentation	215

23	Density Patterns for Adult Sample	216
24	DWI Metric Effect Sizes for Adult Sample	217
25	Density Patterns for Developing Sample	218
26	DWI Metric Effect Sizes for Developing Sample	219
27	Comparison of <i>in vivo</i> Metrics to Histological Density Models	220
28	Age-Related Differences in Neurite Density	221
29	Laterality of Neurite Density in SMA and Caudate Predict Verbal Fluency in ADHD Sample	222
30	Laterality of the SMA Predicts Executive Function in Full Sample	223
31	Orientation Dispersion Predicting Flanker Scores in TD Sample	224
32	Neurite Density of the Left SMA Differentially Predicts Flanker Scores	225
33	Laterality of Orientation Dispersion Differentially Predicts DCCS Scores	226
34	Neurite Density of Tri Predicts Executive Function in the TD Sample	227
35	Orientation Dispersion of Multiple Brain. Regions Predicts Executive Function in the TD Sample	228

CHAPTER 1

INTRODUCTION

The prefrontal cortex and its associated connections have for decades been studied with respect to their contribution to language and executive function development (Diamond, 2002; Fuster, 2002). In addition, prefrontal cortical structure and connectivity are also the focus of investigation in understanding childhood disorders of attention, such as Attention Deficit Hyperactivity Disorder (ADHD) (Casey et al., 1997; Rubia, 2018), which can sometimes present with co-morbid language disorder. Little work has investigated the development of prefrontal regional structure and connectivity in very young children (e.g., preschool and kindergarten aged children), and the field does not generally have an understanding of how development of these regions and connections in the brain relate to behavioral changes in executive function and language. These abilities, nascent in very young children, are potentially informative for early identification and for understanding the progression of disorders of language and attention.

The present investigation of a large sample ($n = 196$) of children with and without a diagnosis of ADHD, and scanned using structural and diffusion-weighted magnetic resonance imaging (DW-MRI), represents a unique opportunity to 1) understand how early brain development in the prefrontal cortex relates to impairment in language and executive function; 2) understand how brain and behavioral profiles in language and executive function manifest along a continuum that crosses traditional diagnostic boundaries (e.g., for those diagnosed with and without ADHD); and 3) understand the establishment and development of hemispheric specialization of particular connectivity profiles for these domains, executive function and language. Understanding the early development of the prefrontal cortex and its associated connections has direct relevance for the definition and characterization

of childhood disorders of attention and language, with potential implications for establishment of therapeutic interventions.

1.1 Attention Deficit Hyperactivity Disorder (ADHD)

Attention Deficit Hyperactivity Disorder is an increasingly common behavioral disorder in young children, frequently characterized by impulsiveness, over-activity, and difficulty paying attention (Desikan et al., 2006; Visser et al., 2014). Children diagnosed with ADHD face increased likelihood of mental illness and academic and social difficulties (Biederman et al., 2006), therefore there is an urgent need for effective treatment and interventions plans to improve outcomes. Even through the use of evidence-based treatments, numerous studies have indicated that intervention programs continue to make very little impact on children’s academic and social well-being (Molina et al., 2009, 2013; Sonuga-Barke et al., 2013). By identifying brain regions and pathways associated with ADHD, more effective, targeted treatment plans can be designed to improve outcomes and developmental trajectories for young children diagnosed with ADHD.

Current neuroimaging research has identified a myriad of neural abnormalities in the ADHD population, including gray matter reductions in the right inferior frontal gyrus (Depue et al., 2010a), increased gray matter in supplementary motor areas (Kaya et al., 2018), lower density and volume in frontal pathways (Wu et al., 2019), and asymmetrical putamen volume (Wellington et al., 2006). There have been mixed findings when examining directionality of water diffusion in fiber pathways in the ADHD population, with some studies reporting decreased directional diffusivity (Chiang et al., 2015; Hamilton et al., 2008) and some indicating increased directional diffusivity (Silk et al., 2009; Tamm et al., 2012) when comparing ADHD samples to

typically developing samples. Differences might be attributed to small sample sizes and age-range differences, and this has yet to be examined in a large, preschool-aged sample. Furthermore, while past work has indicated abnormalities in the structure and activation of the right inferior frontal gyrus (Depue et al., 2010a; Rubia et al., 1999) and supplementary motor areas (Kaya et al., 2018; Suskauer et al., 2008a,b) in individuals with ADHD, the structural connectivity between the two areas, known as the frontal aslant tract (FAT), has yet to be studied in a clinical, ADHD-diagnosed population.

The majority of work surrounding ADHD has primarily focused on executive function aspects, but ADHD can also present with comorbid language disorder (Bellani et al., 2011; Mueller and Tomblin, 2012; Sciberras et al., 2014; Westby and Watson, 2004), which is thought to further contribute to the lower academic performance outcomes observed in ADHD samples (Sciberras et al., 2014). In a large sample of 6- to 8-year old children, Sciberras et al. 2014 found that 41% of children with ADHD also displayed comorbid language problems, which was nearly three times greater than what is seen in typically developing children. Lynam et al. (1993) has suggested that there might be a causal relationship between ADHD and language impairment, in which attention deficits observed in ADHD disrupt the ability to focus on relevant linguistic stimuli required for early language learning. It remains to be seen whether abnormalities in prefrontal regions and pathways can predict both executive function deficits and speech and language outcomes in young children with ADHD.

1.2 Frontal Aslant Tract (FAT)

Prefrontal connectivity studied with DW-MRI has been of increasing interest to researchers interested in both adult and child neural functioning (Thiebaut de Schot-

ten et al., 2014). One intriguing fiber pathway of the brain, the frontal aslant tract (FAT), has recently been evaluated in terms of its association with its development of language and executive function (Catani et al., 2013; Dick et al., 2019; Garic et al., 2019; Mandelli et al., 2016). The FAT fiber pathway is most commonly thought to connect the pre-supplementary motor area (Pre-SMA) to the *pars opercularis* (Op) (Broce et al., 2015; Catani et al., 2012; Ford et al., 2010; Kinoshita et al., 2015; Klein et al., 2007; Kronfeld-Duenias et al., 2016; Oishi et al., 2008; Sierpowska et al., 2015; Vassal et al., 2014; Vergani et al., 2014) but recent research has shown the connections of the FAT could potentially be broken down into four segments involving the connections between the pre-SMA and supplementary motor area (SMA)-proper to the *pars opercularis* (IOp) and the *pars triangularis* (Tri) of the inferior frontal gyrus.

1.2.1 FAT and Language

The left inferior frontal gyrus (IFG) is frequently associated with processing language and has classically been referred to as Broca’s area in the past (Tremblay and Dick, 2016), while the left SMA and pre-SMA brain regions are associated with motor aphasia (Ardila and Lopez, 1984) and word production and selection (Tremblay and Gracco, 2009), respectively. Given that the FAT connects the SMA and pre-SMA to the IFG, it comes as no surprise that most previous research has examined the left FAT’s relation to language and speech almost exclusively. Previous findings have shown that the FAT can cause speech arrest if electrically stimulated (Fujii et al., 2015; Kinoshita et al., 2015; Vassal et al., 2014), is associated with impaired verbal fluency in patients with primary progressive aphasia (Catani et al., 2013; Mandelli et al., 2016), post-stroke aphasia symptoms (Basilakos et al., 2014), deficits in morphological derivation (Sierpowska et al., 2015), speech initiation (Kinoshita

et al., 2015), and with stuttering (Kemerdere et al., 2016; Kronfeld-Duenias et al., 2016). All of the above studies examined the fiber pathway in relation to language in adults, with only one study examining the relationship between the left FAT and language in children. In that study, Broce et al. (2015) found that certain white-matter properties of the tract were associated with receptive language.

While there is convincing evidence and prior work about the left FAT’s association with language, not as much work has been done examining the right hemisphere FAT and its possible relationship to language. We know from other major language fiber pathways, such as the superior longitudinal fasciculus (SLF), arcuate fasciculus (AF) and inferior longitudinal occipital fasciculus (IFOF), that the left hemisphere of the pathway can be more involved in phonemic fluency, while the right hemisphere is associated with category-based semantic fluency (Blecher et al., 2019; Rodriguez-Aranda et al., 2016). Recent work has shown that hemispheric specialization for phonemic versus semantic skills exists in the FAT as well (Blecher et al., 2019), but it remains to be seen whether this hemispheric specialization is already present in early childhood.

A second aspect that remains unknown about the FAT’s relation to language during childhood is whether laterality plays a pivotal role as early as preschool age, and whether the same associations can be found in clinical samples of children, such as those diagnosed with ADHD. The lateralization of brain function, particularly with the left hemisphere being attune to language functions while the right hemisphere becomes increasingly specialized for visuospatial tasks (Herve et al., 2013; Toga and Thompson, 2003), is thought to develop early in life. Recent work has shown that the language network displays left microstructural asymmetry as early as two years of age (Reynolds et al., 2019b). Furthermore, increased left lateralization in language fiber pathways, such as the arcuate fasciculus, has been associated

with improved reading and vocabulary scores in young children (Groen et al., 2012; Reynolds et al., 2019b). Similar results are found with respect to the FAT, with increased left laterality predicting improved lexical decision (Vallesi and Babcock, 2020) and verbal fluency (Tseng et al., 2019) in adults. However, the lateralization of FAT function remains to be tested in young children. We hypothesize that the left lateralization of the FAT will be associated with improved verbal fluency in our sample of typically and atypically developing preschool-aged children.

Given the sparsity of research examining the FAT in developing samples, it comes as no surprise that there is no current work indicating whether the FAT is functionally or structurally different in clinical samples of children. While language impairment is not a diagnostic criteria for ADHD, there has been a long studied comorbidity between ADHD and language disorders (Bellani et al., 2011; Green et al., 2014; Sciberras et al., 2014), most likely associated with the interrelated nature of language and executive function abilities. We set out to examine whether there were microstructural differences in the FAT between our typically developing (TD) sample and ADHD sample, and whether these differences could explain lower verbal fluency performance associated with ADHD.

1.2.2 FAT and Executive Function

While the left IFG has been the primary focus since the time of Broca, research on the right IFG has been gaining traction over the last few decades. Initially, research focused on the right IFG's role in inhibitory control, particularly in Go/NoGo and StopSignal tasks in which the prepotent response (a Go process) must be overridden when a stop-signal occurs (the Stop process) (Swann et al., 2012). More studies have viewed inhibitory control as requiring the support of an extended neural network, involving the dorsolateral prefrontal cortex, pre-SMA, SMA, dorsal anterior cingu-

late, supplementary eye field, frontal eye field, subthalamic nucleus, globus pallidus, and thalamus (Aron, 2007; Aron et al., 2016; Aron and Poldrack, 2006; Chambers et al., 2009; Fife et al., 2017; Garavan et al., 1999; Jahanshahi et al., 2015; Levy and Wagner, 2011; Wiecki and Frank, 2013). The FAT, which connects the IFG and pre-SMA nodes, is an understudied connection within this network.

Garic et al. (2019) examined the FAT and its relation to executive function and externalizing behaviors in a developing sample and found that left laterality of the tract was associated with higher attention problems and executive dysfunction. This study provided initial support that the degree to which the developing brain favors a right lateralized structural dominance of the FAT is directly associated with better executive function. This relationship could provide a new potential biomarker for assessing ADHD during the preschool years, but this remains to be assessed in a sample of children with ADHD.

1.3 Measuring Neuronal Density *in vivo*

There has been a growing interest in identifying biomarkers for ADHD, but research has not yet focused on specific white matter fiber pathways. Through the use of diffusion weighted imaging (DWI) methods, previous studies have been able to establish the structural connectivity of the FAT by examining water diffusion through tissue. By using diffusion tensor imaging (DTI) and generalized q-sampling imaging (GQI) metrics, scientists have been able examine microstructural changes in white matter, such as the directional diffusion of water as well as axonal and myelin integrity. What remains unknown about neuronal microstructure is how to quantify the axonal and neurite density within in these regions *in vivo*. Histological studies have shown that axonal density is related to the progression rate of multiple sclerosis (Tallantyre et al., 2009), hereditary spastic paraplegia (Deluca et al., 2004), as

well as a gradual decline across the lifespan (Pannese, 2011). Being able to quantify these density changes *in vivo* during development could provide essential insight into microstructural differences within brain regions associated with language and executive function. Two new DWI methods have been introduced in order to investigate measuring neuronal density: Neurite Orientation Dispersion and Density Imaging (NODDI) and Restricted Diffusion Imaging (RDI).

1.3.1 Neurite Orientation Dispersion and Density Imaging (NODDI)

The first new measure, Neurite Orientation Dispersion and Density Imaging (NODDI) ascribes the signal of water protons in tissue into three components: isotropic diffusion representing free motion in areas such as ventricles, intracellular volume diffusion representing restricted water in dendrites and neurons, and extracellular volume diffusion representing glial cells, cell bodies, and the extracellular environment (Zhang et al., 2012). Furthermore, Zhang et al. (2012) have shown that NODDI is capable of disentangling the two components contributing to FA, neurite density and orientation dispersion, and allowing the two to be studied individually.

NODDI has the potential to identify critical biomarkers of microstructural changes that occur during neurodegeneration (Andica et al., 2019). Furthermore, past studies have shown that NODDI's intracellular volume fraction is correlated with histological markers of axonal or dendritic processes (Grussu et al., 2017; Seppehrband et al., 2015). Since its implementation, NODDI has been used in numerous adult studies to examine disease progression. In adults with cortical dysplasia, NODDI metrics have been helpful in localizing areas of degradation, above and beyond traditional DTI metrics (Winston et al., 2014). NODDI is also sensitive enough to pick up of white matter abnormalities within fiber pathways in tuberous sclerosis

patients (Taoka et al., 2020) as well as volume atrophy in patients with amyotrophic lateral sclerosis (Broad et al., 2019).

Given the rapid change of dendritic packing and myelination during development, NODDI could potentially be used as a tool to examine neural development across the lifespan (Chang et al., 2015; Lynch et al., 2020), and might be more sensitive to age-related differences than traditional DTI measures (Genc et al., 2017). Infant research has shown that NODDI is capable of differentiating between myelinated and non-myelinated axons (Kunz et al., 2014), mapping the development of structural connectivity (Batalle et al., 2017), and measuring increasing cortical gray matter across maturation (Pecheva et al., 2018). Furthermore, NODDI has shown that higher axon dispersion and lower density in fiber pathways is linked to neurodevelopmental outcomes in children born pre-term (Kelly et al., 2016) and is correlated to dyslexia symptoms (Caverzasi et al., 2018).

The explosion of NODDI implementation in human research in the last several years has led to many exciting discoveries, but the novel DWI method still leaves many questions unanswered. One primary drawback to the NODDI method is the lack of direct diffusivity estimation; instead, it assumes equal intra- and extracellular diffusivity (Jelescu and Budde, 2017), which can bias the parameters. Furthermore, It remains unclear which microstructural characteristic NODDI is the most sensitive to and how reproducible the results are. Chung et al. (2016) used a sample of 8 healthy adults to show that NODDI metrics are prone to more variability than DTI metrics. Reproducibility issues are further exacerbated by the fact that the majority of previous NODDI studies have very small sample sizes. It is still up for question how reliable the metrics are when tested on large samples, and whether it can be used to identify biomarkers for neurodevelopmental disorders, such as ADHD.

1.3.2 Restricted Diffusion Imaging (RDI)

The second new measure, Restricted Diffusion Imaging (RDI), has been proposed to measure changes in cellularity (i.e., cellular density), which affects local diffusion of water molecules. RDI attempts to separate non-restricted diffusion of water molecules from restricted diffusion of water molecules by focusing on the difference in diffusion displacement of each component (Yeh et al., 2017). Unlike relying on the apparent diffusion coefficient (ADC), RDI is calculated through the use of spin density rather than diffusivity. This model-free approach uses q -space imaging to estimate the density of diffusing spins to resolve fast and slow diffusion components; a specificity that other diffusion metrics lack.

This novel metric has only been implemented in two previous studies thus far. In 2017, Yeh et al has been shown to be effective for measuring macrophage infiltration, indicating it can measure cellular density, in rats. By being able to combine both *in vivo* and *ex vivo* methodology, the study showed that a 0.998 correlation between cell density and RDI, thereby providing evidence that RDI has better specificity than traditional DTI metrics. Secondly, RDI was shown to be useful in identifying neural reorganization around lesion sites in patients who underwent a thalamotomy (Sammartino et al., 2019). The study implied that RDI's ability to correct for free water contamination during diffusion can shed more insight to microstructural changes. More work needs to be done to see if this measure will be reliable in a large sample size, as well as its utility in a developing sample.

In order to see whether these novel metrics can be reliably used in measuring density in humans, we replicated a well-known histological corpus callosum density pattern (Aboitiz et al., 1992) in a large sample of adults ($n=842$) and a developing sample ($n=129$) as a proof of concept for Study 2 of this dissertation. Once these

methods were validated with respect to their sensitivity to cellular microstructure, we utilized them to measure neurite and axonal density in brain regions associated with language and executive function in our sample of $n = 196$ pre-school/pre-kindergarten children with and without ADHD. Study 3 examined how the microstructural density differences within prefrontal cortex regions are associated with language and executive function behavioral outcomes in our typically developing children and children diagnosed with ADHD.

1.4 Research Aims

Overall, the three studies comprising this dissertation examined (1) whether the FAT shows age-related differences during the sensitive developmental period between 4- to 7-years of age, and whether the age-related differences differ in children diagnosed with ADHD (2) laterality of the FAT is differentially associated with language and executive function measures in typical children and children with ADHD, (3) showed that novel density DWI models can be reliably applied to human brain imaging, and (4) quantified neuronal density in brain regions associated with language and executive function in typically developing and children diagnosed with ADHD. This multimodal approach aimed to provide insight into brain lateralization and density changes during the critical preschool years in typical and atypical language and executive function development.

CHAPTER 2

STUDY 1

2.1 Research Question

We investigated the age-related differences in the bilateral FAT and related its microstructural properties to behavioral measures of language and executive function development. We expected that the left hemisphere FAT will be associated with language ability, specifically in the phonological, semantic, and speech articulation domains. Given the growing literature on the left FAT's involvement in language in adults (Basilakos et al., 2014; Catani et al., 2013; Kinoshita et al., 2015; Kronfeld-Duenias et al., 2016), we set out to replicate these findings in a developing sample and to elucidate how the FAT impacts language development in typically and atypically developing children.

Secondly, we examined the right hemisphere FAT and its putative relationship to executive function, specifically in the working memory, set shifting, and inhibitory control domains. The right IFG has been previously shown to be related to inhibition and attentional control (Hampshire et al., 2010) and our team has found that the right FAT, specifically, is related to inattention and executive dysfunction in 7- to 18-year-old participants (Garic et al., 2019). Our 2019 paper served as the groundwork for the design of Study 1, and the full publication is available in Appendix A for more information.

Our previous work used the Behavior Rating Inventory of Executive Function (BRIEF) parent and teacher report measures to examine executive function. However, these are rather coarse measures of executive function ability, relying on the report of behaviors by teachers and parents. In the present study, we extended our investigation to the use of empirically validated laboratory measures of executive

function. Furthermore, our previous results indicated that the FAT could serve as a biomarker for dysfunction of attention, but was only tested on a typically developing sample. In the present study, we examined a diverse sample with both typically developing children and children with ADHD to examine the FAT's influence on executive dysfunction. We inspected executive dysfunction among the typical and ADHD participants from both a transdiagnostic approach, in which executive function was viewed on a continuum without respect to diagnostic category (i.e., ADHD or control), and a categorical diagnostic approach, with respect to diagnosis between the ADHD and TD group. The transdiagnostic approach is consistent with the Research Domain Criteria (RDoc) (Casey et al., 2013) and allows for examination of dysfunction across traditional diagnostic categories, while the categorical diagnosis approach allows us to compare the ADHD and TD groups based on DSM-5 classifications.

When we examined executive function from the transdiagnostic approach, we hypothesized that greater directional diffusivity in the left hemisphere FAT will be associated with higher scores on the phonemic subscales of the Developmental NEuroPSYchological Assessment (NEPSY) and more accurate phoneme articulation as measured by the Syllable Repetition Task (SRT). We also predicted that greater directional diffusivity in the right hemisphere FAT would result in higher scores on the semantic sub-scales of the NEPSY and higher executive function performance on the NIH Toolbox Flanker, Card Sort and Head-Toes-Knees-Shoulders (HTKS) task. If we find increased right laterality of the FAT is associated with improved executive function performance, this would build on and further solidify our previous findings with parent and teacher report measures.

When we examined our data from the categorical diagnostic approach, we expected to see that diagnosis moderates the relationships between the FAT and both

language and executive function. For language findings, we predicted that children with ADHD might have lower diffusivity in the FAT when compared to controls. Chiang et al. (2016), for example, found lower directional diffusivity in language fiber pathways in preadolescent children with ADHD. We wanted to test if this result carries over to the FAT in preschool children. Furthermore, previous studies have shown there are significant differences in grey matter volume and activation within the right inferior frontal gyrus in children and adults with ADHD which influence their performance on attention, executive control, and inhibition tasks (Depue et al., 2010b; Wang et al., 2013).

Given previous findings, we expected that the relationship between the FAT and language and executive function differs depending on ADHD diagnosis. When contrasting the typically developing and ADHD samples, we hypothesized that the ADHD sample would have lower scores on the language measures because of the comorbidity between ADHD and speech-language disorders (Efron and Sciberras, 2010; McGrath et al., 2008). We also predicted that the typically developing group will outperform the ADHD group on executive function measures as a result of the well-documented executive dysfunction and lower attentional control symptoms attributed to the disorder (Lambek et al., 2011; Reader et al., 1994). We hypothesized that the FAT would have a larger impact on language and executive function in typically developing children than in children diagnosed with ADHD.

To determine whether the FAT has a unique contribution to language and executive function, we decided to use a control pathway to compare the results to. We chose the corticospinal tract (CST), which originates in the premotor, motor, and primary somatosensory cortex regions of the brain (Kolb and Wishaw, 2014). Since the primary function of the CST is voluntary motor control (Welniarz et al., 2017), we hypothesize that it will not be related to language and executive function.

In sum, we predicted that the left and right FAT serve different but complementary functions within the developing brain. We hypothesized that the left FAT would be more specialized in language-focused executive function while the right FAT would be focused on domain general and visuospatial aspects of executive function and that this relationship could potentially be moderated by ADHD.

2.2 Method

Participants

Recruitment and Eligibility Requirements. Children and their families were recruited from local schools, public family events at zoos and museums, open houses/parent workshops, mental health agencies, and social media to participate in the ADHD Heterogeneity of Executive Function/Emotion Regulation Across Development (AHEAD) study. All children were offered free gifted intelligence testing, while ADHD children were additionally offered a free-of-charge or price-reduced summer treatment program as a behavioral intervention for ADHD. All participants were screened by phone for MRI contraindications and were provided informed consent and written assent (if above the age of 7-years-old) before MRI scanning. Exclusionary criteria for the children included not attending or being enrolled in school, intellectual disability (IQ lower than 70 on the Wechsler Preschool and Primary Scale of Intelligence 4th edition (WPPSI-IV)), history of developmental or psychotic disorders, and currently or previously taking psychotropic medication.

Demographics. We analyzed 196 four to seven-year-old children from the AHEAD project for the final sample. The split between the typically developing sample and the children diagnosed with ADHD was relatively even, with 96 typically developing children and 100 children diagnosed with ADHD. The groups were equivalent on age ($M = 5.64$ years, $p = 0.80$) and SES ($m = 5$, binned variable, equates to

\$50-65,000 average parent income, $p = 0.71$). Because there is a higher prevalence of ADHD diagnosis in males (i.e., Banaschewski et al. 2017), there are more males than females in the sample ($p < 0.05$, $df = 194$). We had 136 males and 60 females in the overall group, with the ADHD group being comprised of 76% males (76 males, 24 females), and the TD group being comprised of 62.5% males (60 males, 36 females). These results can be found in Table 1. Additionally, the Full Scale Intelligence Quotient (FSIQ) indicated that the average IQ in the full sample was 99.90. There was a significant group difference ($p < 0.001$, $df = 193$), with TD ($m = 103.67$) outperforming ADHD ($m = 96.31$).

The majority of our sample was Hispanic (85.2%, $n = 167$), which was representative of the surrounding South Florida population. For race, parents were allowed to select multiple options: majority of our participants self-identified as White (89.2%, $n = 176$), 10% identified as African American ($n = 20$), 2% as Asian ($n = 4$), and 0.5% as American Indian or Alaskan Native ($n = 1$). While all the children in the study spoke fluent English and attended English preschools, more than half of parents identified the child's primary language as a mixture of English and Spanish (55.6%, $n = 109$), while the remainder primarily spoke English (39%, $n = 78$), Spanish (3.1%, $n = 6$), or other (1%, $n = 2$).

General Procedure

Data were collected across three visits. The first visit comprised of diagnosis and academic testing, the second visit was behavioral data collection for the language and executive function tasks, and the third visit was the MRI scan.

ADHD Diagnostic Criteria

To diagnose and place children into the ADHD sample, we used a combination of rating scales to measure the child's parent- and teacher-rated symptomatology as well as structured parent interviews at intake. Symptoms and impairment were measured by the Disruptive Behavior Disorders Rating Scale (DBD; Pelham et al. 1992), Impairment Rating Scale (IRS; Fabiano et al. 2006), and a parent semi-structured interview (DISC-IV; Shaffer et al. 2000). In order to capture the highest level of impairment, parent and teacher ratings were combined by taking the higher of the two ratings for each item (Garcia et al., 2020; Hartman et al., 2007; Sibley et al., 2010). Higher ratings indicate greater impairment.

To be included in the ADHD group, children needed to have 6 or more symptoms of inattention or hyperactivity/impulsivity (American Psychiatric Association, 2013) or a previous diagnosis of ADHD, and impairments in social, academic, or behavior scales on the IRS. Two licensed clinicians reviewed the results to determine diagnosis and severity, with a third clinician being called in when a disagreement occurred. For the purposes of this dissertation, we examined ADHD as a whole, without regard to specific ADHD subtypes. The majority of our sample was diagnosed with ADHD-combined (ADHD-C) type (87%), while 7% were primarily ADHD-hyperactive/impulsive (ADHD-HI) and 6% were primarily ADHD-inattentive (ADHD-I).

Oppositional Defiant Disorder (ODD) Comorbidity

Numerous studies have indicated that there is a large degree of comorbidity between ADHD and ODD (Connor et al., 2010; Efron and Sciberras, 2010; Mohammadi et al., 2019; Reale et al., 2017). In our sample, 68% of children with ADHD also met

diagnostic criteria for ODD. In order to verify whether our comparisons between TD and ADHD groups were valid and ADHD-specific, we decided to control for ODD comorbidity. Using the results from the DBD, the highest parent-teacher rating for the continuous ODD subscale score for each participant was entered as a covariate in the regression models.

Battery of Language and Executive Function Measures.

The following assessments were administered to obtain an understanding of each child’s language skills, executive function, and demographic information.

Measurements of Speech and Language. We measured children’s abilities in speech motor planning, phonemics, and semantics. Language assessments included the phonemic and semantic subscales of the NEuroPSYchological Assessment (NEPSY) and the syllable repetition task (SRT).

NEuroPSYchological Assessment (NEPSY). We analyzed the semantic and phonemic subscales of the NEPSY (Korkman et al., 1998). For the semantic fluency segment, children were tested with NEPSY’s Word Generation Semantic task and were asked to list as many words as they knew in the food category and animal category within a 60 second time limit. The children were also tested with NEPSY’s Word Generation Initial Letter task to test phonemics, which asked them to list out all the words starting with “s” and then “f” that they could within the time limit. The semantic fluency and phonemic subscales have test-retest correlation coefficients of 0.84 and 0.54 respectively (Brooks et al., 2010). While the NEPSY provides scaled contrast scores that indicate specific language impairments, the phonological scaled values were only available for children above the age of 7, which disqualified the majority of our sample. Instead, individual task scores and total semantic and phonological scores are reported and analyzed.

Syllable Repetition Task (SRT). The SRT examined phonological working memory, language impairment, and motor planning deficits and previous work has indicated that it is an accurate and stable task for measuring misarticulation (Shriberg et al., 2009). The task asked children to repeat a list of 18 two to four syllable nonsense words which are played over computer speakers. The task starts with simple, two-syllable words such as ba-da, and increases in difficulty to words such as ba-na-ma-da. The microphone recordings were transcribed by three research assistants and scored according to the SRT scoring manual, which provides a final percentage score for proportion of correct syllables spoken. Syllable additions, or syllables that the participant produced that were not a part of the target word, are tallied and provide a validity check. If four or more responses include additions (25% of items), that participant’s score is deemed invalid. The SRT has a Cronbach’s α coefficient of 0.83 and a Pearson’s correlation coefficient between successive runs of 0.87 (Mahrooghi et al., 2015).

Three transcribers, all Spanish-English bilinguals, were trained by a licensed Spanish-English bilingual speech pathologist. On the task, the three transcribers had moderate to good inter-rater reliability score of $\kappa = 0.587$ (Cohen, 1960). In cases of disagreement, the score for each word was determined by majority (2 out of 3) vote. If agreement could not be reached, the recording was replayed with all raters and a licensed Spanish-English bilingual speech pathologist present for a final determination.

Given the large proportion of bilingual Spanish speaking children enrolled in our study and the fact that the SRT was developed for monolingual participants, we decided to score the SRT using both the traditional scoring manual as well as an updated, bilingual scoring system. The bilingual scoring method allows for b/v substitutions, which are two separate phonemes in English but are commonly both

pronounced as "b" in Spanish. The results from both traditional SRT scoring and our bilingual scoring system were analyzed.

Measurements of Executive Functioning. We assessed inhibition, attentional control, monitoring, working memory, and self-regulation in our sample of typically and atypically developing young children. Executive function assessments included NIH Toolbox's Flanker task and Dimensional Change Card Sort Test (DCCS), and the Head-Toes-Knees-Shoulders (HTKS) task.

NIH Toolbox. The NIH Toolbox tasks that were administered are the list sorting working memory task, the flanker task, and the Dimensional Change Card Sort Test (DCCS). A large proportion of our participants did not make it past the practice sessions and into the scored trials for the working memory task, therefore this task was not analyzed due to missing data. The following analyses will focus on the Flanker task and DCCS.

The flanker task tested a child's inhibition and attentional control in the face of distracting environmental stimulation. The task asked the child to select which direction the middle fish is pointing after being presented with a row of 5 fish. The orientation of the flankers was congruent with the middle/target stimuli on some trials and incongruent on others. The task contained a practice block, the fish block mentioned above, and a more challenging block that switched the fish with arrows.

The DCCS examined the child's ability to plan and monitor behaviors in a goal directed manner. The tasks asked the child to match the shape and color of a target image when given two choices and the task was comprised of practice, pre-switch, post-switch, and mixed blocks. The pre-switch block asked the child to match by color before moving onto the post-switch block which asked the child to now match by shape instead. The shift between the first rule and the second rule caused a conflict which leads to a switch cost, therefore we examined both reaction time

and accuracy. If the child made it to the final block, they were asked to put their finger on a “home base” (a dot on a piece of paper in front of the screen) while the rules alternate between matching for color and for shape, which was referred to the mixed block. The NIH toolbox flanker and DCCS tasks both have excellent test-retest correlation coefficients of 0.92 (Zelazo et al., 2013).

Head-Toes-Knees-Shoulders Task (HTKS). The Head-to-Toes task was developed by Ponitz et al. (2008) to measure multiple aspects of a child’s self-regulation, including attention, executive control, and working memory. The original task asked children to first touch their toes and head but then examined their ability to do the opposite of the dominant response. For example, when told to touch their head, the child would have to touch their toes. We used the Head-Toes-Knees-Shoulders (HTKS) task, an adapted version of the Head-to-Toes task which has been shown to be more appropriate for kindergarten-age children and to increase difficulty and variability in scores (Ponitz et al., 2009). The HTKS required children to perform the opposite of a dominant response for four different oral commands, including switching command associations in the last segment to make the task more taxing on the child’s executive control. The HTKS task not only taxes many aspects of executive function, but the interaction between the child and the experimenter makes this a more ecologically valid task compared to the iPad based NIH Toolbox tasks (McClelland and Cameron, 2012). Ponitz has shown that the HTKS has high construct validity and is significantly related to other measures of children’s attention, inhibitory control performance, and academic performance.

Demographics and Control Variables. We used age, sex, socio-economic status (SES), whole brain microstructure, and movement in the scanner as controls. Age, sex, and SES were all self-reported, with SES being categorically binned. Whole-

brain microstructure data were output directly from DSI Studio to control for any overall neuroanatomical differences between participants. Lastly, the number of directions kept for each DWI scan was used as a proxy for movement in the scanner.

Data Acquisition

Participants were scanned on a 3 Tesla Siemens MAGNETOM Prisma at Florida International University’s Center for Imaging Science. All children first underwent a simulated scan in a mock scanner in order to get familiarized with the MRI scanner, the noises associated with the scans, and the correct laying position (no crossed legs or arms, legs laying flat instead of raised). Data acquisition for the AHEAD project followed the same guidelines as the Adolescent Brain Cognitive Development Study (ABCD), which are detailed in Hagler et al. (2019). Briefly, the 1.7mm isotropic diffusion weighted images were acquired using multiband echo-planar imaging (EPI) with 102 directions. The multishell DWI sequence was compromised of 96 diffusion directions and 6 $b = 0$ frames, with a total of 4 b-values: $b = 500 \text{ s/m}^2$ (6 directions), $b = 1000 \text{ s/m}^2$ (15 directions), $b = 2000 \text{ s/m}^2$ (15 directions), and $b = 3000 \text{ s/m}^2$ (60 directions).

For postprocessing, we used the DTIPrep and TORTOISE DIFFPREP software. The DWI images were processed for motion correction, to remove eddy current artifacts, to correct for EPI B0 susceptibility deformations, to conduct B-matrix reorientation, and to co-register the diffusion series with structural MRI. We also used FSL’s topup tool (Andersson et al., 2003; Smith et al., 2004) to estimate and correct susceptibility-induced distortions.

Subject movement is also an important factor to monitor and correct for when-scanning preschool aged children. We used directions kept after the automated kick-out method from DTIPrep as a proxy for movement. Although the ADHD

group had significantly more movement during the DWI scan ($\beta = -0.20$, $p < 0.01$, $df = 194$), each group provided sufficient data for accurate reconstruction. Out of 102 possible directions, the ADHD group had an average of 84.40 directions after motion correction, while the TD group had 88.74 directions. To control for these differences, number of directions kept was entered as a nuisance covariate in forthcoming analyses.

Finally, a T1w structural scan (1mm isotropic) using a 3D T1w inversion prepared RF-spoiled gradient echo sequence was also collected, using prospective motion correction via Siemens vNAV protocol.

Lausanne Parcellation

We used a semi-automated approach to define regions of interest (ROIs) for tractography. To prevent warping to an adult-based atlas, we created an individual atlas for each participant from the participant’s T1-weighted scan. FreeSurfer v6.0 was used for the initial cortical parcellation and cortical segmentation (e.g., Dale et al. 1999; Fischl et al. 1999, 2001, 2002; Reuter et al. 2010), and has been shown to be successful at creating accurate cortical surface representations for both typically developing children (Tamnes et al., 2010) and young children diagnosed with ADHD (Jacobson et al., 2018). Next, the Desikan-Killiany Freesurfer atlas (Desikan et al., 2006) for each participant was modified using the procedure specified by Cammoun and colleagues (Cammoun et al., 2012), originally defined by Hagmann et al. (2008). In this procedure, the larger ROIs from the Freesurfer parcellation are further divided into smaller units (collectively these atlas modifications are called the Lausanne atlases because they were developed in Lausanne, Switzerland). We used the modification defining 463 total ROIs, which allowed a finer parcellation of the

superior frontal gyrus, allowing for a more accurate subdivision of the preSMA and SMA.

Diffusion Metrics

We calculated and compared four Diffusion Tensor Imaging (DTI) metrics (fractional anisotropy (FA), radial diffusivity (RD), axial diffusivity (AD), and mean diffusivity (MD)) and two Generalized q -sampling Imaging (GQI) metrics (quantitative anisotropy (QA) and generalized fractional anisotropy (GFA)). The diffusion tensor was used to calculate the eigenvalues reflecting diffusion parallel and perpendicular to each of the fibers along 3 axes (x, y, z). The resulting eigenvalues were then used to compute indices of FA, RD, AD, and MD (Basser et al., 1994; Hasan and Narayana, 2006). Fractional anisotropy is an index for the amount of diffusion asymmetry within a voxel, normalized to take values from zero (isotropic diffusion) to one (anisotropic diffusion). Fractional anisotropy is sensitive to microstructural changes in white matter, with higher FA values indicating more directional diffusion of water. The FA value can be decomposed into AD, measuring the parallel eigenvalue (λ_1), and RD, measuring the average of the secondary and tertiary perpendicular eigenvalues ($[(\lambda_2 + \lambda_3)]/2$). The AD and RD quantifications are sensitive to axon integrity and myelin integrity, respectively (Winston, 2012). Mean diffusivity is a summary mean of the three principal eigenvalues ($[\lambda_1 + \lambda_2 + \lambda_3]/3$). Across development, FA increases while RD, AD, and MD decrease with the increase of myelination and white matter organization in the developing brain (Dimond et al., 2020).

Two GQI metrics will also be calculated— Quantitative Anisotropy (QA) and Generalized Fractional Anisotropy (GFA).

Quantitative Anisotropy (QA). QA is defined as the amount of anisotropic spins that diffuse along a fiber orientation, and it is given mathematically by:

$$QA = Z_0(\psi(\hat{a}) - iso(\psi))$$

where ψ is the spin distribution function (SDF) estimated using the generalized q -sampling imaging, \hat{a} is the orientation of the fiber of interest, and $iso(\psi)$ is the isotropic background diffusion of the SDF. Z_0 is a scaling constant that scales free water diffusion to 1 so that the QA value will mean the same thing across different participants (Yeh et al., 2010).

QA can be defined for each peak in the SDF. Because tractography follows individual peaks across a string of voxels, researchers typically have focused on the first peak (QA_0), and have additionally normalized the QA_0 metric so that it can be compared across different participants. The normalized QA metric, nQA, will be calculated according to the generalized q -sampling imaging method from Yeh et al. (2010).

Generalized Fractional Anisotropy (GFA). Generalized fractional anisotropy (GFA) represents an alternative indirect metric of white matter integrity that can be computed from a HARDI diffusion acquisition. It can be thought of as a higher-order generalization of FA (Descoteaux et al., 2007). The GFA metric thus begins with the ODF, and proceeds to rescale it by subtracting off the baseline term. Rescaling the ODF introduces a confound such that noise in the data, which rescales non-linearly, can appear to be anisotropic when in fact that is not the case. The GFA corrects for this by rescaling the min-max normalized ODF with an anisotropy measure. From Tuch (2004), the GFA metric follows the same logic as the FA calculation. Thus:

$$FA = \frac{std(\lambda)}{rms(\lambda)} \quad (2.1)$$

where λ are the eigenvalues of the diffusion tensor.

GFA is given then by:

$$GFA(\psi) = \sqrt{\frac{std(\psi)}{rms(\psi)} = \frac{n \sum_{i=1}^n (\psi(u_i) - (\psi))^2}{(n-1) \sum_{i=1}^n \psi(u_i)^2}} \quad (2.2)$$

where $(\psi) = (\frac{1}{n}) = \sum_{i=1}^n \psi(u_i) = (\frac{1}{n})$ is the mean of the ODF. The output of this transformation is a scalar measure, GFA, which functions in a similar manner as FA to describe the anisotropic direction of water diffusion in the voxel. Like the traditional FA metric from DTI, the values range from 0 to 1.

Fiber Track Identification

The FAT was tracked using a semi-automated method. First, an individualized Lausanne atlas was created for each participant, as described in the Lausanne segmentation section above. Next, we tracked the FAT regions of interest (pre-SMA, SMA, *pars opercularis*, and *pars triangularis*) and visually checked each participant for neuroanatomically correct region-of-interest (ROI) positioning and tract patterns. The FAT anatomy and locations of ROIs is shown in Figure 1.

The control pathway, CST, was tracked with DSI Studio’s built-in automated tractography atlas (Yeh et al., 2018). The atlas was created from 842 participants in the Human Connectome Project (HCP) and is placed on each brain through non-linear registration of a participant’s subject data to MNI space. Since the atlas was

created from an adult brains, left and right CST segments were visually checked for accuracy.

2.3 Statistical Analysis

We analyzed age-related differences and the FAT's relation to language and executive function using FA, MD, AD, RD, GFA, and QA DWI metrics. We used robust linear models (R function `rlm`, R version 3.5.3; <http://www.R-project.org>) to examine both age-related differences as well as the transdiagnostic approach to examine FAT's influence on our behavioral outcomes controlling for age, sex, whole brain microstructure, socioeconomic status, and movement in the scanner. Robust regression was chosen because it is less influenced by outlying values than traditional least-squares methods (Wilcox, 1998). The influence of outliers is reduced using a Huber loss function that applies different weights to each observation, with outliers being downweighed and therefore making a smaller impact on overall results without having to be removed from the dataset. Robust regression results can be interpreted the same was a least square regression and will remain unchanged in the presence of no outliers.

For the categorical diagnosis approach at examining the impact of FAT microstructure in language and executive function in children with and without ADHD, we chose to use robust multiple regression. We used the dummy-coded diagnosis as a predictor variable in the model to investigate whether ADHD moderates the relationship between FAT and our behavioral outcomes. For all analyses, we used the bootstrapping method to improve the estimation of reliability of the parameter estimate (Efron, 1987) and to calculate standard errors and 95% confidence intervals. Laterality was calculated using Thiebaut de Schotten et al. (2014) formula $(\text{left} - \text{right})/(\text{left} + \text{right})$ in which positive values indicate left laterality.

Missing Data. von Hippel (2007) advises against missing data imputation for dependent variables. Therefore we used multiple imputation only for the demographic covariates, particularly highest parental income category. Logistic regression was used to verify whether there was a relationship between missingness and the outcome variable. We used the Multivariate Imputation via Chained Equations (MICE) package in R (version 3.5.1). For the following regression analyses, the missing data were handled using Casewise deletion. The missing data were accounted for by reporting the degrees of freedom for each comparison. Lastly, we reported the analysis without imputation to ensure no potential bias was introduced.

Outlier Detection and Correction. We did not remove outliers but corrected for their influence using a conservative 97.5% Winsorization procedure (Wilcox and Keselman, 2003). Similar to clipping in signal processing, the Winsor statistical transformation limits extreme values in order to reduce the influence of outliers. We report both uncorrected and Winsor-corrected results and plots whenever the Winsor method is used.

Power Estimates. Power is most commonly defined as the probability that a statistical test will reject a null hypothesis when it is false (Cohen, 1988). We ran power analyses in effort to avoid Type II error when dealing with null findings. The risk of Type II error was particularly important when we analyzed interaction effects, since effects can be missed if power is low. Our power was 0.80 to detect a small effect of $r = 0.2$ at $\alpha = .05$ in the full sample, and power = 0.70 to detect a small effect of $r = 0.2$ for interaction effects. For individual group analyses, power = 0.80 to detect moderate effect of $r = 0.3$. All of our Cohen's power estimates are at $\alpha = .05$ (Cohen, 1988).

Code Availability. All software used in the present analysis is open source from the Comprehensive R Archive Network (version 3.5.0). The R code to replicate the analysis is available at https://github.com/deagaric/AHEAD_project.

2.4 Results

All of the following results presented have been Winsor-outlier corrected. Both raw data and Winsor corrected data were analyzed, and the Winsor method did not significantly alter results. Secondly, all of the results below were re-analyzed with ODD symptomatology added as a covariate to account for the comoridity between ADHD and ODD. The addition of the ODD covariate did not significantly change any findings reported.

Tractography Results

Using our Lausanne method, we successfully tracked at least one segment of the bilateral FAT in 195 out of 196 children (99% of the sample). Using the individually defined ROIs, we were able to track four subcomponents of the FAT, in the following percentage of participants from the full sample ($n = 196$; averaged across the hemispheres; preSMA \leftrightarrow Op (91.5%); SMA \leftrightarrow Op (88%); preSMA \leftrightarrow Tri (40%); SMA \leftrightarrow Tri (19.5%).

Across both hemispheres, projections to the *pars opercularis* were observed in 90% of all hemispheres, while *pars triangularis* projections were observed in only 30% of the hemispheres. The disparity between Op and Tri is not uncommon, and has been seen in previous work as well (Szmuda et al., 2017). Given the small proportion of participants with *pars triangularis* projections (for example, laterality analyses within *pars triangularis* projections had sample sizes of 11 for some tasks), our analyses will focus on the projections from the superior frontal gyrus (the preSMA

and SMA) to *pars opercularis* from here on out. The regional contributions of the *pars triangularis* for language and executive function will be re-visited in a region analysis in Study 3.

Out of the entire sample, 100 children had ADHD, while 96 were TD. There were no whole-brain microstructure differences between the TD and ADHD groups in any of the diffusion metrics. The only group difference we found between the FAT segments was that the right preSMA to Op segment had higher FA and lower RD in the ADHD group than the TD group ($\beta = 0.18$, $p < 0.01$, $df = 180$, and $\beta = -0.15$, $p < 0.01$, $df = 180$ for FA and RD, respectively), indicating that the ADHD group displayed higher diffusivity and more myelination of this FAT segment compared to the TD group while controlling for whole brain FA.

Using the tractography atlas, we were able to output data for the CST for all 196 children. We found significant group differences between the CST in TD and ADHD samples for both the left and right CST ($t = -5.09$, $p < 0.001$, $df = 193$, and $t = -4.45$, $p < 0.001$, $df = 193$ for left and right CST, respectively). In the TD group, the CST has a mean FA of 0.38 and 0.36 for left and right CST, while the mean FA for the ADHD group was 0.35 and 0.33, respectively. This indicates that the TD sample has strong structural integrity of the CST compared to the ADHD sample while controlling for whole brain FA.

Age-Related Differences

Using robust linear regression, we examined whether there are significant age-related differences within the FAT during the 4- to 7-year-old age range in our sample, controlling for sex, whole brain microstructure, and movement in the scanner. Upon close examination of our FAT developmental plots, it became evident that we had few but large outliers. To avoid removing them entirely, we ran our findings using

the Winsor approach to reduce the influence of outliers. The Winsor approach had a very minimal effect on our analyses (with the largest change in β being only 0.03), but helped clarify the age-related development plots. We will focus on the Winsor results below, but the non-Winsor results can also be found in Appendix B for comparison.

Even given the narrow age range of 4 to 7, we found that both the left and right hemisphere FAT segments undergo age-related differences that go above and beyond whole brain development. The left preSMA to *pars opercularis* shows a gradual increase in microstructural integrity as measured by FA ($\beta = 0.14$, $p = 0.05$, $df = 171$), which is further supported by very strong decreases in AD ($\beta = -0.29$, $p < 0.001$, $df = 171$) and MD ($\beta = -0.34$, $p < 0.001$, $df = 171$). The left SMA to *pars opercularis* segment had the same findings for AD ($\beta = -0.32$, $p < 0.001$, $df = 163$) and MD ($\beta = -0.33$, $p < 0.001$, $df = 163$). No laterality differences across time were found. On the right hemisphere, we see a similar, but less robust, change across time. The right preSMA to Op segment showed significant tract development, as seen by lower AD ($\beta = -0.19$, $p < 0.01$, $df = 178$) and MD ($\beta = -0.29$, $p < 0.001$, $df = 178$). The same results were also seen in the right SMA to Op ($\beta = -0.23$, $p < 0.01$, $df = 171$, ($\beta = -0.31$, $p < 0.001$, $df = 171$, for AD and MD respectively.)

Since the preSMA to Op segment had the largest sample sizes and was very similar to the pattern seen in the SMA to Op, we chose these segments to plot the developmental change, as seen in Figures 2 and 3. The large sample sizes in these segments give it the highest probability of accurately portraying developmental change within the FAT as it compares to whole brain development. There were no significant differences found in development or whole brain microstructure between the TD and ADHD samples, therefore all age-related tables and figures contain the full sample. Lastly, we did not find significant age related change in FA for the CST,

our control pathway. We did find significant reductions in AD ($\beta = -0.36$, $p < = 0.001$, $df = 191$) and MD ($\beta = -0.17$, $p < = 0.05$, $df = 191$) across development, as seen in Figure 4. No age-related differences in laterality were evident in the CST.

2.4.1 Language Findings

NEPSY-II Results: Transdiagnostic Approach.

First, we analyzed our data without consideration to ADHD diagnosis, with the purpose of examining whether the FAT was associated with fluency in the whole sample when measured with NEPSY. We had NEPSY scores for 194 out of 196 children. The mean of the 4 NEPSY tasks and their associated total scores are reported in Table 3. Overall, children found the phonological tasks more difficult than the semantic tasks, which is typical and implies that the child can produce language adequately but does not have a good search strategy when when information is not categorically organized.

As expected, children’s performance on NEPSY word generation increases significantly with age across all tasks ($p < 0.001$ for all, $df = 194$), indicating children’s vocabulary improves dramatically across 4- to 7-years of age. There were moderate sex differences seen on the semantic food and drink and phonological s-words and total scores, with females outperforming males ($p < 0.05$, $df = 194$). Whole brain microstructure was associated with better performance on semantic animal words and phonological initial letter s-words ($p < 0.05$, $df = 194$), indicating that the more developed the whole brain is, the better performance on those tasks. As a result of the demographic differences, age, sex, and whole-brain were entered in as covariates for all following regression models. We are also controlling for movement in the scanner, as is standard.

Using robust regression models, we examined whether the Op segments of the FAT was associated with NEPSY scores. To simplify analyses, we focused on total phonemic and semantic scores rather than for each task. The full results for all verbal fluency and articulation findings reported below can be found in Table 5. The only significant result for the full sample for was that the right SMA to Op projection was associated with higher scores in semantic fluency when examined with AD ($\beta = 0.16$, $p < 0.05$, $df = 168$). There were no significant findings for other segments or using other metrics.

NEPSY-II Results: Categorical Diagnosis Approach.

We compared the differences between the TD and ADHD samples, with the purpose of examining whether the FAT's relationship with phonemic and semantic fluency was affected by diagnosis. We found group differences on NEPSY performance between TD and ADHD, which are outlined on Table 4 and displayed in Figure 5. The differences we found persisted even when controlling for age, sex, and SES, which is known to be associated with ADHD. We found that the typically developing group outperforms the ADHD group on almost all NEPSY tasks with the exception of food and drink words and initial letter F-words. We looked at this more closely by examining the TD and ADHD groups individually.

NEPSY-II Main Effects for TD Sample. Upon examining the 96 TD children, we found that the left hemisphere FAT segments were associated with phonemic scores while the right FAT segments were associated with semantic scores. In particular, the GFA of the left preSMA to Op segment was associated with higher total phonemic scores ($\beta = 0.26$, $p < 0.05$, $df = 78$), while the AD of the right SMA to Op projection was associated with better semantics ($\beta = 0.25$, $p < 0.05$, df

= 81). The plots for these relationships can be found in Figure 6. There were no significant laterality associations seen in the TD sample.

NEPSY-II Main Effects for ADHD Sample. Upon examining the 100 children with ADHD, we found that the structural integrity of the right FAT actually hampers semantic performance in the ADHD sample. This finding could explain the unexpected results we found when looking at the TD and ADHD combined sample previously. All of the NEPSY findings for the ADHD sample were in the right hemisphere while the left hemisphere remained insignificant. Specifically, the right preSMA to Op projection lowered semantic scores for both FA and GFA ($\beta = -0.25$, $p < 0.05$, $df = 83$, $\beta = -0.29$, $p < 0.05$, $df = 83$, for FA and GFA respectively). The relationship between the right preSMA to Op projection GFA and semantics can be seen in Figure 7.

When we examined any possible laterality differences, we found that higher left lateralization of the preSMA to Op segments were associated with higher semantic scores were in the ADHD sample ($\beta = 0.21$, $p < 0.05$, $df = 77$, $\beta = 0.22$, $p < 0.05$, $df = 77$, for FA and GFA respectively). The lateralization finding in the preSMA to Op connection was also seen with the inversely-interpreted RD metric ($\beta = -0.24$, $p < 0.05$, $df = 77$). Taken together, the degree to which the developing brain favors a left lateralized structural dominance of the FAT is directly associated with semantic fluency in the ADHD sample. The relationship between FAT laterality and fluency is plotted in Figure 8.

NEPSY-II Diagnosis Interaction Effects. We found a significant interaction effect when looking at the right preSMA to Op's association with semantic scores when measured with GFA ($\beta = -0.16$, $p < 0.05$, $df = 171$), with the ADHD group showing an inverse relationship between the right FAT and semantic scores ($\beta = -0.29$, $p < 0.05$, $df = 83$), and the TD group showing a weak upwards trend (β

= 0.15, $p = 0.19$, $df = 85$). As seen in Figure 9, ADHD diagnosis moderates the relationship between the right FAT and semantic scores, with higher GFA in the ADHD group being associated with lower semantic scores while higher GFA of the segment has a positive trending association for the TD group. The same pattern was also seen when using FA ($\beta = -0.14$, $p < 0.05$, $df = 171$).

Furthermore, we found a significant group interaction when looking at the laterality of the preSMA and Op GFA segment's association with semantic scores ($\beta = 0.16$, $p < 0.05$, $df = 156$). In the TD group, the lateralization of the preSMA to Op segment was not significantly associated with semantic outcomes, but for the ADHD group, higher left lateralization of the preSMA to Op segment was associated with higher the semantics scores (see Fig. 10). A similar pattern is also seen with RD ($\beta = -0.16$, $p < 0.05$, $df = 156$), with participants in the ADHD sample exhibiting higher myelination in the left FAT segment while no significant laterality difference is seen in the TD sample.

NEPSY-II Control Pathway Results. Using the bilateral CST as our control pathway, we found no association between the control pathway and any NEPSY fluency outcomes in the full sample (lowest $p = 0.06$) nor any laterality associations (lowest $p = 0.55$). Furthermore, no significant results between the CST and NEPSY were found when looking at the TD sample (lowest $p = 0.16$) or ADHD sample (smallest $p = 0.53$) separately. The association of the corticospinal tract's laterality to NEPSY scores was tested for each group and was insignificant as well (smallest $p = 0.29$).

SRT Results: Transdiagnostic Approach.

As a consequence of technical issues, some inaudible voice recordings in quiet children, and some participants refusing to do the task, we had scores for 115 out of

the 196 children. Across all 18 words, there were 50 total phonemes. Using the traditional SRT scoring, the overall sample had 80.69% accuracy rate, while the bilingual scoring system (which allows for common Spanish phoneme substitutions such as b/v) had an 82.42% accuracy rate in the full sample. We examined the effect of demographics, and while no demographics were associated with the monolingual system scores, bilingual system scores significantly increased across age ($t = 0.29$, $p < 0.01$, $df = 111$) and females outperformed the males ($t = -0.22$, $p < 0.05$, $df = 111$). Age, sex, whole brain microstructure, SES, and movement in the scanner were controlled in the following analyses. Since the differences between the two scoring methods were not significant ($t = -0.74$, $p = 0.46$), we chose to following analyses on the the bilingual scoring system scores to accommodate our large Spanish-speaking population.

When examining the full sample, we find that only the left FAT was associated with phoneme production on the SRT. As Figure 11 shows, the left preSMA to Op was strongly associated with higher accuracy on the SRT using QA ($\beta = 0.63$, $p < 0.01$, $df = 98$). The GFA metric trended in the positive direction. The left SMA to Op was also associated with higher SRT scores, but only in AD ($\beta = 0.22$, $p < 0.01$, $df = 91$). Favoring the left hemisphere for this task was further confirmed when we examined laterality. We found that increased left laterality of the preSMA to Op projection was associated with higher SRT scores with GFA ($\beta = 0.16$, $p < 0.05$, $df = 91$). A similar pattern is seen with the SMA to Op projection for AD ($\beta = 0.21$, $p < 0.05$, $df = 83$) and QA ($\beta = 0.18$, $p < 0.05$, $df = 83$). The laterality findings for SRT can be found on Figure 12.

SRT Results: Categorical Diagnosis Approach.

We compared the differences between the TD and ADHD samples, with the purpose of examining whether the FAT's relationship with phonemic articulation was affected by diagnosis. We found that the TD group significantly outperforms the ADHD group ($\beta = -0.19$, $p < 0.05$, $df = 110$). The TD sample had an 86.19% average accuracy on the task, while ADHD had 78.98% average accuracy. The following analyses will examine whether the FAT was differentially associated with SRT in the TD and ADHD samples.

SRT Main Effects for TD Sample. In the TD sample, we found that the left SMA to Op was associated with higher scores on the SRT when AD was used ($\beta = 0.31$, $p < 0.05$, $df = 39$). The same relationship was also trending when GFA was used ($\beta = 0.17$, $p = 0.07$, $df = 39$). Further, higher left lateralization of the SMA to Op was associated with better SRT performance for QA ($\beta = 0.22$, $p < 0.05$, $df = 36$).

SRT Main Effects for ADHD Sample. While the FAT segments were not directly associated with SRT scores within the ADHD sample, laterality did. Similar to the TD sample, greater left laterality of the SMA to Op projection was associated with higher SRT scores with both AD and QA ($\beta = 0.47$, $p < 0.01$, $df = 40$, $\beta = 0.31$, $p < 0.05$, $df = 40$, respectively).

SRT Diagnosis Interaction Effects. We examined whether an ADHD diagnosis might moderate the relationship between the FAT and phonemic articulation, and there were no significant interactions effects nor laterality differences.

SRT Control Pathway Results. Using the bilateral CST as our control pathway, no significant results between the CST and NEPSY were found when looking at the TD sample (lowest $p = 0.78$) or ADHD sample (smallest $p = 0.48$)

separately. CST laterality's associated with SRT was tested for each group and was insignificant as well (smallest $p = 0.48$). There were no significant associations between the CST and SRT phonemic articulation in the full sample (lowest $p = 0.82$) nor any laterality associations (lowest $p = 0.89$).

2.4.2 Executive Function Findings.

NIH Toolbox Results: Transdiagnostic Approach.

First, we analyzed our data without consideration to ADHD diagnosis, with the purpose of examining whether the FAT was associated with executive function in the whole sample when measured with the NIH Toolbox Flanker and DCCS. We had flanker data for 164 children and DCCS data for 167 out of our 196 children. We used the age-corrected standard score NIH Toolbox results, which compare the test-takers score to that of all other test takers at the same age. The mean score for age-corrected standard scores on NIH Toolbox tasks is 100 with a standard deviation of 15. Since this metric is already normed for age, we did not have to control for age, but kept our gender, movement in the scanner, whole brain microstructure, and parental income covariates in the model. For our full sample, the overall mean scores on the age-corrected standard score was 97.3 on flanker and 96.7 on DCCS. None of the covariates were significantly associated with flanker scores. SES was negatively correlated with DCCS scores, with higher SES being associated lower DCCS scores ($r = -0.17$, $p < 0.05$, $df = 165$). Table 6 displays the mean task scores and how they relate to our control variables.

Using robust regression models we examined whether the 4 segments of the bilateral FAT were associated with flanker and DCCS scores, controlling for sex, movement in the scanner, whole brain microstructure, and SES. The full results for all executive function findings reported below can be found in Table 8. As seen in

Figure 13, we found that increased AD in the left SMA to Op segment was associated with higher flanker scores ($\beta = 0.20, p < 0.05, df = 137$), while the QA of the left preSMA to Op segment was associated with higher DCCS scores ($\beta = 0.55, p < 0.05, df = 145$). When examining laterality, we found that higher left lateralization, as measured by AD, in the SMA to Op segment was associated with higher flanker scores in the full sample ($\beta = 0.23, p < 0.01, df = 124$).

NIH Toolbox Results: Categorical Diagnosis Approach.

We compared the differences between the TD and ADHD samples, with the purpose of examining whether the FAT's relationship with executive function was affected by ADHD diagnosis. We found group differences on NIH toolbox tasks between TD and ADHD, which are outlined on Table 7 and displayed in Figure 14. The differences we found persisted even when controlling for age, sex, and SES. We found that the typically developing group greatly outperforms the ADHD group on both flanker ($\beta = -0.34, p < 0.0001, df = 161$) and card sort tasks ($\beta = -0.27, p < 0.0001, df = 163$). We looked at this more closely by examining the TD and ADHD groups individually.

NIH Toolbox Main Effects for TD Sample. Upon examining the TD group separately, we find no direct significant associations between the FAT and the NIH Toolbox results. We did find that higher left laterality of the SMA to Op segment was related to higher DCCS scores when measured with QA ($\beta = 0.354, p < 0.05, df = 55$).

NIH Toolbox Main Effects for ADHD Sample. When we examined our sample of 100 children with ADHD, we found that greater structural integrity of the left and right preSMA to Op segments was linked to higher scores on the DCCS. In

particular, a positive linear relationship was identified between the FA and GFA of the left preSMA to Op segment's association with better card sort scores ($\beta = 0.226$, $p < 0.05$, $df = 76$; $\beta = 0.275$, $p < 0.05$, $df = 76$ for FA and GFA, respectively). On a similar note, we saw a similar relationship with the RD of the right preSMA to Op segment, with lower RD (therefore, higher myelination) being related to higher DCCS ($\beta = -0.326$, $p < 0.05$, $df = 76$), as shown in Figure 15. There were no laterality differences for these associations in the ADHD sample.

NIH Toolbox Diagnosis Interaction Effects. There were no significant group interaction effects for the NIH toolbox in either direct brain-behavior associations nor laterality effects.

NIH Toolbox Control Pathway Results. Using the bilateral CST as our control pathway, we did find an association between the left ($\beta = 0.27$, $p < 0.01$, $df = 159$) and right ($\beta = 0.45$, $p < 0.01$, $df = 159$) CST FA in relation to higher scores on the flanker task in the full sample. CST was not directly related to DCCS but did indicate that higher left laterality was associated with DCCS ($\beta = 0.17$, $p < 0.05$, $df = 161$). A possible explanation for CST's association with NIH Toolbox scores could be that the CST is a very large white matter pathway that makes contact with many regions and other pathways, and the fact that the iPad NIH Toolbox tasks do require voluntary motor control for successful completion. These findings disappear when the TD (smallest $p = 0.50$ for direct relationship, smallest $p = 0.10$ for laterality) and ADHD (smallest $p = 0.08$ for direct relationship, smallest $p = 0.22$ for laterality) groups are examined individually.

HTKS: Transdiagnostic Approach.

First, we analyzed our data without consideration to ADHD diagnosis, with the purpose of examining whether the FAT was related to executive function in the full

sample when measured with the HTKS. We will use the HTKS total scores for all three parts. The score can range from 0 to 60, depending on how accurately the child did each pair-switch. In our full sample, 179 out of 196 children completed the task with an average score of 32.68. We saw a highly significant correlation with age ($\beta = 0.45$, $p < 0.001$, $df = 177$), sex ($\beta = -0.21$, $p < 0.001$, $df = 177$), and whole brain microstructure ($\beta = 0.26$, $p < 0.001$, $df = 177$), and no significant association with SES. Overall, older children scored higher on the task than younger children, with female participants outperforming males, and a positive association with overall brain microstructure integrity and HTKS performance. These results can be seen on Table 6.

Using robust regression models, we examined whether the 4 segments of the FAT were associated with HTKS performance controlling for age, sex, whole brain microstructure, movement in the scanner, and SES. Going completely against our hypothesis, our results indicated that increased structural integrity of both the right and left FAT was associated with *worse* performance on the HTKS for the full sample. In the left hemisphere, higher mean diffusivity of the preSMA and SMA to Op projections were linked to higher HTKS scores ($\beta = 0.21$, $p < 0.05$, $df = 154$, $\beta = 0.21$, $p < 0.05$, $df = 138$, respectively). MD is frequently interpreted in reverse, with higher MD indicating a less developed structural connection. For the right hemisphere, we find a similar pattern. There was a negative relationship between structural integrity of the right preSMA to Op and HTKS scores when measured with FA ($\beta = -0.19$, $p < 0.05$, $df = 168$). The same relationship is seen with the right SMA to Op when measured with FA and MD ($\beta = -0.19$, $p < 0.05$, $df = 154$, $\beta = 0.19$, $p < 0.05$, $df = 154$, respectively). The only significant laterality finding was that higher left laterality of the SMA to Op projection was associated with better

performance on the HTKS task when measured with axial diffusivity ($\beta = 0.20$, $p < 0.05$, $df = 135$).

HTKS Results: Categorical Diagnosis Approach.

The scores on the HTKS task, which range from 0 to 60, showed large group differences between TD and ADHD. The differences persisted even when controlling for age, sex, and SES. We found that the TD group ($m = 38.78$) greatly outperformed the ADHD group ($m = 28.17$) on HTKS ($\beta = -0.26$, $p < 0.0001$, $df = 172$). We looked at group differences more closely by examining the TD and ADHD groups individually.

HTKS Main Effects for TD Sample. Out of the 96 children in the TD sample, we had HTKS data for 85. Using robust linear regression, we examined the relationships between the FAT segments and HTKS performance controlling for age, sex, whole brain microstructure, movement in the scanner, and SES. The left SMA to Op GFA ($\beta = 0.25$, $p < 0.05$, $df = 66$) and the right preSMA to Op segment GFA (trending, $p = 0.058$) and AD ($\beta = 0.20$, $p < 0.05$, $df = 75$) were associated with higher HTKS scores. These relationships can be seen in Figure 17.

Upon examination of FAT laterality relationships, we found that right laterality was related to better performance on HTKS, which confirms our hypothesis that right laterality contributes to executive function in young children. In particular, the more left lateralized the preSMA to Op ($\beta = -0.25$, $p < 0.01$, $df = 68$; $\beta = -0.25$, $p < 0.01$, $df = 68$ for FA and GFA, respectively), the worse scores on HTKS were. These laterality findings provide support for the developing brain favoring the right hemisphere for taxing, motor executive function tasks. The laterality finding for the TD sample are displayed on Figure 18.

HTKS Main Effects for ADHD Sample. Out of the 100 children in the ADHD sample, we had HTKS data for 94. Using robust linear regression, we examined the relationships between the FAT segments and HTKS performance controlling for age, sex, whole brain microstructure, movement in the scanner, and SES. The results for the ADHD sample were the opposite of what was seen in the TD sample. For the left hemisphere, both preSMA to Op MD ($\beta = 0.35$, $p < 0.01$, $df = 77$, MD metric is inversely interpreted) and SMA to Op GFA ($\beta = -0.31$, $p < 0.05$, $df = 75$, similar results seen with QA, FA, MD and RD) were associated with worse HTKS scores. For the right hemisphere, the preSMA to Op ($\beta = -0.38$, $p < 0.01$, $\beta = -0.40$, $p < 0.01$, $\beta = -0.65$, $p < 0.05$, for FA, GFA, and QA, respectively, $df = 78$ for all) was related to lower HTKS performance. The negative association between the FAT and HTKS scores in the ADHD group is thought to have flipped our HTKS findings in the transdiagnostic findings for the full sample. The full results for all associations between the FAT segments and HTKS can be found on Table 8. The left and right FAT associations with HTKS are plotted on Figure 19. There were no significant associations with laterality.

HTKS Diagnosis Interaction Effects. Using diagnosis as an interaction term, robust regression analyses revealed that there is an interaction between the left SMA to Op and the right preSMA to Op segments' association with HTKS scores when examining FA, RD, and GFA. There was an interaction between diagnosis group and the GFA of the left SMA to Op's association with HTKS ($\beta = -0.18$, $p < 0.05$, $df = 146$), with children in the TD sample significantly benefiting from increased structural integrity of the segment ($\beta = 0.25$, $p < 0.05$, $df = 66$) while the segment was associated with lower scores in the ADHD sample ($\beta = -0.31$, $p < 0.05$, $df = 75$). Similar findings were seen when FA and RD were used, with higher myelination within the pathway being related to worse HTKS scores for the ADHD

group and trending upwards for the TD group. A similar interaction was exhibited in the GFA of the right preSMA to Op segment ($\beta = -0.24$, $p < 0.05$, $df = 158$), with the TD sample showing a trending positive association ($\beta = 0.22$, $p = 0.058$, $df = 75$) while the ADHD group had a significant negative association between the segment and HTKS scores ($\beta = -0.40$, $p < 0.01$, $df = 78$). The interaction effects seen in the left and right FAT's association with HTKS can be seen on Figure 20.

When laterality was examined, a significant interaction effect was found between preSMA to Op and HTKS scores between the two groups. For both FA and GFA, the analysis implicated that there is a significant group interaction effect in FAT laterality's association with HTKS scores ($\beta = 0.24$, $p < 0.05$, $df = 145$; $\beta = 0.23$, $p < 0.05$, $df = 145$ for FA and GFA respectively), with higher right laterality within the segment being significantly related to improved HTKS scores in the TD sample ($\beta = -0.25$, $p < 0.01$; $\beta = -0.25$, $p < 0.01$, both $df = 66$ for FA and GFA, respectively), while there was a trending association with left laterality's relation to higher scores for the ADHD sample ($\beta = 0.22$, $p = 0.08$; $\beta = 0.22$, $p = 0.06$, both $df = 66$, both $df = 72$, for FA and GFA, respectively). The group interaction between FAT laterality, as measured by GFA, and its association to HTKS is plotted in Figure 21, with an almost identical relationship when FA is used.

HTKS Control Pathway Results. Since our control pathway, CST, is responsible for voluntary motor control, it was not surprising to see that it was associated with the HTKS, which is a motor executive function task. Higher FA of both the left ($\beta = 0.18$, $p < 0.05$, $df = 172$) and right CST ($\beta = 0.19$, $p < 0.05$, $df = 172$) were related to higher HTKS scores, but no laterality differences were found ($p = 0.66$). This finding was only found in the full sample. There was no significant association with HTKS in the TD sample (smallest $p = 0.054$) and no laterality differences ($p = 0.23$). There were also no significant associations between the left and right CST

and HTKS in the ADHD sample (smallest $p = 0.27$) nor any laterality relationships ($p = 0.39$).

2.5 Discussion

Study 1 provides unique insight into the FAT's development and relation to language and executive function in young typically and atypically developing preschool-aged children. There is evidence to show that ADHD moderates the relationship between the structural connectivity of the FAT and its association with verbal fluency and motor executive function task performance. Increased structural integrity of the bilateral FAT was linked to improved performance on semantic fluency and motor executive function in the TD group, while being associated with decreased scores for the ADHD group. All of the findings presented here persisted even when ODD comorbidity was entered as a covariate, possibly suggesting that these findings are ADHD-specific. Further, the group interaction effects on language and executive function associations are unique to the FAT, and were not found when we examined the CST control pathway. The CST, which is primarily associated with voluntary motor function, was related to higher scores on motor executive function tasks and NIH Toolbox, but was not able to differentiate between our TD and ADHD samples. Study 1 provides strong evidence that the FAT can potentially serve as a unique biomarker for ADHD diagnosis and is differentially associated with language and executive function in typically and atypically developing children. The development of the FAT, and its association with language and executive function will be discussed in detail below.

Development of the FAT. The significant age-related differences we found in the bilateral FAT offer a novel contribution to the field of prefrontal cortex development during early childhood. The first published study that examined the

development of the FAT in young children (five to eight years of age) did not find significant age-related differences (Broce et al., 2015), most likely as a result of a small sample size ($n = 19$). With our much larger sample size and high-resolution DWI data, we provide counter-evidence against the idea that the FAT does not undergo age-related differences across childhood. Furthermore, our age-related difference findings replicated our previous study (Garic et al., 2019), which found that the FAT rapidly develops in the first 6 years of life, above and beyond what can be explained by whole brain microstructure. We expanded on our previous work by offering a detailed look at the 4- to 7-year-old period of development in a large sample of 196 children, whereas the previous paper only had 18 children within this important age range. We did not find any significant increases in laterality across age, which provides further support for previous work that indicated that left lateralization of language pathways develops early and does not continue to increase in strength (Groen et al., 2012).

Whether children with ADHD have delayed white matter maturation is a topic of debate within the field. Initial studies (e.g., Castellanos et al. 2002) found that ADHD patients had delayed brain development, with decreased cerebellar volumes that remained regardless of stimulant treatment. On the contrary, more recent work has found that in medication-naive children with ADHD, similar to our sample, there are no white matter development delays when compared to TD (Bouziane et al., 2018, 2019). Bouziane and colleagues propose that early stimulant use might be an underlying factor for the delayed white matter developmental trajectories (Bouziane et al., 2019). Our work further supports the latter findings, with the medication-naive children with ADHD showing no indication of delayed white matter development across this age span. Our study provides important, preliminary findings that provide potential evidence that neurobiological differences in children

with ADHD may be more in-depth than just a delay in brain development as a whole.

FAT and Speech and Language. When we examined the data transdiagnostically, we found that the right SMA to Op was related to semantics (but only with AD), while both left FAT segments were associated with better phoneme articulation on the SRT. Higher left laterality of the FAT was associated with higher phoneme articulation as well. These findings support our hypothesis that the left FAT is more involved in phonemic tasks while the right FAT is associated with semantic tasks. This relationship is made more evident we use the categorical diagnosis approach and examine the typically developing and ADHD samples individually.

In our typically developing sample, microstructural integrity of the left preSMA to Op segment was associated with improved scores on the initial letter phonemic task and the left SMA to Op segment was related to phoneme articulation. On the right hemisphere, the SMA to Op segment was only linked to category-based semantic scores. These findings coincide with the organization of other major language fiber pathways, such as the SLF and AF, are associated with letter-based fluency while the right SLF, AF, and IFOF predict category-based semantic fluency (Blecher et al., 2019; Rodriguez-Aranda et al., 2016). In fact, our left and right hemisphere FAT language findings within the typically developing sample align with what Blecher and colleagues found in the left and right FATs of adults. Put together, hemispheric differences in the FAT's association with verbal fluency might be present as early as four years of age and persist into adulthood (Blecher et al., 2019).

In sharp contrast, the relationship between the right FAT and verbal fluency flipped when examining the ADHD sample. In particular, higher structural integrity in the right preSMA to Op segment was associated with *lower* NEPSY semantic

scores. The left FAT was not not related to letter-based phonemic or phoneme articulation directly like it was in the TD sample, but higher left laterality was linked with higher articulation on the SRT task and higher semantic scores on the NEPSY word generation task. We will discuss possible explanations for the semantic and phonemic results individually.

For category-based semantic ability, we were surprised to see that in the ADHD sample, the right FAT was negatively associated with the semantic word generation scores. In fact, a significant group interaction effect was discovered when examining the right FAT's relation to semantic fluency scores. We observed that ADHD diagnosis moderates the relationship between the GFA of the right preSMA to Op and semantic performance, with greater tract integrity being associated with lower semantic scores in the ADHD sample but trending upwards in the TD sample. No microstructural differences, measured in GFA, exist for this segment between the two groups, indicating that structural differences between the connection might not be able to explain the relationship.

One possible explanation is that children diagnosed with ADHD might display atypical laterality associations. While we would expect semantic ability to be more right lateralized from previous work on adults (Blecher et al., 2019; Thompson et al., 2016; Rodriguez-Aranda et al., 2016), higher *left* laterality of the preSMA to Op segment was related to improved semantic verbal fluency scores in the ADHD sample, while partially favoring the right hemisphere in the TD sample. Further, higher structural integrity of the right FAT benefited semantic performance in the TD group, but had an adverse effect for the ADHD group. No significant difference was found in the preSMA to Op laterality between the ADHD and TD groups in our study, but the ADHD group was slightly more right lateralized on average ($p=0.08$). From these findings, it appears that children with ADHD favor the left hemisphere

for semantic tasks, unlike what is seen in typical development, but also show greater right laterality than the TD group, potentially causing the negative association.

It is tempting to think that the semantic scores within the ADHD group might catch up with the TD group across development as laterality becomes further developed, but no significant age-related differences in laterality were found in our sample of 4 to 7 year old children. Furthermore, Groen and colleagues (2012) have shown that the strength of lateralization for language production does not significantly increase between the ages of 6 to 16 years either, therefore making it very unlikely that left lateralization will increase in strength during development and improve the verbal fluency scores seen in the ADHD sample.

A third possible explanation for the group differences seen in semantic scores is the fuzzy categorical distinction between verbal fluency and executive function more broadly defined. While it is still a debate in the field, with some researchers finding evidence to believe that verbal fluency is highly associated with language processing and not significantly correlated to executive function (Whiteside et al., 2016), many believe that executive function might be interconnected with verbal fluency ability (Gustavson et al., 2019; Kramer et al., 2014). Moreover, semantic tasks might be more co-dependent on executive function abilities than phonemic tasks (Aita et al., 2019; Berberian et al., 2016), since they require more cognitive control to to inhibit competing semantic concepts that do not fit into the semantic category at hand. Therefore, there is a chance that the ADHD sample's scores were heavily impacted by their inattention and lower inhibition rather than their semantic skills. With no further direction from the task administrator once the 60 second task starts, a child's lack of focus can lead to much significantly lower scores. Inattention and cognitive control might have had a much larger effect on children in the ADHD sample compared to the TD sample.

The involvement of executive function in the verbal fluency tasks might also explain why, in the ADHD sample, we did not find any significant results for the initial letter phonemic NEPSY task but did for the SRT phoneme articulation task. The NEPSY phonemic task might be more dependent on executive function than the SRT. On the NEPSY task, the child has 60 seconds to list words starting with the letter S or F, while remembering what the prompt was, staying on task, and inhibiting words that do not belong in that segment. For example, many children in the ADHD sample start the S words task with "sun, sand, seashell, beach, vacation, fun!" which shows a lack of attention and inhibition. It could also indicate a lack of task-switching ability, since the semantic category tasks, which asked the child to list animal and food items, had just finished prior. In comparison, the SRT tests phoneme articulation by asking the child to repeat 18 non-sense words ranging from 2 to 4 phonemes. While words with 4 phonemes can be moderately taxing on working memory, it can be said that the NEPSY phoneme task is still more dependent on executive control since the SRT has no gap between the target word and the time the child is supposed to repeat it, therefore not requiring much inhibition or attention. The idea that executive function can explain differences in speech and language task performance is further supported by the fact that there were no group interaction effects with the SRT task, indicating that lower executive function present in the ADHD sample did not cause significant differences between TD and ADHD on SRT performance. In short, children with ADHD potentially could have had insignificant results for the NEPSY phonemic task but not for the SRT phonemic articulation task because the NEPSY task was more dependent on executive function, something that the ADHD sample struggles with.

FAT and Executive Function. Across our three executive function tasks, we saw significant group differences, with the typically developing group continuously

outperforming the ADHD group. Using the transdiagnostic approach, we saw that the axial diffusivity of the left SMA to *pars opercularis* segment was related to flanker scores, while the left preSMA to Op quantitative anisotropy was associated with card sort scores. Further, higher left laterality of the left SMA to Op AD was related to higher flanker scores in the full sample. Since AD and QA both decline with age during brain development, these findings are difficult to interpret without additional FA and GFA findings.

When the TD and ADHD samples were examined individually, we saw a positive relationship between left laterality of the SMA to Op AD and card sort scores, while higher myelination (as indicated by decreased RD values) in the right preSMA to Op and higher structural integrity (indicated by higher FA and GFA) in the left preSMA to Op were both associated with card sort performance in the ADHD sample. It appears as if the left hemisphere FAT is primarily involved in the task switching behaviors tested by the card sort in the TD sample, while the both the left and right FAT is involved in the ADHD sample. No significant interaction effects were found. The null interaction effects could most likely have been caused by the inconsistencies in significant diffusion metrics for the findings between the groups. The findings in the TD sample did not support our hypothesis and failed to replicate our past work (Dick et al., 2019; Garic et al., 2019), but the findings in the ADHD sample moderately confirmed them.

While the NIH toolbox provided interesting, but inconsistent, results, the HTKS stood out with robust, consistent findings that were supported by multiple diffusion metrics. The HTKS is a motor executive function task that taps into task-switching, working memory, and inhibition all within a short 7 to 8 minute task that does not require any additional materials except a researcher providing verbal cues. The transdiagnostic analysis approach found that both the left and right segments of

the FAT were related to lower scores on the task, marked by lower FA and higher MD values. We quickly discovered that this was due to the profound differences between the TD and ADHD groups.

In the TD sample, both the left and right FAT was related to better performance on the HTKS, but laterality analyses revealed that the developing brain favors the right hemisphere for the motor executive task. Higher right laterality of the preSMA to Op projection was associated with higher scores on the HTKS for both FA and GFA. Children with ADHD displayed a completely flipped pattern of results. For the ADHD sample, all segments of the left and right FAT were strongly related to worse outcomes on the HTKS tasks, which was seen with FA, MD, RD, GFA, and QA. There were significant group interaction effects seen with the left SMA to Op and right preSMA to Op projections. With the right SMA to Op, we find that ADHD diagnosis moderates the relationship between the right SMA to Op's association with HTKS, with increased structural integrity in the segment being related to improved HTKS performance for children in the TD sample, but worse performance for the ADHD sample. A similar pattern is seen with the right preSMA to Op segment, with a positive, trending ($p = 0.058$) association with structural integrity of the right FAT and better scores for the TD sample, but significantly lower scores in the ADHD sample.

The HTKS results provided compelling evidence that the FAT has a differential association with motor executive function performance in typically and atypically developing children. We argue that the group differences can be explained, in part, by laterality interaction effects: right laterality was associated with better HTKS performance in the TD sample, while there was a trending association ($p = 0.06$) between left laterality and HTKS performance in the ADHD sample. Given the strong association between the right inferior frontal gyrus and inhibition (Aron,

2007; Aron et al., 2016; Aron and Poldrack, 2006; Fife et al., 2017), it would appear that the right lateralization finding in the TD sample gives them a performance advantage. Furthermore, the direct interaction effects and laterality interaction effects seen between the TD and ADHD groups appear to be specific to motor executive tasks such as the HTKS, because they were not seen when executive function was tested with the NIH toolbox.

Taken together, the executive function results from Study 1 partially confirm our hypothesis that the right FAT is involved in motor, visuospatial executive function tasks. The FAT only was only differentially related to executive function performance in the motor HTKS task, which revealed that right laterality of the FAT was associated with better scores for the TD sample but not for the ADHD group. ADHD diagnosis moderates the association between the left and right FAT and executive function, in which higher structural integrity of the segments were related to higher HTKS scores for TD but worse scores for ADHD. The FAT can potentially differentiate between TD and ADHD samples in motor executive tasks, which makes it a potential biomarker for ADHD diagnosis in preschool-aged children. This can be a huge benefit for future ADHD research and clinical application, especially since the HTKS task is a quick, simple, and low-cost measure to administer.

Limitations. Two primary limitations of Study 1 were sample size and the lack of a direct working memory task. 196 preschool children, 100 diagnosed with ADHD, is a large sample size in the field of developmental neuroimaging, given the cost of MRI scanning and the difficulty of getting high quality scans in young children that struggle to stay perfectly still for 45 minutes in a loud, novel environment. Even so, our sample size was further reduced by 10% because not every child had DWI data for each FAT segment, missing behavioral data as a result of non-compliance, technical issues, or not being able to pass the practice portions, and then further

split when it came to the categorical diagnosis analysis approach which separated the children into TD and ADHD samples. The reduced sample size for some relationships we tested naturally raises the risk of encountering Type II errors. Our power was 0.80 to detect a small effect of $r = 0.2$ at $\alpha = .05$ in the full sample, and power = 0.70 to detect a small effect of $r = 0.2$ for interaction effects, but power = 0.80 to detect moderate effect of $r = 0.3$ $\alpha = .05$ (Cohen, 1988). Reduced power could lead to Type II error for smaller main effects within a group.

A second limitation was the lack of a direct working memory behavioral measure. While the HTKS does tax working memory with multiple task switches through the task, the NIH Toolbox provides a list sorting task that directly isolates and measures working memory. We attempted to administer this task to our sample, but 72% of our TD sample and 82% of our ADHD sample had missing data for the task, thus making the task unfit for analysis. A large portion of the missing data was attributed to the children failing out shortly after the practice rounds, making the score invalid. In the future, we plan to administer a working memory task that will be better fit for our sample's age range.

Conclusions. Our study provides compelling evidence that the FAT is associated with language and executive function development in young, preschool-aged children. We found that even in the narrow age range of 4- to 7-years, the FAT experiences age-related differences above and beyond what can be explained by whole brain development, and the developing structural integrity of the pathway might be differentially associated with behavioral outcomes for typically and atypically developing children. ADHD diagnosis moderates the relationship between the right FAT and semantic performance, with the ADHD sample performing worse with increased structural integrity of the tract. A similar relationship was seen with motor executive function as tested by the HTKS. Brain laterality appears to be related to

behavior differently in children with ADHD: higher right laterality was associated with higher semantic scores while higher left laterality was linked to better motor executive function. This sharply contrasts with the standard ideology of the left hemisphere being more associated with language and the right hemisphere with motor, visuospatial ability (Herve et al., 2013; Toga and Thompson, 2003). Overall, our results suggest that the FAT has the potential to be used as a diagnostic biomarker for ADHD in young children.

CHAPTER 3

STUDY 2

3.1 Research Question

The ability to quantify microstructural properties of neural tissue is important for the diagnosis and treatment of neurologic disease. Significant advances in the acquisition and analysis of diffusion weighted magnetic resonance imaging (DW-MRI) data have allowed researchers to target specific sources of the DW-MRI signal associated with specific tissue properties. Recent analysis approaches, such as restricted diffusion imaging (Yeh et al., 2017) and neurite orientation dispersion and density imaging (Zhang et al., 2012) have provided more fine-grained metrics that augment, and in some cases replace, the more traditional metrics that are reported in diffusion tensor imaging (DTI) studies. The present investigation is an attempt to understand whether such new metrics are sensitive to a particular microstructural property of white matter, that of axonal density. Providing an *in vivo* measure of axonal density has high potential for clinical importance. For example, histological studies have shown that axonal density is related to the progression rate of multiple sclerosis (Tallantyre et al., 2009), hereditary spastic paraplegia (Deluca et al., 2004), and it is a sensitive measure of multiple sclerosis lesion in an animal model (Seehusen and Baumgartner, 2010). The density of fibers of a particular diameter is also important because neural conduction velocity scales with axonal diameter (Ritchie, 1982), influencing the timing and rapidity of information transfer in the nervous system. Thus, being able to quantify these density changes *in vivo* during development could provide essential insight into disease progression, development, and general nervous system structure/function relationships.

The new metrics we investigate extend from previous algorithms used to reconstruct DWI data. The most popular instantiation of DWI reconstruction is diffusion tensor imaging (DTI), which obtains familiar metrics such as fractional anisotropy (FA), mean diffusivity (MD), axial diffusivity (AD), and radial diffusivity (RD), that provide information about the directional nature of water diffusion through tissue. AD measures the longitudinal component or eigenvalue (λ_1) of the diffusion tensor model, and it has been shown to be sensitive to axon integrity (Song et al., 2003). RD is the average of the remaining eigenvalues ($(\lambda_2 + \lambda_3)/2$), which are perpendicular to the longitudinal component, and which have been associated with myelin integrity (Song et al., 2003, 2005). MD is the average of these three principal eigenvalues ($(\lambda_1 + \lambda_2 + \lambda_3)/3$). Finally, FA is the most frequently used metric. This metric indicates how the other diffusion metrics stand in relation to one another, providing a summary index of the directional nature of water diffusion in the voxel (Beaulieu, 2002). It is scaled such that 0 represents unrestricted or isotropic diffusion, and 1 indicates water diffusion that is anisotropic, or restricted in all but one direction. These metrics have been useful in tracking various fiber pathways in health and disease across the lifespan (Chan et al., 2008; Lebel and Beaulieu, 2009; Nir et al., 2013), but none of these DTI metrics are designed to isolate and characterize the specific contributions of axonal density to the diffusion-weighted imaging signal.

With updates in MRI hardware and software, more diffusion directions can be acquired in a shorter amount of time, which has allowed for the use of better imaging reconstruction algorithms. These High Angular Resolution Diffusion Imaging (HARDI) algorithms improve the estimation of water diffusion in multiple directions, leading to better estimation and resolution of such crossing and kissing fibers. For example, Generalized Q-Sampling Imaging (GQI) has been employed to effi-

ciently reconstruct the orientation distribution function (ODF) of water diffusion from HARDI acquisitions (Daducci et al., 2014; Yeh et al., 2010). Two metrics can be recovered from these diffusion models: Quantitative anisotropy (QA) and generalized fractional anisotropy (GFA). QA is defined as the amount of anisotropic spins that diffuse along a fiber orientation, while GFA can be thought of as a higher-order generalization of FA (Cohen-Adad et al., 2008; Tuch, 2004). Regardless of the improvements GQI has provided for MRI, these metrics are still not optimal for measuring axonal density differences (Zhang et al., 2012).

Other imaging reconstruction methods have focused on estimation of microstructural properties of cell body processes—dendrites and axons, i.e., neurites. For example, Neurite Orientation Dispersion and Density Imaging (NODDI) ascribes the signal of water protons in tissue into three components: isotropic diffusion representing free motion in areas such as ventricles, intracellular volume diffusion representing restricted water in dendrites and neurons, and extracellular volume diffusion representing glial cells, cell bodies, and the extracellular environment (Zhang et al., 2012). A number of studies have compared the NODDI signal to known histological patterns in white matter. For example, Zhang et al. 2012 have shown that NODDI is capable of disentangling the two components of FA, neurite density and orientation dispersion, allowing the two to be studied individually. In an important study that serves as a model for our present investigation, Genc et al. 2017 have also used NODDI to map corpus callosum density in children and adolescents. They found that NODDI intracellular volume fraction (ICVF) and orientation distribution function (OD) metrics were sensitive to histologic differences along the longitudinal axis of the corpus callosum. We conducted a partial replication of this study, and will return to the details of it in the Method.

Finally, Restricted Diffusion Imaging (RDI) is a recent measure that has been proposed to measure changes in cellularity (i.e., cellular density), which affects local diffusion of water molecules. RDI attempts to separate non-restricted diffusion of water molecules from restricted diffusion of water molecules by focusing on the difference in diffusion displacement of each component. As such, the model can measure restricted diffusion while ignoring non-restricted diffusion. Yeh et al. 2017 showed that RDI was sensitive to differences in cellular density in a manufactured phantom, and in rat cardiac tissue that sustained a lesion, which resulted in the migration of macrophages to the lesion site. The density changes resulting from this macrophage migration were detectable in changes in RDI. Thus, RDI seems to be sensitive to cellular density and changes in cellular density.

What is unknown, though, from these initial studies is whether RDI metrics are sensitive to density of axonal fibers. It is well known that axons at cross-section differ in diameter (Aboitiz et al., 1992) and this affects the density of axons within the fiber pathway. For example, the Aboitiz et al. (1992) histological examination of 20 post-mortem healthy adult brains showed that the density of small and large diameter axons differs across the anterior-posterior axis of the corpus callosum. This now well-established density pattern has been replicated with other measures in more recent work (Suzuki et al., 2016; Caminiti et al., 2013; Bjornholm et al., 2017), including the study by Genc et al. (2017) that serves as a model of the present investigation. As we noted earlier, it would be important for a number of reasons to establish *in vivo* metrics that are sensitive to differences in axonal density. Given its high sensitivity to diffusion changes as a function of cellular density, we expected RDI to be most sensitive to these changes relative to other established metrics. Thus, the primary aim of this study is to address whether RDI is a candidate metric for measuring axonal density *in vivo*, and further whether it

does so better than other available diffusion metrics. To do this, we measured segments of the corpus callosum, which have been known to differ in axonal density on the anterior-posterior axis (Aboitiz et al., 1992; Reyes-Haro et al., 2013; Riise and Pakkenberg, 2011; Suzuki et al., 2016). We used both a healthy adult sample ($n = 840$) and a healthy developing sample ($n = 129$) to test whether previous histological results match the segmental pattern reflected using RDI *in vivo*. In order to demonstrate that RDI measures a unique characteristic in the imaging modality, we compared the RDI measurements to that of DTI metrics (AD, RD, FA, and MD), GQI diffusion metrics (GFA and QA), and NODDI metrics (ISO, ICVF, and OD). We hypothesized that RDI would most reliably, relative to other measures, replicate the Aboitiz et al. (1992) anterior-posterior density pattern established in histology.

Paradigm and Summary of Both Experiments in Study 2

Two studies were designed to investigate the sensitivity of various diffusion metrics to the anterior-posterior microstructural organization of the corpus callosum. We will refer to them as Study 2.A and Study 2.B from here on out. Our study design uses as a point of departure the study by Genc et al. (2017). We used two publicly available datasets. In Study 2.A we analyzed 840 multi-shell adult high angular resolution diffusion-weighted imaging (HARDI) scans from the Human Connectome Project (<http://www.humanconnectome.org>). Study 2.A was designed to replicate and match the corpus callosum density pattern found in the Aboitiz et al. (1992) histological study. In Study 2.B, we conducted the same analysis on a different dataset of 129 infants, children, and adolescents from the C-MIND study (<https://research.cchmc.org/c-mind/>). We used the single-shell acquisition from this study to establish whether the RDI metric could be sensitive in single-shell data, which are also still common acquisitions, especially in clinical settings.

Simultaneously, the use of the CMIND data allowed us to investigate whether the density pattern can be detected in a developmental sample. For both studies we computed DTI metrics (FA, RD, AD, MD), GQI metrics (QA, GFA, and RDI), and (in Study 2.A only) NODDI metrics (ICVF, OD, ISO). We applied a corpus callosum mask based on Aboitiz et al. (1992) to compute summary statistics of each metric for each subregion. The mask was applied in an automated fashion for Study 2.A, and hand-drawn for Study 2.B (to accommodate the different brain sizes in the developmental sample (Wilke et al., 2008)).

3.2 Study 2.A: Adult Sample

3.2.1 Method

Participants

The adult sample contained 842 participants between the ages of 22- and 35-years-old who underwent MRI scans as part of the Human Connectome Project. Data were provided by the Human Connectome Project, WU-Minn Consortium (Principal Investigators: David Van Essen and Kamil Ugurbil; 1U54MH091657) funded by the 16 NIH Institutes and Centers that support the NIH Blueprint for Neuroscience Research; and by the McDonnell Center for Systems Neuroscience at Washington University. The automated atlas segmentation was successfully applied to 840 of these participants. Therefore, the summary statistics for the DTI and GQI metrics were calculated on 840 participants. The NODDI reconstruction is a time and resource intensive process, and therefore a random sample of 100 participants were selected from the full sample for this reconstruction.

Diffusion Metrics

We calculated and compared four DTI metrics (FA, RD, AD, and MD), three GQI metrics (QA, GFA, and RDI), and three NODDI metrics (ICVF, OD, ISO). The calculations for the four DTI metrics and for two of the GQI metrics were explained in Study 1, so we will mainly focus on explaining the novel RDI and the NODDI metrics below.

Neurite orientation dispersion and density imaging (NODDI) Metrics.

NODDI works by combining the three-component tissue model, which distinguishes between intracellular, extracellular, and cerebrospinal fluid, with the 2-shell HARDI protocol:

$$A = (1 - V_{iso})(V_{ic}A_{ic} + (1 - V_{ic})A_{ec}) + V_{iso}A_{iso} \quad (3.1)$$

This calculates the independent, normalized signal A , comprised of the intra-cellular normalized signal and volume fraction (V_{ic} and A_{ic}), the normalized signal of the extracellular compartment (A_{ec}), and the normalized signal and volume fraction of the cerebrospinal fluid (V_{iso} and A_{iso}) (Zhang et al., 2012). The three tissue components are calculated from a simplified form of the orientation-dispersed cylinder model (Zhang et al., 2011) and the Watson distribution. Using the Watson distribution provides a unique advantage due to its capability of accurately estimating both low and high levels of dispersion across the brain, while truncated spherical harmonic series tend to provide inexact measurements of lower levels of orientation dispersion (Jespersen et al., 2007; Zhang et al., 2012).

NODDI supports the modelling of both gray and white matter, with white matter showing low to moderate axonal dispersion and gray matter showing high axonal

dispersion. Since its implementation, NODDI has been used in numerous adult studies to examine disease progression (Taoka et al., 2020; Broad et al., 2019), and it appears to be useful for differentiating between myelinated and non-myelinated axons (Kunz et al., 2014) and measuring cortical gray matter maturation over development (Pecheva et al., 2018).

The three NODDI metrics we examined were intracellular volume fraction (ICVF), isotropic volume fraction (ISOVF), and orientation dispersion (OD). ICVF measures neurite density, with higher values indicating greater packing of neuronal tissue. ISOVF measures the extracellular, free water compartment of the model. OD measures dispersion of modelled sticks, with greater dispersion seen in gray matter and lower dispersion in white matter regions such as the corpus callosum.

Restricted Diffusion Imaging (RDI). Restricted diffusion imaging (RDI) is a novel metric that aims to measure changes in cellular density. Thus far it has been shown to be sensitive to the inflammatory response (macrophage infiltration) in rats (Yeh et al., 2017). It is for this reason that we expect it might be sensitive to differences in axonal density.

RDI works through the use of q-ball imaging that estimates the density of diffusing spins with respect to their diffusion displacement. RDI separates non-restricted diffusion from restricted diffusion through the use of different diffusion sensitization strengths, which allows RDI to be more sensitive to structural changes. The calculation for the metric is a linear combination of diffusion-weighted imaging signals acquired by the long diffusion time (Yeh et al., 2017);

$$p(L) = \sum_q \frac{Si(2\pi L|\mathbf{q}|)}{2\pi|\mathbf{q}|} W(\mathbf{q}) \quad (3.2)$$

In the formula, $\rho(L)$ represents the density of diffusing spins that are restricted with the displacement distance L . Si is a sine integral, $\text{Si}(x) = \int_0^x \frac{\sin(t)}{t} dt$. In the case where $\mathbf{q} = 0$, the term $\text{Si}(2\pi L - \mathbf{q}) / 2\pi - \mathbf{q}$ would be replaced by L . Overall restricted diffusion, $\rho(L)$, estimates the density of diffusing spins with diffusion displacements less than L (Yeh et al., 2017).

DWI Reconstruction

DTI (Basser et al., 1994) and GQI (Yeh et al., 2010) reconstruction were both done using the January 2018 version of DSISudio (<http://dsi-studio.labsolver.org>) and took approximately one minute for DTI and two minutes for GQI. NODDI reconstruction took considerably longer, at about four to six hours per brain. Since the time we conducted the NODDI reconstruction, reconstruction time has been reduced to one hour per brain through the use of Microstructure Diffusion Toolbox (MDT; Harms et al. 2017), which will be touched upon again in the Discussion. The NODDI reconstruction done here used the AMICO (Daducci et al., 2015) python implementation, along with the DIPY library (Garyfallidis et al., 2014), SParse Modeling Software (SPAMS; Mairal et al. 2010; <http://spams-devel.gforge.inria.fr/>), and the Camino toolkit as dependencies (Cook et al., 2006).

Parcellating the Corpus Callosum: Drawing the Regions of Interest (ROIs).

The corpus callosum was manually segmented into 10 ROIs in DSI Studio, following the segmentation scheme described by Aboitiz et al., (1992). These divisions are shown in Figure 22A, reconstructed from the original Aboitiz et al., (1992) segmentation. To conduct the segmentation, we first drew the midline slice from the coronal view, and then we drew the ROIs from the sagittal view. We then mea-

sured the corpus callosum divided it into three equal length sections going from the anterior to posterior direction: the genu, the midbody, and the isthmus/splenium. We then further divided the genu and the midbody sections into three equal parts. Thus, the genu was divided into G1, G2, and G3, while the midbody was divided into B1, B2, and B3.

Finally, we defined the last third of the corpus callosum as the isthmus and the splenium. The splenium makes up the posterior fifth of the entire corpus callosum and is subdivided into three equal sections, labelled S1, S2, and S3. The isthmus, labelled I, is comprised of the remaining area between the midbody and the splenium sections. All sections of the corpus callosum are arbitrarily divided based on straight length by counting voxels between the parcels. Clarke (1990) showed that whether these sections are portioned based on curvature or straight length makes no difference. For this adult sample, the 10 ROIs were saved as an atlas which was then applied to all participants.

Data Analysis

In the original Aboitiz et al., (1992) paper, the authors used this segmentation to report on densities, based on histological counts, of the following fiber sizes: $>0.4 \mu\text{m}$, $>1 \mu\text{m}$, $>3 \mu\text{m}$, and $>5.0 \mu\text{m}$. The pattern of fiber densities was nearly identical for the $>3 \mu\text{m}$ B and $>5.0 \mu\text{m}$, and thus for simplicity we ignored that pattern for this paper (i.e., the $>5.0 \mu\text{m}$ results would apply in the same way to the $>3.0 \mu\text{m}$ pattern). In order to determine which of the density patterns produced by our two samples best replicated the Aboitiz histological model, we conducted planned contrast analyses (Rosenthal et al., 2000). Planned contrasts allow a test of whether the observed pattern matches an expected pattern, which in this case is defined by the histologic results.

The patterns we modeled are given in Figure 22. Figure 22A shows the segmentation scheme used in the Aboitiz et al., (1992) paper, which we replicated here. This scheme was also used by Genc et al. (2017). Figure 22B shows the density results from Aboitiz et al (1992) for three fiber sizes: $>5.0 \mu\text{m}$, $>1 \mu\text{m}$, and $>0.4 \mu\text{m}$.

The first step in a planned contrast analysis is to establish the contrast weights. These weights are designed to model the pattern of the Aboitiz data for the four comparisons on which they reported (again, note that results for $>3 \mu\text{m}$ are omitted). Figure 3B shows the contrast weights for each of four comparisons that were reported as significant in the Aboitiz paper. For $>5.0 \mu\text{m}$ the contrast weights were: (-5.5, -3.5, -1.5, 0.5, 2.5, 4.5, 2.5, 0.5, -0.5, 0.5). For $>1 \mu\text{m}$, Aboitiz only found significant differences between B3 and S2 segments and S2 and S3 segments. Therefore we created two contrasts to test those specific differences: $>1 \mu\text{m}$ A: (0, 0, 0, 0, 0, -1, 0, 0, 1, 0); $>1 \mu\text{m}$ B: (0, 0, 0, 0, 0, 0, 0, 0, 1, -1). Finally, for $>0.4 \mu\text{m}$ the weights were: (1, 0.5, 0.5, 0, -0.5, -1.5, -0.5, 0, 0.5, 0). As is standard, all contrast weights sum to zero. Once contrast weights are established, the second step is to test them in the context of the linear model, which was done using R v3.6 (R Core Team, 2019).

Power Estimates. In cases where null effects are reported, care must be taken to avoid Type II error. Fortunately, because of the large effect sizes seen and the large sample sizes employed in the present study, power was universally high. In the adult sample, *a posteriori* power analyses for DTI and GQI measures ($n= 840$) showed that power = .95 to detect a small effect of $d = .2$ at $\alpha = .05$. Power was substantially lower for the NODDI measures ($n= 100$) and for the developing sample ($n= 129$) as a consequence of the smaller sample sizes, with power = .80 to detect a moderate effect size of $d = .4$ at $\alpha = .05$. The power analyses presented here are

based on (Cohen, 1988), and provide assurance that we had adequate power to draw accurate conclusions.

Outlier Detection and Correction

We did not remove outliers but corrected for their influence using a conservative 97.5% Winsorization procedure. Similar to clipping in signal processing, this statistical transformation limits extreme values in order to reduce the influence of outliers.

3.2.2 Results

Given the large sample size, even small effects are likely to be statistically significant. Therefore, our reporting of results focuses on effect sizes, which are independent of sample size. However, in organizing the discussion of results it is useful to establish a cutoff on which to base the reporting of the most important results. We established an arbitrary cutoff of $> |2.5|$ standard deviations to organize the discussion of the results. We still report all results in the Tables, regardless of the cutoff values.

As Table 10 and Figure 23 show, based on this cutoff, several measures were sensitive to the longitudinal distribution of fiber sizes in the corpus callosum. From the DTI metrics, AD most closely replicated histological density patterns for both the smallest fiber sizes ($t = -60.50$, $p < 0.001$) and the largest fiber sizes ($t = 70.50$, $p < 0.001$). From the GQI metrics, GFA was the most sensitive to fibers greater than $1 \mu\text{m}$ for both contrasts: B3 and S2 ($t = 52.42$, $p < 0.001$) and S2 and S3 ($t = 22.85$, $p < 0.001$). Figure 24 shows how the effect sizes of each metric compare to each other across differing axonal fiber size models.

As expected, the most significant NODDI metric was ICVF, which accurately detected density patterns at the smallest fiber size ($t = 25.54$, $p < 0.001$) and at the

largest fiber size ($t = -24.66$, $p < 0.001$). The NODDI density patterns seen in this adult sample replicate the patterns reported by Genc et al. (2017) in a developing sample. Across both studies, ICVF was the lowest at the isthmus and the highest at the posterior part of the splenium. Similarly, the novel metric reported here, RDI, accurately replicated the density pattern for the $> 5 \mu\text{m}$ fiber sizes ($t = 58.24$, $p < 0.001$), and for the smallest, $> 0.4 \mu\text{m}$ fiber sizes ($t = -53.29$, $p < 0.001$). These findings indicate that both RDI and NODDI are capable of accurately measuring axonal density for large and small fiber sizes.

3.3 Study 2.B: Developing Sample

In Study 2.B we aimed replicate the results from Study 1 in a developing sample. The same DTI and GQI diffusion metrics and histological model were used, but with a manually-drawn corpus callosum segmentation for each participant as previously detailed. NODDI metrics were not able to be calculated on this sample due to NODDI's multi-shell requirement, not met by this sample's single-shell MRI data. Note that Genc et al. (2017) did examine NODDI metrics using a second acquisition in the CMIND data set, which had different acquisition parameters and a different shell. We focused on the single shell acquisition, as we were interested in determining whether RDI can provide accurate results with one shell acquisition. However, because we used the same segmentation approach as they did, we can compare our findings to theirs in a partial replication.

3.3.1 Method

Participants

The developing sample contained 129 participants between the ages of 7-months-old and 19-years-old ($M = 8.8$ years) from the Cincinnati MR Imaging of NeuroDe-

velopment (C-MIND) database, provided by the Pediatric Functional Neuroimaging Research Network (<https://research.cchmc.org/c-mind/>) and supported by a contract from the Eunice Kennedy Shriver National Institute of Child Health and Human Development (HHSN275200900018C). The data are available from CMIND by request, which facilitates validation of the results we report here. Participants in the database are full-term gestation, healthy, right-handed, native English speakers, without contraindication to MRI. By design, the C-MIND cohort is demographically diverse (38% nonwhite, 55% female, median household income \$42,500), intended to reflect the US population. The summary statistics for the DTI and GQI metrics were calculated for the full sample of 129 participants.

Parcellating the Corpus Callosum

Due to previous studies indicating the problems with applying the MNI normalization to a developing sample, we manually drew the 10 ROIs for the Study 2.A sample, following the same guidelines as were used in Study 2.A. The same data analysis procedure was followed as in Study 2.B.

3.3.2 Results

There were notable differences when the diffusion metrics were applied to the C-MIND developing sample. First, AD was no longer the stand-out DTI metric. Instead, FA was the most effective DTI metric at replicating density patterns for 3 out of 4 models. It was positively related to smaller fiber sizes ($t = 28.66$, $p < 0.001$ for $> 0.4 \mu\text{m}$, $t = 23.88$, $p < 0.001$ for $> 1 \mu\text{m}$ model A) and was inversely related to the largest $> 5 \mu\text{m}$ density model ($t = -27.46$, $p < 0.001$).

For the GQI metrics, GFA continued to be a reliable measure of fiber density for all four models. RDI was also consistent for both the smallest and highest fiber size models. In fact, RDI most closely matched the histological model for fiber sizes

greater than $5 \mu\text{m}$ ($t = 30.36$, $p < 0.001$). The density patterns are shown in Figure 25, effect sizes in Figure 26, and full results can be found in Table 11.

3.4 Discussion

The quantification of microstructural properties of neural tissue can be informed by advances in the modeling of diffusion-weighted imaging data. This is important for the diagnosis and treatment of neurologic disease, especially as it relates to properties of white matter such as axon density. In this study, we examined two separate samples of typical adults and children. In the first sample of 840 adults from the HCP dataset, we segmented the corpus callosum into 10 parts, and measured the diffusion properties of each segment. These diffusion properties were modeled using a variety of reconstruction methods based on DTI, NODDI, and GQI models. For large fiber sizes ($> 5\mu\text{m}$), we found that the best indicators of histologically established axonal density patterns were the DTI AD, NODDI ICVF, and RDI. For mid-range fiber sizes ($> 1\mu\text{m}$), there were no methods that were clear standouts. For the smallest fiber sizes ($> 0.4\mu\text{m}$), the same metrics that were sensitive to large fiber sizes (DTI AD, NODDI ICVF, and RDI) showed the clearest differentiation.

For the developing sample of 129 children and adolescents, we generally found the same results as in the adult sample, but there were a couple of exceptions. Unlike the adult sample, DTI AD was not a clear differentiator. Additional measures (i.e., DTI FA and GQI GFA) were also sensitive measures, but this was not evident in the adult sample. We did, however, replicate the finding for the RDI metric. As in the adult sample, the RDI metric clearly matched the known histologic pattern of the corpus callosum, especially for small and large fiber sizes, and indeed seemed to be sensitive to subtle differences across the longitudinal length of the structure. These results suggest it is possible to quantify, indirectly, differences in axonal density *in*

vivo using DWI in both children and adults. Furthermore, there is clear support that RDI is a useful metric of fiber density in both adults and children, and in single- and multi-shell acquisition paradigms. This information has the potential to inform researchers and clinicians about microstructural differences in a variety of domains, for example in the examination of disease progression, of age-related differences across typical and atypical development, and of general nervous system structure/function relationships.

Comparison of Restricted Diffusion Imaging (RDI) to Other Metrics in Published Literature. Our study can be conceived of as a complement to similar investigations conducted by Genc et al. (2017) and by Raffelt et al. (2015, 2012). These authors showed that other metrics sensitive to fiber density can reliably replicate the longitudinal pattern of axonal density in the corpus callosum. For example, Raffelt et al. (2015, 2012) established the apparent fiber density (AFD) measure, which they showed can be biologically interpreted as a measure of the intra-axonal volume fraction of axons along the corresponding orientation. However, the metric is heavily affected by the space occupied by axons, and not so much by axonal diameter. Thus, for example, fiber bundles consisting of large axons could have lower density than thinner axons, yet their AFD would be comparable. Despite this, Genc et al. (2017) showed that AFD is sensitive to axonal density in larger fiber bundles (their Figure 4), and indeed that metric best matched the histological pattern reported by Aboitiz. But Genc et al., did not assess whether it was similarly sensitive for smaller fiber bundles.

In our complementary investigation, we showed that, for both large and small fiber sizes, in both adult and child samples, RDI was an excellent differentiator of the pattern of axonal density across the longitudinal axis of the corpus callosum (see Figure 27 for comparison with large diameter fibers). Unlike most other diffusion

metrics, RDI does not depend on an underlying diffusion model or numerical optimization to estimate model parameters, making it easily applicable to a wider range of databases and clinical scanner protocols. RDI’s sensitivity to cell density has been useful in differentiating tissue in patients with tumors (Yeh et al., 2019; D’Souza et al., 2019), as well as measuring therapeutic benefits of deep brain stimulation (Anderson et al., 2019). In a phantom study by Yeh et al, the optimized restricted diffusion showed an almost perfect correlation of 0.998 with cell density (Yeh et al., 2017). Notably, that paper also showed that mean diffusivity is associated with cell density. However, we did not corroborate that here with respect to axonal density. That is, MD is not as good as RDI at differentiating the longitudinal pattern of fiber density in the corpus callosum. Thus, despite similar sensitivity to cellular density in a phantom study, RDI seems to be more sensitive than MD to fiber density *in vivo*. Furthermore, RDI was highly consistent across the two samples (see Figure 27). This is in contrast to other common metrics like FA, which was not consistent across the two samples. These results suggest that RDI is a reliable measure of fiber density across a wide age range, and it is robust to different diffusion acquisitions. Furthermore, a main advantage of RDI is the computation time (under a minute) which occurs as part of routine image reconstruction, thus making it appealing in clinical settings.

Genc et al. (2017) also showed that NODDI metrics were reasonably sensitive to the distribution of axon density in the corpus callosum. In our study, for large fiber sizes, NODDI ICVF was the best NODDI differentiator of corpus callosum fiber density. In other research, this measure has also been shown to be effective at capturing axonal density across the corpus callosum (Zhang et al., 2012; Genc et al., 2017). For example, previous studies have found that NODDI is more sensitive to demyelination than DTI metrics in both human (Grussu et al., 2017) and

mouse models (Seppehrband et al., 2015). However, despite the sensitivity, two issues limit the utility of NODDI for clinical samples, especially for pediatric samples. One is the long reconstruction times (several hours per participant in our study), and the second is the requirement of multi-shell data acquisitions. Some software advances have improved reconstruction times for NODDI models (to around 1 hour per participant using Microstructure Diffusion Toolbox (MDT; Harms et al. 2017), but RDI reconstruction times are still much shorter (around 1 minute per participant), and our data suggest that, for fiber density, RDI can provide accurate results even for single-shell acquisitions. This does not entirely discount the effectiveness of NODDI ICVF as a metric for assessing fiber density, but it does suggest that RDI is another useful addition to the diffusion toolkit, and that it has important clinical applicability.

RDI also outperformed DTI metrics. For our adult sample, our density patterns were similar to previous investigations, with an increase in FA seen in the posterior segments of the corpus callosum (Caminiti et al., 2013; Bjornholm et al., 2017) and a peak of MD in the isthmus (Bjornholm et al., 2017), indicating that DTI metrics are sensitive to structural differences in the corpus callosum. But DTI metrics were inconsistent between the adult and child samples. Furthermore, despite being widely utilized as measures of microstructural change, DTI metrics lack specificity when it comes to measuring specific characteristics of microstructure (Daducci et al., 2014). The inconsistencies we saw in our DTI metrics might have been caused by differences in axonal density, but they might also be associated with other tissue properties, such as lower myelination (Lebel and Deoni, 2018; Reynolds et al., 2019a), increased orientation dispersion (Jones et al., 2013), or less mature axonal integrity within the developing sample (Kumar et al., 2012; Qiu et al., 2008). Due to the inherent nonspecific nature of DTI, it remains difficult to discern what caused the differences

in quantification between samples, which highlights well-established drawbacks to DTI metrics.

Limitations. One inherent limitation of this study is that there are many more available diffusion-weighted imaging reconstruction algorithms than we studied here. We restricted our comparison to the novel RDI method and compared it to DTI, GQI, and NODDI techniques, but there are other algorithms that should also be considered. A second limitation of our study is that we only examined one brain region. The corpus callosum is a coherently orientated structure with no crossing fibers. Our study does not address how accurate these metrics would be at measuring density when crossing fibers are present, which is a known drawback of DTI in particular, but might also affect more recently-developed metrics such as NODDI and RDI. While our study provides strong evidence for the utility of NODDI and RDI for measuring axonal density, investigations of other brain regions would further expand these results and potentially elucidate different clinical applications.

Conclusions. The study provided novel evidence that RDI can be used to measure axonal density in children and adults, even for single-shell data. The histological model of corpus callosum anterior-posterior density pattern was replicated using this novel *in-vivo* metric across two independent samples. NODDI's ICVF measure was also sensitive to axonal density in the adult population. The encouraging findings support the hypothesis that RDI and ICVF can be used for measurement of axonal density as a biomarker for demyelination disorders, such as multiple sclerosis, in the future.

Establishing reliable and effective measures of axonal density is potentially significant for the study of early symptomatology, progression, and possible underlying causes of disorders characterized by white matter and other neural pathologies, such as multiple sclerosis (Grussu et al., 2017), amyotrophic lateral sclerosis (Broad et al.,

2019), dysplasia (Winston et al., 2014), epilepsy (Winston et al., 2014), and immune cell infiltration Andica et al. (2019). Many previous relationships between axonal density and clinical disorders were fully dependent on histology, but through the advancements of DWI, these disorders can be studied *in vivo*, which holds potential for making earlier diagnoses and may contribute to the design of more specific, directed treatment plans.

CHAPTER 4

STUDY 3

4.1 Research Question

Diffusion tensor imaging (DTI) has played a pivotal role in mapping brain maturation, indicating increasing amounts of myelination and axonal growth and organization throughout development (Lebel and Beaulieu, 2011; Lebel et al., 2008; Tamnes et al., 2018). While DTI has offered many invaluable insights into the events that occur during brain development, it lacks the specificity required to disentangle individual factors, such as myelination, axonal growth, density, and organization, that are occurring simultaneously. Neurite orientation dispersion and density imaging (NODDI) is a novel, advanced three-component diffusion model that offers more detailed quantification of microstructural changes (Zhang et al., 2012), and could offer more detailed insights into the changes occurring during brain maturation and associated behaviors.

In this study, we used NODDI implementation to measure axonal and dendritic density and coherence within white and gray matter of typically and atypically developing children. NODDI was selected as the model of choice given its ability to measure density and orientation in both white and gray matter (Zhang et al., 2012), therefore allowing us to examine subcortical regions, which other methods that we tested in Study 2 are less suitable for.

The two primary metrics derived from the NODDI model that are of particular interest to us for this study are neurite density index (NDI) and orientation dispersion index (ODI). Increased NDI indicates greater myelination, axonal growth, or neurite density, while ODI measures neurite orientation dispersion, axonal fanning, and neural coherence (Genc et al., 2017; Mah et al., 2017; Zhang et al., 2012). As a

result of increases in myelination and synaptic formation during brain development, we expect to see an increase of NDI across age, while ODI is expected to remain the same.

Within a particular brain region, increased NDI can either be interpreted as greater myelination and development (Mah et al., 2017), or as a lack of proper synaptic pruning (Genc et al., 2018). Delayed pruning has been linked with ADHD in the past (Oades et al., 2010), and the excess synapses could reduce network efficiency needed for processing speed on executive function tasks (Merolla et al., 2014). Increases in ODI typically indicate greater axonal fanning and lack of neural coherence (Merolla et al., 2014), but lower ODI could also indicate lower complexity of neurite branching (Morris et al., 2018; Zhang et al., 2012).

We examined whole brain microstructure differences, particularly neuronal density and orientation, between the typically developing sample and the ADHD-diagnosed sample to examine potential neurobiological differences between the groups. Furthermore, we investigated the microstructural differences in prefrontal cortex regions, specifically the pre-SMA, SMA, *pars opercularis*, and *pars triangularis*, as well as the caudate and putamen, and examined whether these differences were associated with language and executive function performance.

The pre-SMA is involved in higher-order motor control (e.g., planning and sequencing of movements; Ikeda et al. 1999; Peck et al. 2009; Scangos et al. 2013; Vergani et al. 2014). The left pre-SMA, in particular, is thought to be involved in linguistic processing (Catani et al. 2013; Makuuchi et al. 2012; McNealy et al. 2010; Zentgraf et al. 2005). A recent study has suggested that the right hemisphere pre-SMA is involved in language inhibition, especially when it comes to switching between languages (de Bruin et al., 2014). Given the pre-SMA's known relation to choosing correct words, we expect to see both the left and right pre-SMA being

related to higher verbal fluency scores, since these tasks measure one’s ability to list out words that are either in the right category or start with the correct letter while inhibiting incorrect responses.

Due to the SMA’s cytoarchitecture, it is most commonly thought to be involved in motor execution, particularly in speech initiation and production (Bohland and Guenther 2006; Connor et al. 2010; Peck et al. 2009; Vergani et al. 2014). The SMA is also active bilaterally during silent repetition tasks, but the left SMA shows greater activation in the left hemisphere in both the left and right-handed adult participants, possibly as a result of its involvement in speech (Dalacorte et al., 2012). Forster and Webster (2001) examined the role of SMA speech-motor control in stutterers versus non-stutterers, and found that the coordination deficits seen in adult stutterers are mediated by the SMA. Finally, in cases where the SMA is impacted by tumor, it is known to cause what is known as “SMA syndrome”, which leads to contralateral akinesia and mutism (Vergani et al., 2014). This highlights its importance in both speech and motor execution. Given these previous findings, we expect the left SMA would be linked to higher scores on phonemic articulation.

The left inferior frontal gyrus (IFG) has, in particular, been associated with the process of “selection” among competing semantic and/or phonological representations. Thus, the literature suggests several functions associated with the IFG, such as resolution of semantic competition (Grindrod et al., 2008), semantic selection (Grindrod et al. 2008 ; Kan and Thompson-Schill 2004), sentence integration (Zhu et al., 2009), and word retrieval (Gold and Buckner 2002; Smith et al. 2004). Specifically, the *pars opercularis* (Op) is thought to be more involved in phonological processing/phonological selection, while the *pars triangularis* (Tri) is thought to be involved in semantic processing/semantic selection (Booth et al., 2004; Katzev et al.,

2013; Lau et al., 2008). Therefore, we expect to see the right Op being related to semantic fluency scores and left Tri being associated with phonemic fluency scores.

The caudate and putamen have both been linked to language, especially for nouns, verbs, and grammatical learning for people speaking a secondary language (Chan et al., 2008; Tagarelli et al., 2019) as well as being associated with developmental language impairment (Lee et al., 2013). Bilateral damage to these brain regions has been shown to cause deficits in both speech production and sentence comprehension (Pickett et al., 1998).

More specifically, the putamen is thought to be responsible for motor role in speech while the caudate plays a role in cognitive control (Chan et al., 2008; Hervais-Adelman et al., 2015; Robles et al., 2005). In children, the left putamen in particular has been associated with phonological processing (Cherodath et al., 2017) and the right caudate has been linked with specific speech impairment (SLI) (Badcock et al., 2012) and speech motor planning, particularly in children who stutter (Foundas et al., 2013). Therefore, we hypothesize that we expect to find associations between the left putamen and phonemic skills, while right caudate would be associated with semantic verbal fluency.

When it comes to executive function, Scangos et al. (2013) have shown that the pre-SMA and SMA play a role in future action selection, which is a key component of executive control. Similarly, in humans, a pre-SMA lesion preserves a person's ability to inhibit responses, but creates a specific deficit in rapid switching between responses (Smith et al., 2004). Since previous studies suggest that pre-SMA and SMA would be related to task switching, we hypothesized that these regions would be related to successfully being able to adhere to rule changes presented in the Dimensional Change Card Sort (DCCS) task and Head-Toes-Knees-Shoulders (HTKS) task.

Several studies have found that the right hemisphere inferior frontal gyrus, along with the right pre-SMA (Crone et al., 2006; de Bruin et al., 2014; Smith et al., 2004; Scangos et al., 2013), is involved in domain general inhibition (Barber et al., 2013; Chavan et al., 2015; de Bruin et al., 2014; Hampshire et al., 2010; Hughes et al., 2013; Lenartowicz et al., 2011; Swann et al., 2012). Aron et al. (2004) found that a lesion in the right IFG, but not the left, caused deficits in response inhibition, and the severity of the deficit depends on the size of the right IFG lesion. Furthermore, the data more strongly suggested involvement of the right Tri compared to Op. The authors have suggested, in subsequent publications, that the right inferior frontal cortex may act as a “brake” for executive control (Aron et al., 2014). Therefore, we expected that higher organization within the right Op and Tri would lead to improved executive function performance in our participants.

The caudate and putamen have been associated with executive function as well, particularly for executive control and spatial attention (Jarbo and Verstynen, 2015). In particular, increased connectivity of the caudate in adults has been linked with better performance on working memory tasks (Gordon et al., 2015; Huang et al., 2017) while caudate lesions are related to set-shifting difficulties (Svegar et al., 2016). On the other hand, greater volume in the putamen is related to greater performance in attention (Zimmerman et al., 2006) while right lateralization of the putamen has been associated with higher inhibitory control (Ardila et al., 2018). Therefore, we hypothesize that neurite microstructure in the caudate and putamen will be associated with higher scores on our executive function measures.

Children diagnosed with ADHD have been shown to have reduced caudate and putamen volume bilaterally (Mahone et al., 2011; Qiu et al., 2011). One study has also found that if no volume differences between ADHD and control samples are present, there is still a significant asymmetry seen in ADHD samples, such that

the left putamen is smaller than the right (Wellington et al., 2006). In adults, ADHD-related hyperactivation was found in the right caudate and left putamen (Cortese et al., 2016). Therefore, we hypothesize that our ADHD sample will have microstructural differences in the caudate and putamen compared to the typically developing group, and possibly have laterality differences, with the right putamen being larger than the left when compared to controls.

4.2 Method

We used the same 196 4- to 7-year-old children and same language and executive function measures detailed in the Method section of Study 1. We have established that axonal density can be measured *in vivo* in children and adults using Restricted Diffusion Imaging (RDI) and in adult samples using NODDI in Study 2, but we were previously unable to test NODDI’s applicability to a developing sample because the C-MIND dataset was incompatible with NODDI implementation. For Study 3, we will use the multi-shell neuroimaging data from the AHEAD project to measure region-based neurite microstructure in our typically and atypically developing samples using an improved NODDI method, detailed below.

Neurite orientation dispersion and density imaging (NODDI) Metrics.

As explained in Study 2, NODDI works by combining the three-component tissue model, which distinguishes between intracellular, extracellular, and cerebrospinal fluid (Zhang et al., 2012). Given the very long computation times (4 to 6 hours per participant) in Study 2, we chose to use the Microstructure Diffusion Toolbox (MDT; Harms et al. 2017), which improves both run time and robust fit, to compute NODDI metrics for this study. We then focused on neurite density index (NDI) and orientation dispersion index (ODI) metrics. NDI is the fraction of tissue that contains neurites (axons or dendrites), and it is calculated:

$$NDI = \frac{w_{in}}{w_{in} + w_{ex}} \quad (4.1)$$

in which w_{in} represents the intracellular volume fraction and w_{ex} represents the extracellular volume fraction. ODI is a proxy for complexity of neurite branching and spatial configuration, and is calculated:

$$ODI = \arctan2(1, \kappa \times 10) \times \frac{2}{\pi} \quad (4.2)$$

where κ represents the dispersion index of the Watson distribution. Once MDT runs the whole brain NODDI implementation, we extract the mean NDI and ODI values for each of our 12 brain regions using the Lausanne atlas parcellation, as described in Study 1.

Data analysis. The data analysis for Study 3 uses the same approach as Study 1, except now we will look at region-based data rather than structural connectivity. We conducted robust linear regression to examine age-related differences and to test the association between the NDI and ODI values of brain regions to behavioral outcomes. The brain region data was Winsor outlier-corrected to avoid having to completely remove any outliers. Regressions were used to examine the full sample (both TD and ADHD samples) using a transdiagnostic approach, and then a categorical diagnosis approach in which we examined the TD sample separately, ADHD sample separately, and also tested for diagnosis interaction effects.

4.3 Results

Region Means and Group Differences

The NDI and ODI means for each brain region are shown on Table 12. For whole brain microstructure, we see that the ADHD group has lower NDI ($\beta = -0.18$, $p < 0.05$, $df = 194$) and higher ODI ($\beta = 0.15$, $p < 0.05$, $df = 194$). We found significant group differences for both left and right hemisphere using NDI and ODI metrics. The ADHD sample had higher NDI in the left Op ($\beta = 0.15$, $p < 0.05$, $df = 191$) and left caudate ($\beta = 0.17$, $p < 0.05$, $df = 193$) than the typically developing group, controlling for whole brain NDI. The opposite pattern is seen with ODI, with the ADHD group having decreased orientation dispersion in the left and right Tri ($\beta = -0.17$, $p < 0.05$, $df = 191$; $\beta = -0.18$, $p < 0.01$, $df = 191$, respectively), left and right caudate ($\beta = -0.19$, $p < 0.01$, $df = 193$; $\beta = -0.15$, $p < 0.05$, $df = 193$, respectively), and left and right putamen ($\beta = -0.21$, $p < 0.01$, $df = 193$; $\beta = -0.15$, $p < 0.05$, $df = 193$, respectively).

There were also differences in strengths of lateralization. The preSMA ODI was left lateralized in both groups, but significantly more so in the ADHD sample ($\beta = 0.16$, $p < 0.05$, $df = 189$, $\beta = 0.17$, $p < 0.05$, $df = 192$). Secondly, NDI of the putamen was right lateralized in the TD sample, while showing a trending association ($p = 0.08$) towards left lateralization in the ADHD sample ($\beta = 0.19$, $df = 193$). Neurite density is thought to be inversely related to brain volume (Genc et al., 2018), so this implies that the left putamen in the ADHD sample might have less volume than the right.

Age Related Change

We found that NDI captured age-related differences while ODI remained stable across development in 4- to 7-year-old children. This was seen across the whole brain with NDI increasing across age ($\beta = 0.10$, $p < 0.001$, $df = 192$), while remaining insignificant for ODI ($p = 0.92$). NDI steadily increased across development in the right Op ($\beta = 0.10$, $p < 0.05$, $df = 189$), left and right caudate ($\beta = 0.12$, $p < 0.05$, $df = 191$, $\beta = 0.16$, $p < 0.01$, $df = 191$, respectively), and left and right putamen ($\beta = 0.21$, $p < 0.001$, $df = 191$, $\beta = 0.16$, $p < 0.01$, $df = 191$, respectively). The only relationship with laterality we found was that the preSMA NDI becomes more left lateralized across development ($\beta = 0.08$, $p < 0.001$, $df = 188$). The full results are in Table 13, and the significant age-related are plotted in Figure 28.

Neurite density, as measured by NDI, appears to develop in a similar pattern across development for both typically and atypically developing children. In contrast, ADHD moderates the change of orientation dispersion across development. Specifically, there are interactions between ADHD diagnosis and the age-related differences in ODI for both the right Tri and left putamen ($\beta = -0.11$, $p = 0.055$, 95% CI does not cross zero; $df = 187$, $\beta = -0.12$, $p < 0.05$, $df = 189$, respectively). For both regions, ODI significantly decreases across development in the ADHD sample ($\beta = -0.18$, $p < 0.05$, $df = 93$; $\beta = -0.17$, $p < 0.05$, $df = 95$, for right Op and left putamen, respectively), while remaining unchanged in the typically developing sample. There were no significant laterality differences across development.

4.3.1 Language Findings

NEPSY-II Results: Transdiagnostic Approach.

First, we analyzed our data without consideration to ADHD diagnosis, with the purpose of examining which of our 12 brain regions are related to verbal fluency in the full sample when measured with NEPSY. We had NEPSY scores for 194 out of 196 children. Overall, the mean of the 4 NEPSY tasks and their associated total scores are reported in Table 3 and were explained in Study 1.

Using robust regression models, we did not find any direct associations between neurite density or orientation dispersion and verbal fluency. We did find that greater right laterality of neurite density within the caudate is associated with higher category-based semantic verbal fluency scores ($\beta = -0.15$, $p < 0.05$, $df = 186$), which supports our hypothesis that the right hemisphere would be more involved in semantic rather than phonemic tasks.

NEPSY-II Results: Categorical Diagnosis Approach.

We compared the differences between the TD and ADHD samples, with the purpose of examining whether the relationship of neurite density and orientation dispersion in brain regions with phonemics and semantics was affected by diagnosis. We found group differences on NEPSY performance between TD and ADHD, which are outlined on Table 4 and displayed in Figure 5. The behavioral group differences were explained in detail in the results section of Study I, but overall, the TD group outperformed the ADHD group on phonemics and semantics.

NEPSY-II Main Effects for TD Sample. Upon examining the 96 TD children, we found no direct associations between NDI and ODI metrics within the brain regions in relation to verbal fluency, but did find that, in the TD sample, higher left

laterality of SMA neurite density was associated with better semantic verbal fluency ($\beta = 0.29$, $p < 0.05$, $df = 84$).

NEPSY-II Main Effects for ADHD Sample. Within our 100 children in the ADHD sample, we also did not find any direct associations between NODDI metrics and fluency, but did find laterality relationships. Left laterality of neurite density within the SMA was related to better scores on the category-based phonemics task ($\beta = 0.22$, $p < 0.05$, $df = 88$). Greater left laterality of orientation dispersion in the caudate was associated with higher initial-letter phonemic scores ($\beta = 0.19$, $p < 0.05$, $df = 92$), while greater right laterality of neurite density was linked with higher semantic scores ($\beta = -0.23$, $p < 0.05$, $df = 93$). The NDI laterality associations can be found on Figure 29.

NEPSY-II Diagnosis Interaction Effects. There were no significant interaction effects of group on the relationship between the NDI and ODI of our 12 brain regions and NEPSY-II verbal fluency scores.

SRT Results: Transdiagnostic Approach.

As a result of technical issues, some inaudible voice recordings in quiet children, and some participants refusing to do the task, we had scores for 115 out of the 196 children. Across all 18 words, there were 50 total phonemes. The full explanation of overall group means is detailed in the Study 1 results section and is summarized on the bottom of Table 3.

We ran robust regression models to test the association between the ODI and NDI of 12 brain regions and SRT phonemic articulation, controlling for age, sex, whole brain microstructure, movement in the scanner, and SES. We found that the right preSMA NDI was positively related to higher SRT scores ($\beta = 0.18$, $p < 0.05$, $df = 104$), which is further supported by increased right laterality of the region

being associated with higher SRT scores as well ($\beta = -0.20$, $p < 0.05$, $df = 104$). Lastly, greater left laterality, as measured by ODI, in the putamen was related to higher SRT scores ($\beta = 0.15$, $p < 0.05$, $df = 106$).

SRT Results: Categorical Diagnosis Approach.

We compared the differences between the TD and ADHD samples, with the purpose of examining whether the relationships between brain regions and phonemic articulation were affected by diagnosis. We found that the TD group significantly outperforms the ADHD group ($\beta = -0.19$, $p < 0.05$, $df = 110$). The TD sample had an 86.19% average accuracy on the task, while ADHD had 78.98% average accuracy. The following analyses will examine whether the FAT was differentially related to SRT in the TD and ADHD samples.

SRT Main Effects for TD Sample. In the typically developing sample, the only significant association we found was that increased neurite density in the right preSMA has a positive relationship with better phonemic articulation ($\beta = 0.20$, $p < 0.05$, $df = 47$). No significant laterality associations were found.

SRT Main Effects for ADHD Sample. Similar to what was seen in the TD sample, we found that higher NDI in the right preSMA was associated with higher SRT scores in the ADHD sample, but to a greater extent ($\beta = 0.33$, $p < 0.05$, $df = 50$). Secondly, we also see higher right laterality of neurite density in the preSMA was related to better SRT scores ($\beta = -0.47$, $p < 0.05$, $df = 50$).

SRT Diagnosis Interaction Effects. There were no significant interaction effects of group on the relationship between the NDI and ODI of our 12 brain regions and SRT phonemic articulation scores. All significant relationships between brain regions and speech and language scores can be found on Table 14.

4.3.2 Executive Function Findings

NIH Toolbox Results: Transdiagnostic Approach.

First, we analyzed our data without consideration to ADHD diagnosis, with the purpose of examining whether the 12 brain regions were associated with executive function in the whole sample when measured with the NIH Toolbox Flanker and DCCS. We had flanker data for 164 children and DCCS data for 167 out of our 196 children. We have decided to use the age-corrected standard score NIH Toolbox results, which compare the test-takers score to that of all other test takers at the same age. Table 6 displays the mean task scores and how they relate to our control variables.

Using robust regression models. we examined whether the neurite density and orientation dispersion of 12 brain regions were related to flanker and DCCS scores, controlling for sex, movement in the scanner, whole brain microstructure, and SES. Age was controlled for within the task through the use of age-corrected values. The full results for all executive function findings reported below can be found in Table 15. As seen in Figure 30, we found that increased left laterality of neurite density in the SMA was positively related to higher scores on the flanker task ($\beta = 0.20$, $p < 0.05$, $df = 153$). Higher left laterality of the orientation dispersion in SMA was also linked with higher scores on the DCCS ($\beta = 0.20$, $p < 0.05$, $df = 155$).

NIH Toolbox Results: Categorical Diagnosis Approach.

We compared the differences between the TD and ADHD samples, with the purpose of examining whether the association between brain regions and executive function was affected by ADHD diagnosis. We found group differences on NIH toolbox tasks between TD and ADHD, which are outlined on Table 7 and displayed in Figure

14. The differences we found persisted even when controlling for age, sex, and SES. We found that the TD group greatly outperforms the ADHD group on both flanker ($\beta = -0.34, p < 0.0001, df = 161$) and card sort tasks ($\beta = -0.27, p < 0.0001, df = 163$). We looked at this more closely by examining the TD and ADHD groups individually.

NIH Toolbox Main Effects for TD Sample. Upon examining the TD group separately, we find that decreased neurite density in the left SMA was associated with higher flanker scores ($\beta = -0.27, p < 0.05, df = 67$). When we examined orientation dispersion, we found many brain regions associated with executive function. Specifically, we found that the ODI of the left and right SMA ($\beta = -0.26, p < 0.05, df = 68$; $\beta = -0.29, p < 0.05, df = 68$, respectively), left Op ($\beta = -0.31, p < 0.05, df = 70$), and right preSMA ($\beta = -0.27, p < 0.05, df = 69$) were all negatively associated with DCCS scores. Higher orientation dispersion was also linked with lower flanker scores in 10 out of 12 regions that we examined, including the left and right preSMA ($\beta = -0.28, p < 0.05, df = 67$; $\beta = -0.24, p < 0.05, df = 68$, respectively), left and right SMA ($\beta = -0.31, p < 0.05, df = 67$; $\beta = -0.28, p < 0.05, df = 67$, respectively), the left Op ($\beta = -0.26, p < 0.05, df = 69$), the left Tri ($\beta = -0.30, p < 0.05, df = 69$), the left and right caudate ($\beta = -0.34, p < 0.01, df = 69$; $\beta = -0.30, p < 0.05, df = 69$, respectively), and the left and right putamen ($\beta = -0.23, p < 0.05, df = 69$; $\beta = -0.25, p < 0.05, df = 69$, respectively). All ODI results are plotted in Figure 31 for direct comparison.

Laterality of orientation dispersion also plays a role in executive function performance on the NIH Toolbox tasks. Greater left laterality of the preSMA and SMA ($\beta = 0.27, p < 0.05, df = 68$; $\beta = 0.27, p < 0.05, df = 68$, respectively) was related to better outcomes on the DCCS task, while greater right laterality of the Op was associated with higher scores on the same task ($\beta = -0.30, p < 0.05, df = 70$).

Lastly, greater left laterality of the preSMA was associated with better scores on the flanker task ($\beta = 0.26$, $p < 0.05$, $df = 67$).

NIH Toolbox Main Effects for ADHD Sample. There were no significant associations between brain regions and NIH Toolbox scores for the ADHD sample. The direct relationships were all in the negative direction, but none reached significance.

NIH Toolbox Diagnosis Interaction Effects. Results indicated that ADHD directly moderated the relationship between the left SMA NDI and flanker scores ($\beta = 0.13$, $p < 0.05$, $df = 152$). Within the TD group, lower neurite density in the left SMA was related to better flanker scores ($\beta = -0.26$, $p < 0.05$, $df = 67$), while it did not have a significant impact on the ADHD sample. As shown in Figure 32, both the TD and ADHD group showed a decline in scores with an increase of left SMA NDI, but the TD group had a much stronger relationship, thus causing a significant interaction.

We also discovered that ADHD diagnosis affected the relationships between preSMA and Op ODI laterality and DCCS scores ($\beta = -0.15$, $p < 0.05$, $df = 155$, $\beta = 0.15$, $p < 0.05$, $df = 156$, for preSMA and Op, respectively). For the TD sample, greater left laterality of the preSMA ODI was associated with better DCCS scores ($\beta = 0.27$, $p < 0.05$, $df = 68$), while laterality had no significant effect within the ADHD sample. While laterality of the preSMA was not significant within the ADHD group, the relationship was still in the same, positive direction, just to a much smaller extent. Lastly, we found that right laterality of the Op ODI was related to higher scores on the DCCS task in the TD sample ($\beta = -0.30$, $p < 0.05$, $df = 70$), while having no affect in the ADHD sample. These interactions are pictured in Figure 33.

HTKS: Transdiagnostic Approach.

First, we analyzed our data without consideration to ADHD diagnosis, with the purpose of examining whether brain regions were related to executive function in the full sample when measured with the HTKS. We will use the HTKS total scores for all 3 parts. The score can range from 0 to 60, depending on how accurately the child did each pair-switch. 179 out of 196 children in our full sample completed the task with an average score of 32.68. We saw a very high correlation with age ($\beta = 0.45$, $p < 0.001$, $df = 177$), sex ($\beta = -0.21$, $p < 0.001$, $df = 177$), and whole brain microstructure ($\beta = 0.26$, $p < 0.001$, $df = 177$), and no significant association with SES. Overall, older children performed better on the task, with female participants outperforming males, and a positive association with overall brain microstructure integrity and HTKS performance. The full break down can be found on Table 6.

Using robust linear models to test associations between brain regions and HTKS performance, we found that higher neurite density in the right *pars triangularis* region were associated with higher scores ($\beta = 0.16$, $p < 0.001$, $df = 170$). None of the other 11 brain regions were associated within the full sample, and no relationships with brain laterality were found.

HTKS Main Effects for TD Sample. Out of the 96 children in the TD sample, we had HTKS data for 85. Higher neurite density in the right Tri was related to higher HTKS scores ($\beta = 0.25$, $p < 0.05$, $df = 78$). Orientation dispersion, much like the NIH Toolbox results suggested, was negatively associated with executive function on the HTKS task. In particular, higher ODI in the the left preSMA ($\beta = -0.21$, $p < 0.05$, $df = 76$), the left and right SMA ($\beta = -0.23$, $p < 0.05$, $df = 76$; $\beta = -0.23$, $p < 0.05$, $df = 76$, respectively), left caudate ($\beta = -0.24$, $p < 0.05$, $df =$

78), and right putamen ($\beta = -0.21$, $p < 0.05$, $df = 78$) were all negatively related to HTKS scores.

Right laterality of neurite density in the inferior frontal gyrus was associated with better executive function performance. Specifically, greater right laterality of the Op ($\beta = -0.23$, $p < 0.05$, $df = 78$) and Tri ($\beta = -0.23$, $p < 0.05$, $df = 78$) regions were both linked to higher scores on HTKS.

HTKS Main Effects for ADHD Sample. Out of the 100 children in the ADHD sample, we had HTKS data for 94. No significant direct or laterality associations were found for this sample using NODDI metrics.

HTKS Diagnosis Interaction Effects. No significant moderator effect of ADHD diagnosis was discovered for HTKS performance with any metric or brain region.

4.4 Discussion

NODDI is a novel diffusion model that offers enormous promise for illuminating microstructural processes involved in brain development. Through the use of NODDI metrics, our study provided further evidence of how myelination and synapse formation increase across maturation in the developing brain during the formative preschool years. We found that certain brain regions, particularly the right *pars opercularis* and the bilateral caudate and putamen, show a pattern of neurite density increase that is significantly different from that of the whole brain. Further, our findings suggest that children diagnosed with ADHD have lower NODDI neurite density and higher orientation dispersion than typically developing children. While this hasn't been tested with NODDI previously to our knowledge, these findings confirm past work (Wu et al., 2019) that has also found lower neurite density in ADHD populations through the use of return-to-orientation probability (RTOP).

We also showed that orientation dispersion is decreasing between the ages of 4 to 7 in the ADHD sample but not in the typical sample. Taken together, this could indicate that children with ADHD have delayed myelination and synaptic formation, as well as less coherent neural organization. Neurite density and neural coherence differences between our TD and ADHD sample can potentially explain executive function outcomes for children with ADHD.

Relationships between brain regions and speech and language. Our results indicated, regardless of ADHD diagnosis, higher neurite density within the right preSMA was associated with better phoneme articulation. We expected phoneme articulation to be dependent on the left SMA, which is frequently associated with speech production (Bohland and Guenther, 2006; Vergani et al., 2014), rather than the preSMA, which handles higher-order motor control and linguistic processing (Vergani et al., 2014; Zentgraf et al., 2005). While unexpected, the association between right preSMA and SRT coincides with previous work showing that the right preSMA is involved in speech motor control (Aron and Poldrack, 2006) and conflict resolution between competing associations involved in speech production (Ter Minassian et al., 2014). Therefore, we stipulate that young children required the right preSMA to be well-developed in order to inhibit off-target words within the SRT. Besides being a speech articulation task, the more difficult target words (such as 3 and 4 syllable nonsense target words), tax working memory and motor control, so our findings implicate that the right preSMA might contribute to improved performance.

A second surprising finding was that higher left laterality of the SMA was associated with semantic scores in the typically developing sample. In Study 1, we found evidence to support the right hemisphere FAT having a greater association with semantic tasks while the left hemisphere FAT handled phonemic tasks, so we

expected higher right laterality in the SMA to be related with semantic scores. A potential reason for this conflicting result could be the difference between looking at structural connectivity, such as the FAT, compared to region-based neurite density. Greater left laterality of the SMA region might be associated with improved semantic fluency when the region is examined independently, while the structural connection between the SMA and inferior frontal gyrus could benefit from right lateralization for the same task.

In the ADHD sample, the laterality of the caudate confirmed our hypothesis that left hemisphere is involved with phonemics while right is involved in semantic tasks. We find that higher left laterality of caudate ODI and SMA NDI is associated with better NEPSY initial-letter phonemic scores and higher right laterality of caudate NDI is associated with NEPSY category-based semantic fluency. Interpretation of ODI can be two-fold: higher ODI is frequently linked to a less efficient brain network and higher neurite incoherence (Genc et al., 2018; Mah et al., 2017), but it can also indicate higher gray matter complexity and greater connectivity (Morris et al., 2018; Andersson et al., 2003; Zhang et al., 2012).

While we had more significant findings for the ADHD sample than the TD sample for language tasks, all directions were in the same direction and had a similar slope. TD was trending for many of the same associations found in ADHD, and no significant interactions were found. This indicates that differences between neurite density and dispersion within the 12 brain regions we examined in the TD and ADHD samples cannot explain the differences seen in language and speech articulation seen between the groups.

Differential associations between brain regions and executive function.

When we examined the relationships between our 12 brain regions and executive function performance, we found many consistent results within the TD sample. We

found that lower neurite density in the left SMA was associated with higher scores on the flanker task, possibly indicating that proper synaptic pruning in this region caused the lower NDI and improved performance. Lower NDI's relation to better behavioral outcomes is not unheard of; Genc and colleagues have previously reported that lower NDI is associated with higher IQ, processing speed, and a more efficient neural network (Genc et al., 2018).

When orientation dispersion was observed, we found 10 brain regions were associated with flanker task performance. Within the left and preSMA, left and right SMA, left *pars opercularis*, left *pars triangularis*, and left and right caudate and putamen, lower ODI values were related to better performance on the flanker task. Since low ODI values can indicate higher neurite coherence within the area, we take these results to mean that greater organization within these brain areas can potentially be linked to executive function performance in a typically developing sample. Majority of our findings show that both left and right hemisphere contribute to executive function outcomes, implicating a distributed organization of the developing brain. Both left and right preSMA were related to flanker, but laterality analyses showed that higher right laterality of the region was associated with better scores.

Our results suggested that the prefrontal cortex regions were related to task-switching ability, as measured by the DCCS, in the TD sample. In particular, lower orientation dispersion, therefore higher neural coherence, in the right preSMA, left and right SMA, and left Op was associated with better scores on the NIH Toolbox DCCS. This was further supported with laterality analyses. Our findings fit into current literature which shows that the pre-SMA and SMA are related to rapid response/rule switching and inhibitory control (Aron, 2007; Crone et al., 2006; Gruszka et al., 2017; Nachev et al., 2007; Smith et al., 2004), which are required to inhibit a response when the rules of the DCCS game change.

Given the many executive function factors that the HTKS task taps into, it comes as no surprise that many regions of the brain were associated. In the TD sample, lower neurite orientation dispersion in the left preSMA, left and right SMA, left caudate, and right putamen, as well as higher neurite density in the *pars triangularis*, contributed to better HTKS performance. Furthermore, right laterality of neurite density within the *pars opercularis* was associated with improved executive function outcomes as well. These findings further support preSMA and SMA's involvement in rule switching mentioned above, and also confirm previous studies on adults that have shown the right inferior frontal gyrus is important for inhibitory control (Aron et al., 2014; Hampshire et al., 2010; Hughes et al., 2013; Swann et al., 2012).

The striatum's association with executive function on the HTKS task partially confirmed our hypotheses. In our typical sample, greater neurite organization in the right putamen was linked to better HTKS performance, which coincides with previous studies showing that right putamen being related to inhibitory control and motor cancellation (Ardila et al., 2018; Guo et al., 2018). We hypothesized that the right caudate would be associated with executive function, given its relation to set-shifting (Svegar et al., 2016), but our results show that orientation dispersion in the left caudate was related to better HTKS scores. This was surprising, but not unheard of; De Simoni et al. (2018) found that the left caudate consistently predicted switching on the Stroop inhibition task. While we expected more right hemisphere regions to be associated with executive function tasks, both hemispheres are involved. This could be attributed to the right hemisphere handling inhibition while the left hemisphere is responsible for reasoning (Ardila et al., 2018).

While the relationships between the TD and ADHD samples were similar, three significant interactions were identified. Specifically, we found that ADHD diagnosis moderates the relationship between left SMA NDI and flanker scores, with lower

neurite density in the region significantly improving flanker scores ($\beta = -0.27$, $p < 0.05$), while having a much smaller effect within the ADHD group ($\beta = -0.11$, $p > 0.05$). Similar associations were seen with orientation dispersion laterality within the preSMA and Op in relation to rule-switching behavior in the DCCS. We found that higher left laterality of the preSMA and higher right laterality of the Op in the TD sample were both associated with better performance during card sort, while laterality relationships were insignificant for the ADHD sample. This could indicate that children with ADHD do not benefit from neurite density and orientation in the same way that typically developing children do, indicating differences in microstructural brain development. This will be further discussed in the general discussion.

Limitations and future directions. It is important to note that white matter of the brain is saturated with long-range myelinated axons, and contains significantly fewer cell bodies than gray matter (Purves, 2008). Therefore, NODDI might be missing important findings within our white matter prefrontal cortex regions given the lower number of neurites. Secondly, while we examined 12 brain regions, previous work has also implicated differences in the hippocampus and thalamus as being associated with ADHD symptomatology (Rubia, 2018; Hoogman et al., 2017; Zepf et al., 2019), so the neurite characteristics of these regions could be examined in the future.

Conclusions. This study provides novel information about neurite density characteristics within an ADHD sample. We found that, compared to the typically developing group, children in the ADHD sample displayed lower neurite density and higher neurite orientation dispersion throughout the brain, possibly indicating delayed synapse formation and increased axonal fanning. When examining brain-behavior associations across the full sample of typically and atypically developing

children, we found that the neurite density within the right hemisphere preSMA directly contributed to increases in phonemic articulation, while right laterality of the striatum was related to improved semantic fluency and articulation. Regardless of ADHD diagnosis, the transdiagnostic approach revealed that the right *pars triangularis* and right laterality of the SMA were associated with executive function ability. When ADHD diagnosis was added in as an interaction variable, we found that children diagnosed with ADHD do not benefit from neurite microstructure within the preSMA, SMA, and *pars opercularis* to the same degree as those in the TD group. Findings in this study imply that ADHD might be characterized by aberrant brain maturation patterns that could explain differences seen in executive function ability.

CHAPTER 5

GENERAL DISCUSSION

5.1 Summary

This current dissertation set forth to answer the following four questions: Does the frontal aslant tract (FAT) show age-related differences during the sensitive developmental period between 4- to 7-years of age, and do age-related differences differ in children diagnosed with ADHD? Can the microstructural properties of the FAT explain the differences in language and executive function outcomes in children with and without ADHD? Are novel diffusion weighted imaging (DWI) methods capable of reliably mapping neurite density in children and adults and expanding what we currently know about brain microstructure and maturation? If so, are neurite density and orientation within prefrontal and subcortical brain regions associated with behavioral outcomes in typically and atypically developing children? Through the use of multiple DWI methods and a battery of language and executive function behavioral measures, we conducted three separate studies to answer these questions.

In Study 1, we introduced the FAT, a long association white matter pathway that has recently been evaluated in terms of its association with the development of language and executive function (Catani et al., 2013; Dick et al., 2019; Garic et al., 2019; Mandelli et al., 2016). We examined 196 4- to 7-year-old children, 100 of whom had been diagnosed with ADHD, tracked 4 bilateral segments of the pathway, and mapped the age-related differences using the 4 most common diffusion tensor imaging (DTI) metrics (fractional anisotropy (FA), axial diffusivity (AD), radial diffusivity (RD), and mean diffusivity (MD)) and three most common high angular resolution diffusion imaging (HARDI) metrics (generalized fractional anisotropy (GFA), quantitative anisotropy (QA), and normalized quantitative imaging (nQA)) with gener-

alized q-sampling imaging (GQI) reconstruction. We then analyzed brain-behavior associations between FAT segments and 3 speech and language tasks (NEPSY semantic fluency, NEPSY phonemic fluency, and SRT phonemic articulation) and 3 executive function measures (NIH Toolbox flanker task, NIH Toolbox dimensional change card sort task, and Head-Toes-Knees-Shoulders task). Study 1 used DTI and HADI metrics to measure age-related differences within the structural connectivity of the FAT and tested whether the fiber pathway was differentially associated with language and executive function in our TD and ADHD sample.

The 7 diffusion metrics utilized in Study 1 provide invaluable insight into the microstructural properties of the developing brain, but lack the specificity needed to directly measure neurite (axonal and dendritic) density. Axonal density has been associated with many neuropathologies, such as multiple sclerosis (Tallantyre et al., 2009), hereditary spastic paraplegia (Deluca et al., 2004), and epilepsy (Winston et al., 2014), while dendritic density has been associated with neural network efficiency and information processing (Genc et al., 2018). In Study 2, we tested whether two advanced diffusion methodologies, restricted diffusion imaging (RDI) and neurite orientation and dispersion density imaging (NODDI), can accurately match established histological models of axonal density, above and beyond that of DTI and GQI metrics, in large developing and adult samples. NODDI required multishell neuroimaging data which our developing sample in Study 2 did not meet. Hence, we explored this further in Study 3.

In Study 3, we applied the NODDI implementation to our multishell diffusion dataset from Study 1 to measure age-related differences in neurite density and orientation in typical and atypical development. We expand on the structural connectivity findings in Study 1 by examining region-based microstructure in Study 3. Using NODDI to quantify tissue structure offered us an opportunity to a) test the

model in a developing sample, which we were unable to do in Study 2, b) expand our examination of the developing brain from white matter to also include gray matter in subcortical regions since NODDI is sensitive to both white and gray matter of the brain (Zhang et al., 2012). Further, we examined whether neurite density and orientation characteristics within prefrontal and subcortical bilateral brain regions (pre-supplementary motor area (pre-SMA), SMA, *pars opercularis* (Op), *pars triangularis* (Tri), caudate, and putamen) were related to verbal fluency and executive function behavioral outcomes in young, preschool-aged children.

In this General Discussion, I review the processes that occur during typical and atypical brain development and how the age-related findings from Study 1 and Study 3 contribute to extant literature. Next, I will detail how the FAT is differentially associated with language and executive function behavioral outcomes in children with and without ADHD, followed by a discussion of the reliability of mapping neurite density *in vivo* in developing and adult samples and its relation to behavior. I end with an overview of implications of the three current studies, limitations, and future research directions.

Typical and atypical brain development. In order to fully grasp the implications of brain-behavior associations in children, it is important to first understand typical neurodevelopment. Knowledge about the neural processes that occur during brain maturation offers valuable insights for earlier identification of aberrant child development and consequently, earlier clinical diagnosis where intervention can have the greatest impact (Charach et al., 2011; Halperin et al., 2012).

Historically, it is commonly believed that the first year of life is marked by robust myelination, the process by which a fatty-lipid myelin sheath covers the axon to allow for faster electrical impulse transmission (Bean, 2007), which then slows down but gradually continues for the following four decades (Brody et al., 1987;

Yakovlev and Lecours, 1967). The plasticity seen in early development is made possible through synaptic reorganization- a cycle of synaptic formation and synaptic elimination/pruning (Goda and Davis, 2003). The processes of myelination, synaptic formation, and maturational and experience-dependent pruning have long held the interest of neuroscientists, and establishes the foundation of brain development as we understand it.

Magnetic resonance imaging (MRI) has come a long way in expanding the classic histological and animal model findings of brain maturation. Longitudinal MRI studies have consistently indicated increasing white matter and decreasing gray matter from the ages of 4 to 25 (Giedd et al., 2015; Lebel and Beaulieu, 2011). Further, DWI has indicated increasing myelin and microstructural integrity from early childhood to late adolescence, marked by increased FA and decreased RD and MD, with very little change in axonal integrity as measured by AD (Lebel and Beaulieu, 2011; Tamnes et al., 2018). Neurite density, which represents myelination and axonal growth, has also been shown to expand from the ages of 8 to 13, with very little change in orientation dispersion (ODI) (Chang et al., 2015; Mah et al., 2017).

Study 1 of this dissertation has matched previous work by showing significant increases in FA, GFA and NDI, decreases in RD, and stable ODI in the whole brain across the ages of 4 to 7. It was surprising to see MD show no age-related differences during this time period, but the FAT did show the expected age-related pattern. The FAT also moderately confirmed the previous age-related findings in the Garic et al. (2019) study that examined the FAT from infancy to the age of 18. The left FAT FA indicated an age-related increase even in the much narrower range of 4 to 7 years of age, above and beyond what could be explained by whole brain development.

For region-based age-related differences, Study 3 indicated that the neurite density of the right *pars opercularis* and bilateral regions of the striatum show significant increase across age. Mah et al. (2017) have found age-related increases in neurite density in all brain regions except the caudate in their sample of 8- to 13-year old children, but Study 3 indicates that the age-related differences in the caudate might occur before the age of 7. Regional development of neurite density in the *pars opercularis* has yet to be studied directly to my knowledge, but the age-related increases shown coincide with what is known about prefrontal cortex development with DTI (Lebel et al., 2008).

For atypical development, I will focus on what is known about ADHD, and make references to other disorders where ADHD-specific information is not available. Study 1 was the first to examine FAT development in the ADHD population, and results implicated that there are no significant differences on how the pathway develops in the ADHD sample when compared to the typically developing sample. The only difference found was that the right FAT displayed higher FA and lower RD in the ADHD group, indicating more structural integrity and myelination when compared to the TD group. This comes as a sharp contrast to what is seen in other disorders, such as autism spectrum disorder, in which the FAT shows reduced structural integrity compared to TD (Chien et al., 2017; Lo et al., 2017). The results of Study 1 could implicate that the FAT in children with ADHD could be more developed, but still not result in increased task performance like what is seen in the brain-behavior associations within the typically developing sample. This will be discussed further in the next section.

Previous work has primarily implicated lower volume in the right hemisphere caudate and putamen in children with ADHD (Frodal and Skokauskas, 2012; Lu et al., 2019; Qiu et al., 2009; Valera et al., 2007; Wang et al., 2007), as well as

decreased white matter volume in the left inferior frontal gyrus (Kumar et al., 2017). There is increasing evidence to show that the left caudate (O'Dwyer et al., 2016; Wu et al., 2019; Qiu et al., 2009) and left anterior putamen (Qiu et al., 2009) also have reduced volume. Kaya et al. (2018) have argued that gray matter findings in an ADHD population are not consistent, and their study indicates that there might be an increase of gray matter volume within the supplementary motor area in children and adolescents with ADHD, while Qiu et al. (2009) have also found an increase in volume in the bilateral posterior putamen, but only in boys. Inconsistencies across studies is most likely attributed to small sample size of clinical populations ($n = 12$ in some cases). Study 3 aimed to clarify these results by using a large sample of 196 children, 100 of which were diagnosed with ADHD. Results suggest that there is increased neurite density in the left *pars opercularis* and left caudate when compared to the typically developing sample. Neurite density can be interpreted as the inverse of cortical volume (Genc et al., 2018), therefore our inferior frontal gyrus, *pars opercularis*, finding replicated what was seen in Kumar et al.'s work, as well as found more evidence for left hemisphere caudate tissue differences in atypically developing children.

Overall, the process of synaptic formation and elimination in the developing brain sets the stage for neural efficiency. Through maturation and experience-dependent pruning, the brain reduces unnecessary and unused synapses and dendrites in order to increase processing speed and reasoning (Genc et al., 2018; Merolla et al., 2014). In adults, lower neurite density and axonal fanning have been associated with higher intelligence and faster information processing (Genc et al., 2018), but this has not been tested on a clinical, ADHD developing population until this dissertation. Our results indicate that neurite density increases across development for both the ADHD and TD groups, implicating that myelination and synapse formation are

still robustly occurring. Further, the ADHD sample displayed significantly lower neurite density across the brain, hinting that there is delayed myelination and brain development, along with decreased pruning and organization seen in the inferior frontal gyrus and left caudate, regions that are known to be involved in language and executive function. Interestingly, while we found group differences in neurite density and orientation, the developmental slopes for TD and ADHD were not significantly different, suggesting that the two groups have a different starting point but share similar neurite development patterns. This might indicate that the microstructural differences are present before four years of age. The impact of regional neurite density differences on behavioral outcomes will be discussed next.

FAT as a biomarker for ADHD. Study 1 has provided further evidence of the FAT's association in both language and executive function outcomes, and has extended this to a clinical, ADHD population. For semantic fluency, results indicated that increased structural integrity of the right hemisphere FAT was associated with higher semantic performance in the typically developing group, while it was significantly associated with lower performance in the ADHD group. This can partially be explained when examining laterality; semantic fluency has been associated with the right hemisphere in adults (Blecher et al., 2019; Thompson et al., 2016; Rodriguez-Aranda et al., 2016), but results indicate that the ADHD group favor the left hemisphere for improved performance on this task. Significant interactions between the TD and ADHD groups were observed for the right FAT's association with semantic fluency, as well as laterality of the FAT. Results suggest ADHD specifically moderates the FAT's relation to verbal fluency and not to other speech and language aspects, such as phonemic fluency or phonemic articulation. Put together, Study 1 results provide novel indication that the differential association between

both the right FAT and FAT laterality could explain the lower semantic verbal fluency observed in children with ADHD.

Executive function has been the most consistent, core deficit found in ADHD across decades of research, frequently persisting into adulthood (i.e., Barkley 1997; Magnin and Maurs 2017; Pennington and Ozonoff 1996; Sergeant et al. 2002). Results from Study 1 support these findings and indicate that typically developing children greatly surpassed children in the ADHD sample on all three executive function tasks (all $p < 0.001$). Increased myelination and structural integrity of the bilateral FAT was linked with better attentional control and planning and monitoring behaviors as tested by NIH Toolbox tasks, regardless of ADHD diagnosis. Group differences only became strikingly apparent when brain-behavior associations between the FAT and motor executive function ability, as tested by the HTKS, were examined. Regardless of whether FA, RD, MD, GFA, or QA diffusion metrics were used, all indicated that the FAT was negatively associated with HTKS scores in the ADHD sample, which was the opposite of what was seen in the TD sample as well as other executive function tasks. We observed that ADHD diagnosis moderates the relationship between the left and right FAT and motor executive function performance, with higher integrity of the pathway being associated with higher scores for the TD group and lower scores for the ADHD group.

We stipulate that the FAT is differentially related to HTKS performance but not NIH Toolbox task performance because 1) the HTKS task is potentially more ecologically valid than the iPad-based NIH Toolbox tasks and 2) this fiber pathway might be particularly sensitive to motor inhibition. First, the HTKS has been shown to be a very ecologically valid task for examining self-regulation because of the real-time interaction between participant and examiner, and is strongly related to both teacher ratings of behavior regulation in the classroom as well as academic

performance in math and literacy (Wanless et al., 2011). Therefore, the FAT might have been associated to HTKS but not the NIH Toolbox tasks because the HTKS is more sensitive to self-regulation in a real-world setting. Secondly, the FAT connects the preSMA to the inferior frontal gyrus, regions that, alongside the basal ganglia, are thought to play critical roles in the motor inhibitory network (Aron et al., 2007), alongside the basal ganglia. The inverse relationship between structural integrity of the FAT and HTKS performance in the ADHD group was surprising, but we will offer a few plausible explanations below.

Similar to the language findings discussed previously, the differing association between FAT structural integrity and HTKS might be partially explained by differences in brain laterality. Consistent with current literature that implicates the right hemisphere's association with visuospatial and inhibitory control tasks (Aron, 2007; Herve et al., 2013; Toga and Thompson, 2003), higher right laterality of the FAT was strongly related to improved motor executive function performance in typically developing children in Study 1. ADHD diagnosis moderates the association between FAT laterality and motor executive function, with higher left laterality of the FAT being associated with improved scores in the ADHD sample and higher right laterality being related to higher scores for the TD sample. Atypical tract laterality association might explain why children with ADHD perform worse on motor executive control tasks.

Alternative hypotheses for the differential relationship between the FAT and motor executive performance could be group differences in regional microstructure and/or differential brain-behavior associations between TD and ADHD. Upon examining regional density and neurite orientation dispersion in Study 3, we found that participants in the ADHD sample had significantly higher neurite density in the left Op than the TD sample. As previously mentioned, higher neurite den-

sity could indicate delayed synaptic pruning during development, and can reduce network efficiency and processing speed (Genc et al., 2018; Merolla et al., 2014). Therefore, stronger structural connectivity between the Op and the superior frontal regions (which comprise the FAT) could be hindering performance for the ADHD sample since our results suggest that the Op might have delayed synaptic pruning for that sample.

Secondly, there is still disagreement within the field when it comes to interpreting the directionality of DWI findings and what it could implicate for brain-behavior associations. It is commonly believed that higher FA values would be positively associated with behavioral outcomes, but whether this holds true for the ADHD population is still debatable. Neuropathology is frequently linked with a significant reduction in FA (Alexander et al., 2007), but previous studies have found both increases (Silk et al., 2009; Tamm et al., 2012) and decreases (Hamilton et al., 2008) in FA within many white matter pathways in children with ADHD. In Study 1, we found that the right FAT had higher FA and lower RD in the ADHD versus the TD sample, but this was inversely related to motor EF performance for the ADHD group and positively related in the TD group. While unexpected, this is in line with recent findings from Bessette and Stevens (2019), who found a similar pattern of results when they examined numerous pathways and delay aversion task performance. Bessette and colleagues found that higher FA in many pathways, such as the corpus callosum and inferior and superior longitudinal fasciculus, predicted better EF outcomes for TD, while predicting lower scores for ADHD. Taken together, this could indicate widespread alterations of brain-behavior relationships in the ADHD population. The findings from Study 1 and Study 3 offer some evidence that differential brain-behavior associations could result from atypical development, but more work will be needed to rule out whether children with ADHD compensate by relying

on different brain regions and fiber pathways for these tasks (Chiang et al., 2015; Fassbender and Schweitzer, 2006).

Lastly, it is important to note that experience has a fundamental impact on brain-behavior associations. The studies that comprise this dissertation have focused on how brain regions and associated structural connectivity are related to behavior, but the relationships between the brain and behavior can be bidirectional. We do not wish to imply that microstructural properties of brain regions and fiber pathways are solely responsible for behavioral outcomes, because behavior and experience can also impact neural properties. The impact of environment on development can begin prior to birth. In-utero risk factors, such as exposure to cigarette smoke (Kovess et al., 2015; Langley et al., 2012; Mulligan et al., 2013) and alcohol (Aronson et al., 1997), have been linked with later ADHD diagnosis. Further, experience- and activity-dependent maturation can greatly contribute to synaptic pruning (Sweatt, 2016). Therefore, the experiences and environment of participants in our study could be impacting the relationships we observed. We need to consider more comprehensive models, such as the dynamic developmental theory of ADHD, proposed by Sagvolden et al. (2005), which suggests that the core behavioral aspects of ADHD, such as inattention and impulsivity, can arise from a hypofunctioning dopamine system if it is also present in the context of inconsistent parenting and an unpredictable external environment.

Relationship between regional neurite density and behavioral outcomes. In Study 2, we established that NODDI can accurately replicate a histological corpus callosum density model in healthy adults. We expanded on this in Study 3 by applying the model to a large developing sample and testing its relationship to behavioral outcomes. Study 3 was an exploratory investigation on whether regional

neurite density, as measured by the NODDI model, is associated with language and executive function outcomes in typically and atypically developing children.

Our findings suggest that higher regional neurite density, particularly in the right preSMA, are related to higher phonemic articulation in both children with and without ADHD. As Schmitz et al. (2019) have recently suggested, NODDI appears to be particularly sensitive to brain laterality, therefore the majority of Study 3 brain-behavior associations seen in Study 3 were derived from laterality analyses. Across both TD and ADHD samples, we find that higher right laterality of neurite density within the caudate and preSMA is associated with better semantic fluency and phonemic articulation, respectively. Further, we found that higher right laterality of neurite organization, as measured by reduced ODI, in the putamen is related to better articulation. Higher right laterality relating to better semantic scores was expected given previous adult studies (Blecher et al., 2019; Thompson et al., 2016; Rodriguez-Aranda et al., 2016), but the association between higher right laterality and phonemic articulation was an unexpected finding that was not indicated in structural connectivity findings in our Study 1. This suggests that the right preSMA and putamen, which have been associated with speech motor control (Vergani et al., 2014; Zentgraf et al., 2005) and motor planning (Foundas et al., 2013), might also play an important role in halting incorrect articulation during speech production. Lastly, our findings found no significant group interactions on language tasks, likely indicating that neurite microstructure differences within prefrontal regions did not contribute to the FAT's differential association with language and executive function.

Examining executive function outcomes in our typically developing sample revealed that 10 out of 12 brain regions observed were associated with overall executive function across measures. This speaks to the complex, distributed network in the brain that contributes to executive function, in which no single region is indepen-

dently responsible for a behavior (Bettcher et al., 2016; Cole et al., 2013; Medaglia et al., 2018; Rabinovici et al., 2015). Overall, lower neurite density and orientation were linked to better outcomes, implicating that synaptic pruning and more concise, organized dendritic architecture are associated with better cognitive performance in typically developing children.

Surprisingly, no direct brain-behavior associations reached significance when examining the ADHD sample independently. Instead, we found significant group interaction effects that implied that neurite microstructure was similarly related to behavioral outcomes between the groups, but to a lesser extent in children with ADHD. Specifically, we found that ADHD diagnosis moderates the association between left SMA neurite density and inhibition and attention, as tested by the flanker task. Lower neurite density within the left SMA, possibly indicating the effects of synaptic pruning, was associated with higher flanker scores for the TD sample ($\beta = -0.27$) but had a significantly smaller effect on the ADHD sample ($\beta = -0.11$). Similar results were observed with laterality of the preSMA and *pars opercularis* (Op) in relation to task-switching, with the TD group benefiting from higher right laterality in the preSMA and higher left laterality in the Op, while only being weakly associated in the ADHD sample. Differences in laterality's relation to behavior were also seen in Study 1 when structural connectivity of the FAT was examined. Both structure and connectivity laterality differences might be partially resulting from a significant increase of neurite density in the left Op in the ADHD sample, suggesting a lower level of pruning.

It is important to note, that in the speech and language tasks, it appears that higher regional neurite density was associated with better performance, while higher orientation dispersion (ODI) was related to worse performance. For executive function tasks, ODI is still negatively associated with performance, but neurite density

is now related to worse outcomes as well. This could potentially be attributed to the idea that higher neurite density reduces processing speed (Genc et al., 2018), a vital aspect of executive function. Study 3 provides novel evidence that the interpretation of NODDI’s NDI metric in developing children could be dependent on whether the task is probing language or executive function ability.

5.2 Implications

In this dissertation, we have provided compelling, preliminary evidence to show that the frontal aslant tract has the potential to be used as an early biomarker for ADHD in young, preschool-aged children. Our findings suggest that the structural connectivity of the pathway might be differentially related to language and executive function outcomes in children with and without ADHD, specifically for semantic verbal fluency and motor executive function. Further, our findings imply that one specific region of the frontal aslant tract, left *pars opercularis*, displays delayed synaptic pruning in ADHD compared to the typically developing sample.

The ability to identify consistent and reliable biomarkers for ADHD in preschool children can have great implications for improving treatment and intervention programs. Preschool is a critical social and cognitive developmental period in which many of the symptoms of ADHD first become apparent. Targeted interventions that begin in preschool have been associated with improved developmental trajectories for children diagnosed with ADHD (Halperin et al., 2012). In particular, many of the adverse outcomes of ADHD, such as later emotion dysregulation and academic difficulties, can be avoided if treatment is applied during preschool years when the development is displaying the highest rates of neural plasticity (Halperin and Healey, 2011; Halperin et al., 2012; Sonuga-Barke et al., 2011). Biomarkers for ADHD can potentially be used as non-biased indicators for treatment response or as

future targets for non-invasive brain stimulation. By identifying brain regions and pathways associated with ADHD, this can hold clinical implications by allowing for more effective, targeted treatment plans to be designed to improve outcomes for young children diagnosed with ADHD.

Lastly, this is the first study to examine neurite density imaging in an ADHD population and one of the first to associate neurite density to behavior outcomes in young children. With increasing availability of high resolution multishell neuroimaging datasets for developing samples and with the use of the Microstructure Diffusion Toolbox (Harms et al., 2017) to significantly reduce computation time, Study 3 further implicates that the NODDI model is a promising tool for future examination of neural tissue structure in young children. Neurite density index (NDI) is very sensitive to age-related differences, but can be difficult to interpret in developing samples due to robust myelination and synaptic pruning occurring concurrently. Therefore, interpretation of neurite density in young children might be task-dependent. Orientation dispersion index (ODI), on the other hand, was routinely negatively associated with behavioral outcomes, regardless of task or typical or atypical participant sample. While it is not sensitive to age-related differences, ODI could offer a more consistent measurement of brain-behavior associations within the developing brain.

5.3 Limitations

There are a few important limitations to consider when interpreting the findings of this dissertation. First, given the sparsity of NODDI implementation in this age group, as well as the absence of previous work examining neurite density in children with ADHD, our findings are all tentative and would need further replication. Secondly, we examined the caudate and putamen using a Lausanne atlas parcellation,

which did not differentiate between head, body, or tail of the caudate or the dorsal and ventral putamen. Neurite density and orientation characteristics could potentially differ among specific regions of the caudate and putamen, and our results only reflect the average tissue microstructure.

The ADHD sample was comprised of combined (ADHD-C), primarily inattentive (ADHD-I), and primarily hyperactive/impulsive (ADHD-HI) subtypes. Since 87% of our ADHD sample was diagnosed with ADHD-C, our results will most likely be less applicable to children who fall into the ADHD-I or ADHD-HI subtypes. This limits the applicability of our findings because previous work from Saad et al. (2017) has suggested that ADHD subtypes might each have their own connectivity and neural organization profiles. In particular, differing strengths of connection between the anterior cingulate, putamen, and middle frontal gyrus were seen between ADHD-C and ADHD-I, which could impact how our results apply to children who are diagnosed as primarily ADHD-inattentive. Lastly, ADHD is comorbid with speech language impairment and oppositional defiant disorder (Efron and Sciberras, 2010; McGrath et al., 2008; Taurines et al., 2010), therefore some of our results may not be specific to ADHD. This is particularly important to consider for speech language impairment, which frequently preceded ADHD diagnosis in our sample and could alter interpretations.

5.4 Future Directions

The current dissertation contributes to the overall understanding of typical and atypical brain development and suggests a novel biomarker for ADHD. While the research benefited from large sample sizes, this came at the cost of relying on cross-sectional rather than longitudinal neuroimaging data. In the future, longitudinal data would allow us to observe whether the structure and connectivity of the prefrontal cortex

shows direct developmental change across time. Furthermore, longitudinal studies could examine the neurobiological long-term effects of medication on the developing brain, particularly because many of our young medication-naive participants were prescribed medication within a year of participating in our study. Lastly, ADHD is a complex disorder with sub-types and differing levels of severity. Future studies could examine whether the FAT is differentially associated with behavioral outcomes in children with varying ADHD severity.

REFERENCES

- Aboitiz, F., Scheibel, A. B., Fisher, R. S., and Zaidel, E. (1992). Fiber composition of the human corpus callosum. *Brain Res*, 598(1-2):143–53.
- Achenbach, T. M. and Rescorla, L. (2000). *Manual for the ASEBA preschool forms profiles : an integrated system of multi-informant assessment*. ASEBA., Burlington, VT.
- Achenbach, T. M. and Rescorla, L. (2001). *Manual for the ASEBA school-age forms profiles : an integrated system of multi-informant assessment*. ASEBA, Brlington, VT.
- Achenbach, T. M. and Rescorla, L. (2003). *Manual for the ASEBA adult forms profiles : for ages 18-59 : adult self-report, adult behavior checklist*. ASEBA, Burlington, VT.
- Aita, S. L., Beach, J. D., Taylor, S. E., Borgogna, N. C., Harrell, M. N., and Hill, B. D. (2019). Executive, language, or both? an examination of the construct validity of verbal fluency measures. *Appl Neuropsychol Adult*, 26(5):441–451.
- Alexander, A. L., Lee, J. E., Lazar, M., and Field, A. S. (2007). Diffusion tensor imaging of the brain. *Neurotherapeutics*, 4(3):316–29.
- Amador, N. and Fried, I. (2004). Single-neuron activity in the human supplementary motor area underlying preparation for action. *J Neurosurg*, 100(2):250–9.
- Anderson, D. N., Duffley, G., Vorwerk, J., Dorval, A. D., and Butson, C. R. (2019). Anodic stimulation misunderstood: preferential activation of fiber orientations with anodic waveforms in deep brain stimulation. *J Neural Eng*, 16(1):016026.
- Andersson, J. L., Skare, S., and Ashburner, J. (2003). How to correct susceptibility distortions in spin-echo echo-planar images: application to diffusion tensor imaging. *Neuroimage*, 20(2):870–88.
- Andica, C., Kamagata, K., Hatano, T., Saito, Y., Ogaki, K., Hattori, N., and Aoki, S. (2019). Mr biomarkers of degenerative brain disorders derived from diffusion imaging. *J Magn Reson Imaging*.
- Ardila, A., Bernal, B., and Rosselli, M. (2018). Executive functions brain system: An activation likelihood estimation meta-analytic study. *Arch Clin Neuropsychol*, 33(4):379–405.
- Ardila, A. and Lopez, M. V. (1984). Transcortical motor aphasia: one or two aphasias? *Brain Lang*, 22(2):350–3.
- Aron, A. R. (2007). The neural basis of inhibition in cognitive control. *Neuroscientist*, 13(3):214–28.
- Aron, A. R., Behrens, T. E., Smith, S., Frank, M. J., and Poldrack, R. A. (2007). Triangulating a cognitive control network using diffusion-weighted magnetic resonance imaging (mri) and functional mri. *J Neurosci*, 27(14):3743–52.

- Aron, A. R., Herz, D. M., Brown, P., Forstmann, B. U., and Zaghoul, K. (2016). Frontosubthalamic circuits for control of action and cognition. *J Neurosci*, 36(45):11489–11495.
- Aron, A. R. and Poldrack, R. A. (2006). Cortical and subcortical contributions to stop signal response inhibition: role of the subthalamic nucleus. *J Neurosci*, 26(9):2424–33.
- Aron, A. R., Robbins, T. W., and Poldrack, R. A. (2004). Inhibition and the right inferior frontal cortex. *Trends Cogn Sci*, 8(4):170–7.
- Aron, A. R., Robbins, T. W., and Poldrack, R. A. (2014). Inhibition and the right inferior frontal cortex: one decade on. *Trends Cogn Sci*, 18(4):177–85.
- Aronson, M., Hagberg, B., and Gillberg, C. (1997). Attention deficits and autistic spectrum problems in children exposed to alcohol during gestation: a follow-up study. *Dev Med Child Neurol*, 39(9):583–7.
- Badcock, N. A., Bishop, D. V., Hardiman, M. J., Barry, J. G., and Watkins, K. E. (2012). Co-localisation of abnormal brain structure and function in specific language impairment. *Brain Lang*, 120(3):310–20.
- Badre, D., Poldrack, R. A., Pare-Blagoev, E. J., Insler, R. Z., and Wagner, A. D. (2005). Dissociable controlled retrieval and generalized selection mechanisms in ventrolateral prefrontal cortex. *Neuron*, 47(6):907–18.
- Banaschewski, T., Becker, K., Dopfner, M., Holtmann, M., Rosler, M., and Romanos, M. (2017). Attention-deficit/hyperactivity disorder. *Dtsch Arztebl Int*, 114(9):149–159.
- Barber, A. D., Caffo, B. S., Pekar, J. J., and Mostofsky, S. H. (2013). Effects of working memory demand on neural mechanisms of motor response selection and control. *J Cogn Neurosci*, 25(8):1235–48.
- Barkley, R. A. (1997). Behavioral inhibition, sustained attention, and executive functions: constructing a unifying theory of adhd. *Psychol Bull*, 121(1):65–94.
- Barkley, R. A. and Fischer, M. (2011). Predicting impairment in major life activities and occupational functioning in hyperactive children as adults: self-reported executive function (ef) deficits versus ef tests. *Dev Neuropsychol*, 36(2):137–61.
- Barkley, R. A. and Murphy, K. R. (2010). Impairment in occupational functioning and adult adhd: the predictive utility of executive function (ef) ratings versus ef tests. *Arch Clin Neuropsychol*, 25(3):157–73.
- Basilakos, A., Fillmore, P. T., Rorden, C., Guo, D., Bonilha, L., and Fridriksson, J. (2014). Regional white matter damage predicts speech fluency in chronic post-stroke aphasia. *Front Hum Neurosci*, 8:845.
- Basser, P. J., Mattiello, J., and LeBihan, D. (1994). Mr diffusion tensor spectroscopy and imaging. *Biophys J*, 66(1):259–67.

- Batalle, D., Hughes, E. J., Zhang, H., Tournier, J. D., Tusor, N., Aljabar, P., Wali, L., Alexander, D. C., Hajnal, J. V., Nosarti, C., Edwards, A. D., and Counsell, S. J. (2017). Early development of structural networks and the impact of prematurity on brain connectivity. *Neuroimage*, 149:379–392.
- Bean, B. P. (2007). The action potential in mammalian central neurons. *Nat Rev Neurosci*, 8(6):451–65.
- Beaulieu, C. (2002). The basis of anisotropic water diffusion in the nervous system - a technical review. *NMR Biomed*, 15(7-8):435–55.
- Bellani, M., Moretti, A., Perlini, C., and Brambilla, P. (2011). Language disturbances in adhd. *Epidemiol Psychiatr Sci*, 20(4):311–5.
- Berberian, A. A., Moraes, G. V., Gadelha, A., Brietzke, E., Fonseca, A. O., Scarpato, B. S., Vicente, M. O., Seabra, A. G., Bressan, R. A., and Lacerda, A. L. (2016). Is semantic verbal fluency impairment explained by executive function deficits in schizophrenia? *Braz J Psychiatry*, 38(2):121–6.
- Bessette, K. L. and Stevens, M. C. (2019). Neurocognitive pathways in attention-deficit/hyperactivity disorder and white matter microstructure. *Biol Psychiatry Cogn Neurosci Neuroimaging*, 4(3):233–242.
- Bettcher, B. M., Mungas, D., Patel, N., Eloffson, J., Dutt, S., Wynn, M., Watson, C. L., Stephens, M., Walsh, C. M., and Kramer, J. H. (2016). Neuroanatomical substrates of executive functions: Beyond prefrontal structures. *Neuropsychologia*, 85:100–9.
- Biederman, J., Faraone, S. V., Doyle, A., Lehman, B. K., Kraus, I., Perrin, J., and Tsuang, M. T. (1993). Convergence of the child behavior checklist with structured interview-based psychiatric diagnoses of adhd children with and without comorbidity. *J Child Psychol Psychiatry*, 34(7):1241–51.
- Biederman, J., Monuteaux, M. C., Mick, E., Spencer, T., Wilens, T. E., Silva, J. M., Snyder, L. E., and Faraone, S. V. (2006). Young adult outcome of attention deficit hyperactivity disorder: a controlled 10-year follow-up study. *Psychol Med*, 36(2):167–79.
- Bjornholm, L., Nikkinen, J., Kiviniemi, V., Nordstrom, T., Niemela, S., Drakesmith, M., Evans, J. C., Pike, G. B., Veijola, J., and Paus, T. (2017). Structural properties of the human corpus callosum: Multimodal assessment and sex differences. *Neuroimage*, 152:108–118.
- Blecher, T., Miron, S., Schneider, G. G., Achiron, A., and Ben-Shachar, M. (2019). Association between white matter microstructure and verbal fluency in patients with multiple sclerosis. *Front Psychol*, 10:1607.
- Bohland, J. W. and Guenther, F. H. (2006). An fmri investigation of syllable sequence production. *Neuroimage*, 32(2):821–41.
- Booth, J. R., Burman, D. D., Meyer, J. R., Gitelman, D. R., Parrish, T. B., and Mesulam, M. M. (2004). Development of brain mechanisms for processing orthographic and phonologic representations. *J Cogn Neurosci*, 16(7):1234–49.

- Bouziane, C., Caan, M. W. A., Tamminga, H. G. H., Schrantee, A., Bottelier, M. A., de Ruiter, M. B., Kooij, S. J. J., and Reneman, L. (2018). Adhd and maturation of brain white matter: A dti study in medication naive children and adults. *Neuroimage Clin*, 17:53–59.
- Bouziane, C., Filatova, O. G., Schrantee, A., Caan, M. W. A., Vos, F. M., and Reneman, L. (2019). White matter by diffusion mri following methylphenidate treatment: A randomized control trial in males with attention-deficit/hyperactivity disorder. *Radiology*, 293(1):186–192.
- Bozkurt, B., Yagmurlu, K., Middlebrooks, E. H., Karadag, A., Ovalioglu, T. C., Jagadeesan, B., Sandhu, G., Tanriover, N., and Grande, A. W. (2016). Microsurgical and tractographic anatomy of the supplementary motor area complex in humans. *World Neurosurg*, 95:99–107.
- Broad, R. J., Gabel, M. C., Dowell, N. G., Schwartzman, D. J., Seth, A. K., Zhang, H., Alexander, D. C., Cercignani, M., and Leigh, P. N. (2019). Neurite orientation and dispersion density imaging (noddi) detects cortical and corticospinal tract degeneration in als. *J Neurol Neurosurg Psychiatry*, 90(4):404–411.
- Broce, I., Bernal, B., Altman, N., Tremblay, P., and Dick, A. S. (2015). Fiber tracking of the frontal aslant tract and subcomponents of the arcuate fasciculus in 5-8-year-olds: Relation to speech and language function. *Brain Lang*, 149:66–76.
- Brody, B. A., Kinney, H. C., Kloman, A. S., and Gilles, F. (1987). Sequence of central nervous system myelination in human infancy. i. an autopsy study of myelination. *Journal of neuropathology and experimental neurology*, 46 3:283–301.
- Brooks, B., Sherman, E., and Strauss, E. (2010). Nepsy-ii: A developmental neuropsychological assessment, second edition. *Child Neuropsychology.*, 16:80–101.
- Cak, H. T., Cengel Kultur, S. E., Gokler, B., Oktem, F., and Taskiran, C. (2017). The behavior rating inventory of executive function and continuous performance test in preschoolers with attention deficit hyperactivity disorder. *Psychiatry Investig*, 14(3):260–270.
- Caminiti, R., Carducci, F., Piervincenzi, C., Battaglia-Mayer, A., Confalone, G., Visco-Comandini, F., Pantano, P., and Innocenti, G. M. (2013). Diameter, length, speed, and conduction delay of callosal axons in macaque monkeys and humans: comparing data from histology and magnetic resonance imaging diffusion tractography. *J Neurosci*, 33(36):14501–11.
- Cammoun, L., Gigandet, X., Meskaldji, D., Thiran, J. P., Sporns, O., Do, K. Q., Maeder, P., Meuli, R., and Hagmann, P. (2012). Mapping the human connectome at multiple scales with diffusion spectrum mri. *J Neurosci Methods*, 203(2):386–97.
- Carter, A. S., Briggs-Gowan, M. J., and Davis, N. O. (2004). Assessment of young children’s social-emotional development and psychopathology: recent advances and recommendations for practice. *J Child Psychol Psychiatry*, 45(1):109–34.

- Casey, B. J., Castellanos, F. X., Giedd, J. N., Marsh, W. L., Hamburger, S. D., Schubert, A. B., Vauss, Y. C., Vaituzis, A. C., Dickstein, D. P., Sarfatti, S. E., and Rapoport, J. L. (1997). Implication of right frontostriatal circuitry in response inhibition and attention-deficit/hyperactivity disorder. *J Am Acad Child Adolesc Psychiatry*, 36(3):374–83.
- Casey, B. J., Craddock, N., Cuthbert, B. N., Hyman, S. E., Lee, F. S., and Ressler, K. J. (2013). Dsm-5 and rdoc: progress in psychiatry research? *Nat Rev Neurosci*, 14(11):810–4.
- Castellanos, F. X., Lee, P. P., Sharp, W., Jeffries, N. O., Greenstein, D. K., Clasen, L. S., Blumenthal, J. D., James, R. S., Ebens, C. L., Walter, J. M., Zijdenbos, A., Evans, A. C., Giedd, J. N., and Rapoport, J. L. (2002). Developmental trajectories of brain volume abnormalities in children and adolescents with attention-deficit/hyperactivity disorder. *JAMA*, 288(14):1740–8.
- Castellanos, F. X., Sonuga-Barke, E. J., Milham, M. P., and Tannock, R. (2006). Characterizing cognition in adhd: beyond executive dysfunction. *Trends Cogn Sci*, 10(3):117–23.
- Catani, M., Dell’acqua, F., Vergani, F., Malik, F., Hodge, H., Roy, P., Valabregue, R., and Thiebaut de Schotten, M. (2012). Short frontal lobe connections of the human brain. *Cortex*, 48(2):273–91.
- Catani, M., Mesulam, M. M., Jakobsen, E., Malik, F., Martersteck, A., Wieneke, C., Thompson, C. K., Thiebaut de Schotten, M., Dell’Acqua, F., Weintraub, S., and Rogalski, E. (2013). A novel frontal pathway underlies verbal fluency in primary progressive aphasia. *Brain*, 136(Pt 8):2619–28.
- Caverzasi, E., Mandelli, M. L., Hoeft, F., Watson, C., Meyer, M., Allen, I. E., Papinutto, N., Wang, C., Gandini Wheeler-Kingshott, C. A. M., Marco, E. J., Mukherjee, P., Miller, Z. A., Miller, B. L., Hendren, R., Shapiro, K. A., and Gorno-Tempini, M. L. (2018). Abnormal age-related cortical folding and neurite morphology in children with developmental dyslexia. *Neuroimage Clin*, 18:814–821.
- Chambers, C. D., Garavan, H., and Bellgrove, M. A. (2009). Insights into the neural basis of response inhibition from cognitive and clinical neuroscience. *Neurosci Biobehav Rev*, 33(5):631–46.
- Chan, A. H., Luke, K. K., Li, P., Yip, V., Li, G., Weekes, B., and Tan, L. H. (2008). Neural correlates of nouns and verbs in early bilinguals. *Ann N Y Acad Sci*, 1145:30–40.
- Chang, Y. S., Owen, J. P., Pojman, N. J., Thieu, T., Bukshpun, P., Wakahiro, M. L., Berman, J. I., Roberts, T. P., Nagarajan, S. S., Sherr, E. H., and Mukherjee, P. (2015). White matter changes of neurite density and fiber orientation dispersion during human brain maturation. *PLoS One*, 10(6):e0123656.
- Charach, A., Dashti, B., Carson, P., Booker, L., Lim, C. G., Lillie, E., Yeung, E., Ma, J., Raina, P., and Schachar, R. (2011). Comparative Effectiveness Reviews. Rockville (MD).

- Chatham, C. H., Claus, E. D., Kim, A., Curran, T., Banich, M. T., and Munakata, Y. (2012). Cognitive control reflects context monitoring, not motoric stopping, in response inhibition. *PLoS One*, 7(2):e31546.
- Chavan, C. F., Mouthon, M., Draganski, B., van der Zwaag, W., and Spierer, L. (2015). Differential patterns of functional and structural plasticity within and between inferior frontal gyri support training-induced improvements in inhibitory control proficiency. *Hum Brain Mapp*, 36(7):2527–43.
- Cherodath, S., Rao, C., Midha, R., T. A, S., and Singh, N. C. (2017). A role for putamen in phonological processing in children. *Bilingualism: Language and Cognition*, 20(2):318–326.
- Chiang, H. L., Chen, Y. J., Lo, Y. C., Tseng, W. Y., and Gau, S. S. (2015). Altered white matter tract property related to impaired focused attention, sustained attention, cognitive impulsivity and vigilance in attention-deficit/ hyperactivity disorder. *J Psychiatry Neurosci*, 40(5):325–35.
- Chiang, H. L., Chen, Y. J., Shang, C. Y., Tseng, W. Y., and Gau, S. S. (2016). Different neural substrates for executive functions in youths with adhd: a diffusion spectrum imaging tractography study. *Psychol Med*, 46(6):1225–38.
- Chien, Y. L., Chen, Y. J., Hsu, Y. C., Tseng, W. I., and Gau, S. S. (2017). Altered white-matter integrity in unaffected siblings of probands with autism spectrum disorders. *Hum Brain Mapp*, 38(12):6053–6067.
- Chung, A. W., Seunarine, K. K., and Clark, C. A. (2016). Noddi reproducibility and variability with magnetic field strength: A comparison between 1.5 t and 3 t. *Hum Brain Mapp*, 37(12):4550–4565.
- Clarke, J. (1990). *Interhemispheric functions in humans : relationships between anatomical measures of the corpus callosum, behavioral laterality effects, and cognitive profiles*. Thesis, University of California, Los Angeles.
- Cohen, J. (1960). A coefficient of agreement for nominal scales. *Educational and Psychological Measurement*, 20(1):37–46.
- Cohen, J. (1988). *Statistical power analysis for the behavioral sciences*. Erlbaum, Mahwah, NJ, 2nd edition.
- Cohen-Adad, J., Descoteaux, M., Rossignol, S., Hoge, R. D., Deriche, R., and Benali, H. (2008). Detection of multiple pathways in the spinal cord using q-ball imaging. *Neuroimage*, 42(2):739–49.
- Cole, M. W., Reynolds, J. R., Power, J. D., Repovs, G., Anticevic, A., and Braver, T. S. (2013). Multi-task connectivity reveals flexible hubs for adaptive task control. *Nat Neurosci*, 16(9):1348–55.
- Connor, D. F., Steeber, J., and McBurnett, K. (2010). A review of attention-deficit/hyperactivity disorder complicated by symptoms of oppositional defiant disorder or conduct disorder. *J Dev Behav Pediatr*, 31(5):427–40.
- Cook, P. A., Bai, Y., Nedjati-Gilani, S., Seunarine, K. K., Hall, M. G., Parker, G. J., and Alexander, D. C. (2006). Camino: Open-source diffusion-mri reconstruction and processing.

- Cortese, S., Castellanos, F. X., Eickhoff, C. R., D'Acunto, G., Masi, G., Fox, P. T., Laird, A. R., and Eickhoff, S. B. (2016). Functional decoding and meta-analytic connectivity modeling in adult attention-deficit/hyperactivity disorder. *Biol Psychiatry*, 80(12):896–904.
- Coxon, J. P., Van Impe, A., Wenderoth, N., and Swinnen, S. P. (2012). Aging and inhibitory control of action: cortico-subthalamic connection strength predicts stopping performance. *J Neurosci*, 32(24):8401–12.
- Crone, E. A., Donohue, S. E., Honomichl, R., Wendelken, C., and Bunge, S. A. (2006). Brain regions mediating flexible rule use during development. *J Neurosci*, 26(43):11239–47.
- Daducci, A., Canales-Rodriguez, E. J., Descoteaux, M., Garyfallidis, E., Gur, Y., Lin, Y. C., Mani, M., Merlet, S., Paquette, M., Ramirez-Manzanares, A., Reisert, M., Reis Rodrigues, P., Seppehrband, F., Caruyer, E., Choupan, J., Deriche, R., Jacob, M., Menegaz, G., Prckovska, V., Rivera, M., Wiaux, Y., and Thiran, J. P. (2014). Quantitative comparison of reconstruction methods for intra-voxel fiber recovery from diffusion mri. *IEEE Trans Med Imaging*, 33(2):384–99.
- Daducci, A., Canales-Rodriguez, E. J., Zhang, H., Dyrby, T. B., Alexander, D. C., and Thiran, J. P. (2015). Accelerated microstructure imaging via convex optimization (amico) from diffusion mri data. *Neuroimage*, 105:32–44.
- Dalacorte, A., Portuguez, M. W., Maurer das Neves, C. M., Anes, M., and Dacosta, J. C. (2012). Functional mri evaluation of supplementary motor area language dominance in right- and left-handed subjects. *Somatosens Mot Res*, 29(2):52–61.
- Dale, A. M., Fischl, B., and Sereno, M. I. (1999). Cortical surface-based analysis. i. segmentation and surface reconstruction. *Neuroimage*, 9(2):179–94.
- de Bruin, A., Roelofs, A., Dijkstra, T., and Fitzpatrick, I. (2014). Domain-general inhibition areas of the brain are involved in language switching: fmri evidence from trilingual speakers. *Neuroimage*, 90:348–59.
- De Simoni, S., Jenkins, P. O., Bourke, N. J., Fleminger, J. J., Hellyer, P. J., Jolly, A. E., Patel, M. C., Cole, J. H., Leech, R., and Sharp, D. J. (2018). Altered caudate connectivity is associated with executive dysfunction after traumatic brain injury. *Brain*, 141(1):148–164.
- Deluca, G. C., Ebers, G. C., and Esiri, M. M. (2004). The extent of axonal loss in the long tracts in hereditary spastic paraplegia. *Neuropathol Appl Neurobiol*, 30(6):576–84.
- Depue, B. E., Burgess, G. C., Bidwell, L. C., Willcutt, E. G., and Banich, M. T. (2010a). Behavioral performance predicts grey matter reductions in the right inferior frontal gyrus in young adults with combined type adhd. *Psychiatry Res*, 182(3):231–7.
- Depue, B. E., Burgess, G. C., Bidwell, L. C., Willcutt, E. G., and Banich, M. T. (2010b). Behavioral performance predicts grey matter reductions in the right inferior frontal gyrus in young adults with combined type adhd. *Psychiatry Res*, 182(3):231–7.

- Descoteaux, M., Angelino, E., Fitzgibbons, S., and Deriche, R. (2007). Regularized, fast, and robust analytical q-ball imaging. *Magn Reson Med*, 58(3):497–510.
- Desikan, R. S., Segonne, F., Fischl, B., Quinn, B. T., Dickerson, B. C., Blacker, D., Buckner, R. L., Dale, A. M., Maguire, R. P., Hyman, B. T., Albert, M. S., and Killiany, R. J. (2006). An automated labeling system for subdividing the human cerebral cortex on mri scans into gyral based regions of interest. *Neuroimage*, 31(3):968–80.
- Devlin, J. T., Matthews, P. M., and Rushworth, M. F. (2003). Semantic processing in the left inferior prefrontal cortex: a combined functional magnetic resonance imaging and transcranial magnetic stimulation study. *J Cogn Neurosci*, 15(1):71–84.
- Diamond, A. (2002). *Normal development of prefrontal cortex from birth to young adulthood: cognitive functions, anatomy and biochemistry*. Oxford University Press.
- Dick, A. S., Bernal, B., and Tremblay, P. (2014). The language connectome: new pathways, new concepts. *Neuroscientist*, 20(5):453–67.
- Dick, A. S., Garic, D., Graziano, P., and Tremblay, P. (2019). The frontal aslant tract (fat) and its role in speech, language and executive function. *Cortex*, 111:148–163.
- Dick, A. S. and Tremblay, P. (2012). Beyond the arcuate fasciculus: consensus and controversy in the connectonal anatomy of language. *Brain*, 135(Pt 12):3529–50.
- Dimond, D., Rohr, C. S., Smith, R. E., Dhollander, T., Cho, I., Lebel, C., Dewey, D., Connelly, A., and Bray, S. (2020). Early childhood development of white matter fiber density and morphology. *Neuroimage*, 210:116552.
- D’Souza, S., Ormond, D. R., Costabile, J., and Thompson, J. A. (2019). Fiber-tract localized diffusion coefficients highlight patterns of white matter disruption induced by proximity to glioma. *PLoS One*, 14(11):e0225323.
- Duann, J. R., Ide, J. S., Luo, X., and Li, C. S. (2009). Functional connectivity delineates distinct roles of the inferior frontal cortex and presupplementary motor area in stop signal inhibition. *J Neurosci*, 29(32):10171–9.
- Dum, R. P. and Strick, P. L. (1991). The origin of corticospinal projections from the premotor areas in the frontal lobe. *J Neurosci*, 11(3):667–89.
- Duvernoy, H. M., Bourgouin, P., Cabanis, E. A., Cattin, F., Guyot, J., Iba-Zizen, M. T., Vannson, J. L., Maeder, P., Parratte, B., Tatu, L., and Vuillier, F. (1999). *The human brain: Surface, three-dimensional sectional anatomy with MRI, and blood supply*. Springer-Wien.
- Efron, D. and Sciberras, E. (2010). The diagnostic outcomes of children with suspected attention deficit hyperactivity disorder following multidisciplinary assessment. *J Paediatr Child Health*, 46(7-8):392–7.
- Erika-Florence, M., Leech, R., and Hampshire, A. (2014). A functional network perspective on response inhibition and attentional control. *Nat Commun*, 5:4073.

- Everts, R., Lidzba, K., Wilke, M., Kiefer, C., Mordasini, M., Schroth, G., Perrig, W., and Steinlin, M. (2009). Strengthening of laterality of verbal and visuospatial functions during childhood and adolescence. *Hum Brain Mapp*, 30(2):473–83.
- Fabiano, G. A., Pelham, W. E., J., Waschbusch, D. A., Gnagy, E. M., Lahey, B. B., Chronis, A. M., Onyango, A. N., Kipp, H., Lopez-Williams, A., and Burrows-Maclean, L. (2006). A practical measure of impairment: psychometric properties of the impairment rating scale in samples of children with attention deficit hyperactivity disorder and two school-based samples. *J Clin Child Adolesc Psychol*, 35(3):369–85.
- Fassbender, C. and Schweitzer, J. B. (2006). Is there evidence for neural compensation in attention deficit hyperactivity disorder? a review of the functional neuroimaging literature. *Clin Psychol Rev*, 26(4):445–65.
- Favre, E., Ballanger, B., Thobois, S., Broussolle, E., and Boulinguez, P. (2013). Deep brain stimulation of the subthalamic nucleus, but not dopaminergic medication, improves proactive inhibitory control of movement initiation in parkinson’s disease. *Neurotherapeutics*, 10(1):154–67.
- Fife, K. H., Gutierrez-Reed, N. A., Zell, V., Bailly, J., Lewis, C. M., Aron, A. R., and Hnasko, T. S. (2017). Causal role for the subthalamic nucleus in interrupting behavior. *Elife*, 6.
- Fischl, B., Liu, A., and Dale, A. M. (2001). Automated manifold surgery: constructing geometrically accurate and topologically correct models of the human cerebral cortex. *IEEE Trans Med Imaging*, 20(1):70–80.
- Fischl, B., Salat, D. H., Busa, E., Albert, M., Dieterich, M., Haselgrove, C., van der Kouwe, A., Killiany, R., Kennedy, D., Klaveness, S., Montillo, A., Makris, N., Rosen, B., and Dale, A. M. (2002). Whole brain segmentation: automated labeling of neuroanatomical structures in the human brain. *Neuron*, 33(3):341–55.
- Fischl, B., Sereno, M. I., and Dale, A. M. (1999). Cortical surface-based analysis. ii: Inflation, flattening, and a surface-based coordinate system. *Neuroimage*, 9(2):195–207.
- Ford, A., McGregor, K. M., Case, K., Crosson, B., and White, K. D. (2010). Structural connectivity of broca’s area and medial frontal cortex. *Neuroimage*, 52(4):1230–7.
- Forster, D. C. and Webster, W. G. (2001). Speech-motor control and inter-hemispheric relations in recovered and persistent stuttering. *Dev Neuropsychol*, 19(2):125–45.
- Foundas, A. L., Mock, J. R., Cindass, R., J., and Corey, D. M. (2013). Atypical caudate anatomy in children who stutter. *Percept Mot Skills*, 116(2):528–43.
- Frodl, T. and Skokauskas, N. (2012). Meta-analysis of structural mri studies in children and adults with attention deficit hyperactivity disorder indicates treatment effects. *Acta Psychiatr Scand*, 125(2):114–26.

- Fujii, M., Maesawa, S., Motomura, K., Futamura, M., Hayashi, Y., Koba, I., and Wakabayashi, T. (2015). Intraoperative subcortical mapping of a language-associated deep frontal tract connecting the superior frontal gyrus to broca's area in the dominant hemisphere of patients with glioma. *J Neurosurg*, 122(6):1390–6.
- Furniss, T., Beyer, T., and Guggenmos, J. (2006). Prevalence of behavioural and emotional problems among six-years-old preschool children: baseline results of a prospective longitudinal study. *Soc Psychiatry Psychiatr Epidemiol*, 41(5):394–9.
- Fuster, J. M. (2002). Frontal lobe and cognitive development. *J Neurocytol*, 31(3-5):373–85.
- Garavan, H., Ross, T. J., Kaufman, J., and Stein, E. A. (2003). A midline dissociation between error-processing and response-conflict monitoring. *Neuroimage*, 20(2):1132–9.
- Garavan, H., Ross, T. J., and Stein, E. A. (1999). Right hemispheric dominance of inhibitory control: an event-related functional mri study. *Proc Natl Acad Sci U S A*, 96(14):8301–6.
- Garcia, A., Dick, A., and Graziano, P. A. (2020). A multimodal assessment of emotion dysregulation in young children with and without adhd.
- Garic, D., Broce, I., Graziano, P., Mattfeld, A., and Dick, A. S. (2019). Laterality of the frontal aslant tract (fat) explains externalizing behaviors through its association with executive function. *Dev Sci*, 22(2):e12744.
- Garyfallidis, E., Brett, M., Amirbekian, B., Rokem, A., Van Der Walt, S., Descoteaux, M., and Nimmo-Smith, I. (2014). Dipy, a library for the analysis of diffusion mri data. *Frontiers in Neuroinformatics*, 8(8).
- Genc, E., Fraenz, C., Schluter, C., Friedrich, P., Hossiep, R., Voelkle, M. C., Ling, J. M., Gunturkun, O., and Jung, R. E. (2018). Diffusion markers of dendritic density and arborization in gray matter predict differences in intelligence. *Nat Commun*, 9(1):1905.
- Genc, S., Malpas, C. B., Holland, S. K., Beare, R., and Silk, T. J. (2017). Neurite density index is sensitive to age related differences in the developing brain. *Neuroimage*, 148:373–380.
- Giedd, J. N., Raznahan, A., Alexander-Bloch, A., Schmitt, E., Gogtay, N., and Rapoport, J. L. (2015). Child psychiatry branch of the national institute of mental health longitudinal structural magnetic resonance imaging study of human brain development. *Neuropsychopharmacology*, 40(1):43–9.
- Gioia, G. A., Isquith, P. K., Guy, S. C., and Kenworthy, L. (2000). *Behavior Rating Inventory of Executive Function*. Psychological Assessment Resources, Inc., Lutz, Florida.
- Gioia, G. A., Isquith, P. K., Retzlaff, P. D., and Espy, K. A. (2002). Confirmatory factor analysis of the behavior rating inventory of executive function (brief) in a clinical sample. *Child Neuropsychol*, 8(4):249–57.

- Goda, Y. and Davis, G. W. (2003). Mechanisms of synapse assembly and disassembly. *Neuron*, 40(2):243–64.
- Gold, B. T. and Buckner, R. L. (2002). Common prefrontal regions coactivate with dissociable posterior regions during controlled semantic and phonological tasks. *Neuron*, 35(4):803–12.
- Gordon, E. M., Devaney, J. M., Bean, S., and Vaidya, C. J. (2015). Resting-state striato-frontal functional connectivity is sensitive to dat1 genotype and predicts executive function. *Cereb Cortex*, 25(2):336–45.
- Gough, P. M., Nobre, A. C., and Devlin, J. T. (2005). Dissociating linguistic processes in the left inferior frontal cortex with transcranial magnetic stimulation. *J Neurosci*, 25(35):8010–6.
- Green, B. C., Johnson, K. A., and Bretherton, L. (2014). Pragmatic language difficulties in children with hyperactivity and attention problems: an integrated review. *Int J Lang Commun Disord*, 49(1):15–29.
- Grindrod, C. M., Bilenko, N. Y., Myers, E. B., and Blumstein, S. E. (2008). The role of the left inferior frontal gyrus in implicit semantic competition and selection: An event-related fmri study. *Brain Res*, 1229:167–78.
- Groen, M. A., Whitehouse, A. J., Badcock, N. A., and Bishop, D. V. (2012). Does cerebral lateralization develop? a study using functional transcranial doppler ultrasound assessing lateralization for language production and visuospatial memory. *Brain Behav*, 2(3):256–69.
- Grussu, F., Schneider, T., Tur, C., Yates, R. L., Tachrount, M., Ianus, A., Yianakakis, M. C., Newcombe, J., Zhang, H., Alexander, D. C., DeLuca, G. C., and Gandini Wheeler-Kingshott, C. A. M. (2017). Neurite dispersion: a new marker of multiple sclerosis spinal cord pathology? *Ann Clin Transl Neurol*, 4(9):663–679.
- Gruszka, A., Hampshire, A., Barker, R. A., and Owen, A. M. (2017). Normal aging and parkinson’s disease are associated with the functional decline of distinct frontal-striatal circuits. *Cortex*, 93:178–192.
- Guo, Y., Schmitz, T. W., Mur, M., Ferreira, C. S., and Anderson, M. C. (2018). A supramodal role of the basal ganglia in memory and motor inhibition: Meta-analytic evidence. *Neuropsychologia*, 108:117–134.
- Gustavson, D. E., Panizzon, M. S., Franz, C. E., Reynolds, C. A., Corley, R. P., Hewitt, J. K., Lyons, M. J., Kremen, W. S., and Friedman, N. P. (2019). Integrating verbal fluency with executive functions: Evidence from twin studies in adolescence and middle age. *J Exp Psychol Gen*, 148(12):2104–2119.
- Hagler, D. J., J., Hatton, S., Cornejo, M. D., Makowski, C., Fair, D. A., Dick, A. S., Sutherland, M. T., Casey, B. J., Barch, D. M., Harms, M. P., Watts, R., Bjork, J. M., Garavan, H. P., Hilmer, L., Pung, C. J., Sicat, C. S., Kuperman, J., Bartsch, H., Xue, F., Heitzeg, M. M., Laird, A. R., Trinh, T. T., Gonzalez, R., Tapert, S. F., Riedel, M. C., Squeglia, L. M., Hyde, L. W., Rosenberg, M. D., Earl, E. A., Howlett, K. D., Baker, F. C., Soules, M., Diaz, J., de Leon, O. R., Thompson, W. K., Neale, M. C., Herting, M., Sowell, E. R., Alvarez, R. P.,

- Hawes, S. W., Sanchez, M., Bodurka, J., Breslin, F. J., Morris, A. S., Paulus, M. P., Simmons, W. K., Polimeni, J. R., van der Kouwe, A., Nencka, A. S., Gray, K. M., Pierpaoli, C., Matochik, J. A., Noronha, A., Aklin, W. M., Conway, K., Glantz, M., Hoffman, E., Little, R., Lopez, M., Pariyadath, V., Weiss, S. R., Wolff-Hughes, D. L., DelCarmen-Wiggins, R., Feldstein Ewing, S. W., Miranda-Dominguez, O., Nagel, B. J., Perrone, A. J., Sturgeon, D. T., Goldstone, A., Pfefferbaum, A., Pohl, K. M., Prouty, D., Uban, K., Bookheimer, S. Y., Dapretto, M., Galvan, A., Bagot, K., Giedd, J., Infante, M. A., Jacobus, J., Patrick, K., Shilling, P. D., Desikan, R., Li, Y., Sugrue, L., Banich, M. T., Friedman, N., Hewitt, J. K., Hopfer, C., Sakai, J., Tanabe, J., Cottler, L. B., Nixon, S. J., Chang, L., Cloak, C., Ernst, T., Reeves, G., Kennedy, D. N., Heeringa, S., Peltier, S., et al. (2019). Image processing and analysis methods for the adolescent brain cognitive development study. *Neuroimage*, 202:116091.
- Hagmann, P., Cammoun, L., Gigandet, X., Meuli, R., Honey, C. J., Wedeen, V. J., and Sporns, O. (2008). Mapping the structural core of human cerebral cortex. *PLoS Biol*, 6(7):e159.
- Halperin, J. M., Bedard, A. C., and Curchack-Lichtin, J. T. (2012). Preventive interventions for adhd: a neurodevelopmental perspective. *Neurotherapeutics*, 9(3):531–41.
- Halperin, J. M. and Healey, D. M. (2011). The influences of environmental enrichment, cognitive enhancement, and physical exercise on brain development: can we alter the developmental trajectory of adhd? *Neurosci Biobehav Rev*, 35(3):621–34.
- Hamilton, L. S., Levitt, J. G., O’Neill, J., Alger, J. R., Luders, E., Phillips, O. R., Caplan, R., Toga, A. W., McCracken, J., and Narr, K. L. (2008). Reduced white matter integrity in attention-deficit hyperactivity disorder. *Neuroreport*, 19(17):1705–8.
- Hampshire, A. (2015). Putting the brakes on inhibitory models of frontal lobe function. *Neuroimage*, 113:340–55.
- Hampshire, A., Chamberlain, S. R., Monti, M. M., Duncan, J., and Owen, A. M. (2010). The role of the right inferior frontal gyrus: inhibition and attentional control. *Neuroimage*, 50(3):1313–9.
- Harms, R. L., Fritz, F. J., Tobisch, A., Goebel, R., and Roebroeck, A. (2017). Robust and fast nonlinear optimization of diffusion mri microstructure models. *Neuroimage*, 155:82–96.
- Hartman, C. A., Rhee, S. H., Willcutt, E. G., and Pennington, B. F. (2007). Modeling rater disagreement for adhd: are parents or teachers biased? *J Abnorm Child Psychol*, 35(4):536–42.
- Hasan, K. M. and Narayana, P. A. (2006). Retrospective measurement of the diffusion tensor eigenvalues from diffusion anisotropy and mean diffusivity in dti. *Magn Reson Med*, 56(1):130–7.
- Hayes, A. F. (2013). *Introduction to mediation, moderation, and conditional process analysis : a regression-based approach*. The Guilford Press., New York.

- Herbet, G., Lafargue, G., Almairac, F., Moritz-Gasser, S., Bonnetblanc, F., and Duffau, H. (2015). Disrupting the right pars opercularis with electrical stimulation frees the song: case report. *J Neurosurg*, 123(6):1401–4.
- Hervais-Adelman, A., Moser-Mercer, B., Michel, C. M., and Golestani, N. (2015). fmri of simultaneous interpretation reveals the neural basis of extreme language control. *Cereb Cortex*, 25(12):4727–39.
- Herve, P. Y., Zago, L., Petit, L., Mazoyer, B., and Tzourio-Mazoyer, N. (2013). Revisiting human hemispheric specialization with neuroimaging. *Trends Cogn Sci*, 17(2):69–80.
- Holland, S. K., Plante, E., Weber Byars, A., Strawsburg, R. H., Schmithorst, V. J., and Ball, W. S., J. (2001). Normal fmri brain activation patterns in children performing a verb generation task. *Neuroimage*, 14(4):837–43.
- Hoogman, M., Bralten, J., Hibar, D. P., Mennes, M., Zwiers, M. P., Schweren, L. S. J., van Hulzen, K. J. E., Medland, S. E., Shumskaya, E., Jahanshad, N., Zeeuw, P., Szekely, E., Sudre, G., Wolfers, T., Onnink, A. M. H., Dammers, J. T., Mostert, J. C., Vives-Gilabert, Y., Kohls, G., Oberwilling, E., Seitz, J., Schulte-Ruther, M., Ambrosino, S., Doyle, A. E., Hovik, M. F., Dramsdahl, M., Tamm, L., van Erp, T. G. M., Dale, A., Schork, A., Conzelmann, A., Zierhut, K., Baur, R., McCarthy, H., Yoncheva, Y. N., Cubillo, A., Chantiluke, K., Mehta, M. A., Paloyelis, Y., Hohmann, S., Baumeister, S., Bramati, I., Mattos, P., Tovar-Moll, F., Douglas, P., Banaschewski, T., Brandeis, D., Kuntsi, J., Asherson, P., Rubia, K., Kelly, C., Martino, A. D., Milham, M. P., Castellanos, F. X., Frodl, T., Zentis, M., Lesch, K. P., Reif, A., Pauli, P., Jernigan, T. L., Haavik, J., Plessen, K. J., Lundervold, A. J., Hugdahl, K., Seidman, L. J., Biederman, J., Rommelse, N., Heslenfeld, D. J., Hartman, C. A., Hoekstra, P. J., Oosterlaan, J., Polier, G. V., Konrad, K., Vilarroya, O., Ramos-Quiroga, J. A., Soliva, J. C., Durston, S., Buitelaar, J. K., Faraone, S. V., Shaw, P., Thompson, P. M., and Franke, B. (2017). Subcortical brain volume differences in participants with attention deficit hyperactivity disorder in children and adults: a cross-sectional mega-analysis. *Lancet Psychiatry*, 4(4):310–319.
- Huang, H., Nguyen, P. T., Schwab, N. A., Tanner, J. J., Price, C. C., and Ding, M. (2017). Mapping dorsal and ventral caudate in older adults: Method and validation. *Front Aging Neurosci*, 9:91.
- Hughes, M. E., Johnston, P. J., Fulham, W. R., Budd, T. W., and Michie, P. T. (2013). Stop-signal task difficulty and the right inferior frontal gyrus. *Behav Brain Res*, 256:205–13.
- Ikeda, A., Yazawa, S., Kunieda, T., Ohara, S., Terada, K., Mikuni, N., Nagamine, T., Taki, W., Kimura, J., and Shibasaki, H. (1999). Cognitive motor control in human pre-supplementary motor area studied by subdural recording of discrimination/selection-related potentials. *Brain*, 122 (Pt 5):915–31.
- Isquith, P. and Gioia, G. (2000). Brief predictions of adhd: clinical utility of the behavior rating inventory of executive function for detecting adhd subtypes in children. *Archives of Clinical Neuropsychology*, 15(8):780–781.

- Jacobson, L. A., Crocetti, D., Dirlikov, B., Slifer, K., Denckla, M. B., Mostofsky, S. H., and Mahone, E. M. (2018). Anomalous brain development is evident in preschoolers with attention-deficit/hyperactivity disorder. *J Int Neuropsychol Soc*, 24(6):531–539.
- Jahanshahi, M. (2013). Effects of deep brain stimulation of the subthalamic nucleus on inhibitory and executive control over prepotent responses in parkinson’s disease. *Front Syst Neurosci*, 7:118.
- Jahanshahi, M., Obeso, I., Rothwell, J. C., and Obeso, J. A. (2015). A fronto-striato-subthalamic-pallidal network for goal-directed and habitual inhibition. *Nat Rev Neurosci*, 16(12):719–32.
- Jarbo, K. and Verstynen, T. D. (2015). Converging structural and functional connectivity of orbitofrontal, dorsolateral prefrontal, and posterior parietal cortex in the human striatum. *J Neurosci*, 35(9):3865–78.
- Jelescu, I. O. and Budde, M. D. (2017). Design and validation of diffusion mri models of white matter. *Front Phys*, 28.
- Jensen, P. S., Arnold, L. E., Swanson, J. M., Vitiello, B., Abikoff, H. B., Greenhill, L. L., Hechtman, L., Hinshaw, S. P., Pelham, W. E., Wells, K. C., Conners, C. K., Elliott, G. R., Epstein, J. N., Hoza, B., March, J. S., Molina, B. S. G., Newcorn, J. H., Severe, J. B., Wigal, T., Gibbons, R. D., and Hur, K. (2007). 3-year follow-up of the nimh mta study. *J Am Acad Child Adolesc Psychiatry*, 46(8):989–1002.
- Jespersen, S. N., Kroenke, C. D., Ostergaard, L., Ackerman, J. J., and Yablonskiy, D. A. (2007). Modeling dendrite density from magnetic resonance diffusion measurements. *Neuroimage*, 34(4):1473–86.
- Jones, D. K., Knosche, T. R., and Turner, R. (2013). White matter integrity, fiber count, and other fallacies: the do’s and don’ts of diffusion mri. *Neuroimage*, 73:239–54.
- Kan, I. P. and Thompson-Schill, S. L. (2004). Effect of name agreement on prefrontal activity during overt and covert picture naming. *Cogn Affect Behav Neurosci*, 4(1):43–57.
- Katzev, M., Tuscher, O., Hennig, J., Weiller, C., and Kaller, C. P. (2013). Revisiting the functional specialization of left inferior frontal gyrus in phonological and semantic fluency: the crucial role of task demands and individual ability. *J Neurosci*, 33(18):7837–45.
- Kaya, S. B., Metin, B., Tas, Z. C., Buyukaslan, A., Soysal, A., Hatiloglu, D., and Tarhan, N. (2018). Gray matter increase in motor cortex in pediatric adhd: A voxel-based morphometry study. *J Atten Disord*, 22(7):611–618.
- Keenan, K. and Wakschlag, L. S. (2000). More than the terrible twos: the nature and severity of behavior problems in clinic-referred preschool children. *J Abnorm Child Psychol*, 28(1):33–46.

- Kelly, C. E., Thompson, D. K., Chen, J., Leemans, A., Adamson, C. L., Inder, T. E., Cheong, J. L., Doyle, L. W., and Anderson, P. J. (2016). Axon density and axon orientation dispersion in children born preterm. *Hum Brain Mapp*, 37(9):3080–102.
- Kemerdere, R., de Champfleury, N. M., Deverdun, J., Cochereau, J., Moritz-Gasser, S., Herbet, G., and Duffau, H. (2016). Role of the left frontal aslant tract in stuttering: a brain stimulation and tractographic study. *J Neurol*, 263(1):157–67.
- Kim, J. H., Lee, J. M., Jo, H. J., Kim, S. H., Lee, J. H., Kim, S. T., Seo, S. W., Cox, R. W., Na, D. L., Kim, S. I., and Saad, Z. S. (2010). Defining functional sma and pre-sma subregions in human mfc using resting state fmri: functional connectivity-based parcellation method. *Neuroimage*, 49(3):2375–86.
- Kinoshita, M., de Champfleury, N. M., Deverdun, J., Moritz-Gasser, S., Herbet, G., and Duffau, H. (2015). Role of fronto-striatal tract and frontal aslant tract in movement and speech: an axonal mapping study. *Brain Struct Funct*, 220(6):3399–412.
- Kinoshita, M., Shinohara, H., Hori, O., Ozaki, N., Ueda, F., Nakada, M., Hamada, J., and Hayashi, Y. (2012). Association fibers connecting the broca center and the lateral superior frontal gyrus: a microsurgical and tractographic anatomy. *J Neurosurg*, 116(2):323–30.
- Klein, J. C., Behrens, T. E., Robson, M. D., Mackay, C. E., Higham, D. J., and Johansen-Berg, H. (2007). Connectivity-based parcellation of human cortex using diffusion mri: Establishing reproducibility, validity and observer independence in ba 44/45 and sma/pre-sma. *Neuroimage*, 34(1):204–11.
- Kolb, B. and Whishaw, I. (2014). *An Introduction To Brain and Behavior*. Worth Publishers., 4th edition. edition.
- Korkman, M., Kirk, U., and Kemp, S. (1998). *NEPSY: A developmental neuropsychological assessment*. The Psychological Corporation, San Antonio, TX.
- Kovess, V., Keyes, K. M., Hamilton, A., Pez, O., Bitfoi, A., Koc, C., Goelitz, D., Kuijpers, R., Lesinskiene, S., Mihova, Z., Otten, R., Fermanian, C., Pilowsky, D. J., and Susser, E. (2015). Maternal smoking and offspring inattention and hyperactivity: results from a cross-national european survey. *Eur Child Adolesc Psychiatry*, 24(8):919–29.
- Kramer, J. H., Mungas, D., Possin, K. L., Rankin, K. P., Boxer, A. L., Rosen, H. J., Bostrom, A., Sinha, L., Berhel, A., and Widmeyer, M. (2014). Nih examiner: conceptualization and development of an executive function battery. *J Int Neuropsychol Soc*, 20(1):11–9.
- Kronfeld-Duenias, V., Amir, O., Ezrati-Vinacour, R., Civier, O., and Ben-Shachar, M. (2016). The frontal aslant tract underlies speech fluency in persistent developmental stuttering. *Brain Struct Funct*, 221(1):365–81.
- Kumar, R., Nguyen, H. D., Macey, P. M., Woo, M. A., and Harper, R. M. (2012). Regional brain axial and radial diffusivity changes during development. *J Neurosci Res*, 90(2):346–55.

- Kumar, U., Arya, A., and Agarwal, V. (2017). Neural alterations in adhd children as indicated by voxel-based cortical thickness and morphometry analysis. *Brain Dev*, 39(5):403–410.
- Kunz, N., Zhang, H., Vasung, L., O’Brien, K. R., Assaf, Y., Lazeyras, F., Alexander, D. C., and Huppi, P. S. (2014). Assessing white matter microstructure of the newborn with multi-shell diffusion mri and biophysical compartment models. *Neuroimage*, 96:288–99.
- Lambek, R., Tannock, R., Dalsgaard, S., Trillingsgaard, A., Damm, D., and Thomsen, P. H. (2011). Executive dysfunction in school-age children with adhd. *J Atten Disord*, 15(8):646–55.
- Langley, K., Heron, J., Smith, G. D., and Thapar, A. (2012). Maternal and paternal smoking during pregnancy and risk of adhd symptoms in offspring: testing for intrauterine effects. *Am J Epidemiol*, 176(3):261–8.
- Lau, E. F., Phillips, C., and Poeppel, D. (2008). A cortical network for semantics: (de)constructing the n400. *Nat Rev Neurosci*, 9(12):920–33.
- Lauzon, C. B., Asman, A. J., Esparza, M. L., Burns, S. S., Fan, Q., Gao, Y., Anderson, A. W., Davis, N., Cutting, L. E., and Landman, B. A. (2013). Simultaneous analysis and quality assurance for diffusion tensor imaging. *PLoS One*, 8(4):e61737.
- Lebel, C. and Beaulieu, C. (2009). Lateralization of the arcuate fasciculus from childhood to adulthood and its relation to cognitive abilities in children. *Hum Brain Mapp*, 30(11):3563–73.
- Lebel, C. and Beaulieu, C. (2011). Longitudinal development of human brain wiring continues from childhood into adulthood. *J Neurosci*, 31(30):10937–47.
- Lebel, C. and Deoni, S. (2018). The development of brain white matter microstructure. *Neuroimage*, 182:207–218.
- Lebel, C., Walker, L., Leemans, A., Phillips, L., and Beaulieu, C. (2008). Microstructural maturation of the human brain from childhood to adulthood. *Neuroimage*, 40(3):1044–55.
- Lee, J. C., Nopoulos, P. C., and Bruce Tomblin, J. (2013). Abnormal subcortical components of the corticostriatal system in young adults with dli: a combined structural mri and dti study. *Neuropsychologia*, 51(11):2154–61.
- Lenartowicz, A., Verbruggen, F., Logan, G. D., and Poldrack, R. A. (2011). Inhibition-related activation in the right inferior frontal gyrus in the absence of inhibitory cues. *J Cogn Neurosci*, 23(11):3388–99.
- Levy, B. J. and Wagner, A. D. (2011). Cognitive control and right ventrolateral prefrontal cortex: reflexive reorienting, motor inhibition, and action updating. *Ann N Y Acad Sci*, 1224:40–62.
- Lo, Y. C., Chen, Y. J., Hsu, Y. C., Tseng, W. I., and Gau, S. S. (2017). Reduced tract integrity of the model for social communication is a neural substrate of social communication deficits in autism spectrum disorder. *J Child Psychol Psychiatry*, 58(5):576–585.

- Lu, L., Zhang, L., Tang, S., Bu, X., Chen, Y., Hu, X., Hu, X., Li, H., Guo, L., Sweeney, J. A., Gong, Q., and Huang, X. (2019). Characterization of cortical and subcortical abnormalities in drug-naive boys with attention-deficit/hyperactivity disorder. *J Affect Disord*, 250:397–403.
- Lu, M. T., Preston, J. B., and Strick, P. L. (1994). Interconnections between the prefrontal cortex and the premotor areas in the frontal lobe. *J Comp Neurol*, 341(3):375–92.
- Luppino, G., Matelli, M., Camarda, R. M., Gallese, V., and Rizzolatti, G. (1991). Multiple representations of body movements in mesial area 6 and the adjacent cingulate cortex: an intracortical microstimulation study in the macaque monkey. *J Comp Neurol*, 311(4):463–82.
- Lynam, D., Moffitt, T., and Stouthamer-Loeber, M. (1993). Explaining the relation between iq and delinquency: class, race, test motivation, school failure, or self-control? *J Abnorm Psychol*, 102(2):187–96.
- Lynch, K. M., Cabeen, R. P., Toga, A. W., and Clark, K. A. (2020). Magnitude and timing of major white matter tract maturation from infancy through adolescence with noddi. *Neuroimage*, 212:116672.
- Madsen, K. S., Baare, W. F., Vestergaard, M., Skimminge, A., Ejersbo, L. R., Ramsoy, T. Z., Gerlach, C., Akeson, P., Paulson, O. B., and Jernigan, T. L. (2010). Response inhibition is associated with white matter microstructure in children. *Neuropsychologia*, 48(4):854–62.
- Magnin, E. and Maurs, C. (2017). Attention-deficit/hyperactivity disorder during adulthood. *Rev Neurol (Paris)*, 173(7-8):506–515.
- Mah, A., Geeraert, B., and Lebel, C. (2017). Detailing neuroanatomical development in late childhood and early adolescence using noddi. *PLoS One*, 12(8):e0182340.
- Mahone, E. M., Crocetti, D., Ranta, M. E., Gaddis, A., Cataldo, M., Slifer, K. J., Denckla, M. B., and Mostofsky, S. H. (2011). A preliminary neuroimaging study of preschool children with adhd. *Clin Neuropsychol*, 25(6):1009–28.
- Mahrooghi, E., Zarifian, T., Shirazi, T., and Azizi, A. (2015). Adaptation of the syllable repetition task (srt) and determining its validity and reliability in 4-6 persian speaking children. *Iranian Rehabilitation Journal*, 13(2).
- Mairal, J., Bach, F., Ponce, J., and Sapiro, G. (2010). Online learning for matrix factorization and sparse coding. *J. Mach. Learn. Res.*, 11:19–60.
- Makuuchi, M., Bahlmann, J., and Friederici, A. D. (2012). An approach to separating the levels of hierarchical structure building in language and mathematics. *Philos Trans R Soc Lond B Biol Sci*, 367(1598):2033–45.
- Mandelli, M. L., Caverzasi, E., Binney, R. J., Henry, M. L., Lobach, I., Block, N., Amirbekian, B., Dronkers, N., Miller, B. L., Henry, R. G., and Gorno-Tempini, M. L. (2014). Frontal white matter tracts sustaining speech production in primary progressive aphasia. *J Neurosci*, 34(29):9754–67.

- Mandelli, M. L., Vilaplana, E., Brown, J. A., Hubbard, H. I., Binney, R. J., Attygalle, S., Santos-Santos, M. A., Miller, Z. A., Pakvasa, M., Henry, M. L., Rosen, H. J., Henry, R. G., Rabinovici, G. D., Miller, B. L., Seeley, W. W., and Gorno-Tempini, M. L. (2016). Healthy brain connectivity predicts atrophy progression in non-fluent variant of primary progressive aphasia. *Brain*, 139(Pt 10):2778–2791.
- Martino, J. and De Lucas, E. M. (2014). Subcortical anatomy of the lateral association fascicles of the brain: A review. *Clin Anat*, 27(4):563–9.
- McCandless, S. and O’Laughlin, L. (2007). The clinical utility of the behavior rating inventory of executive function (brief) in the diagnosis of adhd. *J Atten Disord*, 10(4):381–9.
- McClelland, M. M. and Cameron, C. E. (2012). Self-regulation in early childhood: Improving conceptual clarity and developing ecologically valid measures.
- McGrath, L. M., Hutaff-Lee, C., Scott, A., Boada, R., Shriberg, L. D., and Pennington, B. F. (2008). Children with comorbid speech sound disorder and specific language impairment are at increased risk for attention-deficit/hyperactivity disorder. *J Abnorm Child Psychol*, 36(2):151–63.
- McNealy, K., Mazziotta, J. C., and Dapretto, M. (2010). The neural basis of speech parsing in children and adults. *Dev Sci*, 13(2):385–406.
- Medaglia, J. D., Satterthwaite, T. D., Kelkar, A., Ciric, R., Moore, T. M., Ruparel, K., Gur, R. C., Gur, R. E., and Bassett, D. S. (2018). Brain state expression and transitions are related to complex executive cognition in normative neurodevelopment. *Neuroimage*, 166:293–306.
- Merolla, P. A., Arthur, J. V., Alvarez-Icaza, R., Cassidy, A. S., Sawada, J., Akopyan, F., Jackson, B. L., Imam, N., Guo, C., Nakamura, Y., Brezzo, B., Vo, I., Esser, S. K., Appuswamy, R., Taba, B., Amir, A., Flickner, M. D., Risk, W. P., Manohar, R., and Modha, D. S. (2014). Artificial brains. a million spiking-neuron integrated circuit with a scalable communication network and interface. *Science*, 345(6197):668–73.
- Mohammadi, M. R., Zarafshan, H., Khaleghi, A., Ahmadi, N., Hooshyari, Z., Mostafavi, S. A., Ahmadi, A., Alavi, S. S., Shakiba, A., and Salmanian, M. (2019). Prevalence of adhd and its comorbidities in a population-based sample. *J Atten Disord*, page 1087054719886372.
- Molina, B. S., Hinshaw, S. P., Eugene Arnold, L., Swanson, J. M., Pelham, W. E., Hechtman, L., Hoza, B., Epstein, J. N., Wigal, T., Abikoff, H. B., Greenhill, L. L., Jensen, P. S., Wells, K. C., Vitiello, B., Gibbons, R. D., Howard, A., Houck, P. R., Hur, K., Lu, B., Marcus, S., and Group, M. T. A. C. (2013). Adolescent substance use in the multimodal treatment study of attention-deficit/hyperactivity disorder (adhd) (mta) as a function of childhood adhd, random assignment to childhood treatments, and subsequent medication. *J Am Acad Child Adolesc Psychiatry*, 52(3):250–63.
- Molina, B. S. G., Hinshaw, S. P., Swanson, J. M., Arnold, L. E., Vitiello, B., Jensen, P. S., Epstein, J. N., Hoza, B., Hechtman, L., Abikoff, H. B., Elliott, G. R., Greenhill, L. L., Newcorn, J. H., Wells, K. C., Wigal, T., Gibbons, R. D.,

- Hur, K., Houck, P. R., and Group, M. T. A. C. (2009). The mta at 8 years: prospective follow-up of children treated for combined-type adhd in a multisite study. *J Am Acad Child Adolesc Psychiatry*, 48(5):484–500.
- Morris, L. S., Dowell, N. G., Cercignani, M., Harrison, N. A., and Voon, V. (2018). Binge drinking differentially affects cortical and subcortical microstructure. *Addict Biol*, 23(1):403–411.
- Mostofsky, S. H., Cooper, K. L., Kates, W. R., Denckla, M. B., and Kaufmann, W. E. (2002). Smaller prefrontal and premotor volumes in boys with attention-deficit/hyperactivity disorder. *Biol Psychiatry*, 52(8):785–94.
- Mueller, K. L. and Tomblin, J. B. (2012). Examining the comorbidity of language disorders and adhd. *Top Lang Disord*, 32(3):228–246.
- Mulligan, A., Anney, R., Butler, L., O’Regan, M., Richardson, T., Tulewicz, E. M., Fitzgerald, M., and Gill, M. (2013). Home environment: association with hyperactivity/impulsivity in children with adhd and their non-adhd siblings. *Child Care Health Dev*, 39(2):202–12.
- Nachev, P., Wydell, H., O’Neill, K., Husain, M., and Kennard, C. (2007). The role of the pre-supplementary motor area in the control of action. *Neuroimage*, 36 Suppl 2:T155–63.
- Naeser, M. A., Martin, P. I., Theoret, H., Kobayashi, M., Fregni, F., Nicholas, M., Tormos, J. M., Steven, M. S., Baker, E. H., and Pascual-Leone, A. (2011). Tms suppression of right pars triangularis, but not pars opercularis, improves naming in aphasia. *Brain Lang*, 119(3):206–13.
- Neef, N. E., Anwander, A., Butfering, C., Schmidt-Samoa, C., Friederici, A. D., Paulus, W., and Sommer, M. (2018). Structural connectivity of right frontal hyperactive areas scales with stuttering severity. *Brain*, 141(1):191–204.
- Neely, K. A., Wang, P., Chennavasin, A. P., Samimy, S., Tucker, J., Merida, A., Perez-Edgar, K., and Huang-Pollock, C. (2017). Deficits in inhibitory force control in young adults with adhd. *Neuropsychologia*, 99:172–178.
- Nigg, J. T., Willcutt, E. G., Doyle, A. E., and Sonuga-Barke, E. J. (2005). Causal heterogeneity in attention-deficit/hyperactivity disorder: do we need neuropsychologically impaired subtypes? *Biol Psychiatry*, 57(11):1224–30.
- Nir, T. M., Jahanshad, N., Villalon-Reina, J. E., Toga, A. W., Jack, C. R., Weiner, M. W., Thompson, P. M., and Alzheimer’s Disease Neuroimaging, I. (2013). Effectiveness of regional dti measures in distinguishing alzheimer’s disease, mci, and normal aging. *Neuroimage Clin*, 3:180–95.
- Oades, R. D., Dauvermann, M. R., Schimmelmann, B. G., Schwarz, M. J., and Myint, A. M. (2010). Attention-deficit hyperactivity disorder (adhd) and glial integrity: S100b, cytokines and kynurenine metabolism—effects of medication. *Behav Brain Funct*, 6:29.
- Obeso, I., Wilkinson, L., Casabona, E., Speekenbrink, M., Luisa Bringas, M., Alvarez, M., Alvarez, L., Pavon, N., Rodriguez-Oroz, M. C., Macias, R., Obeso, J. A., and Jahanshahi, M. (2014). The subthalamic nucleus and inhibitory control: impact of subthalamotomy in parkinson’s disease. *Brain*, 137(Pt 5):1470–80.

- O'Dwyer, L., Tanner, C., van Dongen, E. V., Greven, C. U., Bralten, J., Zwiers, M. P., Franke, B., Heslenfeld, D., Oosterlaan, J., Hoekstra, P. J., Hartman, C. A., Groen, W., Rommelse, N., and Buitelaar, J. K. (2016). Decreased left caudate volume is associated with increased severity of autistic-like symptoms in a cohort of adhd patients and their unaffected siblings. *PLoS One*, 11(11):e0165620.
- Oishi, K., Zilles, K., Amunts, K., Faria, A., Jiang, H., Li, X., Akhter, K., Hua, K., Woods, R., Toga, A. W., Pike, G. B., Rosa-Neto, P., Evans, A., Zhang, J., Huang, H., Miller, M. I., van Zijl, P. C., Mazziotta, J., and Mori, S. (2008). Human brain white matter atlas: identification and assignment of common anatomical structures in superficial white matter. *Neuroimage*, 43(3):447–57.
- Pannese, E. (2011). Morphological changes in nerve cells during normal aging. *Brain Struct Funct*, 216(2):85–9.
- Papachristou, E., Schulz, K., Newcorn, J., Bedard, A. C., Halperin, J. M., and Frangou, S. (2016). Comparative evaluation of child behavior checklist-derived scales in children clinically referred for emotional and behavioral dysregulation. *Front Psychiatry*, 7:146.
- Pecheva, D., Kelly, C., Kimpton, J., Bonthron, A., Batalle, D., Zhang, H., and Counsell, S. J. (2018). Recent advances in diffusion neuroimaging: applications in the developing preterm brain. *F1000Res*, 7.
- Peck, K. K., Bradbury, M., Psaty, E. L., Brennan, N. P., and Holodny, A. I. (2009). Joint activation of the supplementary motor area and presupplementary motor area during simultaneous motor and language functional mri. *Neuroreport*, 20(5):487–91.
- Pelham, W. E., J., Gnagy, E. M., Greenslade, K. E., and Milich, R. (1992). Teacher ratings of dsm-iii-r symptoms for the disruptive behavior disorders. *J Am Acad Child Adolesc Psychiatry*, 31(2):210–8.
- Pennington, B. F. and Ozonoff, S. (1996). Executive functions and developmental psychopathology. *J Child Psychol Psychiatry*, 37(1):51–87.
- Pickett, E. R., Kuniholm, E., Protopapas, A., Friedman, J., and Lieberman, P. (1998). Selective speech motor, syntax and cognitive deficits associated with bilateral damage to the putamen and the head of the caudate nucleus: a case study. *Neuropsychologia*, 36(2):173–88.
- Ponitz, C. C., McClelland, M. M., Jewkes, A. M., Connor, C. M., Farris, C. L., and Morrison, F. J. (2008). Touch your toes! developing a direct measure of behavioral regulation in early childhood. *Early Childhood Research Quarterly*, 23:141–158.
- Ponitz, C. C., McClelland, M. M., Matthews, J. S., and Morrison, F. J. (2009). A structured observation of behavioral self-regulation and its contribution to kindergarten outcomes. *Dev Psychol*, 45(3):605–19.
- Purves, D. (2008). *Neuroscience*. Sinauer, Sunderland, Mass., 4th edition.
- Qiu, A., Crocetti, D., Adler, M., Mahone, E. M., Denckla, M. B., Miller, M. I., and Mostofsky, S. H. (2009). Basal ganglia volume and shape in children with attention deficit hyperactivity disorder. *Am J Psychiatry*, 166(1):74–82.

- Qiu, D., Tan, L. H., Zhou, K., and Khong, P. L. (2008). Diffusion tensor imaging of normal white matter maturation from late childhood to young adulthood: voxel-wise evaluation of mean diffusivity, fractional anisotropy, radial and axial diffusivities, and correlation with reading development. *Neuroimage*, 41(2):223–32.
- Qiu, M. G., Ye, Z., Li, Q. Y., Liu, G. J., Xie, B., and Wang, J. (2011). Changes of brain structure and function in adhd children. *Brain Topogr*, 24(3-4):243–52.
- R Core Team (2019). *R: A Language and Environment for Statistical Computing*. R Foundation for Statistical Computing, Vienna, Austria.
- Rabinovici, G. D., Stephens, M. L., and Possin, K. L. (2015). Executive dysfunction. *Continuum (Minneapolis, Minn)*, 21(3 Behavioral Neurology and Neuropsychiatry):646–59.
- Raffelt, D., Tournier, J. D., Rose, S., Ridgway, G. R., Henderson, R., Crozier, S., Salvado, O., and Connelly, A. (2012). Apparent fibre density: a novel measure for the analysis of diffusion-weighted magnetic resonance images. *Neuroimage*, 59(4):3976–94.
- Raffelt, D. A., Smith, R. E., Ridgway, G. R., Tournier, J. D., Vaughan, D. N., Rose, S., Henderson, R., and Connelly, A. (2015). Connectivity-based fixel enhancement: Whole-brain statistical analysis of diffusion mri measures in the presence of crossing fibres. *Neuroimage*, 117:40–55.
- Reader, M., Harris, L., Schuerholz, L., and Denckla, M. (1994). Attention deficit hyperactivity disorder and executive dysfunction. *Developmental Neuropsychology*, 10(4):493–512.
- Reale, L., Bartoli, B., Cartabia, M., Zanetti, M., Costantino, M. A., Canevini, M. P., Termine, C., Bonati, M., and Lombardy, A. G. (2017). Comorbidity prevalence and treatment outcome in children and adolescents with adhd. *Eur Child Adolesc Psychiatry*, 26(12):1443–1457.
- Reuter, M., Rosas, H. D., and Fischl, B. (2010). Highly accurate inverse consistent registration: a robust approach. *Neuroimage*, 53(4):1181–96.
- Reyes-Haro, D., Mora-Loyola, E., Soria-Ortiz, B., and Garcia-Colunga, J. (2013). Regional density of glial cells in the rat corpus callosum. *Biol Res*, 46(1):27–32.
- Reynolds, J. E., Grohs, M. N., Dewey, D., and Lebel, C. (2019a). Global and regional white matter development in early childhood. *Neuroimage*, 196:49–58.
- Reynolds, J. E., Long, X., Grohs, M. N., Dewey, D., and Lebel, C. (2019b). Structural and functional asymmetry of the language network emerge in early childhood. *Dev Cogn Neurosci*, 39:100682.
- Ridderinkhof, K. R., Ullsperger, M., Crone, E. A., and Nieuwenhuis, S. (2004). The role of the medial frontal cortex in cognitive control. *Science*, 306(5695):443–7.
- Riise, J. and Pakkenberg, B. (2011). Stereological estimation of the total number of myelinated callosal fibers in human subjects. *J Anat*, 218(3):277–84.

- Ritchie, J. M. (1982). On the relation between fibre diameter and conduction velocity in myelinated nerve fibres. *Proc R Soc Lond B Biol Sci*, 217(1206):29–35.
- Roalf, D. R., Quarmley, M., Elliott, M. A., Satterthwaite, T. D., Vandekar, S. N., Ruparel, K., Gennatas, E. D., Calkins, M. E., Moore, T. M., Hopson, R., Prabhakaran, K., Jackson, C. T., Verma, R., Hakonarson, H., Gur, R. C., and Gur, R. E. (2016). The impact of quality assurance assessment on diffusion tensor imaging outcomes in a large-scale population-based cohort. *Neuroimage*, 125:903–919.
- Roberts, B. A., Martel, M. M., and Nigg, J. T. (2017). Are there executive dysfunction subtypes within adhd? *J Atten Disord*, 21(4):284–293.
- Robles, G., Gatignol, P., Capelle, L., Mitchell, M. C., and Duffau, H. (2005). The role of dominant striatum in language: a study using intraoperative electrical stimulations. *J Neurol Neurosurg Psychiatry*, 76(7):940–6.
- Rodriguez-Aranda, C., Waterloo, K., Johnsen, S. H., Eldevik, P., Sparr, S., Wikran, G. C., Herder, M., and Vangberg, T. R. (2016). Neuroanatomical correlates of verbal fluency in early alzheimer’s disease and normal aging. *Brain Lang*, 155–156:24–35.
- Rosenthal, R., Rosnow, R. L., and Rubin, D. B. (2000). *Contrasts and effect sizes in behavioral research: A correlational approach*. Contrasts and effect sizes in behavioral research: A correlational approach. Cambridge University Press, New York, NY, US.
- Rubia, K. (2018). Cognitive neuroscience of attention deficit hyperactivity disorder (adhd) and its clinical translation. *Front Hum Neurosci*, 12:100.
- Rubia, K., Overmeyer, S., Taylor, E., Brammer, M., Williams, S. C., Simmons, A., and Bullmore, E. T. (1999). Hypofrontality in attention deficit hyperactivity disorder during higher-order motor control: a study with functional mri. *Am J Psychiatry*, 156(6):891–6.
- Saad, J. F., Griffiths, K. R., Kohn, M. R., Clarke, S., Williams, L. M., and Korgaonkar, M. S. (2017). Regional brain network organization distinguishes the combined and inattentive subtypes of attention deficit hyperactivity disorder. *Neuroimage Clin*, 15:383–390.
- Sagvolden, T., Johansen, E. B., Aase, H., and Russell, V. A. (2005). A dynamic developmental theory of attention-deficit/hyperactivity disorder (adhd) predominantly hyperactive/impulsive and combined subtypes. *Behav Brain Sci*, 28(3):397–419; discussion 419–68.
- Sammartino, F., Yeh, F. C., and Krishna, V. (2019). Longitudinal analysis of structural changes following unilateral focused ultrasound thalamotomy. *Neuroimage Clin*, 22:101754.
- Scangos, K. W., Aronberg, R., and Stuphorn, V. (2013). Performance monitoring by presupplementary and supplementary motor area during an arm movement countermanding task. *J Neurophysiol*, 109(7):1928–39.

- Schachar, R., Mota, V. L., Logan, G. D., Tannock, R., and Klim, P. (2000). Confirmation of an inhibitory control deficit in attention-deficit/hyperactivity disorder. *J Abnorm Child Psychol*, 28(3):227–35.
- Schmitz, J., Fraenz, C., Schluter, C., Friedrich, P., Jung, R. E., Gunturkun, O., Genc, E., and Ocklenburg, S. (2019). Hemispheric asymmetries in cortical gray matter microstructure identified by neurite orientation dispersion and density imaging. *Neuroimage*, 189:667–675.
- Sciberras, E., Mueller, K. L., Efron, D., Bisset, M., Anderson, V., Schilpzand, E. J., Jongeling, B., and Nicholson, J. M. (2014). Language problems in children with adhd: a community-based study. *Pediatrics*, 133(5):793–800.
- Seehusen, F. and Baumgartner, W. (2010). Axonal pathology and loss precede demyelination and accompany chronic lesions in a spontaneously occurring animal model of multiple sclerosis. *Brain Pathol*, 20(3):551–9.
- Sepehrband, F., Clark, K. A., Ullmann, J. F., Kurniawan, N. D., Leanage, G., Reutens, D. C., and Yang, Z. (2015). Brain tissue compartment density estimated using diffusion-weighted mri yields tissue parameters consistent with histology. *Hum Brain Mapp*, 36(9):3687–702.
- Sergeant, J. A., Geurts, H., and Oosterlaan, J. (2002). How specific is a deficit of executive functioning for attention-deficit/hyperactivity disorder? *Behav Brain Res*, 130(1-2):3–28.
- Shaffer, D., Fisher, P., Lucas, C. P., Dulcan, M. K., and Schwab-Stone, M. E. (2000). Nih diagnostic interview schedule for children version iv (nih disc-iv): description, differences from previous versions, and reliability of some common diagnoses. *J Am Acad Child Adolesc Psychiatry*, 39(1):28–38.
- Shriberg, L. D., Lohmeier, H. L., Campbell, T. F., Dollaghan, C. A., Green, J. R., and Moore, C. A. (2009). A nonword repetition task for speakers with misarticulations: the syllable repetition task (srt). *J Speech Lang Hear Res*, 52(5):1189–212.
- Sibley, M. H., Pelham, W. E., Molina, B. S., Waschbusch, D. A., Gnagy, E. M., Babinski, D. E., and Biswas, A. (2010). Inconsistent self-report of delinquency by adolescents and young adults with adhd. *J Abnorm Child Psychol*, 38(5):645–56.
- Sierpowska, J., Gabarros, A., Fernandez-Coello, A., Camins, A., Castaner, S., Juncadella, M., de Diego-Balaguer, R., and Rodriguez-Fornells, A. (2015). Morphological derivation overflow as a result of disruption of the left frontal aslant white matter tract. *Brain Lang*, 142:54–64.
- Silk, T. J., Vance, A., Rinehart, N., Bradshaw, J. L., and Cunnington, R. (2009). White-matter abnormalities in attention deficit hyperactivity disorder: a diffusion tensor imaging study. *Hum Brain Mapp*, 30(9):2757–65.
- Smith, S. M., Jenkinson, M., Woolrich, M. W., Beckmann, C. F., Behrens, T. E., Johansen-Berg, H., Bannister, P. R., De Luca, M., Drobnjak, I., Flitney, D. E., Niazy, R. K., Saunders, J., Vickers, J., Zhang, Y., De Stefano, N., Brady, J. M., and Matthews, P. M. (2004). Advances in functional and structural mr image analysis and implementation as fsl. *Neuroimage*, 23 Suppl 1:S208–19.

- Song, S. K., Sun, S. W., Ju, W. K., Lin, S. J., Cross, A. H., and Neufeld, A. H. (2003). Diffusion tensor imaging detects and differentiates axon and myelin degeneration in mouse optic nerve after retinal ischemia. *Neuroimage*, 20(3):1714–22.
- Song, S. K., Yoshino, J., Le, T. Q., Lin, S. J., Sun, S. W., Cross, A. H., and Armstrong, R. C. (2005). Demyelination increases radial diffusivity in corpus callosum of mouse brain. *Neuroimage*, 26(1):132–40.
- Sonuga-Barke, E. J., Brandeis, D., Cortese, S., Daley, D., Ferrin, M., Holtmann, M., Stevenson, J., Danckaerts, M., van der Oord, S., Dopfner, M., Dittmann, R. W., Simonoff, E., Zuddas, A., Banaschewski, T., Buitelaar, J., Coghill, D., Hollis, C., Konofal, E., Lecendreux, M., Wong, I. C., Sergeant, J., and European, A. G. G. (2013). Nonpharmacological interventions for adhd: systematic review and meta-analyses of randomized controlled trials of dietary and psychological treatments. *Am J Psychiatry*, 170(3):275–89.
- Sonuga-Barke, E. J., Koerting, J., Smith, E., McCann, D. C., and Thompson, M. (2011). Early detection and intervention for attention-deficit/hyperactivity disorder. *Expert Rev Neurother*, 11(4):557–63.
- Suskauer, S. J., Simmonds, D. J., Caffo, B. S., Denckla, M. B., Pekar, J. J., and Mostofsky, S. H. (2008a). fmri of intrasubject variability in adhd: anomalous premotor activity with prefrontal compensation. *J Am Acad Child Adolesc Psychiatry*, 47(10):1141–50.
- Suskauer, S. J., Simmonds, D. J., Fotedar, S., Blankner, J. G., Pekar, J. J., Denckla, M. B., and Mostofsky, S. H. (2008b). Functional magnetic resonance imaging evidence for abnormalities in response selection in attention deficit hyperactivity disorder: differences in activation associated with response inhibition but not habitual motor response. *J Cogn Neurosci*, 20(3):478–93.
- Suzuki, Y., Hori, M., Kamiya, K., Fukunaga, I., Aoki, S., and M, V. A. N. C. (2016). Estimation of the mean axon diameter and intra-axonal space volume fraction of the human corpus callosum: Diffusion q-space imaging with low q-values. *Magn Reson Med Sci*, 15(1):83–93.
- Svegar, D., Antulov, R., Tkalčić, M., and Antončić, I. (2016). Lesions of left basal ganglia and insula structures impair executive functions but not emotion recognition: A case report. *Brain Impairment*, 17(3):233–241.
- Swann, N. C., Cai, W., Conner, C. R., Pieters, T. A., Claffey, M. P., George, J. S., Aron, A. R., and Tandon, N. (2012). Roles for the pre-supplementary motor area and the right inferior frontal gyrus in stopping action: electrophysiological responses and functional and structural connectivity. *Neuroimage*, 59(3):2860–70.
- Sweatt, J. D. (2016). Neural plasticity and behavior - sixty years of conceptual advances. *J Neurochem*, 139 Suppl 2:179–199.
- Szmuda, T., Rogowska, M., Sloniewski, P., Abuhaïmed, A., Szmuda, M., Springer, J., Sabisz, A., Dzierzanowski, J., Starzyska, A., and Przewozny, T. (2017). Frontal aslant tract projections to the inferior frontal gyrus. *Folia Morphol (Warsz)*, 76(4):574–581.

- Tagarelli, K. M., Shattuck, K. F., Turkeltaub, P. E., and Ullman, M. T. (2019). Language learning in the adult brain: A neuroanatomical meta-analysis of lexical and grammatical learning. *Neuroimage*, 193:178–200.
- Tallantyre, E. C., Bo, L., Al-Rawashdeh, O., Owens, T., Polman, C. H., Lowe, J., and Evangelou, N. (2009). Greater loss of axons in primary progressive multiple sclerosis plaques compared to secondary progressive disease. *Brain*, 132(Pt 5):1190–9.
- Tamm, L., Barnea-Goraly, N., and Reiss, A. L. (2012). Diffusion tensor imaging reveals white matter abnormalities in attention-deficit/hyperactivity disorder. *Psychiatry Res*, 202(2):150–4.
- Tamnes, C. K., Ostby, Y., Fjell, A. M., Westlye, L. T., Due-Tønnessen, P., and Walhovd, K. B. (2010). Brain maturation in adolescence and young adulthood: regional age-related changes in cortical thickness and white matter volume and microstructure. *Cereb Cortex*, 20(3):534–48.
- Tamnes, C. K., Roalf, D. R., Goddings, A. L., and Lebel, C. (2018). Diffusion mri of white matter microstructure development in childhood and adolescence: Methods, challenges and progress. *Dev Cogn Neurosci*, 33:161–175.
- Taoka, T., Aida, N., Fujii, Y., Ichikawa, K., Kawai, H., Nakane, T., Ito, R., and Naganawa, S. (2020). White matter microstructural changes in tuberous sclerosis: Evaluation by neurite orientation dispersion and density imaging (noddi) and diffusion tensor images. *Sci Rep*, 10(1):436.
- Taurines, R., Schmitt, J., Renner, T., Conner, A. C., Warnke, A., and Romanos, M. (2010). Developmental comorbidity in attention-deficit/hyperactivity disorder. *Atten Defic Hyperact Disord*, 2(4):267–89.
- Ter Minassian, A., Ricalens, E., Nguyen The Tich, S., Dinomais, M., Aube, C., and Beydon, L. (2014). The presupplementary area within the language network: a resting state functional magnetic resonance imaging functional connectivity analysis. *Brain Connect*, 4(6):440–53.
- Thiebaut de Schotten, M., Cohen, L., Amemiya, E., Braga, L. W., and Dehaene, S. (2014). Learning to read improves the structure of the arcuate fasciculus. *Cereb Cortex*, 24(4):989–95.
- Thomas, J. M. and Guskin, K. A. (2001). Disruptive behavior in young children: what does it mean? *J Am Acad Child Adolesc Psychiatry*, 40(1):44–51.
- Thompson, H. E., Henshall, L., and Jefferies, E. (2016). The role of the right hemisphere in semantic control: A case-series comparison of right and left hemisphere stroke. *Neuropsychologia*, 85:44–61.
- Toga, A. W. and Thompson, P. M. (2003). Mapping brain asymmetry. *Nat Rev Neurosci*, 4(1):37–48.
- Tournier, J. D., Calamante, F., and Connelly, A. (2007). Robust determination of the fibre orientation distribution in diffusion mri: non-negativity constrained super-resolved spherical deconvolution. *Neuroimage*, 35(4):1459–72.

- Tremblay, P. and Dick, A. S. (2016). Broca and wernicke are dead, or moving past the classic model of language neurobiology. *Brain Lang*, 162:60–71.
- Tremblay, P. and Gracco, V. L. (2009). Contribution of the pre-sma to the production of words and non-speech oral motor gestures, as revealed by repetitive transcranial magnetic stimulation (rtms). *Brain Res*, 1268:112–124.
- Tremblay, P. and Gracco, V. L. (2010). On the selection of words and oral motor responses: evidence of a response-independent fronto-parietal network. *Cortex*, 46(1):15–28.
- Tseng, C. J., Froudust-Walsh, S., Kroll, J., Karolis, V., Brittain, P. J., Palamin, N., Clifton, H., Counsell, S. J., Williams, S. C. R., Murray, R. M., and Nosarti, C. (2019). Verbal fluency is affected by altered brain lateralization in adults who were born very preterm. *eNeuro*, 6(2).
- Tuch, D. S. (2004). Q-ball imaging. *Magn Reson Med*, 52(6):1358–72.
- Valera, E. M., Faraone, S. V., Murray, K. E., and Seidman, L. J. (2007). Meta-analysis of structural imaging findings in attention-deficit/hyperactivity disorder. *Biol Psychiatry*, 61(12):1361–9.
- Vallesi, A. and Babcock, L. (2020). Asymmetry of the frontal aslant tract is associated with lexical decision. *Brain Struct Funct*, 225(3):1009–1017.
- van Wouwe, N. C., Pallavaram, S., Phibbs, F. T., Martinez-Ramirez, D., Neimat, J. S., Dawant, B. M., D’Haese, P. F., Kanoff, K. E., van den Wildenberg, W. P. M., Okun, M. S., and Wylie, S. A. (2017). Focused stimulation of dorsal subthalamic nucleus improves reactive inhibitory control of action impulses. *Neuropsychologia*, 99:37–47.
- Vassal, F., Boutet, C., Lemaire, J. J., and Nuti, C. (2014). New insights into the functional significance of the frontal aslant tract: an anatomo-functional study using intraoperative electrical stimulations combined with diffusion tensor imaging-based fiber tracking. *Br J Neurosurg*, 28(5):685–7.
- Vergani, F., Lacerda, L., Martino, J., Attems, J., Morris, C., Mitchell, P., Thiebaut de Schotten, M., and Dell’Acqua, F. (2014). White matter connections of the supplementary motor area in humans. *J Neurol Neurosurg Psychiatry*, 85(12):1377–85.
- Visser, S. N., Danielson, M. L., Bitsko, R. H., Holbrook, J. R., Kogan, M. D., Ghandour, R. M., Perou, R., and Blumberg, S. J. (2014). Trends in the parent-report of health care provider-diagnosed and medicated attention-deficit/hyperactivity disorder: United states, 2003-2011. *J Am Acad Child Adolesc Psychiatry*, 53(1):34–46 e2.
- von Hippel, P. T. (2007). Regression with missing ys: An improved strategy for analyzing multiply imputed data. *Sociological Methodology*, 37:83–117.
- Wang, J., Jiang, T., Cao, Q., and Wang, Y. (2007). Characterizing anatomic differences in boys with attention-deficit/hyperactivity disorder with the use of deformation-based morphometry. *AJNR Am J Neuroradiol*, 28(3):543–7.

- Wang, S., Yang, Y., Xing, W., Chen, J., Liu, C., and Luo, X. (2013). Altered neural circuits related to sustained attention and executive control in children with adhd: an event-related fmri study. *Clin Neurophysiol*, 124(11):2181–90.
- Wanless, S. B., McClelland, M. M., Acock, A. C., Ponitz, C. C., Son, S. H., Lan, X., Morrison, F. J., Chen, J. L., Chen, F. M., Lee, K., Sung, M., and Li, S. (2011). Measuring behavioral regulation in four societies. *Psychol Assess*, 23(2):364–78.
- Wellington, T. M., Semrud-Clikeman, M., Gregory, A. L., Murphy, J. M., and Lancaster, J. L. (2006). Magnetic resonance imaging volumetric analysis of the putamen in children with adhd: combined type versus control. *J Atten Disord*, 10(2):171–80.
- Welniarz, Q., Dusart, I., and Roze, E. (2017). The corticospinal tract: Evolution, development, and human disorders. *Dev Neurobiol*, 77(7):810–829.
- Westby, C. and Watson, S. (2004). Perspectives on attention deficit hyperactivity disorder: executive functions, working memory, and language disabilities. *Semin Speech Lang*, 25(3):241–54.
- Whiteside, D. M., Kealey, T., Semla, M., Luu, H., Rice, L., Basso, M. R., and Roper, B. (2016). Verbal fluency: Language or executive function measure? *Appl Neuropsychol Adult*, 23(1):29–34.
- Wiecki, T. V. and Frank, M. J. (2013). A computational model of inhibitory control in frontal cortex and basal ganglia. *Psychol Rev*, 120(2):329–55.
- Wilcox, R. R. (1998). How many discoveries have been lost by ignoring modern statistical methods? *American Psychologist*, 53(3):300–314.
- Wilcox, R. R. and Keselman, H. J. (2003). Modern robust data analysis methods: measures of central tendency. *Psychol Methods*, 8(3):254–74.
- Wilke, M., Holland, S. K., Altaye, M., and Gaser, C. (2008). Template-o-matic: a toolbox for creating customized pediatric templates. *Neuroimage*, 41(3):903–13.
- Winston, G. P. (2012). The physical and biological basis of quantitative parameters derived from diffusion mri. *Quant Imaging Med Surg*, 2(4):254–65.
- Winston, G. P., Micallef, C., Symms, M. R., Alexander, D. C., Duncan, J. S., and Zhang, H. (2014). Advanced diffusion imaging sequences could aid assessing patients with focal cortical dysplasia and epilepsy. *Epilepsy Res*, 108(2):336–9.
- Wood, S. (2006). *Generalized Additive Models: An Introduction with R*. Chapman and Hall/CRC., New York.
- Wu, W., McAnulty, G., Hamoda, H. M., Sarill, K., Karmacharya, S., Gagoski, B., Ning, L., Grant, P. E., Shenton, M. E., Waber, D. P., Makris, N., and Rathjens, Y. (2019). Detecting microstructural white matter abnormalities of frontal pathways in children with adhd using advanced diffusion models. *Brain Imaging Behav*.
- Yakovlev, P. I. and Lecours, A. R. (1967). The myelogenetic cycles of regional maturation of the brain.

- Yeh, F. C., Liu, L., Hitchens, T. K., and Wu, Y. L. (2017). Mapping immune cell infiltration using restricted diffusion mri. *Magn Reson Med*, 77(2):603–612.
- Yeh, F. C., Panesar, S., Barrios, J., Fernandes, D., Abhinav, K., Meola, A., and Fernandez-Miranda, J. C. (2019). Automatic removal of false connections in diffusion mri tractography using topology-informed pruning (tip). *Neurotherapeutics*, 16(1):52–58.
- Yeh, F. C., Panesar, S., Fernandes, D., Meola, A., Yoshino, M., Fernandez-Miranda, J. C., Vettel, J. M., and Verstynen, T. (2018). Population-averaged atlas of the macroscale human structural connectome and its network topology. *Neuroimage*, 178:57–68.
- Yeh, F. C., Verstynen, T. D., Wang, Y., Fernandez-Miranda, J. C., and Tseng, W. Y. (2013). Deterministic diffusion fiber tracking improved by quantitative anisotropy. *PLoS One*, 8(11):e80713.
- Yeh, F. C., Wedeen, V. J., and Tseng, W. Y. (2010). Generalized q-sampling imaging. *IEEE Trans Med Imaging*, 29(9):1626–35.
- Zelazo, P. D., Anderson, J. E., Richler, J., Wallner-Allen, K., Beaumont, J. L., and Weintraub, S. (2013). Ii. nih toolbox cognition battery (cb): measuring executive function and attention. *Monogr Soc Res Child Dev*, 78(4):16–33.
- Zentgraf, K., Stark, R., Reiser, M., Kunzell, S., Schienle, A., Kirsch, P., Walter, B., Vaitl, D., and Munzert, J. (2005). Differential activation of pre-sma and sma proper during action observation: effects of instructions. *Neuroimage*, 26(3):662–72.
- Zepf, F. D., Bubenzer-Busch, S., Runions, K. C., Rao, P., Wong, J. W. Y., Mahfouda, S., Morandini, H. A. E., Stewart, R. M., Moore, J. K., Biskup, C. S., Eickhoff, S. B., Fink, G. R., and Langner, R. (2019). Functional connectivity of the vigilant-attention network in children and adolescents with attention-deficit/hyperactivity disorder. *Brain Cogn*, 131:56–65.
- Zhang, H., Hubbard, P. L., Parker, G. J., and Alexander, D. C. (2011). Axon diameter mapping in the presence of orientation dispersion with diffusion mri. *Neuroimage*, 56(3):1301–15.
- Zhang, H., Schneider, T., Wheeler-Kingshott, C. A., and Alexander, D. C. (2012). Noddi: practical in vivo neurite orientation dispersion and density imaging of the human brain. *Neuroimage*, 61(4):1000–16.
- Zhu, Z., Zhang, J. X., Wang, S., Xiao, Z., Huang, J., and Chen, H. C. (2009). Involvement of left inferior frontal gyrus in sentence-level semantic integration. *Neuroimage*, 47(2):756–63.
- Zimmerman, M. E., Brickman, A. M., Paul, R. H., Grieve, S. M., Tate, D. F., Gunstad, J., Cohen, R. A., Aloia, M. S., Williams, L. M., Clark, C. R., Whitford, T. J., and Gordon, E. (2006). The relationship between frontal gray matter volume and cognition varies across the healthy adult lifespan. *The American journal of geriatric psychiatry : official journal of the American Association for Geriatric Psychiatry*, 14 10:823–33.

APPENDIX A: Laterality of the frontal aslant tract (FAT) explains externalizing behaviors through its association with executive function.

Laterality of the frontal aslant tract (FAT) explains externalizing behaviors through its association with executive function. Dea Garic¹, Iris Broce², Paulo Graziano¹, Aaron Mattfeld¹, and Anthony Steven Dick¹

¹Department of Psychology, Florida International University, Miami, FL, 33199

²Department of Radiology and Biomedical Imaging, University of California, San Francisco, San Francisco, CA, 94143

ABSTRACT

We investigated the development of a recently-identified white matter pathway, the frontal aslant tract (FAT) and its association to executive function and externalizing behaviors in a sample of 129 neurotypical male and female human children ranging in age from 7 months to 19-years. We found that the FAT could be tracked in 92% of those children, and that the pathway showed age-related differences into adulthood. The change in white matter microstructure was very rapid until about 6-years, and then plateaued, only to show age-related increases again after the age of 11-years. In a subset of those children (5-18-years; $n = 70$), left laterality of the microstructural properties of the FAT was associated with greater attention problems as measured by the Child Behavior Checklist (CBCL). However, this relationship was fully mediated by higher executive dysfunction as measured by the Behavior Rating Inventory of Executive Function (BRIEF). This relationship was specific to the FAT—we found no relationship between laterality of a control pathway, or of the white matter of the brain in general, and attention and executive function. These findings suggest that the degree to which the developing brain favors a right lateralized structural dominance of the FAT is directly associated with executive function and attention. This novel finding provides a new potential structural biomarker to assess attention

deficit hyperactivity disorder (ADHD) and associated executive dysfunction during development.

Laterality of the frontal aslant tract (FAT) explains externalizing behaviors through its association with executive function.

It is critical to understand the etiology of children’s externalizing behavior problems, including symptoms of Attention-Deficit/Hyperactivity Disorder (ADHD) such as inattention, hyperactivity, and impulsivity. These are the most common reason for early childhood mental health referrals (Keenan and Wakschlag, 2000; Thomas and Guskin, 2001) and can present early in development, occurring in 10-25% of preschoolers (Carter et al., 2004; Furniss et al., 2006). Despite successful development of evidence-based treatments for such problems, early interventions have little impact on children’s long-term academic and social impairment (Jensen et al., 2007; Molina et al., 2013, 2009; Sonuga-Barke et al., 2013). Researchers, clinicians, and patients are thus desperate for tangible progress in identifying biomarkers for treatment of mental illness in both adults and children. Identifiable biomarkers can serve as indicators of treatment response, as indicators of heterogeneity within broadly defined disorders, or as future targets of non-invasive brain stimulation treatments, and are necessary for applying precision medicine approaches to mental health treatment.

Here we investigate a recently-identified white matter fiber pathway, the frontal aslant tract (FAT), and attempt to define its functional relevance to executive function and externalizing behaviors—namely, attention problems—in a sample of typically developing children. The function of the FAT remains a matter of speculation, and its investigation in children has been minimal (Broce et al., 2015; Madsen et al., 2010). Based on the fiber pathway’s putative connectivity joining the posterior inferior frontal gyrus (IFG) with the pre-supplementary and supplementary motor areas (Bozkurt et al., 2016; Catani et al., 2012; Kinoshita et al., 2012; Martino and De Lucas, 2014; Szmuda et al., 2017), investigators have focused on its involvement

in speech and language function. For example, stimulation of the left FAT during awake surgery induces speech arrest (Fujii et al., 2015; Kinoshita et al., 2015; Vassal et al., 2014), and the left FAT is associated with executive control of speech and language in other tasks, such as verbal fluency and stuttering (Basilakos et al., 2014; Broce et al., 2015; Catani et al., 2013; Kemerdere et al., 2016; Kinoshita et al., 2015; Kronfeld-Duenias et al., 2016; Mandelli et al., 2014; Sierpowska et al., 2015).

However, given the well-known laterality of function in the brain (Herve et al., 2013; Toga and Thompson, 2003), the possibility remains that the function of the left FAT differs from its homologue on the right. Indeed, Aron et al. (2014) suggested that the right posterior IFG, the pre-SMA, and the connections between those regions (i.e., via the FAT) are associated with inhibitory control in executive function tasks (Aron et al., 2007), a possibility supported by fMRI, electrocorticography (ECoG), and diffusion-weighted imaging (DWI) data in adults (Swann et al., 2012). It is thus possible that while the left FAT might be associated with executive control of speech and language function (e.g., in the case of verbal fluency or speech initiation), the right FAT might be associated with executive control of action (e.g., inhibitory control of action). Consistent with this proposition, functional imaging data suggest that lateralization of these functions emerges during childhood (Everts et al., 2009; Holland et al., 2001). Furthermore, ADHD is associated with structural and functional abnormalities in the pre-SMA and right IFG regions connected by the FAT (Mostofsky et al., 2002; Rubia et al., 1999; Suskauer et al., 2008b,a). However, the direct contribution of the FAT to executive function, to attention, or to externalizing behaviors more broadly, during development has not been investigated.

We explored this issue in a DWI study of neurotypical children between the ages of 7-months and 19-years. We tracked the left and right FAT in these participants and related diffusion metrics of white matter microstructure to behavioral invento-

ries of executive function, and attention. Based on the right-lateralized associations with IFG and pre-SMA function and executive function, we predicted that deviation from right lateralization of this pathway would be associated with poorer executive function, and increased instances of externalizing behaviors.

Materials and Methods

Participants

In the present study, we analyzed a publicly available data set of neurotypical children from the Cincinnati MR Imaging of NeuroDevelopment (C-MIND) database, provided by the Pediatric Functional Neuroimaging Research Network (<https://research.cchmc.org/c-mind/>) and supported by a contract from the Eunice Kennedy Shriver National Institute of Child Health and Human Development (HHSN275200900018C). The data are available from CMIND by request, which facilitates validation of the results we report here. Participants in the database are full-term gestation, healthy, right-handed, native English speakers, without contraindication to MRI. By design, the C-MIND cohort is demographically diverse (38% nonwhite, 55% female, median household income \$42,500), intended to reflect the US population.

We tracked the FAT in all available participants ($n = 129$; 70 females). The age range for the full sample was 7-months to 19-years ($M = 8.8$ years; $SD = 5.0$ years). From the full sample, 70 participants had behavioral data on all of the measures of interest, and also had the tracked fiber pathways of interest. Thus, the sample size for the mediation analysis we report below is $n = 70$. In this subset, the participants were equally split by gender (35 females), and ranged in age from 5-years to 18-years ($M = 10.9$ years; $SD = 3.7$ years). A wide range was represented on the measure of socioeconomic status, which was coded on a 10-point ordinal scale of household

income ('0' = \$0 - \$5000 to '10' = Greater than \$150,000; $M = 5.1$; $SD = 2.6$). In the subsample, all of the children were typically developing and the sample was made up of 94% Non-Hispanic/Non-Latino participants. The study was approved by the Cincinnati Children's Hospital Medical Center Institutional Review Board. The Florida International University Institutional Review Board approved the data use agreement.

Experimental Design and Statistical Analysis

We employed analysis of a quasi-experimental design on a publicly available dataset consisting of DWI MRI scans, and parent/teacher report measures of executive function (i.e., the Behavior Rating Inventory of Executive Function; BRIEF) and externalizing behaviors (focusing on Attention Problems with the Child Behavior Checklist; CBCL). We conducted High Angular Resolution Diffusion Imaging (HARDI)-based analysis of the DWI data using a generalized q-sampling imaging (GQI) model-free reconstruction method (Yeh et al., 2010). We manually reconstructed the FAT in each hemisphere of each subject, defined on the original image space of the subject. We then explored the age-related change in the pathway's microstructure, and calculated laterality of the pathway. Following that, we conducted a simple mediation analysis in which laterality of the FAT was entered as a predictor, executive function as measured by the BRIEF was entered as a mediator, and CBCL Attention Problems was entered as the outcome. The same analysis was conducted on the laterality of the whole-brain white matter, on the left and right FAT separately, and on a control pathway (the Inferior Longitudinal Fasciculus; ILF). The details of these steps are presented below.

MRI Scans

Single shell, 61 direction HARDI scans were created using a spin-echo, EPI method with intravoxel incoherent motion imaging (IVIM) gradients for diffusion weighting of the scans. They were acquired using a 32-channel head coil (SENSE factor of 3), which obtained 2 x 2 x 2 mm spatial resolution at $b = 3000$ (EPI factor = 38, 1752.6 Hz EPI bandwidth, 2 x 2.05 x 2 acquisition voxel; 2 x 2 x 2 reconstructed voxel; 112 x 109 acquisition matrix). The scan took under 12 minutes, with an average scan time of 11 minutes and 34 seconds. Seven $b = 0$ images were also acquired at intervals of 8 images apart in the diffusion direction vector. These b_0 images are used for co-registration and averaged to form the baseline for computation of the diffusion metrics of interest.

HARDI post-processing. The image quality of the HARDI data was assessed using DTIPrep (<http://www.nitrc.org/projects/dtiprep>), which discards volumes as a result of slice dropout artifacts, slice interlace artifacts, and/or excessive motion. The number of volumes remaining was included as a covariate in all subsequent analyses, which is important for mitigating the effects of motion on the reported findings (Lauzon et al., 2013; Roalf et al., 2016). All usable data were registered to the reference image ($b = 0$), using a rigid body mutual information algorithm and were eddy current corrected for distortion.

Using DSI Studio, we used the GQI model-free reconstruction method, which quantifies the density of diffusing water at different orientations (Yeh et al., 2010) to reconstruct the diffusion orientation distribution function (ODF), with a regularization parameter equal to 0.006 (Descoteaux et al., 2007). From this, we obtained normalized Quantitative Anisotropy (nQA). GQI reconstruction was preferred over the simpler diffusion-tensor model because it is empirically shown to more accurately resolve multiple fiber orientations within voxels (Daducci et al., 2014; Yeh et al., 2013). In this HARDI data set we can take advantage of the large number of

diffusion directions to conduct this reconstruction algorithm. The major advantage of GQI, in terms of the measurement of microstructural properties of the tissue, is the improved resolution of crossing/kissing fiber orientations. This is particularly important for an oblique fiber pathway like the FAT, which courses through white matter of the frontal lobe containing a number of laterally and longitudinally oriented fibers of proximal pathways (e.g., the superior longitudinal fasciculus or of the coronal radiation emanating from the rostrum of the corpus callosum).

In the GQI framework, QA is defined as the amount of anisotropic spins that diffuse along a fiber orientation, and it is given mathematically by:

$$QA = Z_0(\psi(\hat{a}) - iso(\psi))$$

where ψ is the spin distribution function (SDF) estimated using the generalized q-sampling imaging, \hat{a} is the orientation of the fiber of interest, and $iso(\psi)$ is the isotropic background diffusion of the SDF. Z_0 is a scaling constant that scales free water diffusion to 1 (i.e., it is scaled to the maximum ODF of all voxels, typically found in cerebral spinal fluid).

QA can be defined for each peak in the SDF. Because deterministic tractography (which we use in this study) follows individual peaks across a streamline of voxels, we have focused on the first peak (QA_0). Unlike typical diffusion-tensor imaging (DTI) metrics such as FA, QA must be further normalized so that it can be compared across different participants. This normalized QA metric, nQA, was calculated according to the generalized q-sampling imaging method described above (Yeh et al., 2010), and essentially normalizes the maximum QA value to 1. GQI performs as well as other HARDI metrics, such as Constrained Super-resolved Spherical Deconvolution (CSD; Tournier et al. 2007; Yeh et al. 2013) and better than standard DTI algorithms

(Daducci et al., 2014; Yeh et al., 2013). To facilitate comparisons with prior work, we also reconstructed the FA metric using the standard diffusion-tensor algorithm.

In summary, we used the GQI reconstruction to map the streamlines, with deterministic tractography following the QA_0 at each voxel. We used the nQA_0 component in our analysis of the relation of white matter microstructure to behavior. To facilitate comparisons with prior literature, we report the DTI FA metric for assessment of age-related differences, and in mediation analyses that accompany the main analyses.

Defining the Tracks of Interest. To define the FAT, we identified eight total regions of interest (ROIs) for each participant, four per hemisphere. In each hemisphere, we identified ROIs for two superior frontal gyri: the pre-SMA and SMA; and two inferior frontal gyri ROIs, the IFGOp and the IFGTr.

We systematically identified the eight ROIs for each participant following the same sequence of steps, starting from identification of the brain’s midline slice. From the midline slice, the anterior commissure was located, which represents the arbitrary dividing line between the pre-SMA and SMA ROIs (Kim et al., 2010; Vergani et al., 2014). The superior border for both ROIs is the top of the brain, and the inferior border is the cingulate gyrus. The pre-SMA ROI’s anterior border is the anterior tip of the cingulate gyrus while the posterior border for the SMA is the precentral sulcus. The inferior frontal gyri ROIs—*pars triangularis* (IFGTr) and *pars opercularis* (IFGOp)—were parcellated with reference to the Duvernoy atlas (Duvernoy et al., 1999), and were defined by the semi-automated Freesurfer parcellation (Desikan et al., 2006). After semi-automated parcellation, all ROIs were visually inspected and edited to include the underlying white matter. Fiber tracking was terminated when the relative QA for the incoming direction dropped

below a preset threshold (0.02-0.06, depending on the subject; Yeh et al. 2010) or exceeded a turning angle of 40°.

We also tracked the left and right inferior longitudinal fasciculus (ILF) as a control, expecting this long association fiber pathway to have little association with attention problems or executive function (the pathway courses through the ventral temporal lobe as part of the ventral visual stream, has no parietal or frontal terminations or origins, and is typically associated with semantic processing and reading; Dick et al. 2014; Dick and Tremblay 2012). To track the ILF we used an automated approach available as part of the DSI studio software. This approach applies an atlas-based ROI (from reconstruction of the Human Connectome Project group atlas) of both the left and right ILF.

Calculation of Laterality. We calculated FAT laterality (L) following the standard formula (Thiebaut de Schotten et al., 2014):

$$L = \frac{(left - right)}{(left + right)} \quad (5.1)$$

According to the laterality equation, positive values indicate greater left laterality. The HARDI metric nQA_0 was used as the main measure of interest.

Behavioral Measures

Behavior Rating Inventory of Executive Function (BRIEF). The Behavior Rating Inventory of Executive Function (BRIEF; Gioia et al. 2000) was used to assess executive function. The BRIEF is a parent- and teacher-report measure of executive function. It has eight subscales, which have been grouped, based on factor analysis of these scales, into two indices, the Metacognitive Index (MI) and

the Behavioral Regulation Index (BRI). The BRI is comprised of the Inhibit, Shift, and Emotional Control subscales, and reflects the ability to set shift and control behavior through the administration of appropriate inhibitory control. The MI is comprised by the Initiate, Working Memory, Plan/Organize, Organization of Materials, and Monitor subscales. This index assesses the ability to initiate, plan, and organize behavior, and to apply and sustain appropriate working memory to control behavior (Gioia et al., 2002). All eight subscales comprise a Global Executive Composite (GEC) score. The BRIEF has clinical utility for the diagnosis of ADHD (Isquith and Gioia, 2000). For example, McCandless and O' Laughlin (2007) found that the MI was sensitive to the diagnosis of ADHD, while the BRI was most sensitive to dissociating among subtypes of ADHD. The MI, BRI, and GEC composite scores were the focus of the present investigation.

Child Behavior Checklist (CBCL). The Child Behavior Checklist (CBCL; Achenbach and Rescorla 2000, 2001, 2003) was administered using either the preschool, school-age, or adult form (depending on the participant's age). We focused on the Attention Problems outcome scale, which has high reliability ($r = 0.78$ for the preschool form; $r = 0.92$ for the school age form, with $r = 0.70$ and 0.60 for 12- and 24-month follow-up, respectively; $r = 0.87$ for the adult form). This scale is also highly associated with ADHD diagnosis (Biederman et al., 1993; Papachristou et al., 2016).

Simple Mediation Analysis

We examined the relationships among the laterality of the FAT, executive function, and attention in typical individuals using a simple mediation model. This model was statistically analyzed in SPSS v23 within the PROCESS regression framework from Hayes (2013). We used Model 4 in the framework. Three mediation

models were tested. In the first model, we tested whether the BRIEF GEC—which includes all subtests of the BRIEF—mediates the relation between laterality of the FAT and Attention Problems. Because some of the ratings on the BRIEF are directly related to items on the CBCL Attention Problems subscale (e.g., “Impulsive or acts without thinking”), we re-ran the same analysis replacing GEC with MI as a mediator, which mitigates that potential confound. Although not completely orthogonal, we also ran the analysis with BRI as the mediator. In the mediation analysis, the following covariates were included: gender, number of available HARDI volumes (to index movement), age (in days), whole brain nQA (to control for general white matter microstructure), and household income (on a 10-point scale, to control for SES). Because these controls were included, raw scores were used for the outcome variables. In addition, to confirm whether the results we report were specific to the FAT, we also ran the same mediation model with laterality of the whole brain white matter, and for laterality of the ILF, as the predictor of interest. Finally, to see if the pattern of results differs across hemispheres, the mediation analysis was run on the separate left and right FAT pathways.

Results

Identification of the Fiber Tracts

Using the individually defined ROIs, we were able to track four subcomponents of the FAT, in the following percentage of participants from the full sample ($n = 129$; averaged across the hemispheres; Figure 1): IFGOp $\leftarrow - \rightarrow$ pre-SMA (92%); IFGTr $\leftarrow - \rightarrow$ pre-SMA (66%); IFGOp $\leftarrow - \rightarrow$ SMA (76%); IFGTr $\leftarrow - \rightarrow$ SMA (26%). However, the largest component defined the connections between the IFGOp and pre-SMA, and this was tracked in almost all participants for both hemispheres. This

replicates the pattern of connectivity reported in adults (Bozkurt et al., 2016; Catani et al., 2012; Kinoshita et al., 2012; Martino and De Lucas, 2014; Szmuda et al., 2017). Furthermore, components overlap to a significant degree as they traverse the frontal white matter, and thus analysis of these components introduces a dependency in the results. Finally, the available literature suggests that the IFGOp and pre-SMA are most likely to be associated with executive function (Aron, 2007; Swann et al., 2012). Therefore, for analytic and conceptual simplicity, we focused on the IFGOp < - > pre-SMA component for the age-related and mediation analyses described below.

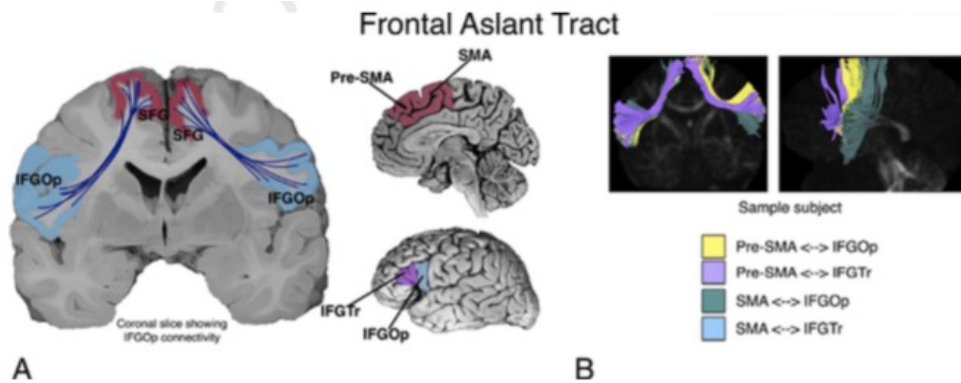


Figure 1. Illustration of the putative connectivity of the frontal aslant tract (FAT). (a) Connectivity of the tract is bilateral between the inferior frontal gyrus (pars opercularis (Op) and pars triangularis (Tri) and the superior frontal gyrus (namely, pre-supplementary motor area (pre-SMA) and supplementary motor area (SMA)). (b) The pathway can be further differentiated into four parts connecting two parts of the IFG to the pre-SMA and SMA.

Age-related Differences in Fractional Anisotropy

In Figure 2 we show the age-related differences in FA of the left (purple) and right FAT (in teal; IFGOp < - > pre-SMA component), and left (purple) and right ILF (in teal). These are mapped along with the general trend of white matter development in the whole brain (grey line). Shading represents the 95% confidence intervals.

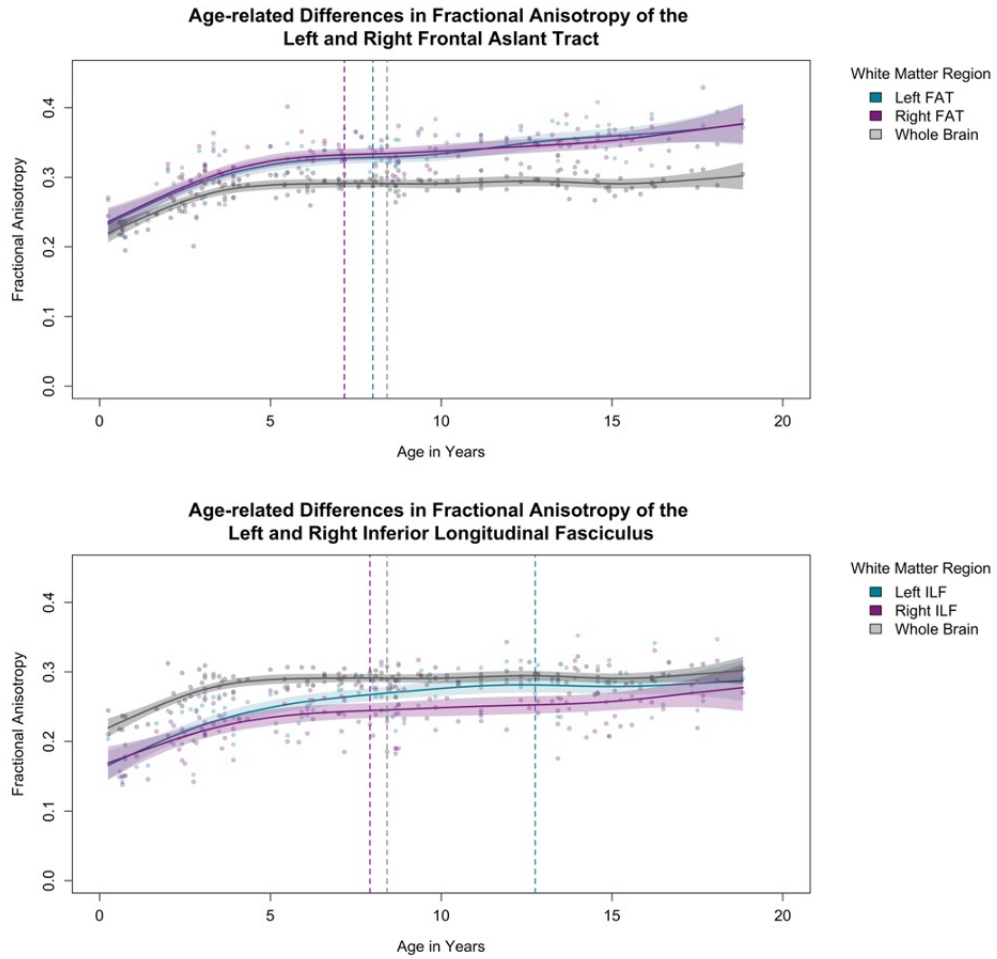


Figure 2. Top: Age-related differences in FA of the left (purple) and right FAT (in teal; IFGOp \leftrightarrow pre-SMA component). Bottom: Age-related differences in FA of the left (purple) and right ILF (in teal). These are mapped along with the general trend of white matter development in the whole brain (grey). Shading represents the 95% confidence intervals. Vertical hashed lines mark the first derivative, which indicates the asymptote of the curve and at what age this occurs.

Visual inspection of the scatter plots indicated that the data might be summarized by a non-linear model. To accomplish this, we fit two models for each dependent measure. The first was a linear model of age and gender predicting FA. The second was a generalized additive model (GAM; R 3.4.3; package *gam*; Wood

2006) with the same variables. Integrated smoothness estimation was applied (of the form $\text{gam}(dv \sim s(\text{predictor}))$). We computed Akaike Information Criterion (AIC) and Bayesian Information Criterion (BIC) values for each model. In addition, we computed the first derivative to identify the “peak” of the curve, in cases where the function was non-linear.

There were no effects of gender in any of the models (smallest $p = 0.26$), so that variable was dropped. In addition, compared to the linear models, AIC and BIC fit indices were smaller for the non-linear (i.e., GAM) models (Left FAT Linear: AIC = -512.8; BIC = -504.5; Non-linear: AIC = -534.4; BIC = -517.7; Right FAT Linear: AIC = -509.1; BIC = -500.8; Non-linear: AIC = -540.9; BIC = -524.3; Whole brain Linear: AIC = -635.2; BIC = -626.6; Non-linear: AIC = -697.4; BIC = -680.2) Thus, the non-linear models are reported here, and were significant for the left FAT ($F(4, 114) = 47.1, p < .001$), the right FAT ($F(4, 114) = 44.4, p < .001$), and the whole brain ($F(4, 124) = 36.89, p < .001$). We implemented the same procedure for the ILF. Left ILF Linear: AIC = -512.8; BIC = -504.5; Non-linear: AIC = -534.4; BIC = -517.7; Right ILF Linear: AIC = -509.1; BIC = -500.8; Non-linear: AIC = -540.9; BIC = -524.3; Left ILF non-linear ($F(4, 114) = 47.1, p < .001$), right ILF non-linear ($F(4, 114) = 44.4, p < .001$). We also calculated the first derivative of the curves to determine where an asymptote was reached following the early increase in FA in the first few years of life. For the FAT, inspection of the plot reveals that age-related differences in white matter appear rapidly over the first 6-7-years. However, while for the whole brain the differences in white matter plateau, for the FAT there is subsequent increase in FA after about age 11. For the ILF, a similar pattern was found, although the left ILF appeared to evidence small age-related differences until about age 13. In addition, unlike the FAT, the average ILF FA is less than

that seen in the whole-brain average.

Mediation Analysis

The age-related differences in white matter suggest that age might be a potential “third variable” driving the association between white matter and behavior. Therefore, we first explored whether age was associated with the behavioral scores. It was not for BRIEF GEC or MI ($r = -0.16$ for BRIEF GEC, $t(68) = 1.31$, $p = 0.20$; $r = -0.14$ for BRIEF MI, $t(68) = 1.18$, $p = 0.24$) or for CBCL Attention Problems ($r = -0.10$, $t(68) = 0.80$, $p = 0.42$). However, there was a small correlation between age and BRIEF BRI scores ($r = -0.27$, $t(68) = 2.31$, $p = 0.03$). To mitigate this possible confound, we controlled for age and other covariates (sex, whole brain white matter, movement in the scanner, and SES) in the analysis. With the exception of the relation between age and BRIEF BRI, no significant effects for the covariates were found, and the findings are reported with the covariates included in the model. This suggests that the mediation analysis speaks to individual differences in the measures of FAT white matter correlates that predict differences in executive function and externalizing behaviors.

Figure 3 shows the results of the mediation analysis. Specifically, the results show that left laterality of the FAT predicted higher CBCL Attention Problems scores. It also predicted higher BRIEF scores. Thus, when considered in a mediation model, the relation between FAT laterality and Attention Problems was fully mediated by executive function as measured by the BRIEF. This finding held for the full executive function index of the BRIEF (i.e., GEC), and also for the MI and BRI considered separately. It also held when we entered as a predictor the FA measure instead of nQA (the 95% CI for the ab parameter covered zero for all models; $B = 42.4$ (10.2 to 80.5) for BRIEF GEC, $B = 32.8$ (6.32 to 69.7) for BRIEF MI, and $B = 32.9$ (7.4

to 68.6) for BRIEF BRI). Because higher scores on each of the outcome variables reflect greater executive function and attention problems, our analysis shows that greater left laterality predicts more executive dysfunction, and higher reports of attention problems, but the relation between laterality and attention is mediated by executive function.

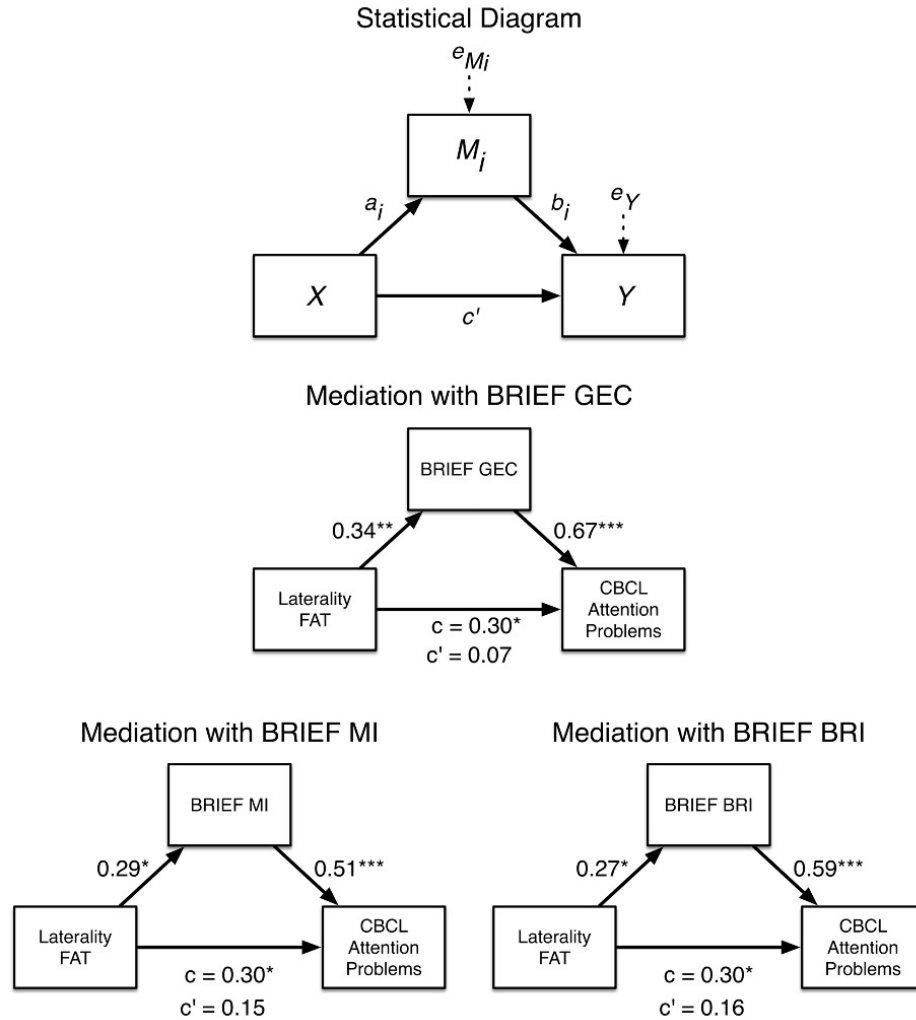


Figure 3. Mediation analysis showing greater left laterality of the FAT predicts more executive dysfunction on the BRIEF, and higher reports of attention problems on the CBCL. The statistical model is presented (top), and is tested with BRIEF GEC as the mediator (middle), BRIEF MI as the mediator (bottom left), and BRIEF BRI as the mediator (bottom right).

This pattern of results was not apparent when we assessed laterality of the whole brain white matter. Laterality of the whole brain white matter did not predict CBCL Attention Problems ($B = 18.6$, $t(63) = 0.34$, $p = 0.73$, 95% CI = -89.8 to 126.9), nor did it predict BRIEF GEC ($B = 88.8$, $t(63) = 0.41$, $p = 0.68$, 95% CI = -343.5 to 521.1), BRIEF MI ($B = 27.1$, $t(63) = 0.86$, $p = 0.39$, 95% CI = -36.0 to 90.1), or BRIEF BRI ($B = 67.4$, $t(63) = 0.90$, $p = 0.37$, 95% CI = -81.6 to 216.3). There was no mediation effect (the 95% CI for the ab parameter covered zero for all models; $B = 15.6$ (-62.4 to 83.9) for BRIEF GEC, $B = 25.4$ (-44.2 to 78.7) for BRIEF MI, and $B = 29.8$ (-38.3 to 97.6) for BRIEF BRI).

We also assessed a control long association fiber pathway, the ILF, that we predicted would not be associated with our attention and executive function measures. Consistent with this prediction, laterality of the ILF white matter did not predict CBCL Attention Problems ($B = -2.63$, $t(62) = -0.20$, $p = 0.84$, 95% CI = -28.6 to 23.4), nor did it predict BRIEF GEC ($B = -46.7$, $t(62) = -0.91$, $p = 0.37$, 95% CI = -149.7 to 56.4), BRIEF MI ($B = -2.0$, $t(62) = -0.27$, $p = 0.79$, 95% CI = -17.1 to 13.1), or BRIEF BRI ($B = -25.0$, $t(62) = -1.42$, $p = 0.16$, 95% CI = -59.9 to 10.2). There was no mediation effect (the 95% CI for the ab parameter covered zero for all models; $B = -8.3$ (-25.4 to 7.2) for BRIEF GEC, $B = -1.9$ (-17.3 to 11.5) for BRIEF MI, and $B = 11.3$ (-28.9 to 3.7) for BRIEF BRI). These results suggest that the finding we report is specific to the FAT.

Finally, we examined whether each tract—left and right FAT—separately evidenced any relation to attention problems and executive function. The left FAT did not predict CBCL Attention Problems ($B = -17.5$, $t(63) = -0.40$, $p = 0.69$, 95% CI = -69.7 to 104.7), nor did it predict BRIEF GEC ($B = 243.1$, $t(63) = 1.43$, $p = 0.16$, 95% CI = -97.9 to 584.1), BRIEF MI ($B = 41.2$, $t(63) = 1.68$, $p = 0.10$, 95% CI = -8.0 to 90.3), or BRIEF BRI ($B = 61.8$, $t(63) = 1.05$, $p = .30$, 95% CI = -55.7

to 179.4). There was no mediation effect (the 95% CI for the ab parameter covered zero for all models; $B = -8.3$ (-25.4 to 7.2) for BRIEF GEC, $B = 43.6$ (-11.8 to 104.2) for BRIEF MI, and $B = 27.8$ (-14.0 to 84.8) for BRIEF BRI). In contrast, the right FAT did predict CBCL Attention Problems ($B = -75.6$, $t(63) = -2.07$, $p = 0.04$, 95% CI = -148.5 to -2.8), but it did not predict BRIEF GEC ($B = -208.3$, $t(63) = 1.42$, $p = 0.16$, 95% CI = -502.3 to 85.8), BRIEF MI ($B = -18.1$, $t(63) = -.84$, $p = 0.40$, 95% CI = -61.2 to 25.0), or BRIEF BRI ($B = -58.0$, $t(63) = 1.14$, $p = .26$, 95% CI = -159.2 to 43.2). There was also no mediation effect (the 95% CI for the ab parameter covered zero for all models; $B = -8.3$ (-25.4 to 7.2) for BRIEF GEC, $B = -35.4$ (-101.6 to 12.4) for BRIEF MI, and $B = -24.9$ (-90.1 to 21.8) for BRIEF BRI).

Discussion

We investigated the development of the FAT and its association to executive function and externalizing behaviors in a sample of 129 children ranging in age from 7-months to 19-years. We found that the FAT could be tracked in over 90% of those children, and that the pathway showed age-related differences into adulthood. The change in white matter microstructure was very rapid until about 6-years, and then plateaued, only to show age-related increases again after the age of 11-years. In a subset of those children for whom behavioral data was available (5-18-years; $n = 70$), left laterality of the microstructural properties of the FAT predicted greater attention problems as measured by the CBCL. However, this relationship was fully mediated by higher executive dysfunction as measured by the BRIEF. This relationship was specific to the FAT—we found no relationship between laterality of the white matter of the brain in general and attention problems, or executive function. It was also specific to the laterality measure—although the right, but not left, FAT

was associated with attention problems, this was not mediated by executive function. These findings suggest that the degree to which the developing brain favors a right lateralized structural dominance of the FAT is directly associated with developing executive function and attention. This novel finding provides a new potential structural biomarker for attention problems and associated executive dysfunction, which would lay the foundation for future exploration as a biological indicator of treatment response in developmental externalizing disorders, such as ADHD.

The Role of the Frontal Aslant Tract in Executive Function

Our findings are consistent with current neurobiological models of executive function in adults. For example, several authors (Aron, 2007; Aron et al., 2016, 2014; Jahanshahi et al., 2015; Wiecki and Frank, 2013) have proposed a model for stopping behavior—i.e., countermanding an initiated response tendency via top-down executive control, recruited during Go/NoGo and Stop-Signal experimental paradigms. In these tasks, a prepotent response is initiated (a Go process) that must be overridden when a stop-signal occurs (the Stop process). These models propose that stopping requires the integrity of the right IFG and the pre-SMA, and that these regions form part of a cortico-basal ganglia “network for inhibition” (Jahanshahi et al., 2015).

In our study, we replicate the structural connection of the IFG and pre-SMA via the fibers of the FAT, and other research confirms the functional connectivity of these two regions (Duann et al., 2009). The establishment of this monosynaptic connection between the IFG and pre-SMA is important for exploring the distinct roles each region plays within this “network for inhibition” (Ridderinkhof et al., 2004). In the Wiecki/Frank computational model (Wiecki and Frank, 2013), the

right IFG directly activates neurons of the subthalamic nucleus, which plays an explicit role in stopping motor behavior (Favre et al., 2013; Jahanshahi, 2013; Obeso et al., 2014; van Wouwe et al., 2017). However, others suggest that this connection may proceed via the pre-SMA (Aron et al., 2016). This is important to work out, and our results suggest that the connection between IFG and pre-SMA is an important structural component of this network. Further, it may be that the modulation of subthalamic nucleus activity proceeds through this link. From this perspective, the right FAT is a pathway for inhibition. Indeed, higher FA in the white matter under the pre-SMA and right IFG is associated with better response inhibition in children (Madsen et al., 2010) and older adults (Coxon et al., 2012).

It is also possible, though, that the pathway does not play a role in inhibition, but rather in conflict detection. Thus, the pre-SMA may be critical for the detection of and resolution of conflicting action representations—the “winning” representation is reinforced, and the “losing” representation is suppressed (Nachev et al., 2007). Indeed, Nachev and colleagues (2007) found that a patient with a focal lesion to the right pre-SMA was significantly impaired on a task requiring the resolution of conflict between competing action plans. This is consistent with fMRI task paradigms showing activation of right pre-SMA in situations in which a participant must choose to perform a new response in favor of an established response (Garavan et al., 2003), and in single-unit recording of a human in which pre-SMA neurons appear to play a role in the selection and preparation of movements (Amador and Fried, 2004). The pre-SMA and its connections with the IFG appear to be important for these processes.

The Role of the Frontal Aslant Tract in Externalizing Behaviors and Attention

We also showed that microstructural properties of the FAT, as measured by DWI, are associated with increased reports of attention problems in children, a finding that was particularly apparent for the right FAT. The left FAT did not show this pattern. This is consistent with prior neuroimaging research in people with ADHD showing activation differences compared to neurotypical people in right IFG and pre-SMA during executive function tasks. For example, people with ADHD show hypoactivation of the right IFG during Go/NoGo and SST tasks (Rubia et al., 1999). Anatomic and functional differences in children with ADHD are also reported for the pre-SMA (Mostofsky et al., 2002; Suskauer et al., 2008a,b).

Thus, one interpretation of our results is that the FAT is involved in attention *per se*, and not necessarily inhibitory control or conflict detection. Indeed, one critique of the notion that the right IFG is associated with inhibition is that the typical experimental paradigms employed are assessing attentional processes (Chatham et al., 2012; Hampshire et al., 2010). For example, Chatham and colleagues (2012) and Hampshire and colleagues (Erika-Florence et al., 2014; Hampshire, 2015; Hampshire et al., 2010) have suggested that so-called “inhibitory control tasks” really tap into controlled context-monitoring processes, not inhibition. The authors further suggested that impairments in context-monitoring, supported by right IFG and associated circuits, might explain deficits seen in ADHD. They pointed to increased reaction time variability in SST paradigms in people with ADHD as support for such a contention (Castellanos et al., 2006), and suggest that treatments focusing on improving context-monitoring, rather than improving inhibitory control, might be more appropriately targeting the underlying deficit in ADHD. But these tasks

confound context monitoring, conflict detection, and inhibitory control processes proposed to recruit the right IFG (Castellanos et al., 2006). Although some attempts have been made to tease these processes apart (Erika-Florence et al., 2014; Hampshire, 2015), there is still debate about whether right IFG is involved in attention more generally (Ridderinkhof et al., 2004), or more specifically inhibitory control (Aron et al., 2014).

It has also been proposed that a primary deficit in ADHD is in fact one of inhibitory control (Barkley and Murphy, 2010; Neely et al., 2017; Schachar et al., 2000). However, inhibitory control and more broadly defined executive function deficits are not a universal feature of ADHD (Nigg et al., 2005), and in fact there may be executive function subtypes of ADHD, with an inhibitory control dysfunction profile describing only one of the subtypes (Roberts et al., 2017). These subtypes are defined at the behavioral level, and further progress in demarcating them may require the additional of data at other levels of analysis, such as at the neurobiological level. In this case, our findings suggest that delineation of the FAT in people with ADHD, and exploration of its functional relationship to executive function, might be important for understanding and dissociating ADHD subtypes. Indeed, our data reinforce the notion that attention problems associated with the FAT are explained by individual differences in executive function. There is a caveat here though—the mediation only held for the laterality measure. Although the right (but not left) FAT predicted attention, this particular association was not mediated by executive function. This raises an interesting possibility. That is, the degree to which functions best supported by a particular fiber pathway are co-opted by the contralateral pathway may predict dysfunction. Some evidence indicates this is the case for the FAT’s involvement in stuttering. Thus, a recent study by Neef and colleagues (Neef et al., 2018) showed that stronger structural connectivity of the right, but not left,

FAT is associated with worse stuttering. They interpreted this as indication of hyperactivity of the network involved in global response suppression, which disrupts fluent speech that typically relies strongly on left perisylvian networks, supported by the left FAT and associated perisylvian pathways. This proposal requires additional research, but it represents an interesting way of thinking about how fiber pathways that mirror each other across hemispheres might support sometimes complimentary and dissociable functions. A second caveat is worth noting as well. That is, our sample is a typical sample, and does not speak to whether there are subtypes that might be apparent in a clinical population. This would require further work in clinical populations, such as people diagnosed with ADHD.

Sub-Components of the Frontal Aslant

Our analysis of the relation between the FAT and attention and executive function focused on one subcomponent of the tract, namely the component connecting the pre-SMA with the IFGOp. On the right hemisphere, the IFGOp is associated with inhibitory control (Aron et al., 2016; Herbet et al., 2015). However, the IFGTr also has efferent/afferent fibers coursing as part of the FAT. On the left hemisphere, this region is consistently associated with controlled lexical retrieval and selection, which is dissociated from the more posterior IFGOp associated with phonological selection and retrieval (Badre et al., 2005; Devlin et al., 2003; Gough et al., 2005). Even on the right hemisphere, there appears to be some role for semantic selection for IFGTr. For example, transcranial magnetic stimulation (TMS) of the right IFGTr, but not IFGOp, improves semantic retrieval in a naming task in people with aphasia (Naeser et al., 2011).

SMA and pre-SMA also have different functional associations. The pre-SMA is especially thought to play a role in motor selection, as it does not make a direct connection to the primary motor cortex, the spinal cord, or the cranial nerve motor nuclei. Actual execution of movements is more associated with SMA and is dependent on and its direct connections with motor cortex (Dum and Strick, 1991; Lu et al., 1994; Luppino et al., 1991). The pre-SMA thus seems to be involved in higher-order selection, and conflict monitoring and resolution (Tremblay and Gracco, 2009, 2010). Differential connectivity of these medial frontal regions with the IFGTr and IFGOp may support somewhat complementary functions in the service of selecting among competing thoughts and actions. In the case of connections with IFGTr, this may be more important in situations involving semantic conflict. Connection with IFGOp may be associated with action selection and inhibitory control of actions more broadly. However, since the FAT is only a relatively recently identified fiber pathway, these proposals remain somewhat speculative and await further investigation.

Limitations

One potential limitation of our study is the use of behavior report measures as a proxy for executive function and attention. This is a legitimate criticism, and the study should be in part viewed as a point of departure for future detailed investigations using laboratory paradigms. However, the behavioral ratings we used here have substantial construct validity and reliability (Achenbach and Rescorla 2000, 2001, 2003; Gioia et al. 2000), and provide information that cannot necessarily be obtained from laboratory tasks. For example, Barkley and colleagues (Barkley and Fischer, 2011; Barkley and Murphy, 2010) found that ratings of executive function

can sometimes be a better predictor of everyday impairment than laboratory tests of executive function. Rating scales are also effective with preschool children and perform as well as laboratory tasks, such as continuous performance tasks, at differentiating children with ADHD from typical children (Cak et al., 2017). Thus, while future research should incorporate laboratory tasks, it does not discount the utility of the results we report here.

Conclusions

The work we report here shows that the FAT develops in a protracted manner into late adolescence/early adulthood, and that right lateralization of the fiber pathway is significantly associated with executive function. This fits with the putative functional roles of the regions the pathway connects—the right IFG and right pre-SMA. These results suggest that the FAT should be explored more carefully in research on developing executive function, or dysfunction as occurs in externalizing disorders such as ADHD.

APPENDIX B: Non-Winsor Age-Related Changes.

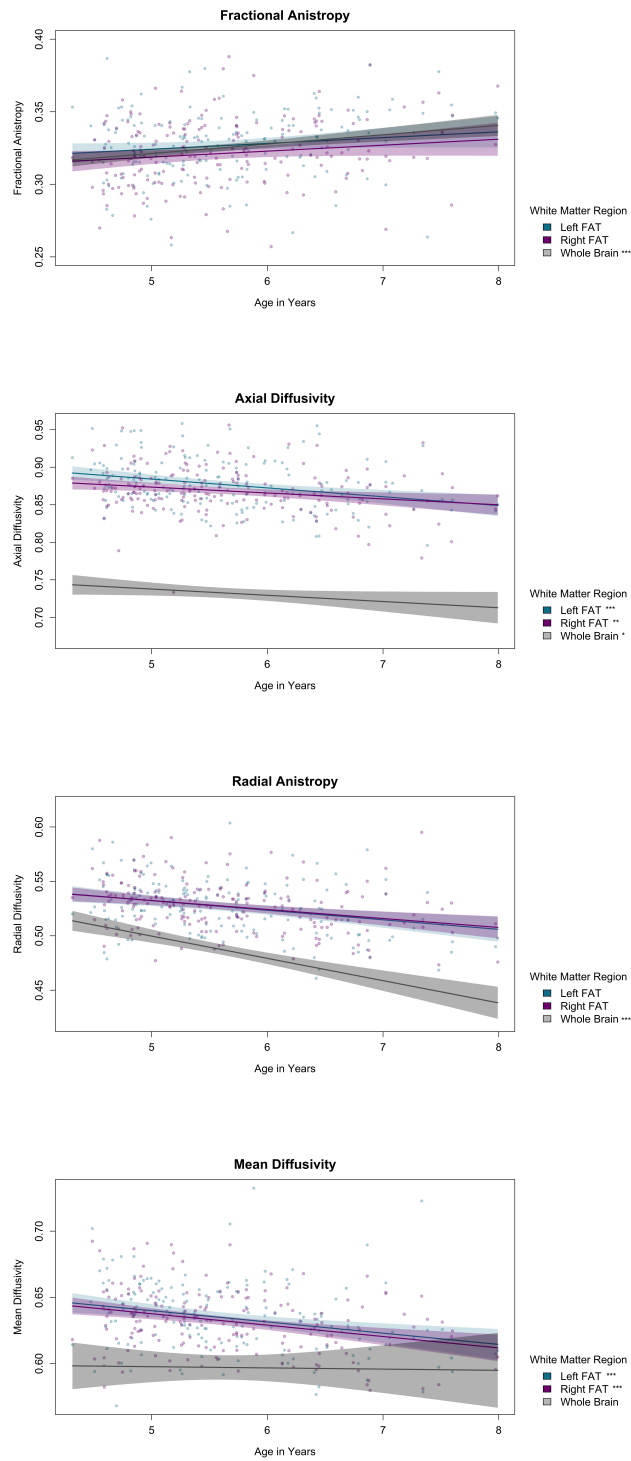
The tables and plots included in this section show age-related change displayed with non-Winsor corrected data points. As mentioned in the main text, the significance of findings remained almost unchanged, but the plots did become easier to interpret since the outliers had a smaller effect.

Table 1: Age-Related Changes in the FAT: Non-Winsor

Metrics	Hemi	PreSMA Op	SMA Op
FA	Left	0.13 (171)	0.04 (163)
	Right	0.11 (178)	0.13 (171)
	Lat	0.004(163)	-0.09 (149)
AD	Left	-0.28*** (171)	-0.31*** (163)
	Right	-0.17** (178)	-0.22** (171)
	Lat	-0.05 (163)	-0.07 (149)
RD	Left	-0.02 (171)	-0.03 (163)
	Right	-0.05 (178)	-0.12 (171)
	Lat	0.08 (163)	0.06 (149)
MD	Left	-0.31*** (171)	-0.31*** (163)
	Right	-0.28*** (178)	-0.29*** (171)
	Lat	0.01 (163)	-0.09 (149)
GFA	Left	0.05 (171)	-0.04 (163)
	Right	0.05 (178)	0.07 (171)
	Lat	-0.04(163) (34)	-0.09 (149)
QA	Left	-0.03 (171)	-0.02 (163)
	Right	-0.01 (178)	0.01 (171)
	Lat	-0.09(163)	-0.08 (149)
nQA	Left	-0.04 (171)	-0.04 (163)
	Right	-0.01 (178)	0.005 (171)
	Lat	-0.09(163)	-0.07 (149)

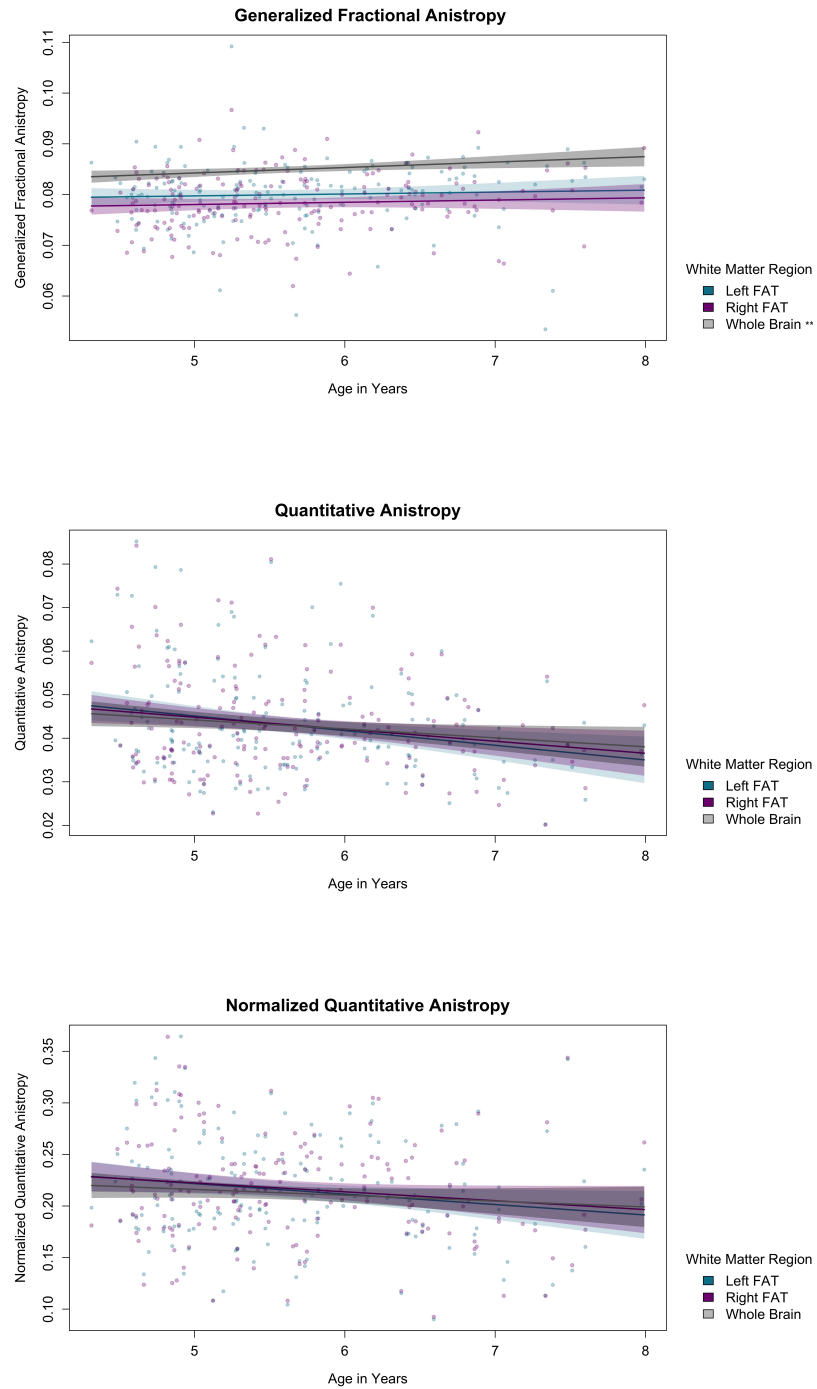
β from the robust regression coefficient is shown for each FAT segment, degrees of freedom in parentheses. Calculations controlled for sex, whole brain microstructure, and movement in the scanner. Laterality ("Lat") is calculated as (Left - Right)/(Left + Right). FA = fractional anisotropy, AD = axial diffusion, RD = radial diffusion, MD = mean diffusivity, GFA = generalized fractional anisotropy, QA = quantitative anisotropy, nQA = normalized quantitative anisotropy. $p < 0.05^*$, $p < 0.01^{**}$, $p < 0.001^{***}$

Figure 1: Age-related changes in the FAT by DTI metric.



Age-related changes, as measured in DTI metrics, in the FAT compared to whole brain microstructural development. Primary segment (preSMA to Op) selected since it had the largest sample sizes. Significance is indicated by *s in the key. $p < 0.05^*$, $p < 0.01^{**}$, $p < 0.001^{***}$.

Figure 2: Age-related changes in the FAT by HARDI metric.



Age-related changes, as measured in HARDI metrics, in the FAT compared to whole brain microstructural development. Primary segment (preSMA to Op) selected since it had the largest sample sizes. Significance is indicated by *s in the key. $p < 0.05^*$, $p < 0.01^{**}$, $p < 0.001^{***}$.

TABLES

Table 1: Group Differences in Demographics

Demographics	Mean (<i>SE</i>)	ADHD Mean (<i>SE</i>)	TD Mean (<i>SE</i>)	Difference β
Age	5.64 (0.06)	5.62 (0.08)	5.65 (0.09)	-0.02
Sex (% Males)	69.39% (3.3%)	76% (4.3%)	62.5% (5%)	0.15*
SES	5.30 (0.18)	5.23 (0.23)	5.37 (0.28)	-0.03
Movement	86.53 (0.77)	84.40 (1.18)	88.74 (0.95)	-0.20**
Whole Brain FA	0.33 (0.001)	0.32 (0.002)	0.33 (0.002)	-0.06

Table 1 shows the mean age, sex, socioeconomic status (SES), movement in the scanner, and whole brain microstructure for full sample and for typically developing (TD) and ADHD group. Age is shown in years, sex is shown in percentage of males per group, SES was a binned variable with 5 indicating \$50-65,000 annual income, and DWI directions kept was used as a proxy for movement in the scanner. No whole brain microstructure differences were found between any DWI metrics, but fractional anisotropy (FA) is shown as an example. β values represent standardized regression slope parameter estimates for group differences. $p < 0.05^*$, $p < 0.01^{**}$, $p < 0.001^{***}$

Table 2: Age-Related Differences in the FAT

Metrics	Hemi	PreSMA Op	SMA Op
FA	Left	0.14* (171)	0.04 (163)
	Right	0.11 (178)	0.14 (171)
	Lat	0.01(163)	-0.10 (149)
AD	Left	-0.29*** (171)	-0.32*** (163)
	Right	-0.19** (178)	-0.23** (171)
	Lat	-0.05 (163)	-0.07 (149)
RD	Left	-0.04 (171)	-0.04 (163)
	Right	-0.05 (178)	-0.14 (171)
	Lat	0.05 (163)	0.08 (149)
MD	Left	-0.34*** (171)	-0.33*** (163)
	Right	-0.29*** (178)	-0.31*** (171)
	Lat	0.03 (163)	-0.08 (149)
GFA	Left	0.10 (171)	-0.02 (163)
	Right	0.07 (178)	0.09 (171)
	Lat	-0.02(163)	-0.12 (149)
QA	Left	-0.03 (171)	-0.02 (163)
	Right	-0.01 (178)	0.01 (171)
	Lat	-0.07(163)	-0.07 (149)
nQA	Left	-0.04 (171)	-0.04 (163)
	Right	-0.01 (178)	0.00 (171)
	Lat	-0.09 (163)	-0.06 (149)

The β from the robust regression coefficient is shown for each FAT segment, degrees of freedom in parentheses. Calculations controlled for sex, whole brain microstructure, and movement in the scanner. This table represents the Winsor corrected values for outliers. Laterality ("Lat") is calculated as $(\text{Left} - \text{Right}) / (\text{Left} + \text{Right})$. FA = fractional anisotropy, AD = axial diffusivity, RD = radial diffusivity, MD = mean diffusivity, GFA = generalized fractional anisotropy, QA = quantitative anisotropy, nQA = normalized quantitative anisotropy. $p < 0.05^*$, $p < 0.01^{**}$, $p < 0.001^{***}$.

Table 3: Language Task Means and Main Effects of Demographic Variables

Task	Mean (<i>SE</i>)	Age <i>r</i>	Sex <i>r</i>	Whole Brain <i>r</i>	SES <i>r</i>
NEPSY Semantics					
Animal Words	8.72 (0.27)	0.40***	-0.05	0.16*	0.10
Food-Drink Words	8.09 (0.25)	0.39***	-0.15*	0.07	0.04
Total Score	16.82 (0.43)	0.46***	-0.12	0.13	0.08
NEPSY Phonemics					
Initial Letter S-Words	4.37 (0.20)	0.43***	-0.16*	0.17*	0.10
Initial Letter F-Words	3.88 (0.20)	0.32***	-0.12	0.07	0.10
Total Score	8.22 (0.36)	0.41***	-0.16*	0.13	0.11
SRT Scores					
Monolingual Scoring	80.69% (1.80%)	0.17	-0.07	-0.12	-0.04
Bilingual Scoring	82.42% (1.52%)	0.29**	-0.22*	-0.05	-0.02

This table shows mean scores for full sample for all NEPSY-II tasks and SRT scores. Scaled scores for NEPSY were unavailable for children under the age of 7 for phonological tasks so they are unreported. The SRT scores represent an percentage of accurate phonemes articulated by the participant. β = Standardized regression slope parameter estimate. SE = Standard error of the regression slope parameter estimate. The Pearson correlation coefficients (r) are reported for age, sex, whole-brain FA, and parental socioeconomic status (SES). For sex, males were scored as 1, so negative scores indicate advantage for females. Whole-brain is shown with FA, but was consistent among other metrics as well. $p < 0.05^*$, $p < 0.01^{**}$, $p < 0.001^{***}$.

Table 4: Group Differences on Language Tasks

Task	ADHD Mean (<i>SE</i>)	TD Mean (<i>SE</i>)	<i>B</i> (<i>SE</i>)	β
Semantic Scores				
Animal Words	8.14 (0.36)	9.39 (0.38)	-1.20 (0.49)	-0.16*
Food-Drink Words	7.69 (0.35)	8.55 (0.34)	-0.70 (0.45)	-0.10
Total Score	15.83 (0.62)	17.96 (0.59)	-1.91 (0.77)	-0.16*
Phonological Scores				
Initial Letter S-Words	3.94 (0.26)	4.86 (0.29)	-0.80 (0.35)	-0.15*
Initial Letter F-Words	3.58 (0.29)	4.24 (0.29)	-0.56 (0.39)	-0.10
Total Score	7.51 A(0.49)	9.07 (0.53)	-1.34 (0.65)	-0.13*
SRT Scores				
Bilingual Scoring	78.98% (2.3%)	86.19% (1.82%)	-6.16(2.90)	-0.19*

This table shows mean scores for full sample, the ADHD sample, and TD sample. For diagnosis group, ADHD was scored as 1, so negative scores indicate advantage for TD. β = Standardized regression slope parameter estimate. *SE* = Standard error of the regression slope parameter estimate. The regressions were ran controlling for age, gender, and SES. $p < 0.05^*$, $p < 0.01^{**}$, $p < 0.001^{***}$.

Table 5: The FAT's Association with Language

Predictor -- > Outcome	<i>df</i>	<i>B (SE)</i>	β	<i>t</i>	<i>p</i>
<u>FAT Predicting Language in Full Sample</u>					
Left PreSMA Op QA -- > SRT Phonemic Articulation	98	886.79 (307)	0.63	2.89	0.01
Left SMA Op AD -- > SRT Phonemic Articulation	91	118 (44.10)	0.22	2.68	0.01
PreSMA Op GFA Laterality -- > SRT Phonemic Articulation	91	77.93 (37.27)	0.16	2.09	0.04
SMA Op AD Laterality -- > SRT Phonemic Articulation	83	183.53 (73.34)	0.21	2.50	0.01
SMA Op QA Laterality -- > SRT Phonemic Articulation	83	50.85 (20.93)	0.18	2.43	0.02
Right SMA Op AD -- > NEPSY Semantics	168	31.53 (13.96)	0.16	2.26	0.03
<u>FAT Predicting Language in TD Sample</u>					
Left SMA Op AD -- > SRT Phonemic Articulation	39	113.81 (51.33)	0.31	2.61	0.01
SMA Op QA Laterality -- > SRT Phonemic Articulation	36	53.73 (23.49)	0.22	2.29	0.03
Left PreSMA Op GFA -- > NEPSY Phonemics	78	280.85 (136.68)	0.26	2.08	0.04
Right SMA Op AD -- > NEPSY Semantics	81	47.87 (21.23)	0.25	2.26	0.03
<u>FAT Predicting Language in ADHD Sample</u>					
SMA Op AD Laterality -- > SRT Phonemic Articulation	40	408.92 (133.35)	0.47	3.07	0.004
SMA Op QA Laterality -- > SRT Phonemic Articulation	40	91.99 (41.06)	0.31	2.24	0.03
Right PreSMA Op FA -- > NEPSY Semantics	83	-67.40 (25.07)	-0.25	-2.69	0.01
Right PreSMA Op GFA -- > NEPSY Semantics	83	-325.93 (121.72)	-0.29	-2.68	0.01
PreSMA Op FA Laterality -- > NEPSY Semantics	77	35.50 (16.09)	0.21	2.21	0.03
PreSMA Op RD Laterality -- > NEPSY Semantics	77	-81.64 (36.10)	-0.21	-2.26	0.03
PreSMA Op GFA Laterality -- > NEPSY Semantics	77	41.51 (16.51)	0.22	2.51	0.01
<u>FAT Group Interactions Predicting Language</u>					
Right PreSMA Op FA -- > NEPSY Semantics	171	-139.25 (48.85)	-0.16	-2.13	0.03
Right PreSMA Op RD -- > NEPSY Semantics	171	-83.25 (34.54)	-0.14	-2.00	0.046
Right PreSMA Op GFA -- > NEPSY Semantics	171	-375.60 (145.61)	-0.16	-2.05	0.04

Continued on next page

Table 5 – continued from previous page

Robust linear regression models were ran to test the association of the bilateral FAT and our three language measures. Laterality is calculated as $(\text{Left} - \text{Right})/(\text{Left} + \text{Right})$. B = Unstandardized regression slope parameter estimate. SE = Standard error of the regression slope parameter estimate. β = Standardized regression slope parameter estimate. All findings control for age, sex, whole brain microstructure, movement in the scanner, and parental SES. In order to be concise, only findings where the confidence interval did not cross zero are reported. All p -values are two-tailed.

Table 6: EF Means and Main Effects of Demographic Variables

Task	Mean (<i>SE</i>)	Age <i>r</i>	Sex <i>r</i>	Whole Brain <i>r</i>	SES <i>r</i>
NIH Toolbox Flanker	97.30 (1.04)	NA	-0.02	0.06	-0.08
NIH Toolbox DCCS	96.74 (1.03)	NA	-0.05	-0.03	-0.17*
HTKS Total	32.68 (1.37)	0.45***	-0.21***	0.26***	0.10

This table shows mean scores for full sample for all NIH Toolbox and HTKS scores. B = Unstandardized regression slope parameter estimate. β = Standardized regression slope parameter estimate. SE = Standard error of the regression slope parameter estimate. The Pearson correlation coefficients (r) are reported for age, sex, whole-brain FA, and parental socioeconomic status (SES). NA for age in NIH Toolbox tasks is because age-corrected scores were used so age was already calculated into the NIH Toolbox score output. For sex, males were scored as 1, so negative scores indicate advantage for females. Whole-brain is shown with FA, but was consistent among other metrics as well. $p < 0.05^*$, $p < 0.01^{**}$, $p < 0.001^{***}$.

Table 7: Executive Functioning Group Differences.

Task	ADHD Mean (<i>SE</i>)	TD Mean (<i>SE</i>)	<i>B</i> (<i>SE</i>)	β
NIH Toolbox Flanker	93.44 (1.50)	101.92 (1.23)	-9.10 (2.05)	-0.34***
NIH Toolbox DCCS	93.73 (1.39)	100.36 (1.44)	-7.19 (2.03)	-0.27***
HTKS Total	27.17 (1.84)	38.78 (1.85)	-9.55 (2.36)	-0.26***

This table shows mean scores for full sample, the ADHD sample, and TD sample. NIH Toolbox scores are age-corrected standard scores, with 100 representing the population mean. HTKS scores range from 0 to 60. For diagnosis group, ADHD was scored as 1, so negative scores indicate advantage for TD. β = Standardized regression slope parameter estimate. *SE* = Standard error of the regression slope parameter estimate. The regressions were ran controlling for age, gender, and SES. $p < 0.05^*$, $p < 0.01^{**}$, $p < 0.001^{***}$.

Table 8: The FAT's Association with Executive Function

Predictor -- > Outcome	<i>df</i>	<i>B (SE)</i>	β	<i>t</i>	<i>p</i>
<u>FAT Predicting Executive Function in Full Sample</u>					
Left SMA Op AD -- > Flanker Task	137	87.79 (34.36)	0.20	2.56	0.01
SMA Op AD Laterality -- > Flanker Task	124	167.65 (57.08)	0.23	2.94	0.004
Left PreSMA Op QA -- > DCCS	145	637.18 (320.12)	0.55	1.99	0.048
Left PreSMA Op MD -- > HTKS	154	160.68 (63.86)	0.21	2.52	0.01
Left SMA Op MD -- > HTKS	148	175.81 (69.21)	0.21	2.54	0.01
Right PreSMA Op FA -- > HTKS	160	-153.06 (64)	-0.19	-2.39	0.02
Right SMA Op FA -- > HTKS	154	-135.16 (59.28)	-0.18	-2.28	0.02
Right SMA Op MD -- > HTKS	154	169.91 (70.27)	0.19	2.42	0.02
SMA Op AD Laterality -- > HTKS	135	194.08 (79.85)	0.20	2.43	0.02
<u>FAT Predicting Language in TD Sample</u>					
SMA Op QA Laterality -- > DCCS	55	79.32 (35.67)	0.35	2.22	0.03
Left SMA Op GFA -- > HTKS	66	733.35 (325.54)	0.25	2.25	0.03
Right PreSMA Op AD -- > HTKS	75	118.93 (55.85)	0.20	2.13	0.04
PreSMA Op FA Laterality -- > HTKS	68	-118.01 (43.84)	-0.25	-2.69	0.01
PreSMA Op GFA Laterality -- > HTKS	68	-124.03 (45.53)	-0.25	-2.72	0.01
<u>FAT Predicting Language in ADHD Sample</u>					
Left PreSMA Op FA -- > DCCS	76	135.03 (65.48)	0.23	2.06	0.04
Left PreSMA Op GFA -- > DCCS	76	667.11 (287.44)	0.28	2.32	0.02
Right PreSMA Op RD -- > DCCS	76	-189.96 (90.13)	-0.33	-2.11	0.04
Left PreSMA Op MD -- > HTKS	77	272.65 (86.03)	0.35	3.17	0.002
Left SMA Op FA -- > HTKS	75	-260.89 (100.3)	-0.33	-2.60	0.01
Left SMA Op RD -- > HTKS	75	370.07 (126.28)	0.46	2.93	0.004
Left SMA Op MD -- > HTKS	75	238.96 (96.2)	0.28	2.48	0.02
Left SMA Op GFA -- > HTKS	75	-974.28 (411.96)	-0.31	-2.36	0.02
<u>FAT Predicting Language in ADHD Sample, continued.</u>					

Continued on next page

Table 8 – continued from previous page

Predictor -- > Outcome	<i>df</i>	<i>B</i> (<i>SE</i>)	β	<i>t</i>	<i>p</i>
Left SMA Op QA -- > HTKS	75	-1057.46 (528.19)	-0.6	-2.00	0.049
Right PreSMA Op FA -- > HTKS	78	-289.5 (87.14)	-0.38	-3.32	0.001
Right PreSMA Op GFA -- > HTKS	78	-1294.06 (411.66)	-0.4	-3.14	0.002
Right PreSMA Op QA -- > HTKS	78	-1104.43 (448.54)	-0.65	-2.46	0.02
Right SMA Op FA -- > HTKS	76	-171.84 (82.63)	-0.25	-2.08	0.04
<u>FAT Group Interactions Predicting Executive Function</u>					
Left SMA Op FA -- > HTKS	146	-293.42 (105.84)	-0.17	-2.12	0.04
Left SMA Op RD -- > HTKS	146	239.99 (102.88)	0.15	1.98	0.049
Left SMA Op GFA -- > HTKS	146	-1137.93 (416.33)	-0.18	-2.10	0.04
Right PreSMA Op FA -- > HTKS	158	-333.67 (102.47)	-0.23	-2.23	0.03
Right PreSMA Op GFA -- > HTKS	158	-1526.79 (439.62)	-0.24	-2.27	0.02
PreSMA Op FA Laterality -- > HTKS	145	212.52 (69.36)	0.24	2.18	0.03
PreSMA Op GFA Laterality -- > HTKS	145	237.37 (73.45)	0.23	2.22	0.03

Robust linear regression models were ran to test the association of the bilateral FAT and our three executive function measures. Laterality is calculated as $(\text{Left} - \text{Right})/(\text{Left} + \text{Right})$. B = Unstandardized regression slope parameter estimate. SE = Standard error of the regression slope parameter estimate. β = Standardized regression slope parameter estimate. All findings control for age, sex, whole brain microstructure, movement in the scanner, and parental SES. In order to be concise, only findings where the confidence interval did not cross zero are reported. All p -values are two-tailed.

Table 9: DWI Metrics in Study 2.A and 2.B

Metrics	n	Measure
Study 2.A: HCP Adults		
multi-shell data		
b values = 500, 1000, 2000		
90 directions per shell		
<u>DTI Metrics</u>		
	840	Radial Diffusivity (RD)
	840	Axial Diffusivity (AD)
	840	Mean Diffusivity (MD)
	840	Fractional Anisotropy (FA)
<u>GQI Metrics</u>		
	840	Generalized Fractional Anisotropy (GFA)
	840	Normalized Quantitative Anisotropy (NQA)
<u>NODDI Metrics</u>		
	100	Intracellular Volume Fraction (ICVF)
	100	Isotropic Volume Fraction (ISOVF)
	100	Orientation Dispersion (OD)
<u>RDI Metric</u>		
	840	Restricted Diffusion Imaging (RDI)
Study 2.B: CMIND Developing		
single shell data		
b value = 3000		
61 directions		
<u>DTI Metrics</u>		
	129	Radial Diffusivity (RD)
	129	Axial Diffusivity (AD)
	129	Mean Diffusivity (MD)
	129	Fractional Anisotropy (FA)
<u>GQI Metrics</u>		
	129	Generalized Fractional Anisotropy (GFA)
	129	Normalized Quantitative Anisotropy (NQA)
<u>RDI Metric</u>		
	129	Restricted Diffusion Imaging (RDI)

This summary table provides a breakdown of the metrics that were analyzed for each study. Given the long computation time, a random sample of 100 out of 840 were chosen for NODDI analyses in Study 2.A. Furthermore, NODDI is only available for multi-shell acquisitions, so it could not be applied to the single-shell data in Study 2.B.

Table 10: Contrast Analyses for Axonal Density in Adult Sample

Metric	<i>n</i>	<i>t</i>	<i>d</i>	<i>p</i>
>0.4 μm Fiber Size				
Fractional Anisotropy (FA)	840	9.70	0.47	<0.001***
Radial Diffusivity (RD)	840	-28.48	-1.39	<0.001***
Axial Diffusivity (AD)	840	-60.60	-2.96	<0.001***
Mean Diffusivity (MD)	840	-41.90	-2.05	<0.001***
Generalized Fractional Anisotropy (GFA)	840	7.18	0.35	<0.001***
Normalized Quantitative Anisotropy (NQA)	840	-19.92	-0.97	<0.001***
Intracellular Volume Fraction (ICVF)	100	25.54	3.61	<0.001***
Isotropic Volume Fraction (ISOVF)	100	-4.56	-0.65	<0.001***
Orientation Dispersion (OD)	100	-0.06	-0.01	0.95
Restricted Diffusion Imaging (RDI)	840	-53.29	-2.60	<0.001***
>1 μm (A) Fiber Size Comparing B3 and S2				
Fractional Anisotropy (FA)	840	48.51	2.37	<0.001***
Radial Diffusivity (RD)	840	-39.68	-1.94	<0.001***
Axial Diffusivity (AD)	840	-6.27	-0.31	<0.001***
Mean Diffusivity (MD)	840	-34.47	-1.68	<0.001***
Generalized Fractional Anisotropy (GFA)	840	52.42	2.56	<0.001***
Normalized Quantitative Anisotropy (NQA)	840	32.28	1.58	<0.001***
Intracellular Volume Fraction (ICVF)	100	17.35	2.45	<0.001***
Isotropic Volume Fraction (ISOVF)	100	-7.71	-1.09	<0.001***
Orientation Dispersion (OD)	100	-7.28	-1.03	<0.001***
Restricted Diffusion Imaging (RDI)	840	-22.92	-1.12	<0.001***
>1 μm (B) Fiber Size Comparing S2 and S3				
Fractional Anisotropy (FA)	840	17.53	0.86	<0.001***
Radial Diffusivity (RD)	840	-13.99	-0.68	<0.001***
Axial Diffusivity (AD)	840	4.29	0.21	<0.001***
Mean Diffusivity (MD)	840	-10.88	-0.53	<0.001***
Generalized Fractional Anisotropy (GFA)	840	22.85	1.12	<0.001***
Normalized Quantitative Anisotropy (NQA)	840	5.30	0.26	<0.001***
Intracellular Volume Fraction (ICVF)	100	-6.28	-0.89	<0.001***
Isotropic Volume Fraction (ISOVF)	100	-9.73	-1.38	<0.001***
Orientation Dispersion (OD)	100	-12.09	-1.71	<0.001***
Restricted Diffusion Imaging (RDI)	840	-6.02	-0.29	<0.001***
>5 μm Fiber Size				
Fractional Anisotropy (FA)	840	4.73	0.23	<0.001***
Radial Diffusivity (RD)	840	20.65	1.01	<0.001***
Axial Diffusivity (AD)	840	70.50	3.44	<0.001***
Mean Diffusivity (MD)	840	38.56	1.88	<0.001***
Generalized Fractional Anisotropy (GFA)	840	7.83	0.38	<0.001***
Normalized Quantitative Anisotropy (NQA)	840	35.17	1.72	<0.001***
Intracellular Volume Fraction (ICVF)	100	-24.66	-3.49	<0.001***

Continued on next page

Table 10 – continued from previous page

Metric	<i>n</i>	<i>t</i>	<i>d</i>	<i>p</i>
Isotropic Volume Fraction (ISOVF)	100	3.14	0.44	<0.001***
Orientation Dispersion (OD)	100	-1.21	-0.17	0.23
Restricted Diffusion Imaging (RDI)	840	58.24	2.84	<0.001***

Contrast analyses for corpus callosum density patterns in the adult sample. These values have been Winsor outlier corrected. $p < 0.05^*$, $p < 0.01^{**}$, $p < 0.001^{***}$.

Table 11: Contrast Analyses for Axonal Density in Developing Sample

Metric	<i>n</i>	<i>t</i>	<i>d</i>	<i>p</i>
>0.4 μm Fiber Size				
Fractional Anisotropy (FA)	129	28.66	3.57	<0.001***
Radial Diffusivity (RD)	129	-21.23	-2.64	<0.001***
Axial Diffusivity (AD)	129	-0.10	-0.01	0.92
Mean Diffusivity (MD)	129	-15.40	-1.92	<0.001***
Generalized Fractional Anisotropy (GFA)	129	27.86	3.47	<0.001***
Normalized Quantitative Anisotropy (NQA)	129	4.88	0.61	<0.001***
Restricted Diffusion Imaging (RDI)	129	-24.79	-3.09	<0.001***
>1 μm (A) Fiber Size Comparing B3 and S2				
Fractional Anisotropy (FA)	129	23.88	2.97	<0.001***
Radial Diffusivity (RD)	129	-15.29	-1.90	<0.001***
Axial Diffusivity (AD)	129	3.67	0.46	<0.001***
Mean Diffusivity (MD)	129	-9.71	-1.21	<0.001***
Generalized Fractional Anisotropy (GFA)	129	25.16	3.13	<0.001***
Normalized Quantitative Anisotropy (NQA)	129	18.70	2.33	<0.001***
Restricted Diffusion Imaging (RDI)	129	-0.85	-0.11	0.40
>1 μm (B) Fiber Size Comparing S2 and S3				
Fractional Anisotropy (FA)	129	1.15	0.22	0.08
Radial Diffusivity (RD)	129	-1.67	-0.21	0.10
Axial Diffusivity (AD)	129	-0.02	-0.003	0.98
Mean Diffusivity (MD)	129	-1.16	-0.14	0.24
Generalized Fractional Anisotropy (GFA)	129	3.64	0.45	<0.001***
Normalized Quantitative Anisotropy (NQA)	129	1.17	0.17	0.24
Restricted Diffusion Imaging (RDI)	129	-2.44	-0.30	<0.05*
>5 μm Fiber Size				
Fractional Anisotropy (FA)	129	-27.46	-3.42	<0.001***
Radial Diffusivity (RD)	129	21.94	2.73	<0.001***
Axial Diffusivity (AD)	129	2.87	0.36	<0.01**
Mean Diffusivity (MD)	129	16.93	2.11	<0.001***
Generalized Fractional Anisotropy (GFA)	129	-25.55	-3.18	<0.001***
Normalized Quantitative Anisotropy (NQA)	129	1.04	0.13	0.30
Restricted Diffusion Imaging (RDI)	129	30.36	3.78	<0.001***

Contrast analyses for corpus callosum density patterns in the developing sample. These values have been Winsor outlier corrected. $p < 0.05^*$, $p < 0.01^{**}$, $p < 0.001^{***}$.

Table 12: NODDI Means and Group Differences

Region	Hemi	NDI (<i>SE</i>) [Group β]	ODI (<i>SE</i>) [Group β]
PreSMA	Left	0.28 (.004) [0.1]	0.41 (.006) [-0.12]
	Right	0.27 (.005) [0.11]	0.40 (.007) [-0.12]
	Lat	0.04 (.012) [-0.03]	0.04 (.011) [0.16*]
SMA	Left	0.29 (.004) [0.11]	0.42 (.006) [-0.08]
	Right	0.29 (.005) [0.13]	0.41 (.006) [-0.07]
	Lat	-0.01 (.005) [-0.09]	0.02 (.005) [-0.01]
Op	Left	0.28 (.004) [0.15*]	0.45 (.005) [-0.11]
	Right	0.29 (.003) [0.000]	0.45 (.004) [-0.06]
	Lat	-0.02 (.007) [0.1]	-0.01 (.005) [-0.08]
Tri	Left	0.28 (.003) [0.07]	0.43 (.006) [-0.17*]
	Right	0.25 (.004) [-0.12]	0.41 (.007) [-0.18**]
	Lat	-0.02 (.009) [-0.01]	.03 (.011) [0.03]
Caudate	Left	0.37 (.004) [0.17*]	0.43 (.006) [-0.19**]
	Right	0.36 (.004) [0.11]	0.43 (.005) [-0.15*]
	Lat	0.002 (.005) [0.08]	.004 (.007) [-0.02]
Putamen	Left	0.36 (.003) [0.03]	0.45 (.004) [-0.21**]
	Right	0.36 (.003) [-0.11]	0.44 (.005) [-0.15*]
	Lat	0.001 (.003) [0.19**]	0.01 (.005) [0.00]

First number represents the region mean, SE in parenthesis, and group difference (β) in brackets. ADHD was dummy coded as 1, so higher β indicates higher value for ADHD compared to TD, controlling for whole brain microstructure. *SE* = Standard error of the regression slope parameter estimate. β = Standardized regression slope parameter estimate. Laterality ("Lat") is calculated as (Left - Right)/(Left + Right). $p < 0.05^*$, $p < 0.01^{**}$, $p < 0.001^{***}$.

Table 13: Region-Based Age Related Change

Region	Hemi	NDI	ODI
PreSMA	Left	0.002	-0.02
	Right	-0.04	-0.02
	Lat	0.08***	0.01
SMA	Left	-0.01	-0.02
	Right	-0.04	0.004
	Lat	0.05	-0.02
Op	Left	-0.03	0.04
	Right	0.10*	-0.05
	Lat	-0.05	0.03
Tri	Left	-0.02	-0.03
	Right	0.02	-0.05
	Lat	-0.07	0.01
Caudate	Left	0.12***	-0.01
	Right	0.16***	-0.09
	Lat	-0.02	0.03
Putamen	Left	0.21***	-0.02
	Right	0.16***	-0.02
	Lat	-0.01	0.003

The β from the robust regression coefficient is shown for each brain region/ Calculations controlled for sex, whole brain microstructure, and movement in the scanner. PreSMA = presupplementary motor area, SMA = supplementary motor area, Op = *pars opercularis*, Tri = *pars triangularis*. Diffusion metrics, NDI = neurite density imaging, ODI = orientation dispersion imaging. Laterality ("Lat") is calculated as $(\text{Left} - \text{Right}) / (\text{Left} + \text{Right})$. $p < 0.05^*$, $p < 0.01^{**}$, $p < 0.001^{***}$.

Table 14: Neurite Density and Orientation Predicting Language Outcomes

Predictor -- > Outcome	<i>df</i>	<i>B (SE)</i>	β	<i>t</i>	<i>p</i>
<u>Brain Regions Predicting Language in Full Sample</u>					
Caudate NDI Laterality -- > NEPSY Semantics	186	-17.52 (7.59)	-0.15	-2.31	0.02
Right PreSMA NDI -- > SRT Phonemic Articulation	104	46.18 (20.78)	0.18	2.22	0.03
PreSMA NDI Laterality -- > SRT Phonemic Articulation	104	-24.57 (11.53)	-0.20	-2.13	0.04
Putamen ODI Laterality -- > SRT Phonemic Articulation	106	58.11 (27.66)	0.15	2.10	0.04
<u>Brain Regions Predicting Language in TD Sample</u>					
SMA NDI Laterality -- > NEPSY Semantics	84	48.84 (20.49)	0.29	2.34	0.02
Right PreSMA NDI -- > SRT Phonemic Articulation	47	53.90 (23.77)	0.20	2.27	0.03
<u>FAT Predicting Language in ADHD Sample</u>					
Caudate ODI Laterality -- > NEPSY Phonemics	92	12.76 (6.33)	0.19	2.02	0.05
SMA NDI Laterality -- > NEPSY Phonemics	88	22.38 (9.18)	0.22	2.44	0.02
Caudate NDI Laterality -- > NEPSY Semantics	93	-23.37 (8.48)	-0.23	-2.76	0.01
Right PreSMA NDI -- > SRT Phonemic Articulation	50	77.94 (39.65)	0.33	1.97	0.05
PreSMA NDI Laterality -- > SRT Phonemic Articulation	50	-55.57 (21.81)	-0.47	-2.55	0.01

Robust linear regression models were ran to test the association of the bilateral FAT and our three language measures. Laterality is calculated as (Left - Right)/(Left + Right). B = Unstandardized regression slope parameter estimate. SE = Standard error of the regression slope parameter estimate. β = Standardized regression slope parameter estimate. All findings control for age, sex, whole brain microstructure, movement in the scanner, and parental SES. In order to be concise, only findings where the confidence interval did not cross zero are reported. All p -values are two-tailed.

Table 15: Neurite Density and Orientation Predicting Executive Function

Predictor -- > Outcome	<i>df</i>	<i>B (SE)</i>	β	<i>t</i>	<i>p</i>
<u>Brain Regions Predicting Executive Function in Full Sample</u>					
SMA NDI Laterality -- > Flanker Task	153	65.71 (25.73)	0.20	2.55	0.01
SMA ODI Laterality -- > DCCS	155	60.39 (23.98)	0.20	2.52	0.01
Right Tri NDI -- > HTKS	170	94.75 (48.47)	0.15	1.95	0.05
<u>Brain Regions Predicting Executive Function in TD Sample</u>					
Left SMA NDI -- > Flanker Task	67	-75.44 (34.68)	-0.27	2.18	0.03
Left PreSMA ODI -- > Flanker Task	67	-47.01 (18.17)	-0.28	-2.59	0.01
Left SMA ODI -- > Flanker Task	67	-51.92 (19.07)	-0.31	-2.72	0.01
Left Op ODI -- > Flanker Task	69	-43.99 (18.48)	-0.26	-2.38	0.02
Left Tri ODI -- > Flanker Task	69	-52.18 (18.13)	-0.30	-2.88	0.01
Left Caudate ODI -- > Flanker Task	69	-57.55 (19.03)	-0.34	-3.02	0.004
Left Putamen ODI -- > Flanker Task	69	-46.44 (23.12)	-0.23	-2.01	0.05
Right PreSMA ODI -- > Flanker Task	68	-31.06 (12.54)	-0.24	-2.48	0.02
Right SMA ODI -- > Flanker Task	67	-46.40 (18.51)	-0.28	-2.51	0.02
Right Caudate ODI -- > Flanker Task	69	-52.59 (22.51)	-0.30	-2.34	0.02
Right Putamen ODI -- > Flanker Task	69	-44.96 (19.21)	-0.25	-2.34	0.02
PreSMA ODI Laterality -- > Flanker Task	67	47.98 (19.48)	0.26	2.47	0.02
Left SMA ODI -- > DCCS	68	-51.71 (25.54)	-0.26	-2.02	0.05
Left Op ODI -- > DCCS	70	-61.35 (24.87)	-0.31	-2.47	0.02
Right PreSMA ODI -- > DCCS	69	-40.28 (16.71)	-0.27	-2.41	0.02
Right SMA ODI -- > DCCS	68	-56.08 (24.19)	-0.29	-2.32	0.02
PreSMA ODI Laterality -- > DCCS	68	56.31 (24.88)	0.27	2.26	0.03
SMA ODI Laterality -- > DCCS	68	86.82 (38)	0.26	2.28	0.03
Op ODI Laterality -- > DCCS	70	-94.85 (41.50)	-0.30	-2.29	0.03
Left PreSMA ODI -- > HTKS	76	-54.55 (25.77)	-0.21	-2.12	0.04
Left SMA ODI -- > HTKS	76	-60.78 (26.77)	-0.23	-2.27	0.03
Left Caudate ODI -- > HTKS	78	-65.72 (29.09)	-0.24	-2.26	0.03

Continued on next page

Table 15 – continued from previous page

Predictor -- > Outcome	<i>df</i>	<i>B</i> (<i>SE</i>)	β	<i>t</i>	<i>p</i>
Right SMA ODI -- > HTKS	76	-61.16 (26.76)	-0.23	-2.29	0.03
Right Putamen ODI -- > HTKS	78	-60.17 (29.27)	-0.21	-2.06	0.04
Right Tri NDI -- > HTKS	78	95.88 (35.27)	0.25	2.72	0.01
Op NDI Laterality -- > HTKS	78	-68.60 (29.12)	-0.23	-2.36	0.02
Tri NDI Laterality -- > HTKS	78	-49.92 (22.82)	-0.23	-2.19	0.03
<u>FAT Group Interactions Predicting Executive Function</u>					
Left SMA NDI -- > Flanker Task	152	97.49 (42.49)	0.13	2.02	0.05
PreSMA ODI Laterality -- > DCCS	155	-56.34 (27.11)	-0.15	-2.06	0.04
Op ODI Laterality -- > DCCS	156	94.75 (48.47)	0.15	1.99	0.05

Robust linear regression models were ran to test the association of 12 brain regions and executive function, as measured by NIH Toolbox tasks (flanker and DCCS) and HTKS. Laterality is calculated as (Left – Right)/(Left + Right). *B* = Unstandardized regression slope parameter estimate. *SE* = Standard error of the regression slope parameter estimate. β = Standardized regression slope parameter estimate. All findings control for age, sex, whole brain microstructure, movement in the scanner, and parental SES. In order to be concise, only findings where the confidence interval did not cross zero are reported. All *p*-values are two-tailed.

FIGURES

Figure 1: FAT Anatomy

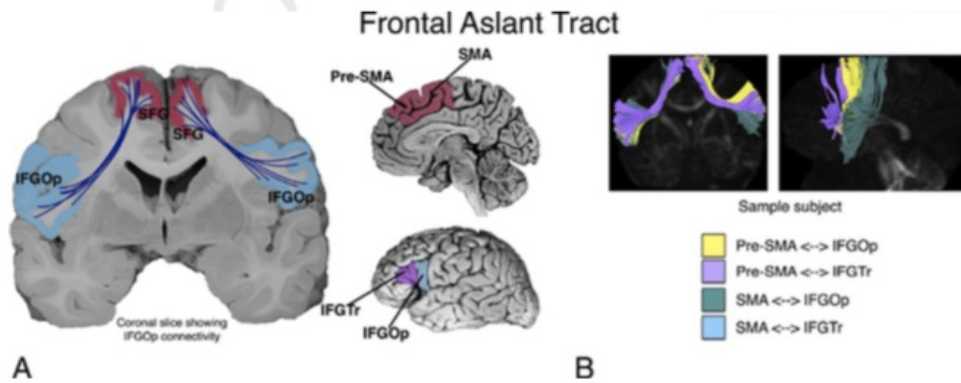
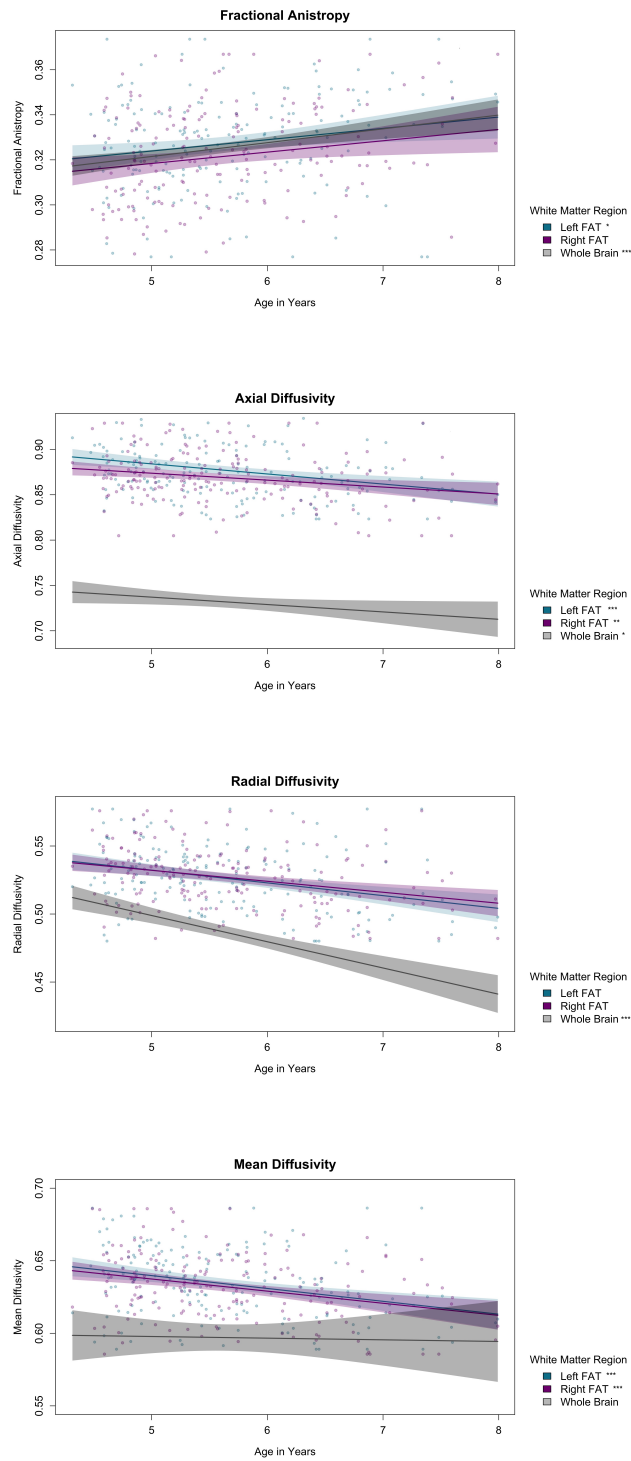


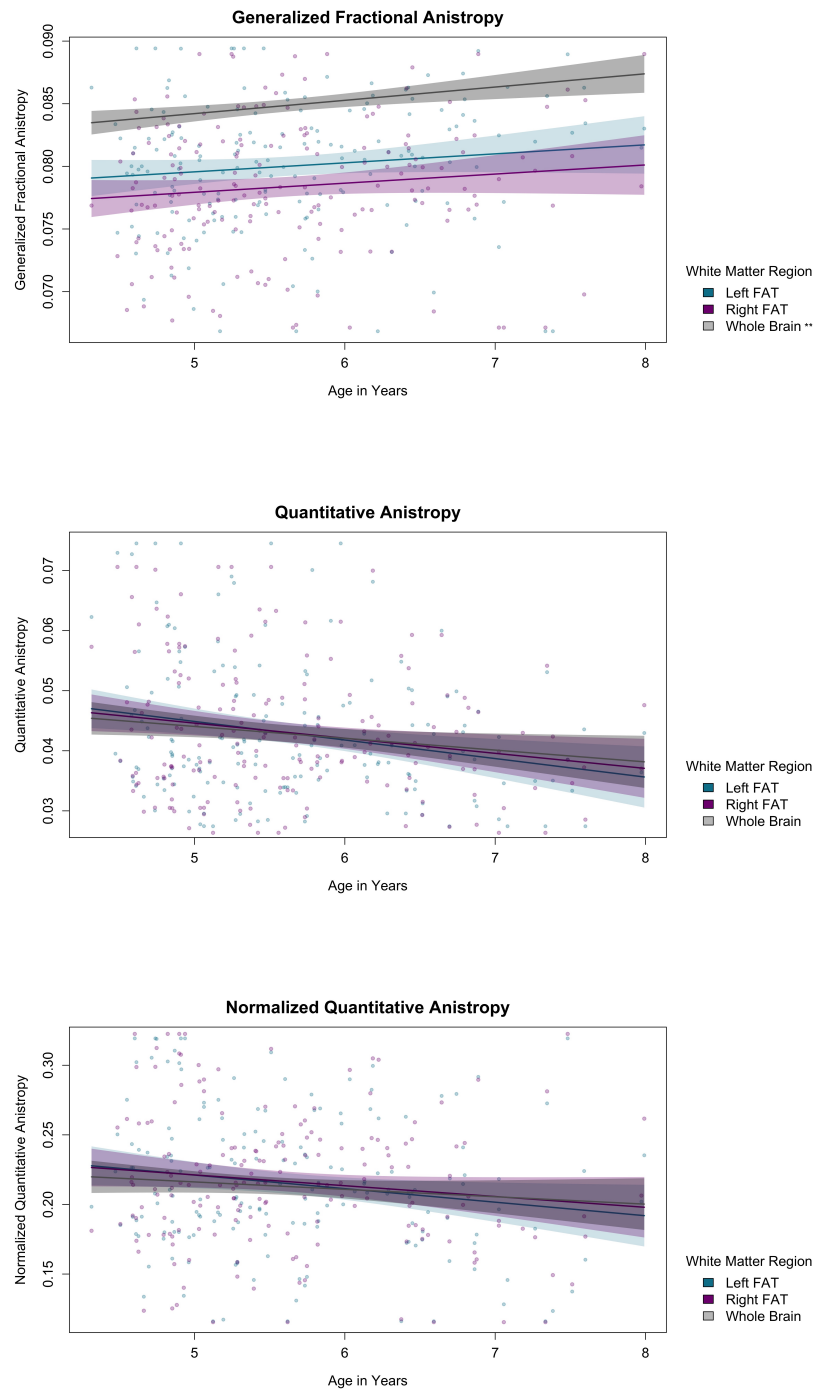
Illustration of the putative connectivity of the frontal aslant tract (FAT). (a) Connectivity of the tract is bilateral between the inferior frontal gyrus (pars opercularis (Op) and pars triangularis (Tri) and the superior frontal gyrus (namely, pre-supplementary motor area (pre-SMA) and supplementary motor area (SMA)). (b) The pathway can be further differentiated into four parts connecting two parts of the IFG to the pre-SMA and SMA.

Figure 2: Age-related differences in the FAT by DTI metric: Winsor.



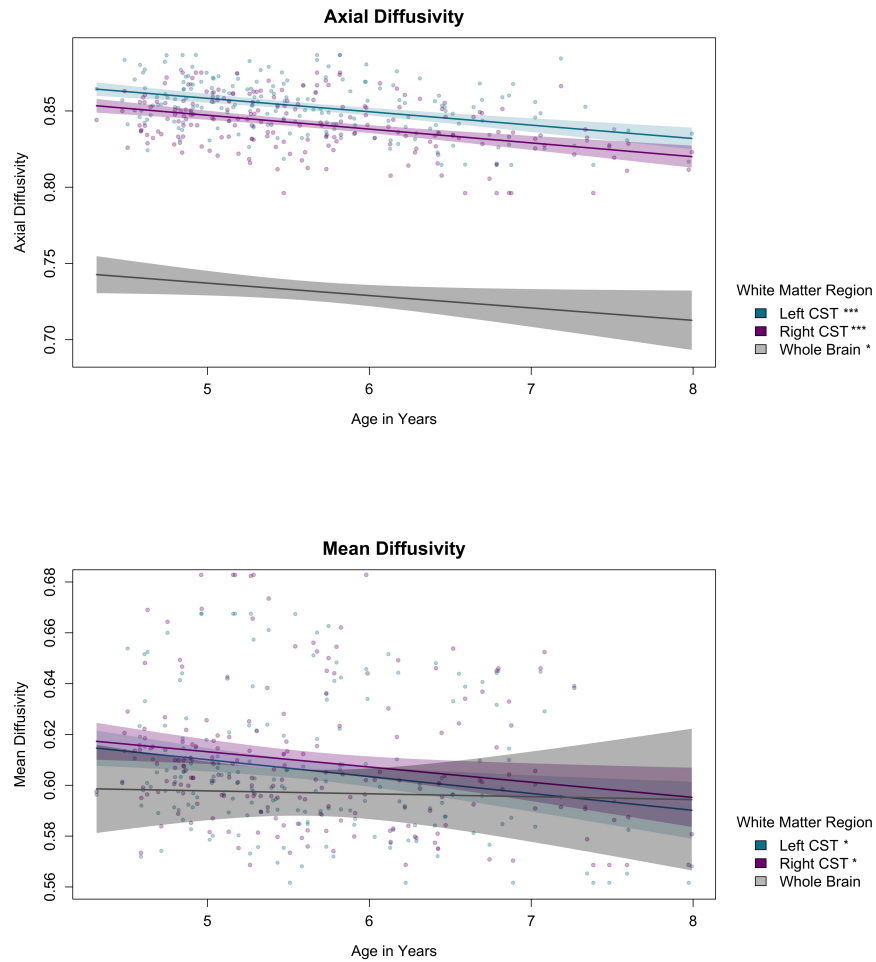
Age-related differences, as measured in DTI metrics, in the FAT compared to whole brain microstructural development. These plots display the Winsor outlier corrections. Primary segment (preSMA to Op) selected since it had the largest sample sizes. Significance is indicated by *s in the key. $p < 0.05^*$, $p < 0.01^{**}$, $p < 0.001^{***}$.

Figure 3: Age-related changes in the FAT by HARDI metric: Winsor.



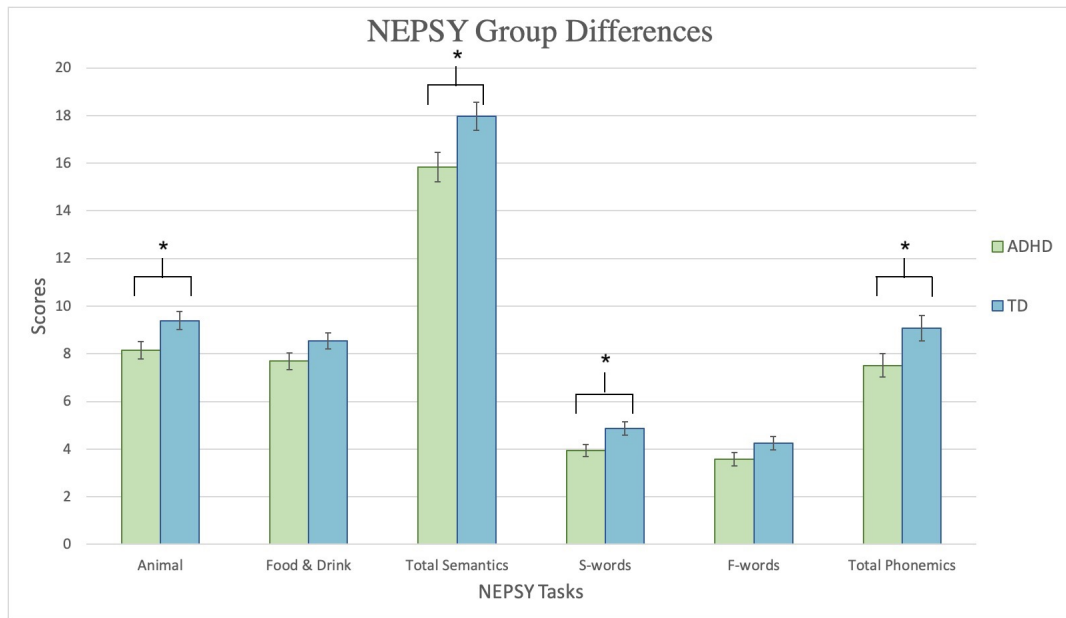
Age-related differences, as measured in HARDI metrics, in the FAT compared to whole brain microstructural development. These plots display the Winsor outlier corrections. Primary segment (preSMA to Op) selected since it had the largest sample sizes. Significance is indicated by *s in the key. $p < 0.05^*$, $p < 0.01^{**}$, $p < 0.001^{***}$.

Figure 4: Significant Age-related differences in the CST: Winsor.



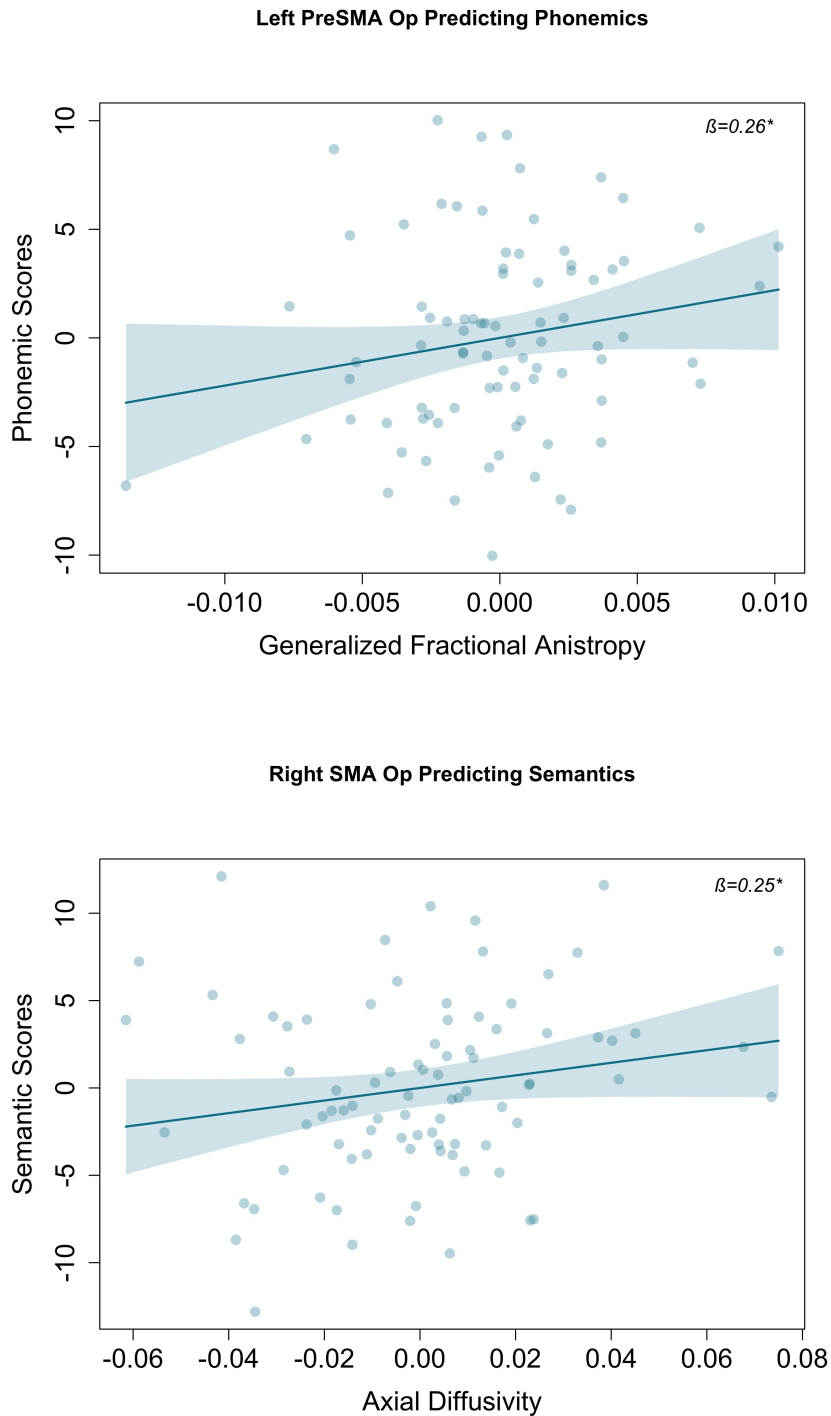
Age-related differences in the CST, the control pathway, compared to whole brain microstructural development. These plots display the Winsor outlier corrections. Only significant metrics for the control pathway are displayed. Significance is indicated by *s in the key. $p < 0.05^*$, $p < 0.01^{**}$, $p < 0.001^{***}$.

Figure 5: NEPSY Group Differences



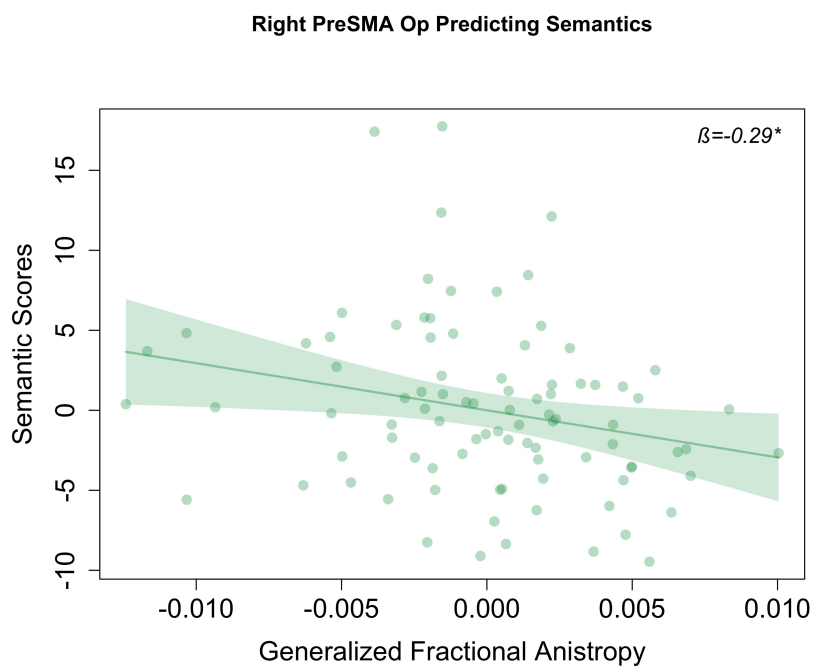
This figure shows the mean scores on all NEPSY tasks, with gray representing TD group scores and blue representing ADHD group scores. The findings also control for age, sex, and SES. $p < 0.05^*$, $p < 0.01^{**}$, $p < 0.001^{***}$.

Figure 6: FAT Predicting Phonemic and Semantic Scores in TD Sample



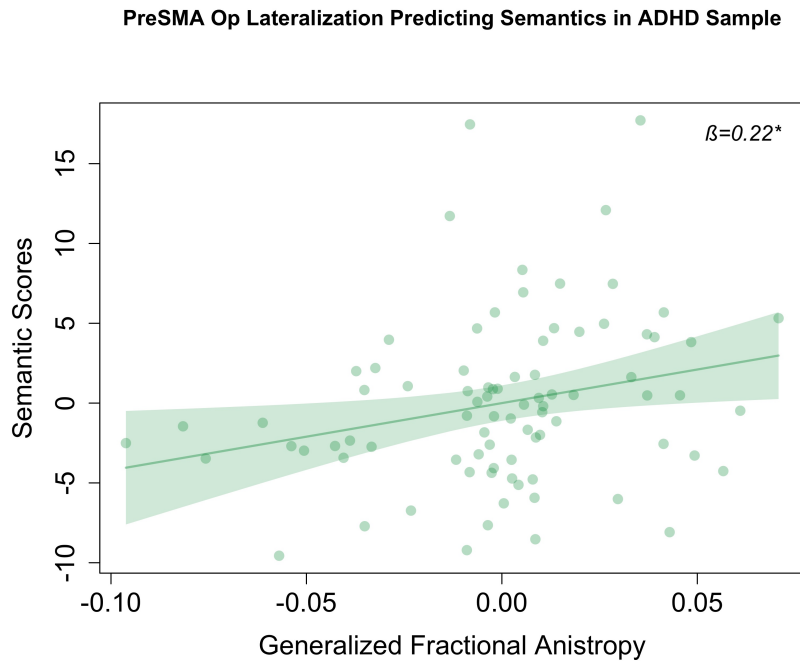
Left and right hemisphere FAT segments in the TD sample predicting NEPSY phonemic and semantic scores in a robust linear regression, controlling for age, sex, whole brain microstructure, movement in the scanner, and SES. $p < 0.05^*$, $p < 0.01^{**}$, $p < 0.001^{***}$.

Figure 7: FAT Predicting Semantic Scores in ADHD Sample



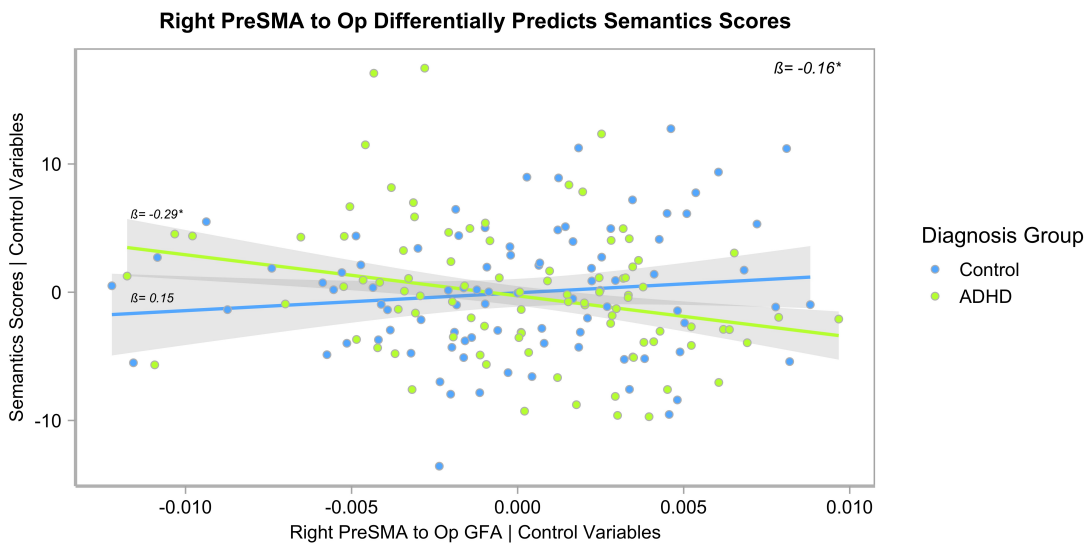
Right preSMA to Op segment in the ADHD sample negatively predicting NEPSY semantic scores in a robust linear regression, controlling for age, sex, whole brain GFA, movement in the scanner, and SES. $p < 0.05^*$, $p < 0.01^{**}$, $p < 0.001^{***}$.

Figure 8: FAT Lateralization Association with Semantic Scores in ADHD Sample



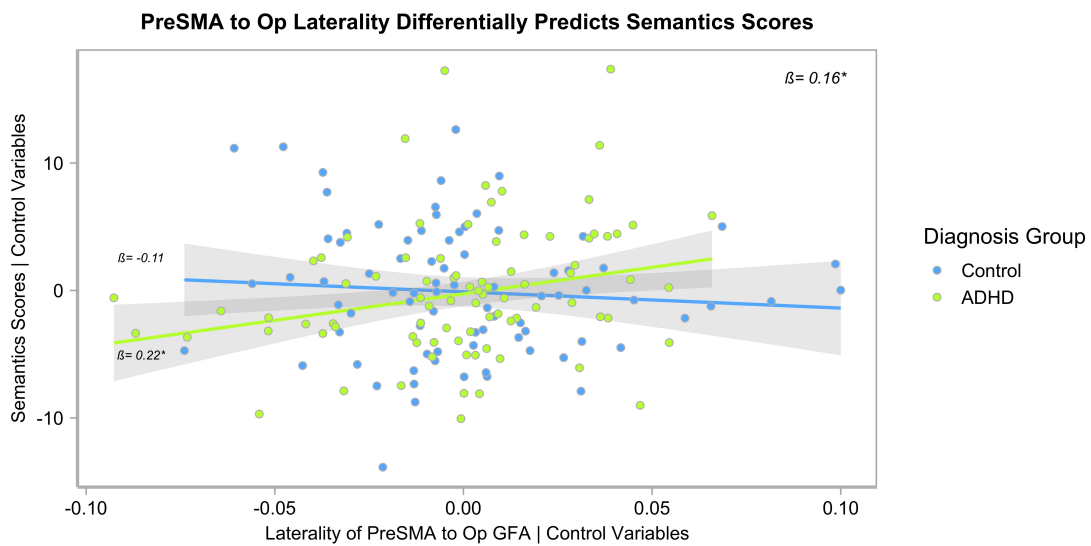
This plot shows how increased left lateralization in the primary FAT segment, the preSMA to Op, predicts higher semantic scores in the ADHD sample. Laterality was calculated using Thiebaut de Schotten et al. (2014) formula $(\text{left} - \text{right}) / (\text{left} + \text{right})$ in which positive values indicate left laterality. $p < 0.05^*$, $p < 0.01^{**}$, $p < 0.001^{***}$.

Figure 9: ADHD Diagnosis Moderates Relationship Between Right FAT and Semantics



Significant interaction between group diagnosis and the preSMA to Op segment predicting NEPSY semantic scores, with higher GFA within the segment predicting lower semantic scores in the ADHD sample while having a trending, positive effect for the TD sample. $p < 0.05^*$, $p < 0.01^{**}$, $p < 0.001^{***}$.

Figure 10: ADHD Diagnosis Moderates Effect of PreSMA Op Laterality's Relationship with Semantics



Significant interaction between group diagnosis and the lateralization of the preSMA to Op segment predicting NEPSY semantic scores, with higher left lateralization predicting higher semantic scores in the ADHD sample while having no significant impact for the TD sample. Laterality was calculated using Thiebaut de Schotten et al. (2014) formula $(\text{left} - \text{right}) / (\text{left} + \text{right})$ in which positive values indicate left lateralization. $p < 0.05^*$, $p < 0.01^{**}$, $p < 0.001^{***}$.

Figure 11: Left FAT Predicting Phoneme Articulation in Full Sample

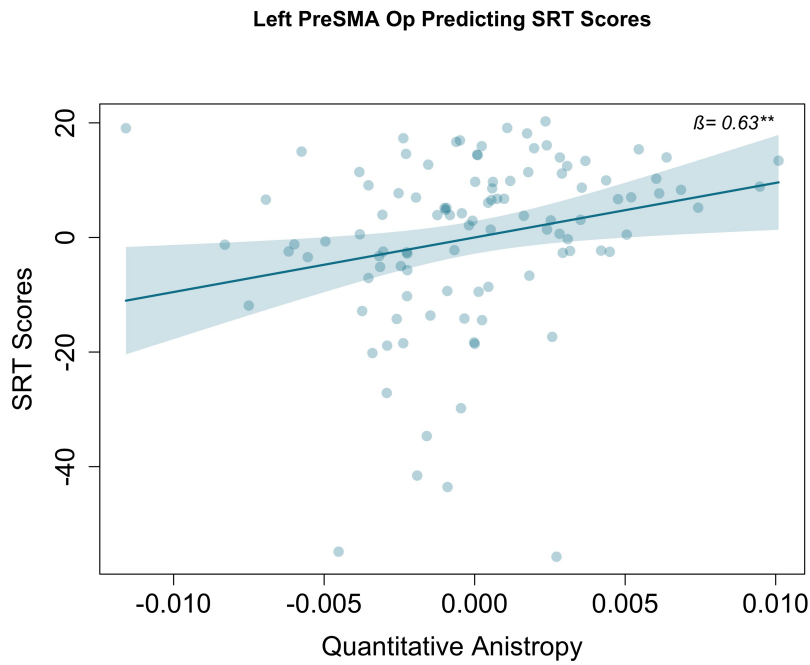
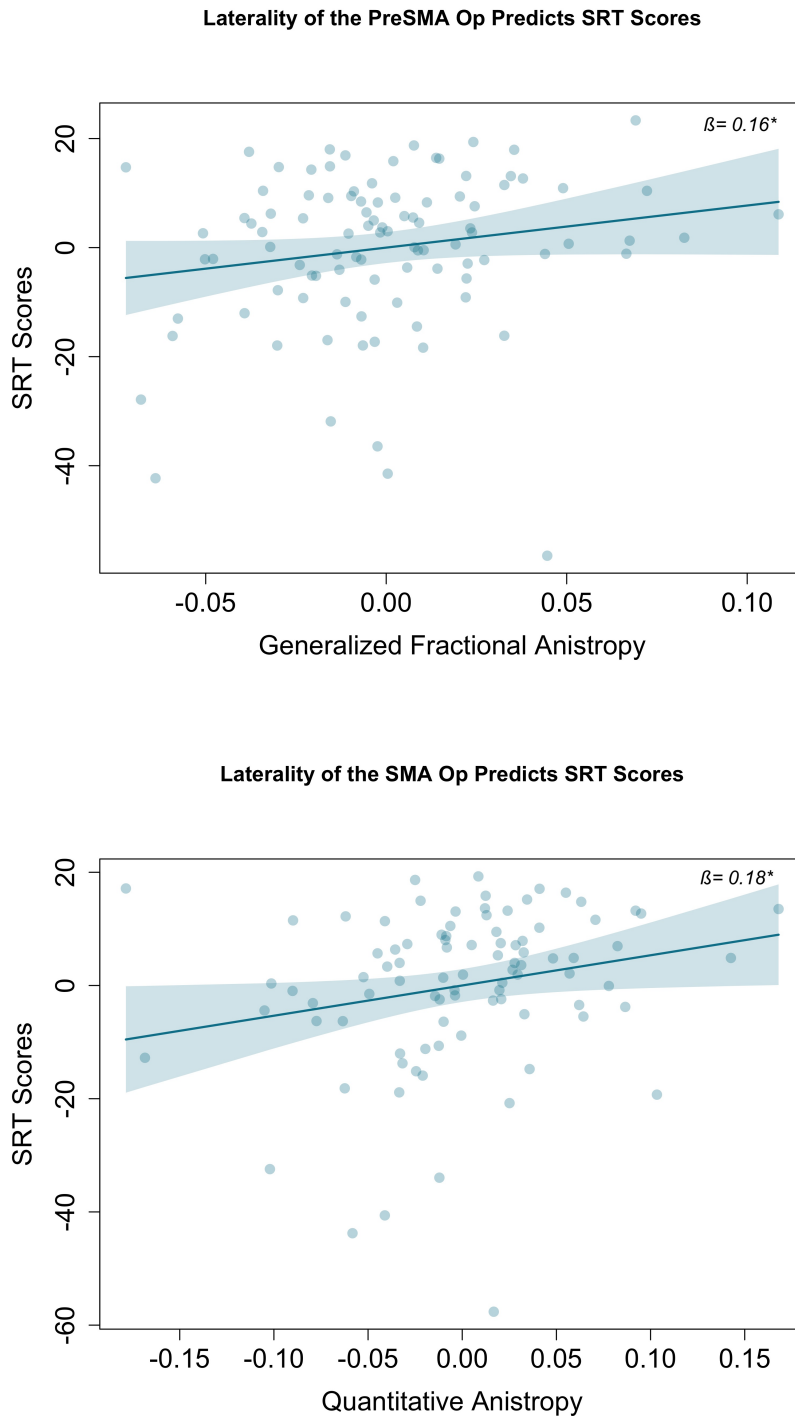


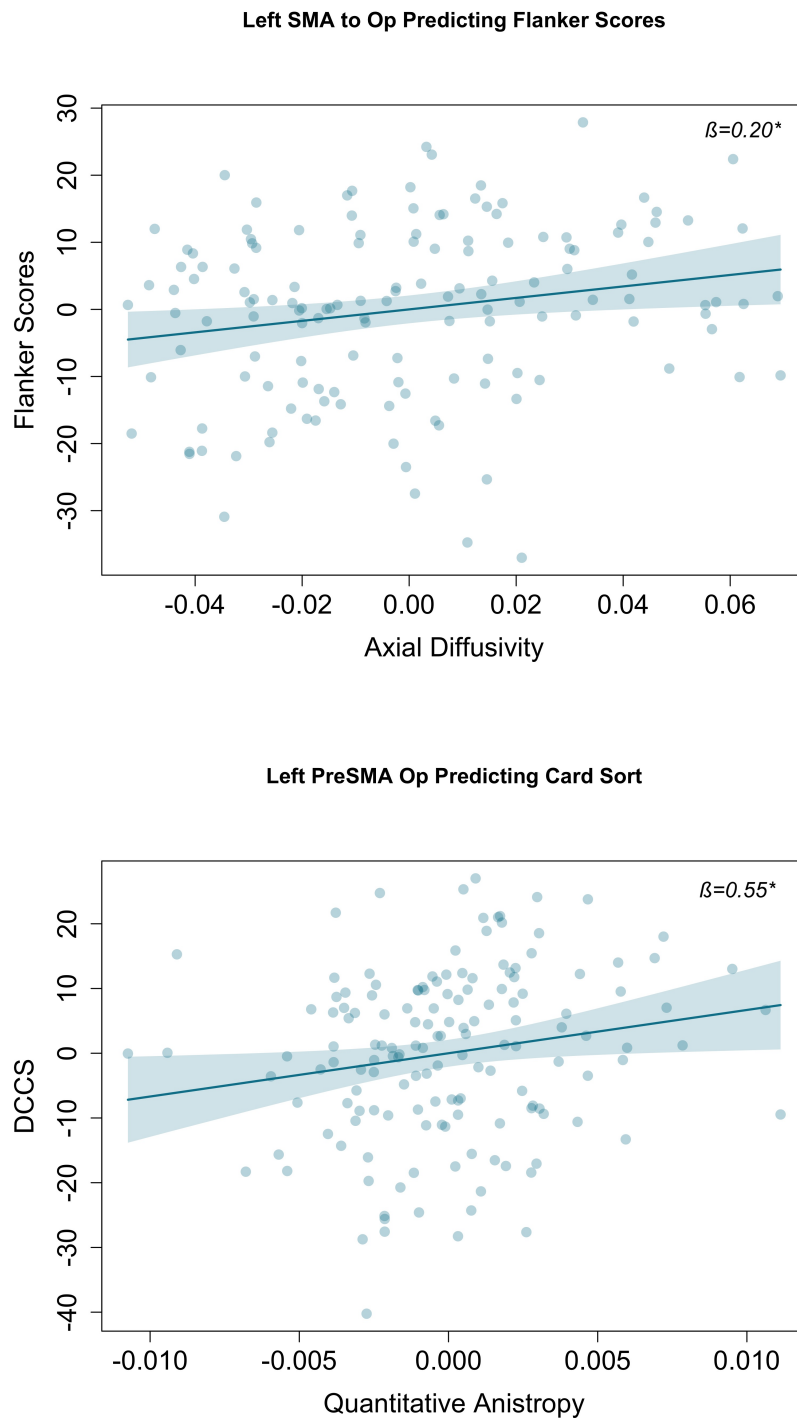
Figure 11 illustrates the association between the left PreSMA to Op projection and phoneme articulation as measured by the SRT. In the full sample, higher QA in this FAT segment predicted higher accuracy on the SRT task. $p < 0.05^*$, $p < 0.01^{**}$, $p < 0.001^{***}$.

Figure 12: Left Lateralization of the FAT Predicts SRT in Full Sample



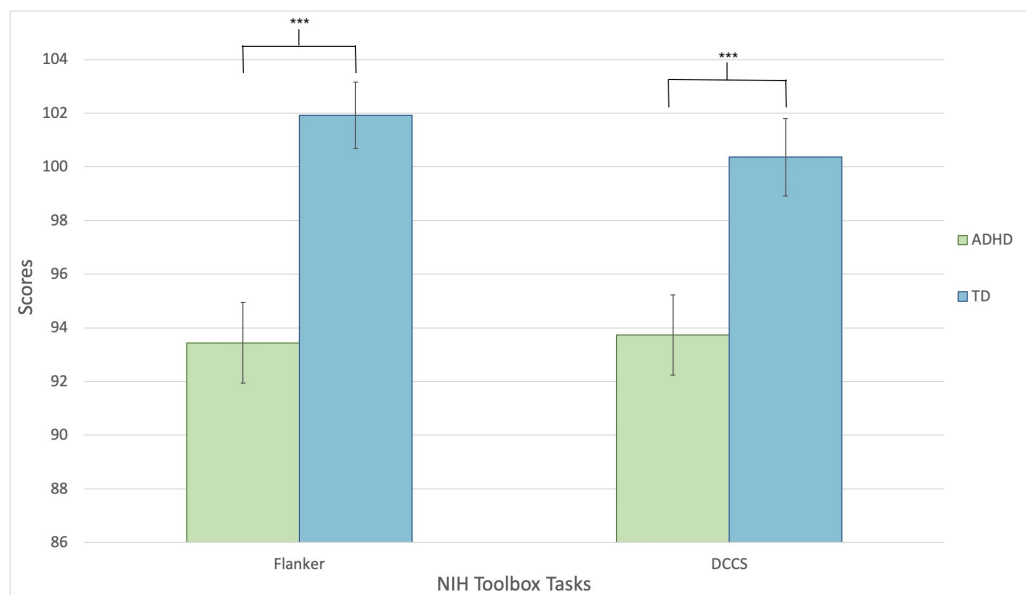
Higher left lateralization of the FAT predicts better phonemic articulation in the full sample, controlling for age, gender, whole brain microstructure, movement in the scanner, and SES. $p < 0.05^*$, $p < 0.01^{**}$, $p < 0.001^{***}$.

Figure 13: Left FAT Predicting Flanker and DCCS Scores in Full Sample



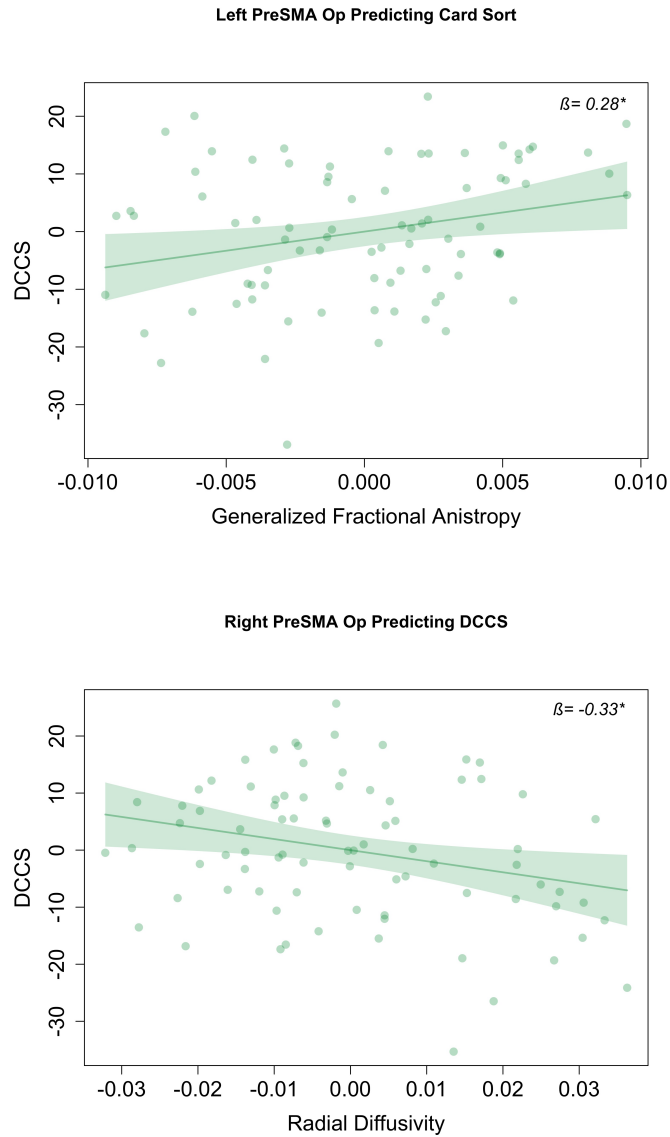
The left SMA to Op projection predicted flanker scores, while the left preSMA to Op predicted DCCS. The NIH Toolbox results represent age-correct scores, additionally controlling for gender, whole brain microstructure, movement in the scanner, and SES. This plot depicts the full sample of children. $p < 0.05^*$, $p < 0.01^{**}$, $p < 0.001^{***}$.

Figure 14: Group Differences in NIH Toolbox Tasks



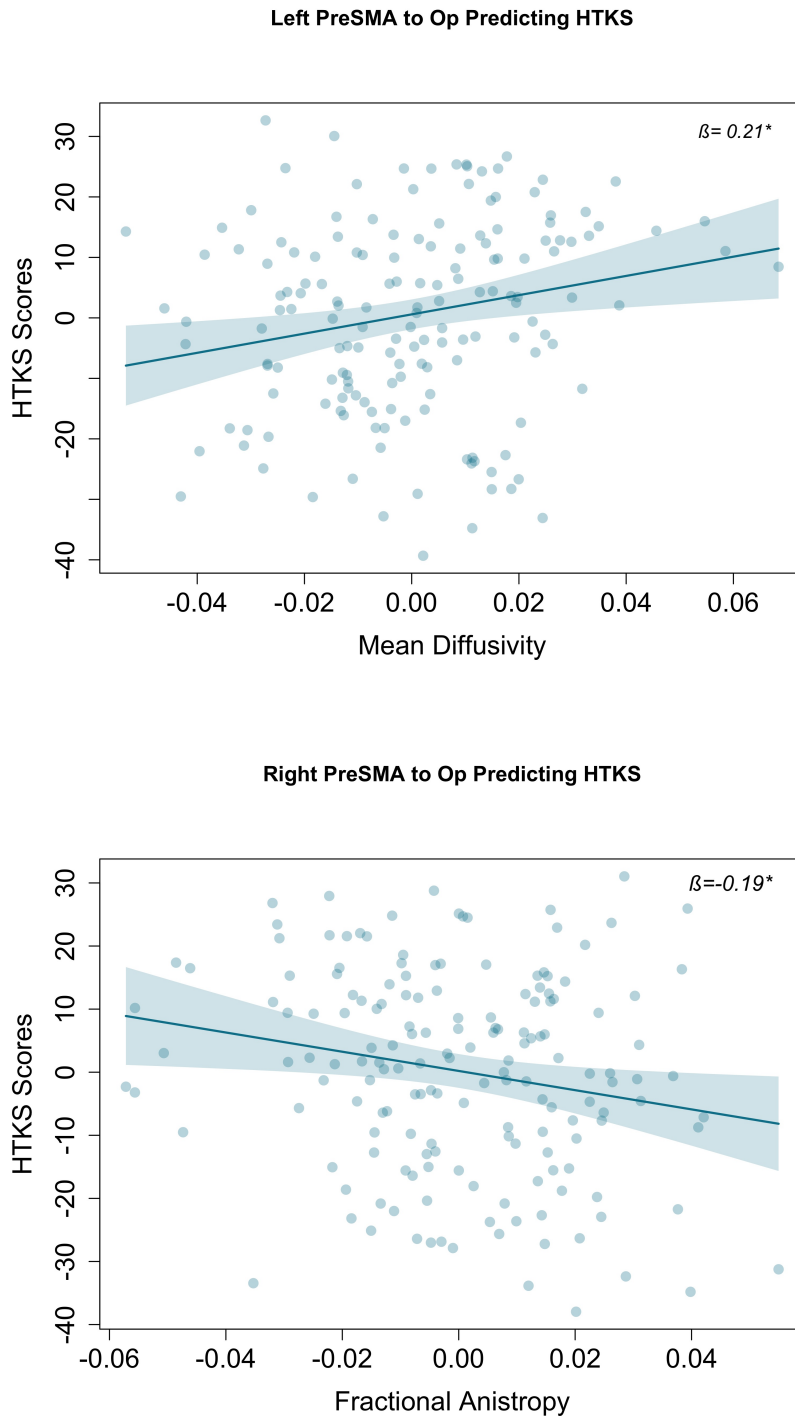
This figure shows the mean scores for the flanker and DCCS tasks, with blue representing TD group scores and green representing ADHD group scores. The findings also control for age, sex, and SES. $p < 0.05^*$, $p < 0.01^{**}$, $p < 0.001^{***}$.

Figure 15: Bilateral FAT Predicting NIH Toolbox in ADHD Sample



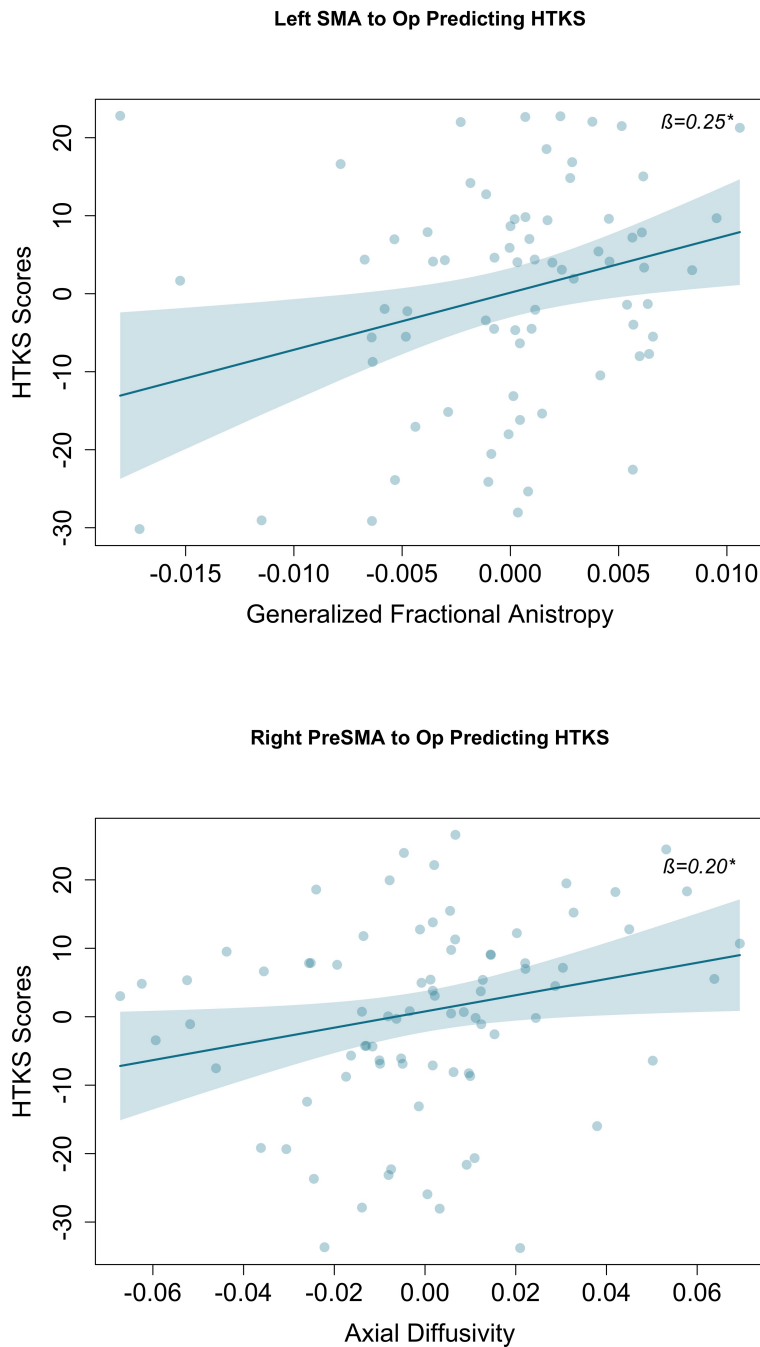
This figure shows how segments of the left and right preSMA projections predict age-corrected standard scores on the NIH Toolbox DCCS, controlling for sex, whole brain GFA, movement in the scanner, and SES. Lower RD represents higher myelination, therefore the bottom plot is inversely interpreted. $p < 0.05^*$, $p < 0.01^{**}$, $p < 0.001^{***}$.

Figure 16: Bilateral FAT Predicting HTKS Scores in Full Sample



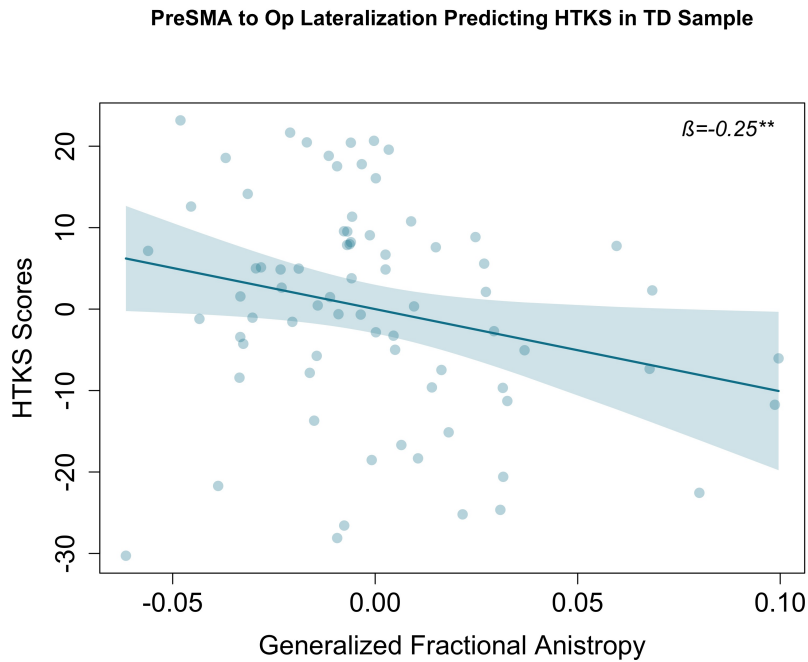
The left and right FAT predicted worse performance on the HTKS controlling for age, gender, whole brain microstructure, movement in the scanner, and SES. MD results are inversely interpreted, with higher MD indicating a less developed pathway. These plots depict the full sample of children. $p < 0.05^*$, $p < 0.01^{**}$, $p < 0.001^{***}$.

Figure 17: Bilateral FAT Predicting HTKS Scores in TD Sample



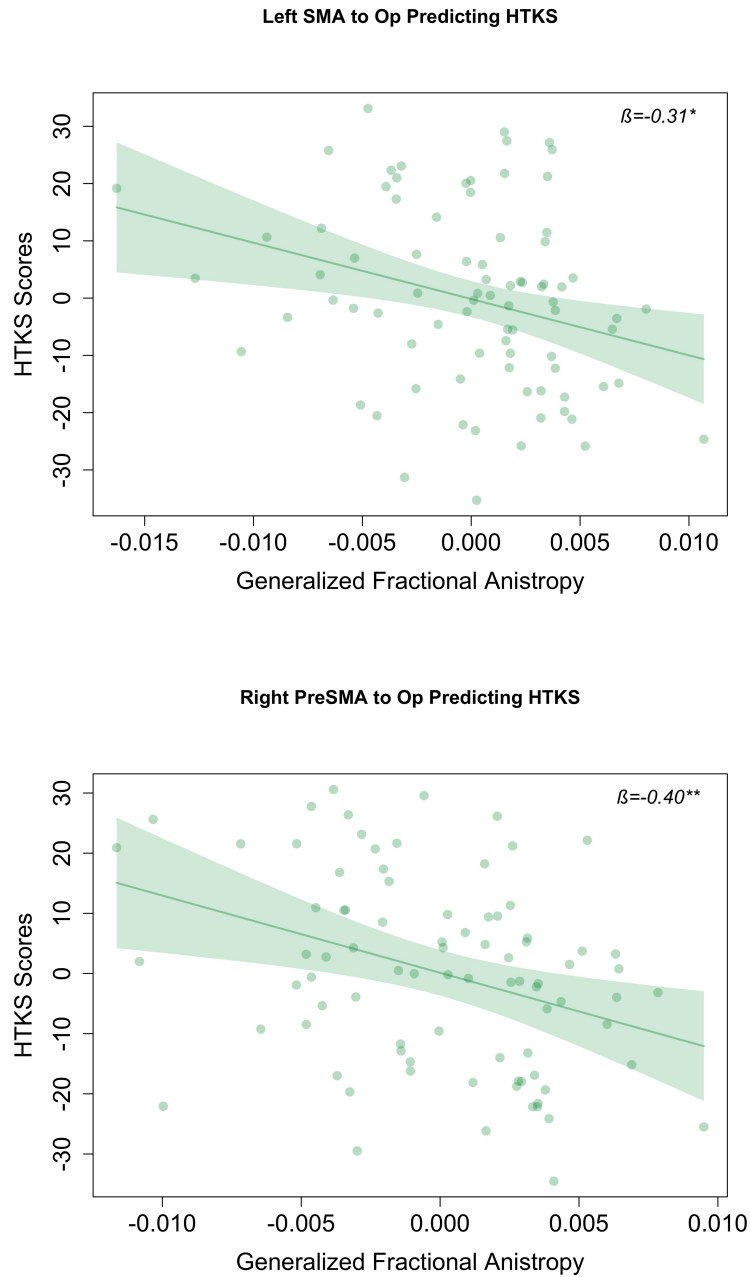
The left SMA to Op GFA predicted higher HTKS scores, controlling for age, gender, whole brain microstructure, movement in the scanner, and SES. A similar relationship can be seen with the right preSMA to Op segment with AD. This relationship is also trending when GFA is used. These plots depict the TD sample of children. $p<0.05^*$, $p<0.01^{**}$, $p<0.001^{***}$.

Figure 18: FAT Laterality Predicting HTKS Scores in TD Sample



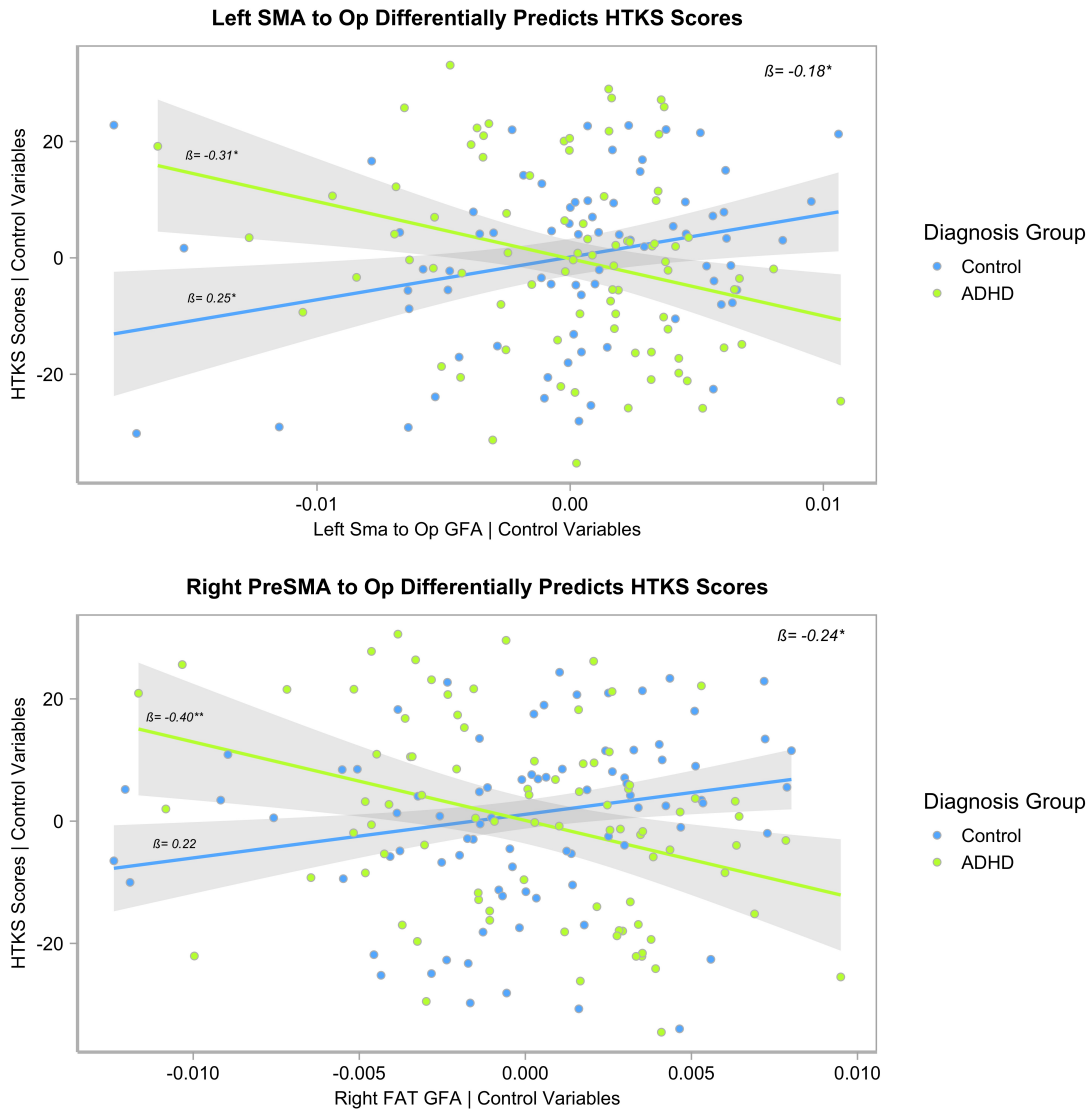
This plot indicates that the left laterality of the FAT is associated with lower HTKS scores. In other words, the developing brain favors the right hemisphere for executive function tasks. These plots depict the TD sample of children. Laterality was calculated using Thiebaut de Schotten et al. (2014) formula $(\text{left} - \text{right}) / (\text{left} + \text{right})$ in which positive values indicate left laterality. $p < 0.05^*$, $p < 0.01^{**}$, $p < 0.001^{***}$.

Figure 19: Bilateral FAT Predicting HTKS Scores in ADHD Sample



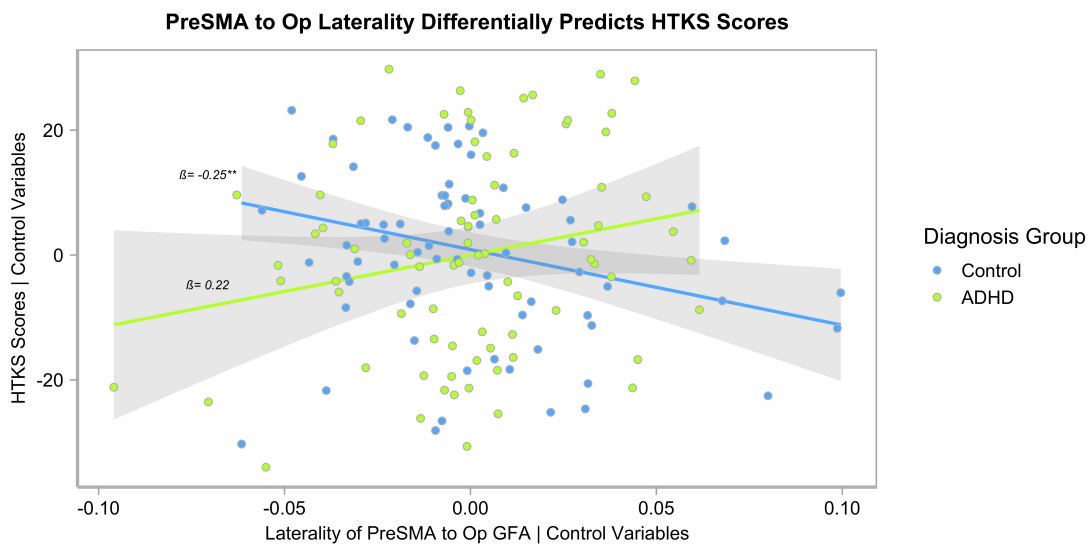
The left and right FAT segments predicted lower HTKS scores, controlling for age, sex, whole brain GFA, movement in the scanner, and SES. These plots depict the ADHD sample of children. $p < 0.05^*$, $p < 0.01^{**}$, $p < 0.001^{***}$.

Figure 20: ADHD Diagnosis Moderates Relationship Between Left and Right FAT and HTKS



ADHD diagnosis moderates the effect of the right and left FAT on HTKS performance, with higher GFA in the segments predicting higher semantic scores in the TD sample and lower scores in the ADHD sample. $p < 0.05^*$, $p < 0.01^{**}$, $p < 0.001^{***}$.

Figure 21: ADHD Diagnosis Moderates Effect of PreSMA to Op Laterality's Relationship with HTKS



Significant interaction between group diagnosis and the lateralization of the preSMA to Op segment predicting HTKS, with lower left lateralization predicting higher HTKS scores in the TD sample, while higher left lateralization had a trending association with higher HTKS scores. Laterality was calculated using Thiebaut de Schotten et al. (2014) formula $(\text{left} - \text{right}) / (\text{left} + \text{right})$ in which positive values indicate left laterality. $p < 0.05^*$, $p < 0.01^{**}$, $p < 0.001^{***}$.

Figure 22: Corpus Callosum Segmentation

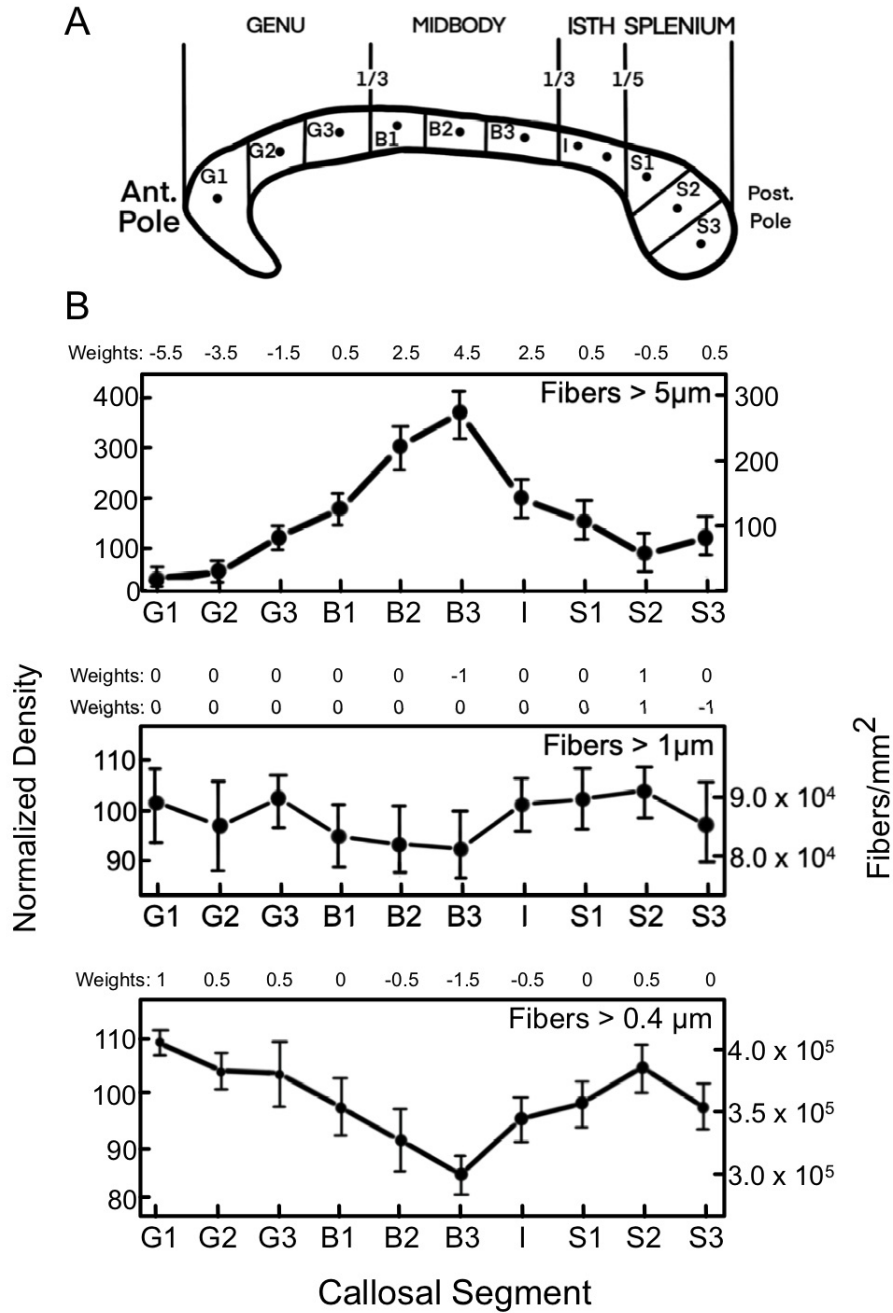
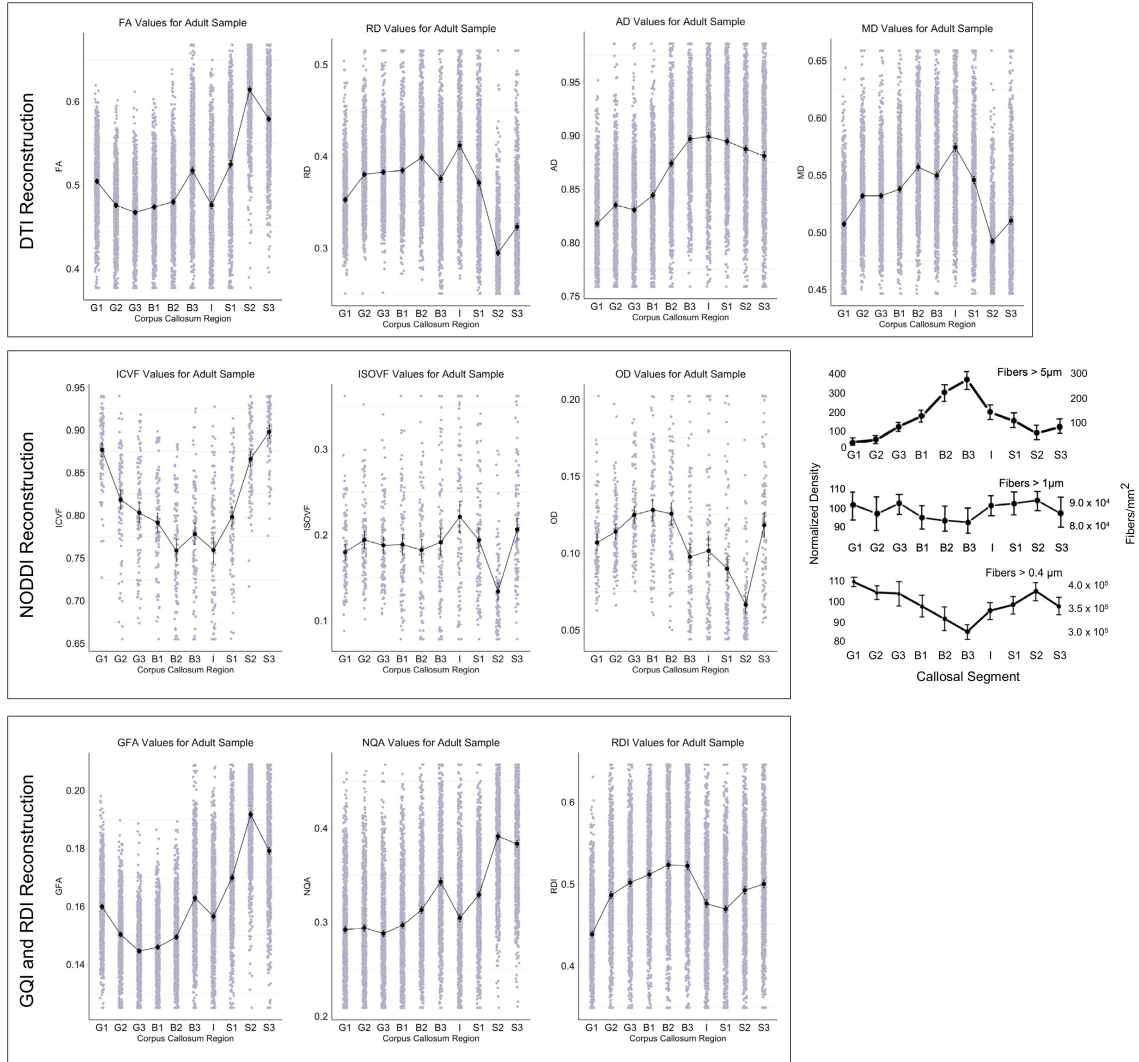


Figure 22A: Corpus callosum segmentation scheme from the Aboitiz et al (1992) paper which we replicated for the current studies. Figure 22B: Density results from Aboitiz et al (1992) for three fiber sizes: >5.0 μ m, >1 μ m, and >0.4 μ m, along with the associated contrast weights we applied.

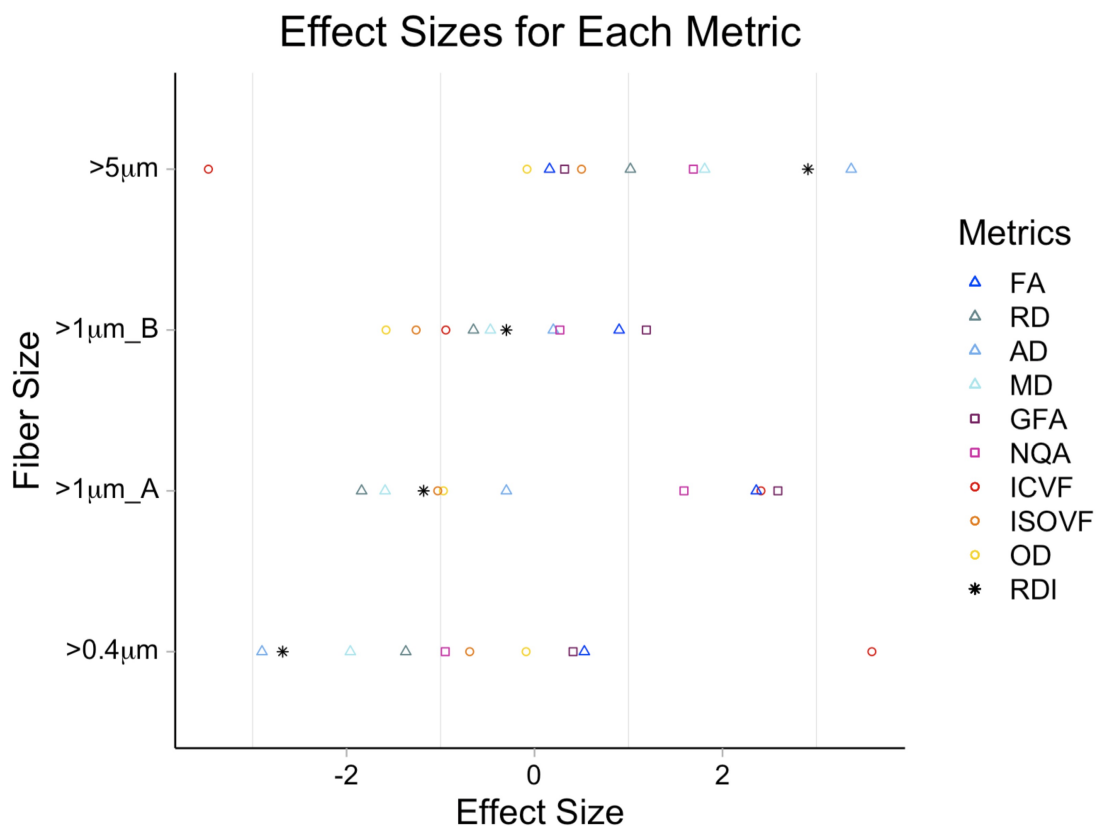
Figure 23: Density Patterns for Adult Sample

DTI, GQI, NODDI, and RDI Metrics for the Adult Sample



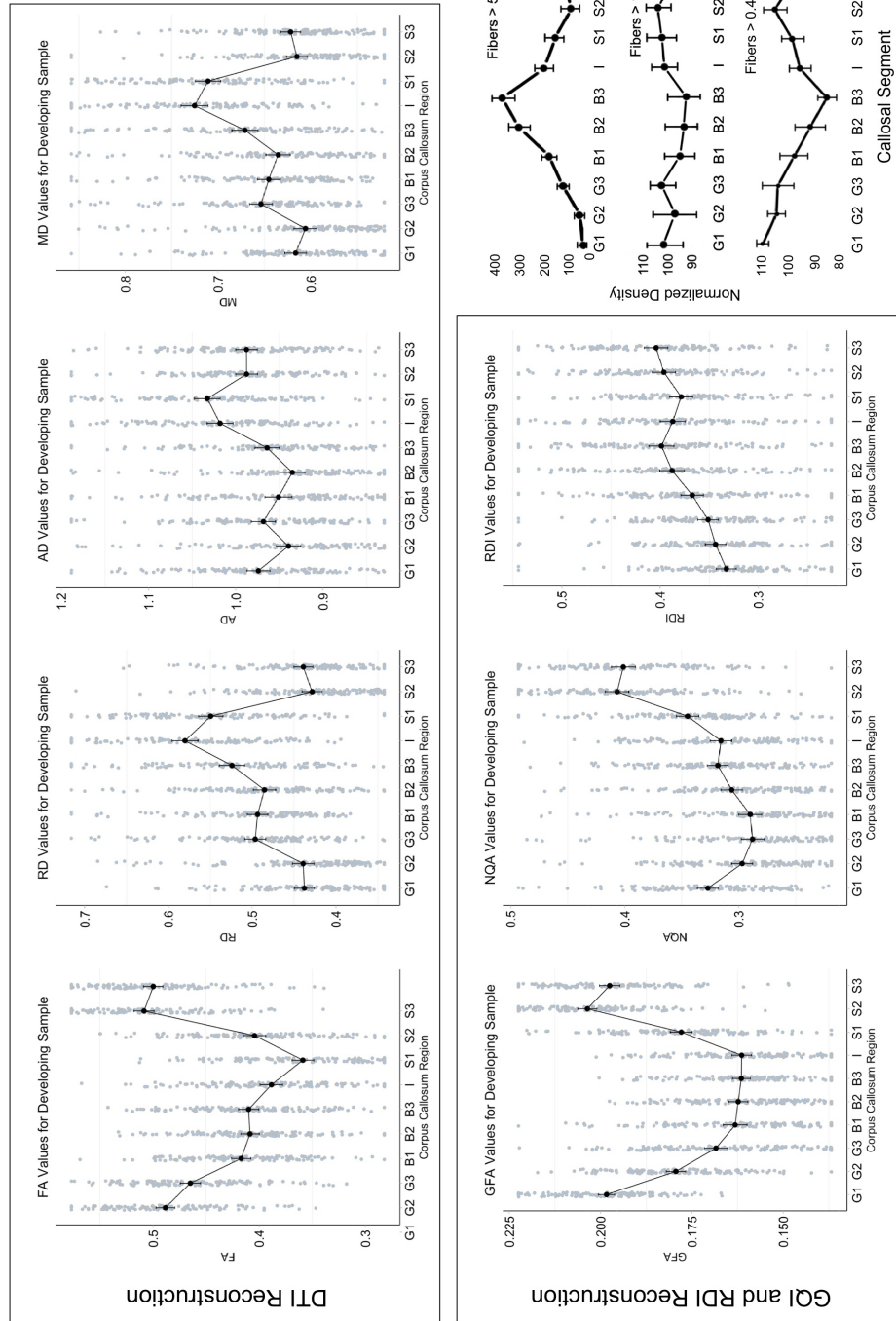
Anterior to posterior corpus callosum density patterns for the adult sample are plotted for each metric and grouped by reconstruction method. The density patterns acquired in the *in vivo* DWI acquisitions are being compared to the Aboitiz (1992) histological patterns, shown on the right.

Figure 24: DWI Metric Effect Sizes for Adult Sample



This figure shows the effect size of each diffusion metric predicting the Aboitiz model in the adult sample, based on fiber size. Fiber sizes above $1\mu\text{M}$ compared the differences in B3 and S2 for model A, and differences between fiber sizes greater than $1\mu\text{M}$ in S2 and S3 for model B.

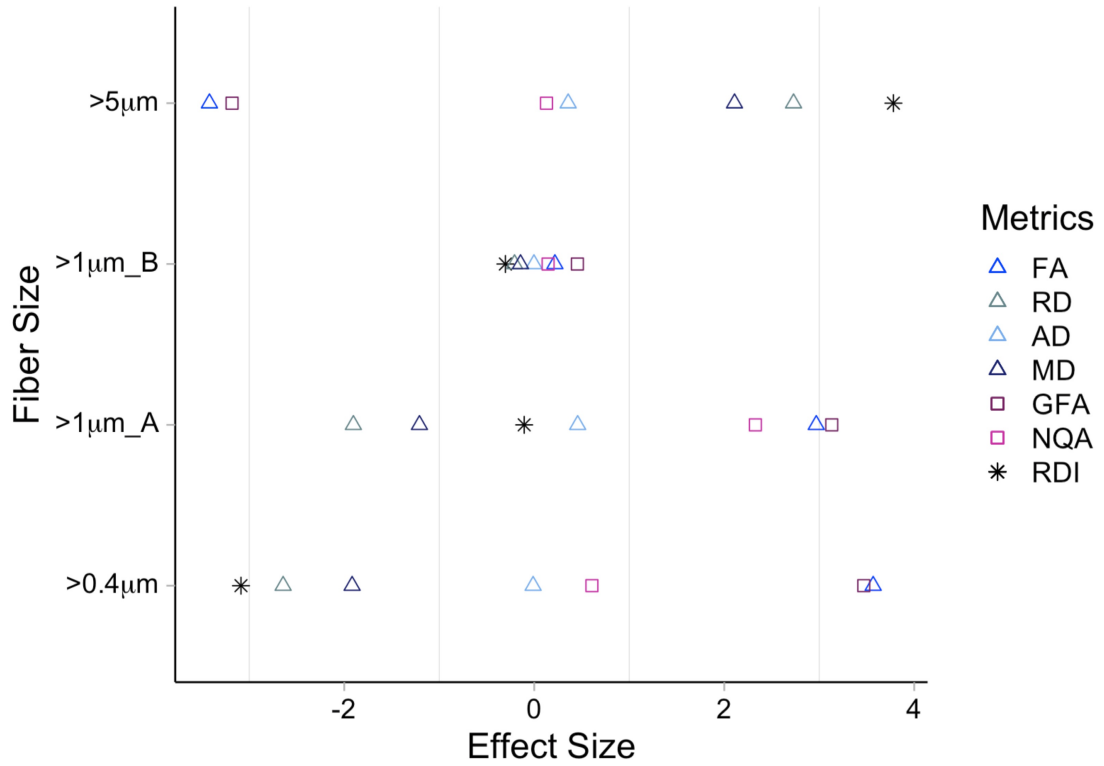
Figure 25: Density Patterns for Developing Sample
 DTI, GQI, and RDI Metrics for the Developing Sample



Corpus callosum density patterns for the developing sample are plotted for each of the 7 metrics and grouped by reconstruction method. The density patterns acquired in the *in vivo* DWI acquisitions are being compared to the Aboitiz (1992) histological patterns, shown on the bottom right.

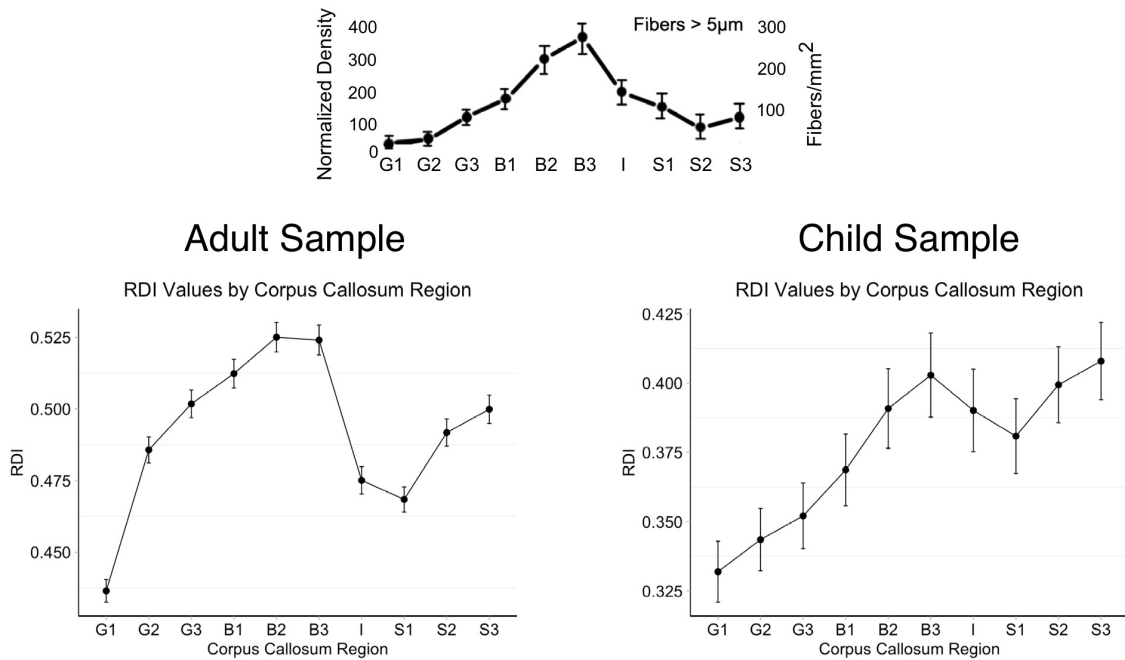
Figure 26: DWI Metric Effect Sizes for Developing Sample

Effect Sizes for Each Metric in Developing Sample



This figure shows the effect size of each diffusion metric predicting the Aboitiz model in the developing sample, based on fiber size. Fiber sizes above $1\mu\text{M}$ compared the differences in B3 and S2 for model A, and differences between fiber sizes greater than $1\mu\text{M}$ in S2 and S3 for model B.

Figure 27: Comparison of *in vivo* Metrics to Histological Density Models



The Aboitiz (1992) histological density model for large fiber sizes is shown above. The bottom plots illustrate the density patterns for the adult and child samples as measured by RDI. RDI accurately captures the peaks and troughs of histologically-established axonal density patterns along the longitudinal axis of the corpus callosum.

Figure 28: Age-Related Differences in Neurite Density

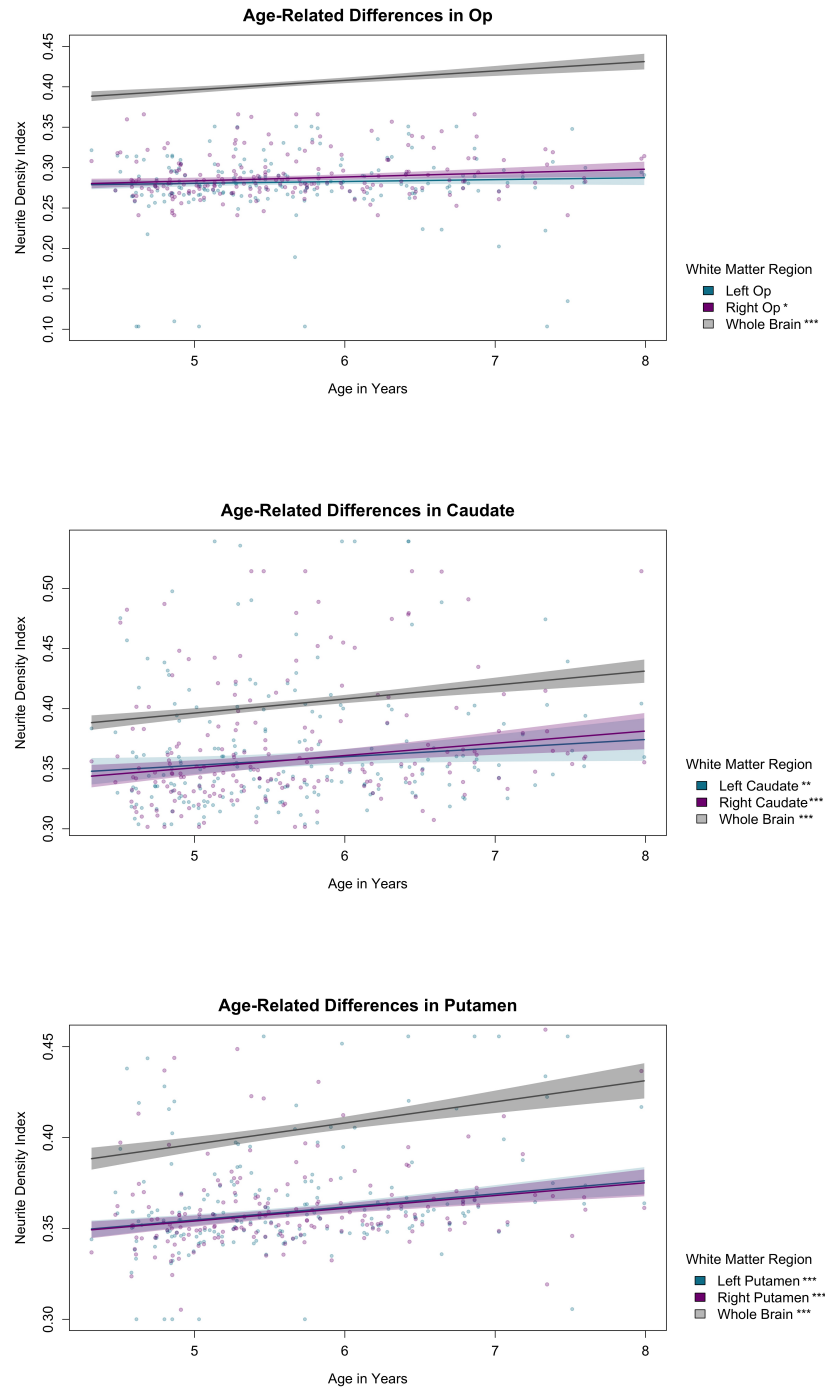


Figure 28 displays the significant age-related differences in neurite density within the *pars opercularis* (Op), caudate, and putamen with Winsorized values in a robust linear model, controlling for age, sex, and whole brain NDI. Significance is indicated by *s in the key. $p < 0.05^*$, $p < 0.01^{**}$, $p < 0.001^{***}$.

Figure 29: Laterality of Neurite Density in SMA and Caudate Predict Verbal Fluency in ADHD Sample

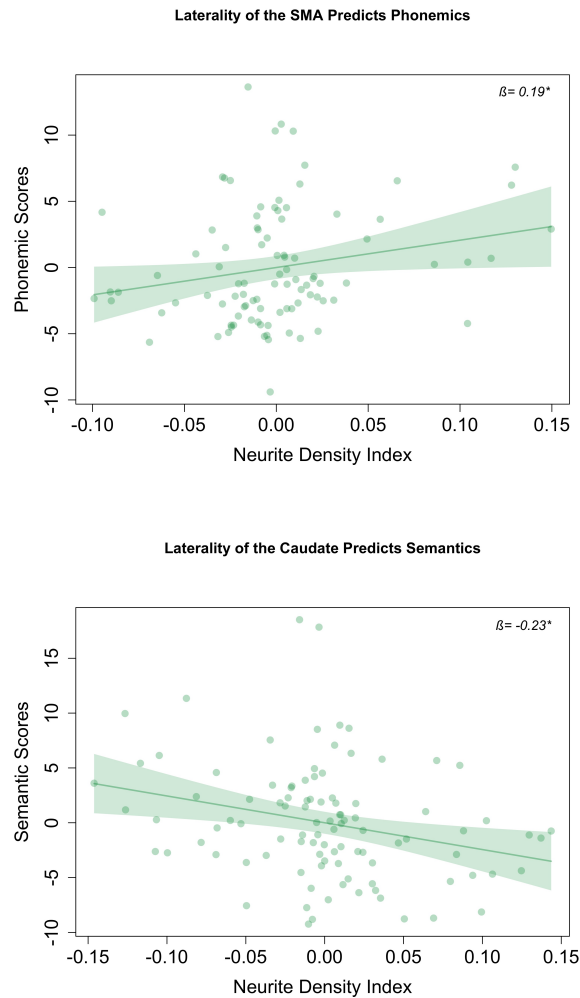


Figure 29 shows how the laterality of the neurite density index (NDI) in the supplementary motor area (SMA) and caudate predict phonemic and semantic scores, controlling for age, sex, whole brain NDI, movement in the scanner, and socioeconomic status. Laterality was calculated using Thiebaut de Schotten et al. (2014) formula $(\text{left} - \text{right}) / (\text{left} + \text{right})$ in which positive values indicate left laterality. β = Standardized regression slope parameter estimate. $p < 0.05^*$, $p < 0.01^{**}$, $p < 0.001^{***}$.

Figure 30: Laterality of the SMA Predicts Executive Function in Full Sample

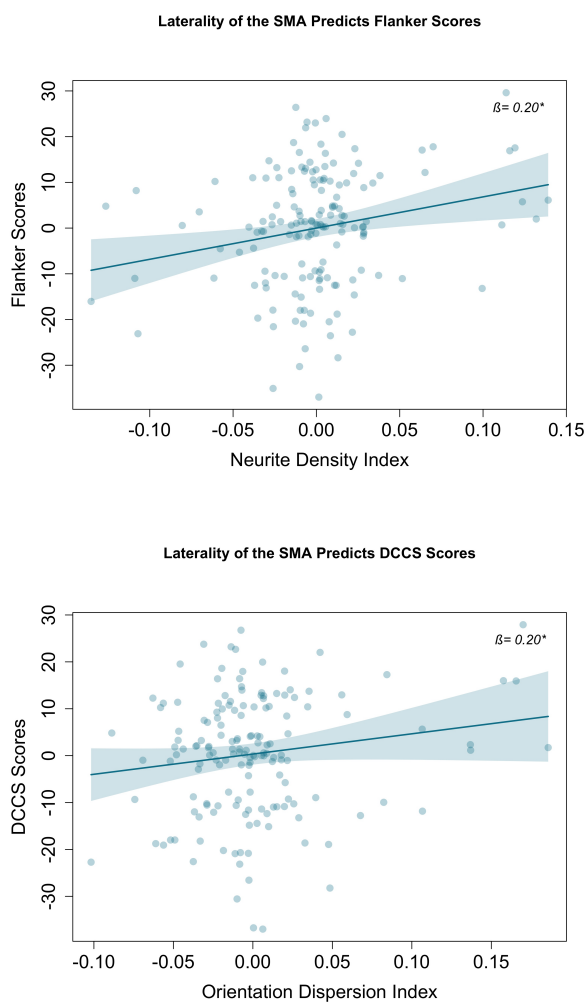


Figure 30 shows how the laterality of the supplementary motor area (SMA) predicts age-corrected NIH Toolbox executive function scores, controlling for sex, whole brain microstructure, movement in the scanner, and socioeconomic status. Laterality was calculated using Thiebaut de Schotten et al. (2014) formula (left - right)/(left + right) in which positive values indicate left laterality. β = Standardized regression slope parameter estimate. $p < 0.05^*$, $p < 0.01^{**}$, $p < 0.001^{***}$.

Figure 31: Orientation Dispersion Predicting Flanker Scores in TD Sample

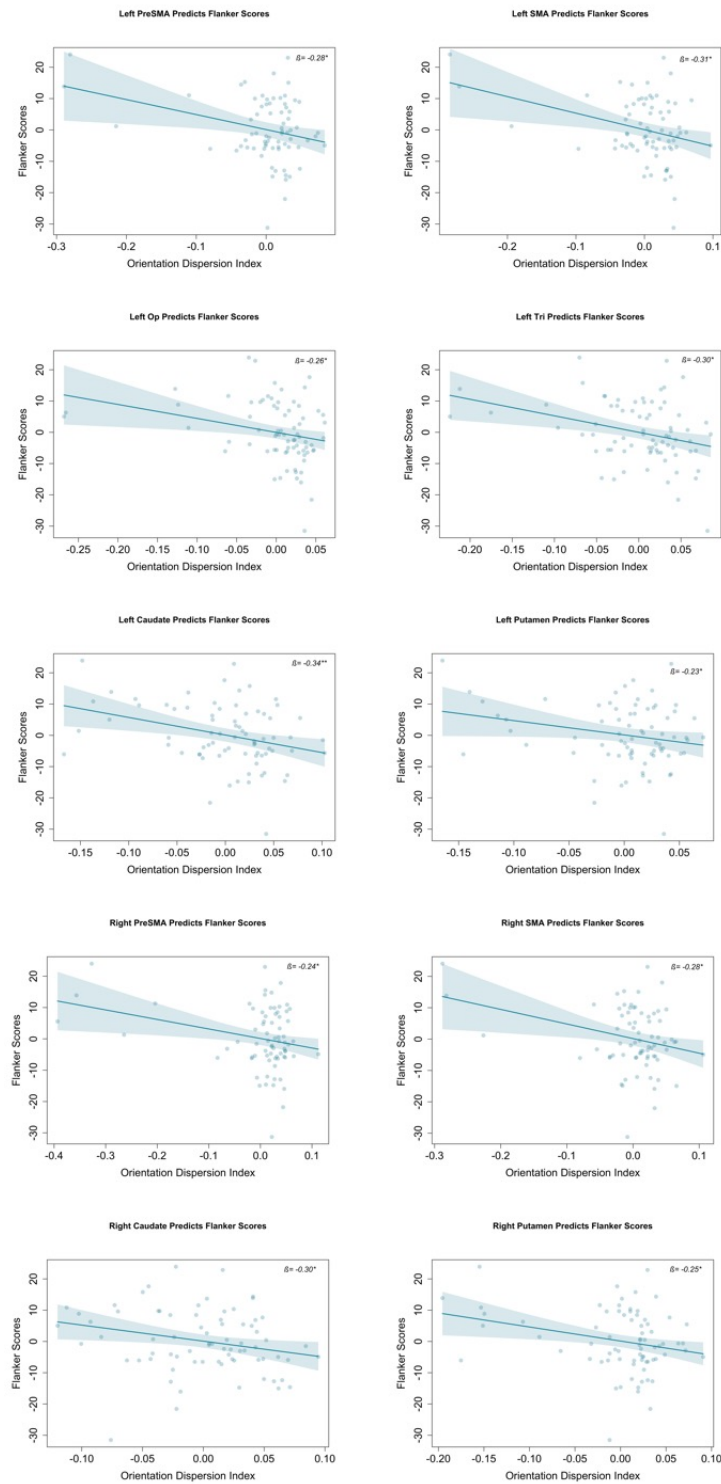


Figure 31 shows how 10 out of 12 brain regions predicted flanker scores, controlling for sex, whole brain microstructure, movement in the scanner, and socioeconomic status. Similar results were seen with FAT regions for DCCS. β = Standardized regression slope parameter estimate. $p < 0.05^*$, $p < 0.01^{**}$, $p < 0.001^{***}$.

Figure 32: Neurite Density of the Left SMA Differentially Predicts Flanker Scores

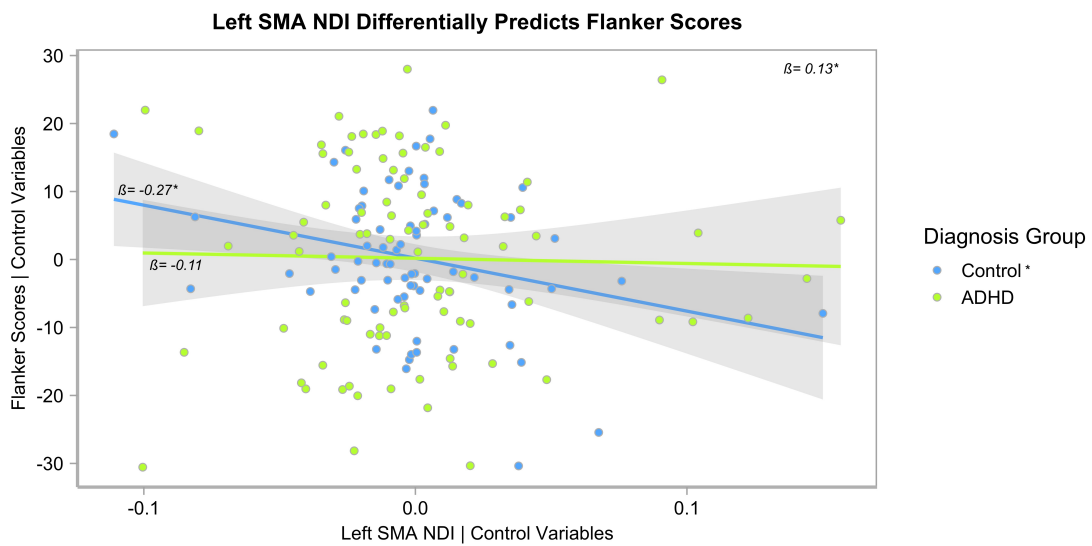


Figure 32 displays the moderation effect of ADHD diagnosis, with lower neurite density (measured with NDI) in the left supplementary motor area (SMA) predicting higher flanker scores in the TD sample, while having no affect in the ADHD sample. β = Standardized regression slope parameter estimate. $p < 0.05^*$, $p < 0.01^{**}$, $p < 0.001^{***}$.

Figure 33: Laterality of Orientation Dispersion Differentially Predicts DCCS Scores

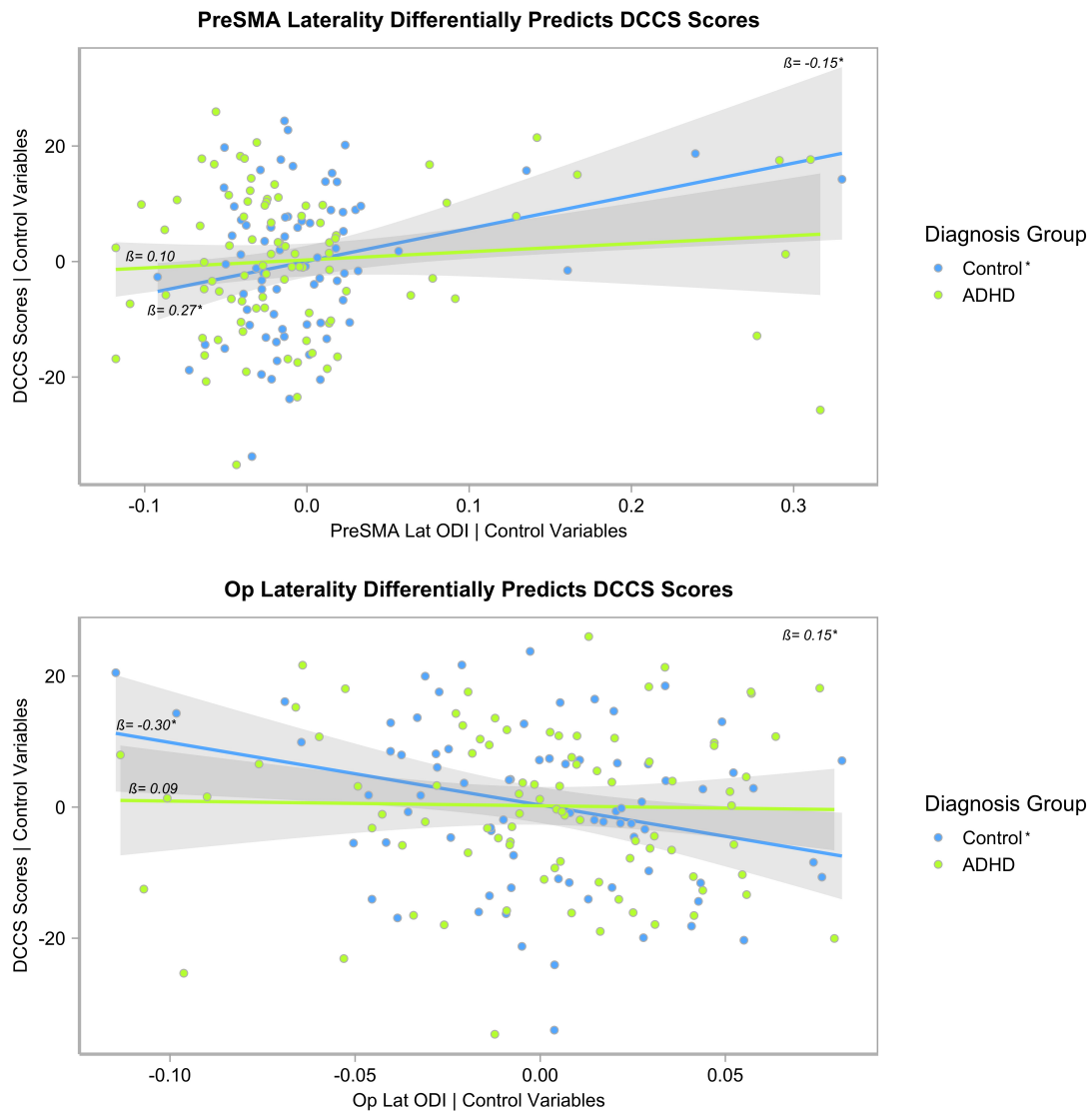


Figure 33 displays how ADHD diagnosis moderates the association between ODI laterality in the pre-supplementary motor area (preSMA) and *pars opercularis* (Op) and DCCS scores. Laterality was calculated using Thiebaut de Schotten et al. (2014) formula (left - right)/(left + right) in which positive values indicate left laterality. β = Standardized regression slope parameter estimate. β = Standardized regression slope parameter estimate. $p < 0.05^*$, $p < 0.01^{**}$, $p < 0.001^{***}$.

Figure 34: Neurite Density of Tri Predicts Executive Function in the TD Sample

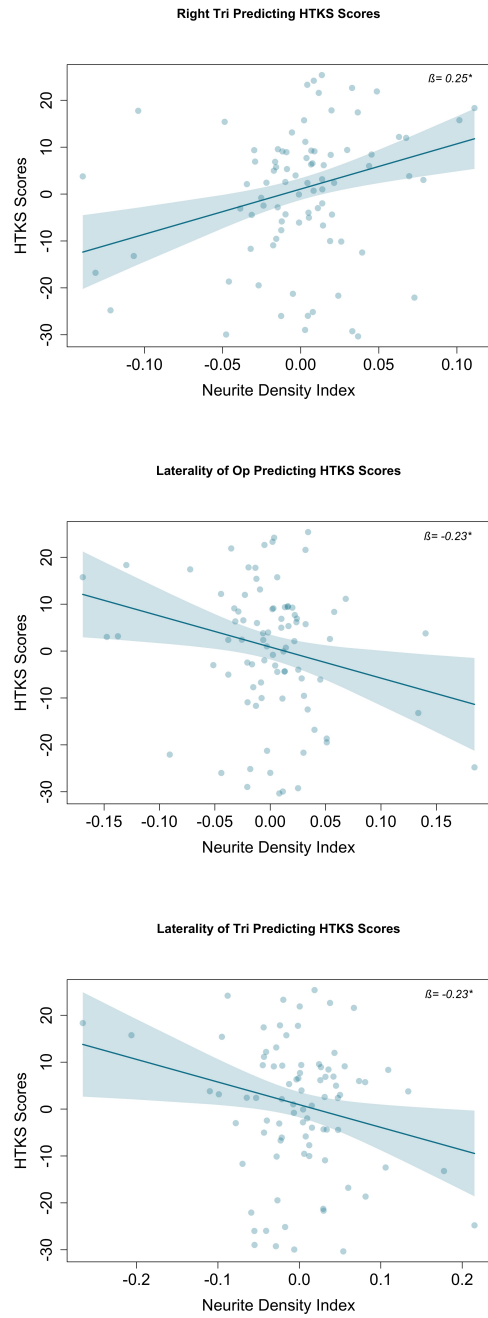


Figure 34 shows the association of the inferior frontal gyrus and executive function, measured by HTKS, in the typically developing sample. Laterality was calculated using Thiebaut de Schotten et al. (2014) formula (left - right)/(left + right) in which positive values indicate left laterality. β = Standardized regression slope parameter estimate. $\beta < 0.05^*$, $p < 0.01^{**}$, $p < 0.001^{***}$.

Figure 35: Orientation Dispersion of Multiple Brain Regions Predicts Executive Function in the TD Sample

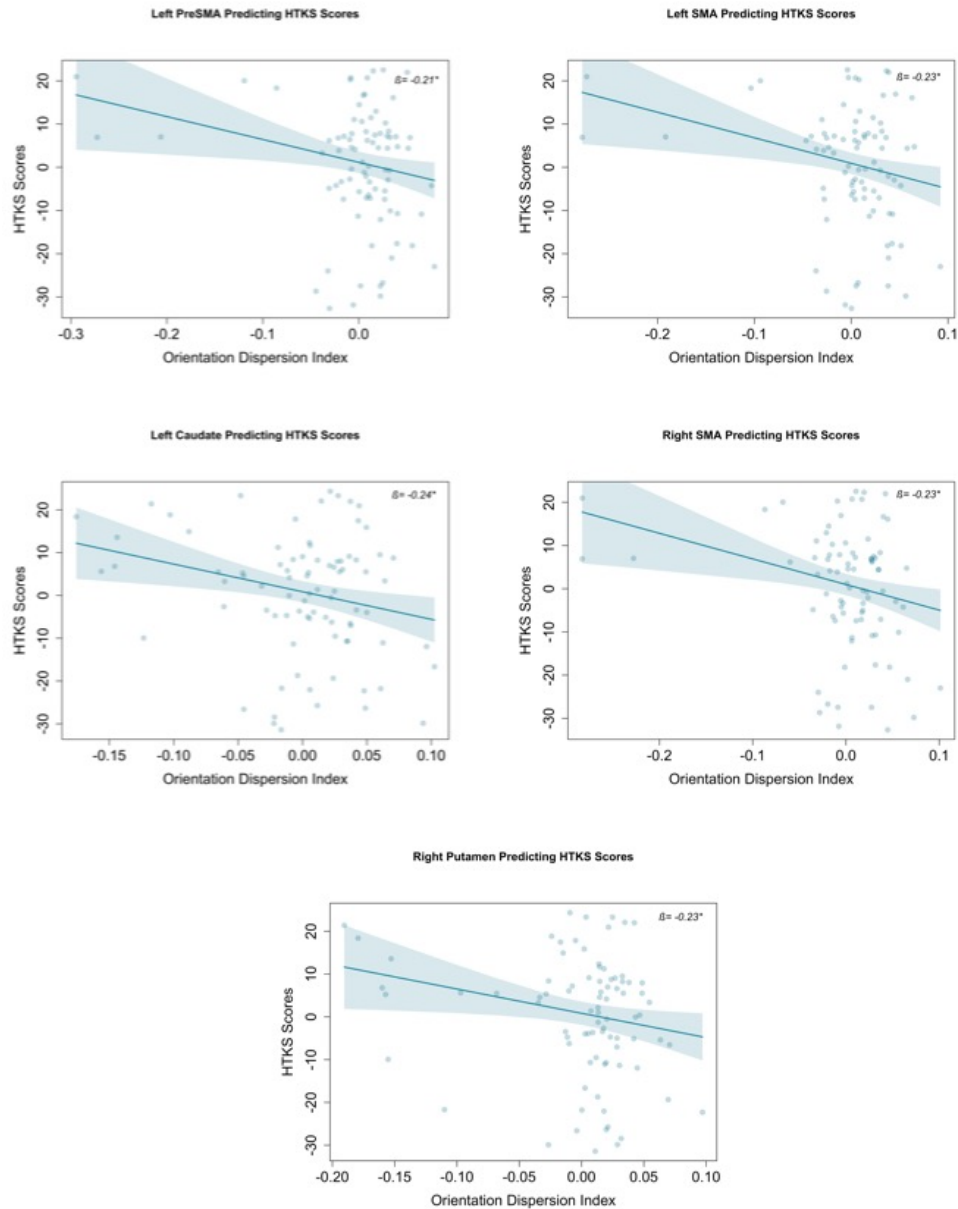


Figure 35 shows the association of the orientation dispersion of multiple brain regions and executive function, measured by HTKS, in the typically developing sample. β = Standardized regression slope parameter estimate. $p < 0.05^*$, $p < 0.01^{**}$, $p < 0.001^{***}$.

VITA

DEA GARIC

2009-2013	B.S., Psychology University of Florida Gainesville, Florida.
2013-2015	M.A., Experimental Psychology Florida Atlantic University Boca Raton, Florida.
2015-2018	M.S., Psychology Florida International University Miami, Florida.
2018-2020	Doctoral Candidate, Psychology Florida International University Miami, Florida.

PUBLICATIONS AND PRESENTATIONS

Garic, D., Badran, R., Borges, H., Graziano, P.A., Dick, A.S. (2020). Bilateral Frontal Aslant Tract association with verbal fluency in young children with and without ADHD. Poster presented at the Cognitive Neuroscience Society, Boston, Massachusetts.

Dick, A.S., Garic, D., Graziano, P.A. (2020). The frontal aslant tract (FAT) white matter microstructure differentiates young children with ADHD from typical controls. Poster presented at the Cognitive Neuroscience Society, Boston, Massachusetts.

Graziano, P.A., Garic, D., Hare, M., Dick, A.S. (2020). Disruption to the Uncinate Fasciculus among young children with ADHD: The role of co-morbid Callous-Unemotional Traits. Poster presented at the Cognitive Neuroscience Society. Boston, Massachusetts.

Garic, D., Badran, R., Behar, D., Torres, A., Garcia, A., Hernandez, M., Borges, H., Graziano, P., Dick, A.S. (2019). Frontal Aslant Tract Structure Differentially Predicts Language and Executive Function Performance in Young Children With and Without ADHD. Poster presented at the International Society for Developmental Psychobiology conference. Chicago, Illinois.

Dick, A.S., Garic, D., Graziano, P., Tremblay, P. (2019). The frontal aslant tract (FAT) and its role in speech, language, and executive function. *Cortex*, 111, 148-163.

Garic, D., Broce, I., Graziano, P., Mattfeld, A. Dick, A. S. (2019). Laterality of the frontal aslant tract (FAT) explains externalizing behaviors through its association with executive function. *Developmental Science*.

Garic, D., Dick, A.S. (2019). Comparison of diffusion-weighted imaging density metrics: Examining neurite and axonal density *in vivo*. Poster presented at the Neural Engineering Research Symposium. Coral Gables, Florida.

Garic, D. Dick, A.S. (2018). Morphology of the Corpus Callosum: Implementing Neurite Orientation Dispersion and Density Imaging (NODDI). Talk presented at regional Brainhack 2018 meeting. Miami, Florida.

Garic, D., Broce, I., Dick, A.S. (2018). Bilateral differences in Frontal Aslant Tract development predicting verbal fluency: A Diffusion Tensor Imaging study. Poster presented at the International Society for the Study of Behavioural Development conference. Gold Coast, Queensland, Australia.

McNew, M.E., Garic, D. (2017). Inclusion of disability status in investigations of child maltreatment prevalence. *American Journal of Public Health*, 107.

Garic, D. Dick, A.S. (2017). Development of The Structural Connectome Supporting Language and Executive Function. Talk presented at the University of Miami Cognitive Studies Graduate Symposium, Miami, Florida.

Garic, D., Zetina, H., Dick, A.S. (2017). Development of the Lateral Lemniscus and Its Relation to Receptive Vocabulary. Poster presented at the International Society for Developmental Psychobiology conference. Washington, DC.

Broce, I., Garic, D., Mattfeld, A., Dick, A.S. (2017). Dorsal and ventral streams supporting literacy: Connectivity of the vertical occipital fasciculus. Poster presented Society for Research in Child Development conference. Austin, Texas.

Garic, D., Broce, J., Lyew, T., Lobo, J., Zetina, H., Dick, A.S. (2016). Development of the Frontal Aslant Tract (FAT) and its relation to executive function. Talk presented at the South Florida Child Psychology Collaborative Research Conference, Miami, Florida.